Analysis of the 1978 Brooks Peninsula, Vancouver Island Earthquakes

by

Christopher William Leonard Spindler
B.Sc., University of Western Ontario, 1987

A Thesis Submitted in Partial Fulfillment of the
Requirements for the Degree of

MASTER OF SCIENCES

in the Department of Physics and Astronomy

[redacted]
Dr. G.C. Rogers, Co-Supervisor
(Department of Physics and Astronomy)

[redacted]
Dr. G.D. Spence, Co-Supervisor
(Department of Physics and Astronomy)

[redacted]
Dr. R.W. Stewart, Departmental Member
(Department of Physics and Astronomy)

[redacted]
Dr. D.D. Olesky, Outside Member
(Department of Computer Science)

[redacted]
Dr. D. Weichert, External Examiner
(Pacific Geoscience Centre, Geological Survey of Canada)

Supervisors: Dr. G.C. Rogers and Dr. G.D. Spence

ABSTRACT

Two earthquakes occurred on the Brooks Peninsula on June 2nd and July 25th, 1978. They were the largest events to have been recorded in the region. Both were followed by extensive aftershock sequences and a field program was mounted to monitor part of the first sequence.

Using the field program data for reference, the main shock epicentres were relocated and the teleseismic and regional location biases identified. The main shock epicentres were coincident within location uncertainties and located on the NW shore of the peninsula at a depth of between 10 and 20 km. Teleseismic epicentre solutions, using the Jeffreys-Bullen model and all available data, misplaced the epicentres to the NE by 12 km. This was corrected by using only data from $\Delta \geq 20°$. The regional bias was on the order of 4-6 km to the east or west, depending on whether the Canadian Shield or Georgia Straits model was being used.

The focal mechanisms, determined using a combination of first-motion and surface wave data, were found to be essentially identical. The preferred fault plane displayed sinistral, normal strike-slip faulting along a NE striking fault, dipping 30°-45° northwest. The other plane displayed dextral motion on a steeply dipping, north striking fault. There was no strong evidence to favour either plane as the fault plane. The pressure axes of the mechanisms were oriented NE-SW, consistent with present convergence vector of the Explorer plate with North America.

Using the surface wave data, the seismic moments were found to be 1.60×10^{24} dyne·cm for June and 1.19×10^{24} dyne·cm for July. The surface wave magnitudes were redetermined using additional data (June: 5.2, July 5.1) and agreed with the I.S.C. values. The stress drops were calculated from the far field displacement spectra and averaged 16 bars for both events. The rupture surface radii for June and July were found to be 3.5 km and 3.2 km respectively.

Other earthquakes in the Brooks Peninsula region, spanning the period from 1978 to 1987, were relocated using the corrections developed from the aftershock data. The events were found to be concentrated off the NW shore of the peninsula and not spread over the entire region, as the original G.S.C. data indicated.

The orientations of the pressure axes of the focal mechanisms suggest that the Brooks Peninsula earthquakes are directly related to the relative motions of the Explorer and North American plates. If this is also true of the regional seismicity, then the data imply that there is coupling between between the plates in the region, possibly due to the subsidence of the peninsula. The placement of the events in the overlying plate further implies that the plates are locked at the interface and that the stress across the interface has been transmitted into the interior of that plate. The relatively low stress drops indicate that the earthquakes did not take place on a new or well cemented fault and that motion on this fault is not uncommon.

Examiners:

[redacted]

Dr. G.C. Rogers, Co-Supervisor
(Department of Physics and Astronomy)

[redacted]

Dr. G.D. Spence, Co-Supervisor
(Department of Physics and Astronomy)

[redacted]

Dr. R.W. Stewart, Departmental Member
(Department of Physics and Astronomy)

[redacted]

Dr. D.D. Olesky, Outside Member
(Department of Computer Science)

[redacted]

Dr. D. Weichert, External Examiner
(Pacific Geoscience Centre, Geological Survey of Canada)

TABLE OF CONTENTS

ABSTRACT ii

TABLE OF CONTENTS iv

LIST OF TABLES vi

LIST OF FIGURES vii

ACKNOWLEDGEMENTS ix

CHAPTER 1 INTRODUCTION 1

1.1 Outline of Thesis Problem 1
1.2 Tectonic Setting of Vancouver Island 3
1.2.1 Tectonic History 5
1.2.2 Plate Boundaries 7
1.2.3 Contemporary Motions 8
1.3 The Brooks Peninsula 10
1.4 Regional Seismicity 12

CHAPTER 2 AFTERSHOCK STUDY 16

2.1 Introduction 16
2.1.1 Chronology 16
2.2 Local Study 18
2.2.1 Method 18
2.2.2 Analysis 20
2.3 Regional Study 23
2.3.1 Method 25
2.3.2 Relocation of Regional Aftershocks 25
2.3.3 Determination of Corrections 30
2.4 Regional Seismicity 37
2.4.1 Relocations 37
2.5 Summary of Results 40

CHAPTER 3 MAINSHOCK EPICENTRE LOCATIONS 42

3.1 Introduction 42
3.2 Teleseismic Study 42
3.2.1 Method 43
3.2.2 Analysis : Epicentre Locations 43
3.3 Focal Depth Determination 50
3.4 Summary of Results 53

CHAPTER 4 FIRST-MOTION ANALYSIS 56

4.1 Introduction 56
4.2 Focal Mechanism Determination 56
4.2.1 Method 58
4.2.2 Analysis of June Mainshock 59
4.2.3 Analysis of Aftershock data 62
4.2.4 Composite of June Mainshock and Aftershock data . . 65
4.2.5 Analysis of July Mainshock 65
4.3 First-Motion Comparisons 70
4.3.1 Analysis 70
4.4 Summary of Results 71

CHAPTER 5 SURFACE WAVE ANALYSIS 72

5.1 Introduction 72
5.2 M_s Determination 72
5.2.1 Method 74
5.2.2 Analysis 74
5.3 Surface Wave Analysis 76
5.3.1 Method 77
5.3.2 Analysis 82
5.4 Constraining P-nodal Solutions 85
5.5 Love-Rayleigh Amplitude Ratios 89
5.5.1 Method 91
5.5.2 Analysis 91
5.7 Summary of Results 92

CHAPTER 6 STRESS DROP DETERMINATION 95

6.1 Introduction 95
6.2 Method 95
6.3 Analysis 96
6.4 Rupture Surface 99
6.5 Summary of Results 100

CHAPTER 7 DISCUSSION AND CONCLUSION 101

7.1 Summary of Results 101
7.2 Discussion 104
7.2.1 Tectonic Implications 105
7.3 Conclusion 109

BIBLIOGRAPHY 111

APPENDIX A TABLES 115

A-1 Locally Detected Aftershock Epicentres 116
A-2 Regionally Detected Aftershock Epicentres 118
A-3 Regional Earthquakes 1978-1987 119
A-4 Teleseismic Arrival Time Data 121
A-5 First-motion Data 130

APPENDIX B FIGURES 135

B-1 First-motion Wave Forms 136
B-2 Digitized Seismograms 145
B-3 Dispersion Curves 172

List of Tables

Table 1 Local crustal model for the Brooks Peninsula. 20

Table 2 Nominal epicentre for the June 2nd event 21

Table 3 Georgia Straits and Canadian Shield earth models. 23

Table 4 *S-P* Intervals at the temporary array stations. 32

Table 5 Final coordinates for the reference event. 32

Table 6 Travel time corrections for the regional stations. . . . 34

Table 7 Epicentre solutions, Jeffreys-Bullen model 45

Table 8 Epicentre solutions determined using stations at $\Delta \geq 20°$ 46

Table 9 Epicentre solutions, Dziewonski-Anderson model 49

Table 10 Epicentre solutions, common stations 50

Table 11 First-motion weighting scheme 60

Table 12 Focal mechanism of the June 2nd event 62

Table 13 Composite focal mechanism of the June aftershocks 63

Table 14 Composite focal mechanism, June main shock and aftershock data 65

Table 15 Focal mechanism of the July 25th event 67

Table 16 M_s values obtained from the I.S.C. 73

Table 17 M_s values determined from the C.S.S.N. data 76

Table 18 Continental crust earth model 80

Table 19 Focal mechanisms of the Brooks Peninsula events 83

Table 20 Variations of the first-motion focal mechanism for the June event 88

Table 21 Variations of the first-motion focal mechanism for the July event 89

Table 22 Stress drop estimates from the WCTN stations 99

Table 23 Summary of the source parameters for the Brooks Peninsula earthquakes 102

List of Figures

Figure 1 The Brooks Peninsula, main shock epicentres and aftershock region 2

Figure 2 The Juan de Fuca plate system 4

Figure 3 Miocene position of the northern edge of the Juan de Fuca plate 6

Figure 4 Rotation poles of the Explorer plate 9

Figure 5 Geology of the Brooks Peninsula 11

Figure 6 Tectonic setting of the Taitao Peninsula 13

Figure 7 Seismicity around the Brooks Peninsula 15

Figure 8 Aftershock activity observed at PHC 17

Figure 9 Location of temporary array and all aftershocks detected by the array 19

Figure 10 Aftershock cross-sections 22

Figure 11 Aftershocks detected and located by the G.S.C. 24

Figure 12 Permanent seismigraph stations in B.C. 26

Figure 13 Regionally detected aftershocks relocated using CANSESS 28

Figure 14 Regionally detected aftershocks relocated using HYPOELLIPSE 29

Figure 15 Various local hypocentre solutions for the reference event 31

Figure 16 Epicentre solutions for the reference event 33

Figure 17 Regionally detected aftershocks relocated using travel time corrections 35

Figure 18 Plot of all aftershock activity 36

Figure 19 Seismicity of the Brooks Peninsula region 38

Figure 20 Relocated regional events, $M_L \geq 2.0$ 39

Figure 21 Main shock epicentres determined using all data 44

Figure 22 Main shock epicentres determined using data at $\Delta \geq 20°$ 47

Figure 23 Main shock epicentres determined using Dziewonski-Anderson model, without corrections 48

Figure 24 Main shock epicentres determined using Dziewonski-Anderson model, with corrections 51

Figure 25 Main shock epicentres determined using common stations 52

Figure 26 Variation of RMS residuals with depth 54

Figure 27 First-motion focal mechanism for the June event 61

Figure 28 First-motion focal mechanism for the June aftershocks 64

Figure 29 Composite focal mechanism using June main shock and aftershock data 66

Figure 30 First-motion focal mechanism for the July event 68

Figure 31 June aftershock data superimposed on July mechanism . . . 69

Figure 32 Azimuthal distribution of M_s values 75

Figure 33 Stations which provided surface wave data 78

Figure 34 Theoretical surface wave dispersion curves 79

Figure 35 Surface wave focal mechanism solution for June 84

Figure 36 Surface wave focal mechanism solution for July 86

Figure 37 Variations on the June first-motion mechanism 87

Figure 38 Variations on the July first-motion mechanism 90

Figure 39 Variation of Love/Rayleigh amplitudes with depth 93

Figure 40 Far field displacement spectra for June 97

Figure 41 Far field displacement spectra for July 98

Figure 42 Main shock epicentres in relation to geology 106

Figure 43 Explorer/North America rotation pole 108

Acknowledgements

I would like to thank my supervisor, Dr. Garry Rogers, for his invaluable support and guidance. I would also like to thank the staff at the Pacific Geoscience Centre who provided the facilities and data for my reasearch, as well as advice and comments on the many facets of the project. Others who provided much appreciated aid and support were: Dr. George Spence, Dr. Roy Hyndman, Dr. Robert Stewart, Mr. Richard Baldwin and Dr. John Cassidy.

Chapter 1 : Introduction

1.1 Outline of Thesis Problem

In the summer of 1978, two earthquakes occurred on the Brooks Peninsula of Vancouver Island, the first on June 2nd having a body wave magnitude (m_b) of 5.0 and the second on July 25th with m_b 5.2 (*Bulletin of the I.S.C.*, 1979). Both events were followed by extensive aftershock sequences.

These were the largest events to have occurred on northern Vancouver Island since 1927, when one of similar size occurred in the same region (Rogers, 1983). The 1978 earthquakes were large enough to provide data for first-motion focal mechanisms, though neither was large enough to provide data in all quadrants of the focal sphere. The earthquakes were also small enough to permit a surface wave analysis of data from relatively nearby stations. Larger events would have pushed the traces at nearby stations off scale.

The aftershock sequence associated with the June event was monitored for 4 days by a temporary array established on the peninsula in a field study. These local data provided some control for subsequent teleseismic and regional epicentre location trials. The initial teleseismic (I.S.C.) and regional (G.S.C.) epicentres were not coincident with the aftershock locations (Fig. 1).

The aim of this thesis was to learn as much as possible about the 1978 Brooks Peninsula earthquakes. The current interpretation of contemporary tectonics was examined in the light of the new results. In the course of the study, the following were done:

1) The pattern of the June aftershocks detected by the local, temporary array was examined. Aftershocks detected by the regional stations were relocated using one of the locally detected events as a reference point. Other earthquakes in the immediate vicinity of

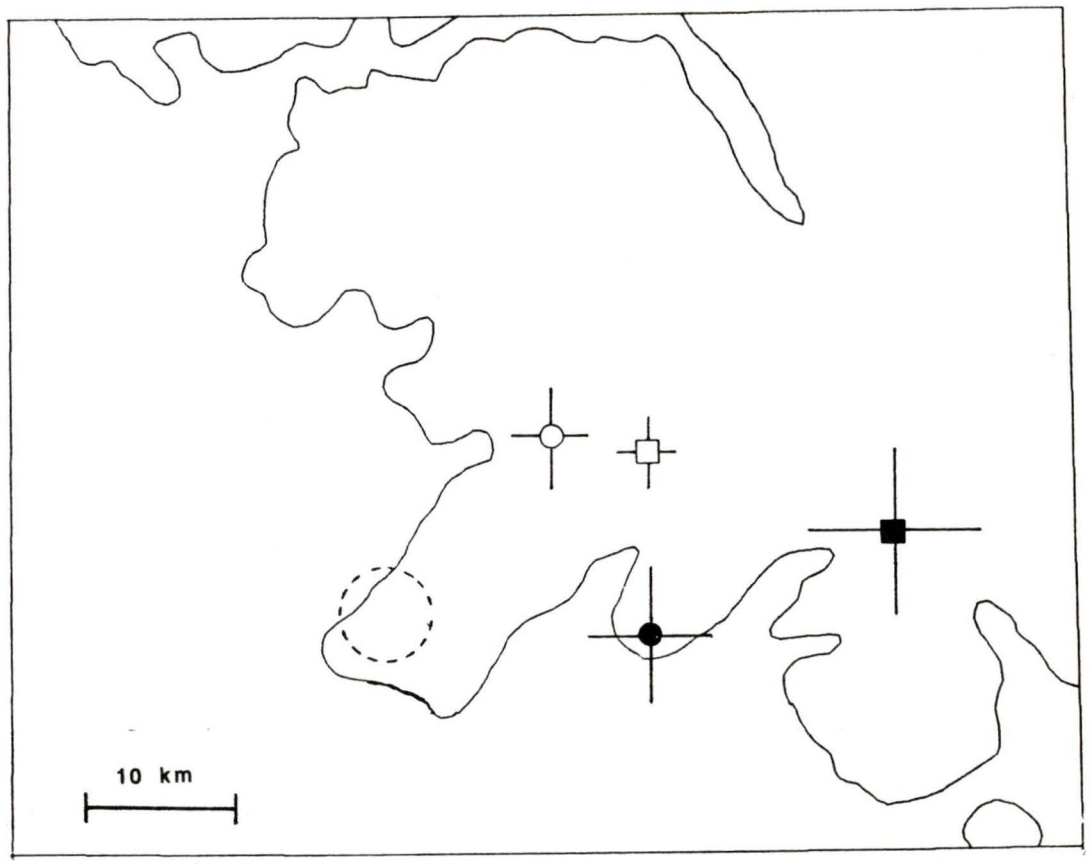

Figure 1 : The Brooks Peninsula and the mainshock epicentres, teleseismic (open) and regional (solid) solutions, from the I.S.C. and G.S.C. respectively. The June 2nd event is indicated by circles and the July 25th event by squares. The aftershock region determined by the field program is delimited by the dashed circle.

the peninsula were relocated using travel time corrections generated from the aftershock data.

2) The teleseismic arrival time data were used to locate the July mainshock with respect to the June event. The effects of the upper mantle bias on the epicentre solutions were also examined.

3) First motion focal mechanisms were determined using the program of Wickens and Hodgson (1967). The *P* waveforms were examined at stations common to both events.

4) The surface wave magnitudes were re-determined for both events. The program suite of Herrmann (1978) was used to obtain focal mechanism solutions and seismic moments from surface wave data. A Love/Rayleigh amplitude ratio technique was used to obtain the focal depth of the June event.

5) The stress drops of the events were determined using seismic moments, rupture area and corner frequencies of the *S* wave displacement spectra. This was done using short period data in the 250 to 400 km distance range.

Work done before the start of this project was carried out by Dr. Garry Rogers at Pacific Geoscience Centre. Dr. Rogers was responsible for the aftershock field program and the reading of those seismic records. He also produced preliminary first-motion mechanisms and initial mainshock and aftershock locations.

1.2 Tectonic Setting of Vancouver Island

There are four lithospheric plates in the Vancouver Island region; the North American (NAM) plate, the Pacific (PAC) plate, the Juan de Fuca (JDF) plate and the Explorer (EXP) plate (Fig. 2). The Winona block (Davis and Riddihough, 1982) occupies the northwestern end of the Explorer plate.

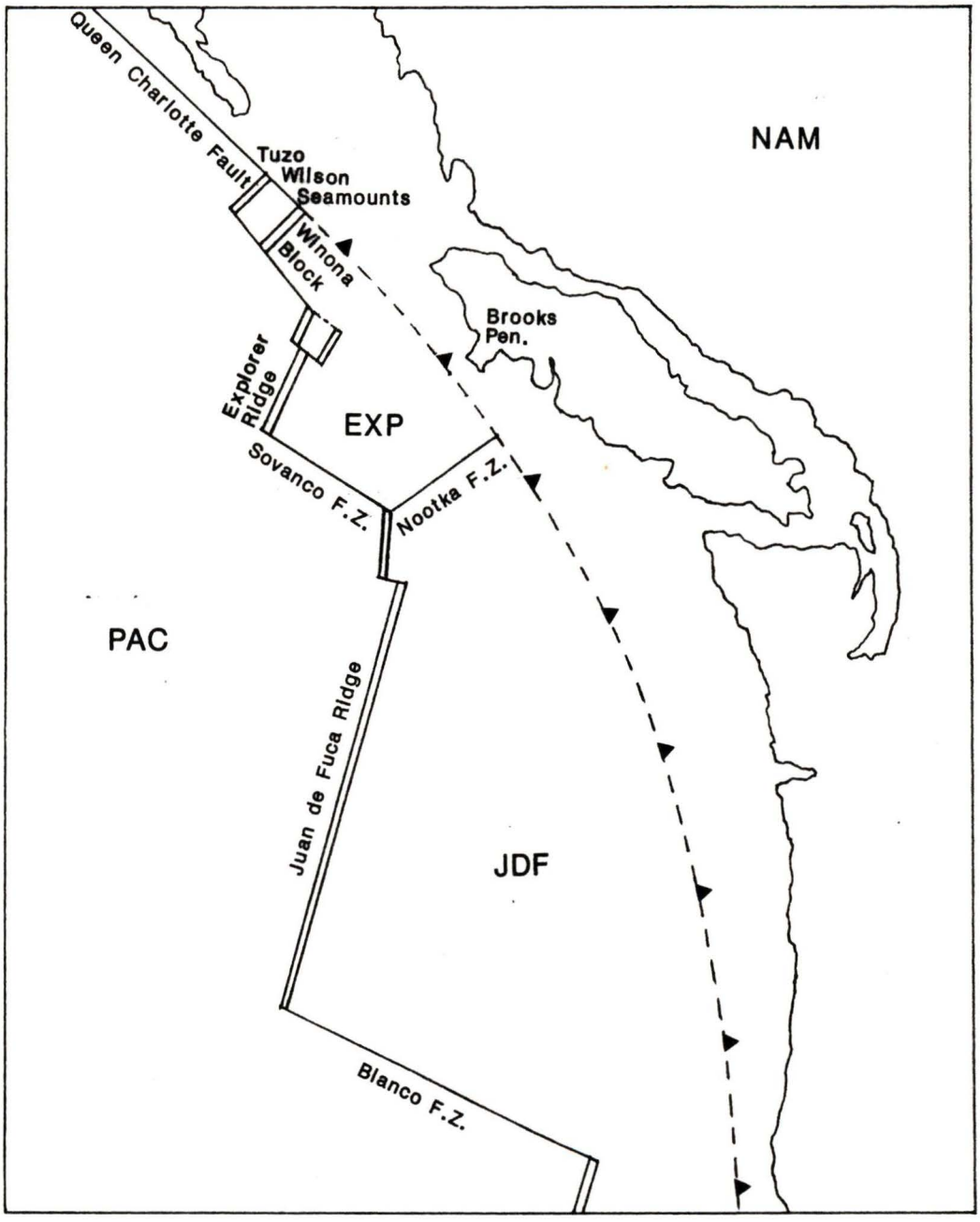

Figure 2 : The Juan de Fuca plate system, showing the Pacific (PAC), Explorer (EXP), Juan de Fuca (JDF) and North American (NAM) plates. Spreading ridges are shown by double lines, transform boundaries by single lines and the subduction by solid triangles. Adapted from Riddihough (1984).

1.2.1 Tectonic History

The Juan de Fuca plate is a remnant of the Farallon plate which has converged with the Americas over the past 150 million years (Riddihough, 1984). The oldest portions of the Juan de Fuca plate exposed on the sea floor are on the order of 10 million years old. The plate interactions were reconstructed from an analysis sea floor magnetic anomalies (Riddihough, 1977).

At 10 Ma BP, the Explorer plate was part of the Juan de Fuca plate which was converging with North America at a rate of 5.5 cm/yr. From 9.0 to 3.5 Ma BP, convergence occurred at azimuths of between 035° and 050° and the convergence rate fell to 4.5 cm/yr (Riddihough, 1977). The JDF-NAM-PAC triple junction was positioned just off the Brooks Peninsula from 10 to 4.0 Ma BP and the northernmost edge of the subducted Juan de Fuca plate struck NE from the peninsula, across the island (Fig. 3). Volcanism in the Alert Bay Volcanic Belt, which was probably associated with the descending plate edge, started at 8 Ma BP (Armstrong *et al.*, 1985).

Significant changes occurred between 4.0 and 3.5 Ma BP, when the Explorer plate started moving independently of the Juan de Fuca plate (Riddihough, 1984). The JDF-NAM convergence rate decreased abruptly at this time, falling from 4.5 cm/yr to 3.5 cm/yr. The EXP-NAM convergence rate went from 4.0 cm/yr to 1.9 cm/yr and azimuth of convergence with NAM changed from between 026° and 038° to between 051° and 062° (Riddihough, 1977). The azimuth of JDF-NAM convergence did not change significantly. These events also coincided with a peak in volcanic activity in the Alert Bay Volcanic Belt (Armstrong *et al.*, 1985). At the same time, the triple junction began migrating north from its position near the Brooks Peninsula at a rate of 1-2 cm/yr (Riddihough *et al.*, 1983). The Winona block began to decouple from the Pacific plate between 1.5 and 2.0 Ma BP and was fully decoupled by 1.0 Ma BP (Davis and Riddihough, 1982).

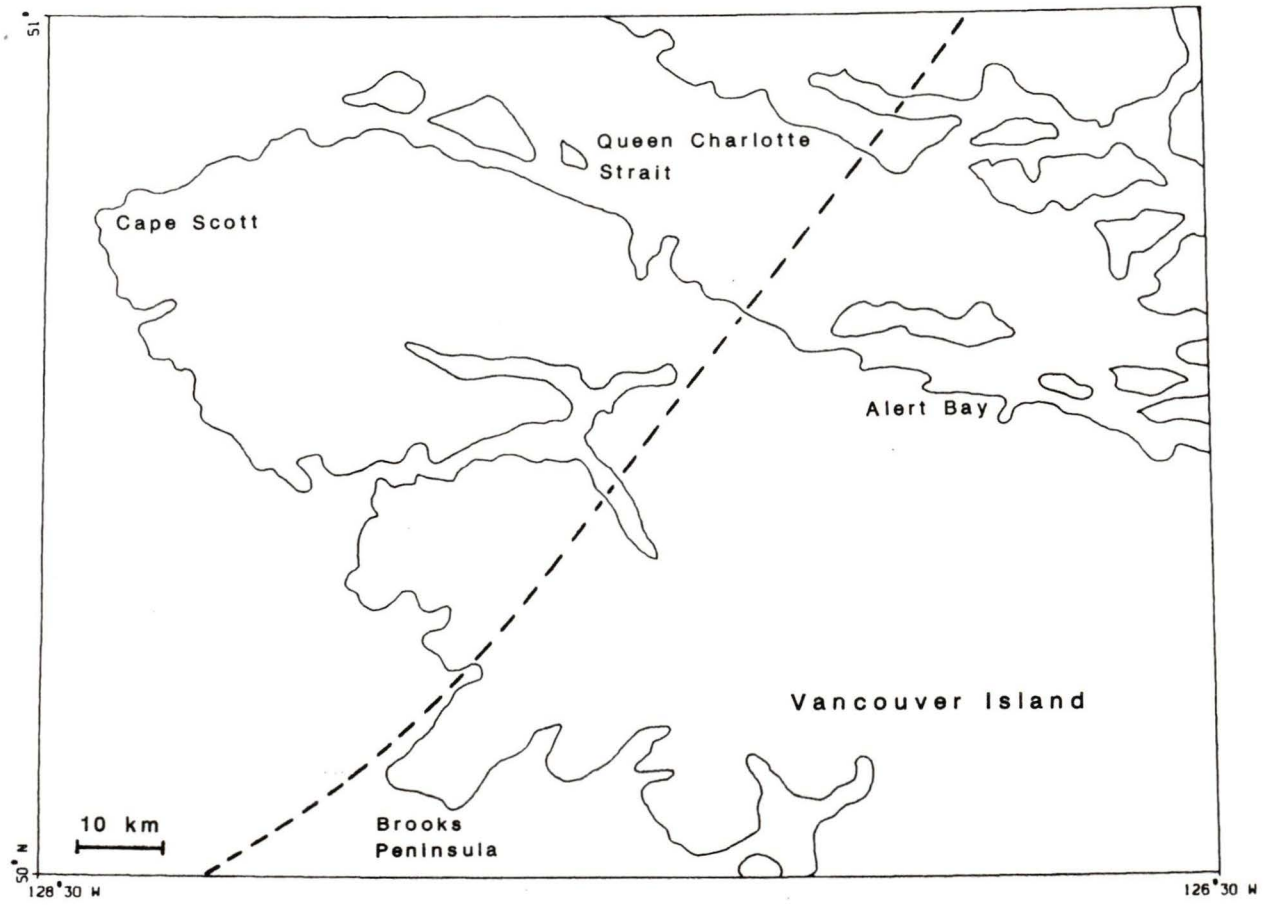

Figure 3 : The estimated trace of the northern edge of the subducted Juan de Fuca plate at 10 Ma (Riddihough, 1977).

1.2.2 Plate Boundaries

The Queen Charlotte fault extends north from the Tuzo Wilson seamounts to the Aleutian trench and forms the NAM-PAC boundary (Fig. 2), striking between 320° and 325°. The focal mechanisms of earthquakes located along the Queen Charlotte fault are consistent with right-lateral strike-slip motion but show a convergence component near the southern end (Rogers, 1983).

The Explorer and Pacific plates are separated by a series of spreading ridges and transform faults. Recent studies of the regional seismicity (Wahlström and Rogers, 1990; Wahlström *et al.*, 1990) show that the activity is concentrated along the ridge offsets, although the Sovanco fracture zone is not clearly defined by seismicity. The Juan de Fuca and Pacific plates are bounded by the Juan de Fuca Ridge, which is a series of offset spreading ridges. The Nootka fault zone marks the contact between the JDF and EXP plates (Hyndman *et al.*, 1979). It is primarily defined by the seismicity pattern (Keen and Hyndman, 1979) and by the consistency of the focal mechanisms in the region. Wahlström and Rogers (1990) have shown this to be more complicated than a simple transform fault.

The boundary between the North American plate and the Juan de Fuca and Explorer plates is marked by a deformation front which lies to the west of Vancouver Island. The subduction zone lacks the deep trench commonly associated with other convergent margins (Keen and Hyndman, 1979). The Benioff zone seismicity is shallow and does not extend below 80 km (Rogers, 1983). The continuing convergence of NAM with the EXP and JDF plates is indicated primarily by sediment deformation (Davis and Riddihough, 1982; Davis and Hyndman, 1989). Riddihough (1984) suggests that the Explorer plate is simply being overridden by North America.

The Winona block was a portion of the Pacific plate but Davis and Riddihough suggest that the block became detached from the PAC plate and

started to underthrust NAM when the EXP-NAM-PAC triple junction jumped northwards from the Brooks Peninsula.

The triple junction is not a single point but a complex region of deformation defined in part by seismicity and bathymetry (Riddihough, 1977). The active spreading centre between the Explorer plate and the Pacific plate at the triple junction lies near the Tuzo Wilson seamounts (Carbotte *et al.*, 1989). The triple junction is likely a complex group of three triple junctions between four plates, including the Winona Basin block (Carbotte *et al.*, 1989). The close proximity of these spreading centres to the subduction zone results in the oceanic crust in this vicinity being relatively thin and hot.

1.2.3 Contemporary Motions

The contemporary motions of the plates are based on magnetic anomaly data which can only be resolved to 0.5 Ma. The motion between the North American plate and the Pacific plate is dextral and proceeding at approximately 5.5 cm/yr (Riddihough, 1977). Relative to one another, the Juan de Fuca and Explorer plates are moving left-laterally along the Nootka fault zone at 2 cm/yr. The Explorer and Juan de Fuca plates are diverging from the Pacific plate with full spreading rates of 4 cm/yr and 6 cm/yr respectively (Riddihough *et al.*, 1983). The Juan de Fuca plate is converging with North America at 3.2 cm/yr while the Explorer plate is converging with North America in a northeasterly direction at 1.4 cm/yr (Riddihough, 1984). The Winona block is presently converging slowly with North America at roughly 1 cm/yr (Davis and Riddihough, 1982).

The rotation poles of the Explorer plate, with respect to NAM, PAC and the hot spot frame, have been migrating northwards (Fig. 4) at a decreasing rate over the last 3.5 Ma (Riddihough, 1984). Assuming a constant deceleration, the extrapolated pole positions are SW, SE and E of the Explorer plate relative to PAC, NAM and the hot spot frame,

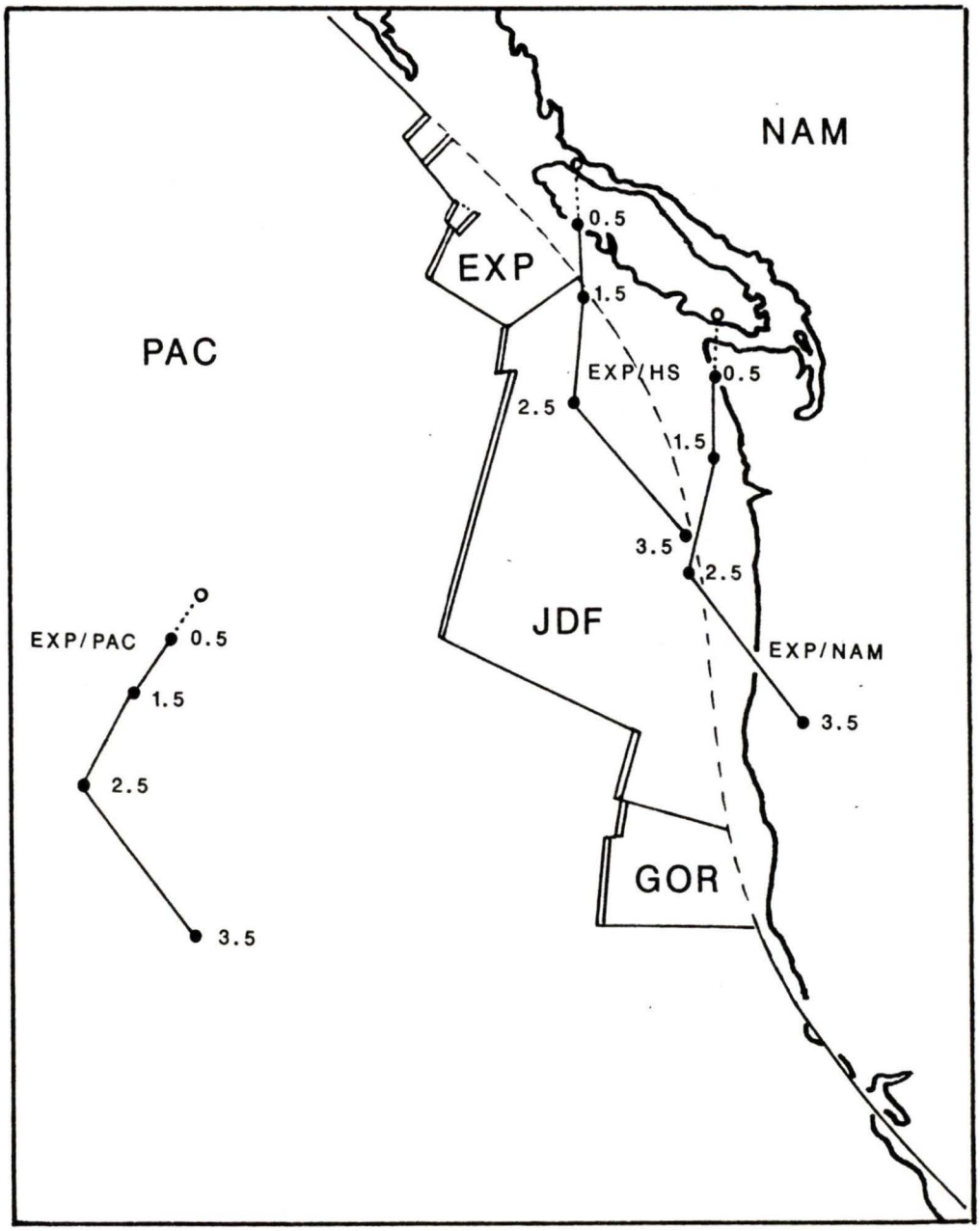

Figure 4 : Migration of the rotation poles for the Explorer with respect to the Pacific plate (EXP/PAC), the North American plate (EXP/NAM) and the hot spot reference frame (EXP/HS) (Riddihough, 1984). The ages of the rotation poles (●) are given in Ma BP. The present positions of the poles (o) have been extrapolated from the past locations. Transform boundaries are shown as solid lines, spreading ridges as double lines and the dashed lined is the convergent margin.

respectively. The poles of the Juan de Fuca plate show the same pattern but at much greater distances from the plate (Riddihough, 1984).

Riddihough (1984) suggests that the Explorer plate has stopped moving with respect to the hot spot reference frame. This would imply that the pole of rotation is within or very near to the plate, which is consistent with projected position of the EXP/HS pole. With continuing convergence between EXP and NAM, the tectonic stresses on northern Vancouver Island should be oriented N-S or NE-SW.

1.3 The Brooks Peninsula

The Brooks Peninsula is located on the west coast of the northern end of Vancouver Island (Fig. 2) and covers an area of roughly 170 square kilometres. The peninsula is inaccessible by land and uninhabited. Dense vegetation and difficult terrain have made detailed geological surveys impossible. The four major geological elements identified on the peninsula (Smyth, 1985) are the West Coast Fault, the West Coast Complex, the Cape Cook Fault and the Pacific Rim Complex (Fig. 5). Despite its proximity to a major subduction zone, the seismicity of the peninsula is quite low.

The northern end of Vancouver Island is characterized by extensive block faulting. The main faults in the area strike northwest, dipping steeply to the northeast. They are cross-cut by steeply dipping, northeast striking faults. The faults are normal or strike-slip with right-lateral displacement. The Brooks Peninsula is itself a distinct fault block bounded on three sides, and possibly on the fourth, by faults. Muller *et al.* (1974) were unable to locate a fault off the NW coast of the peninsula.

The West Coast Fault strikes northwest, separating the peninsula from the rest of Vancouver Island. The Cape Cook Fault runs from the SE corner of the peninsula to the northwest corner. The latter fault separates the two major geological complexes on the peninsula: the West

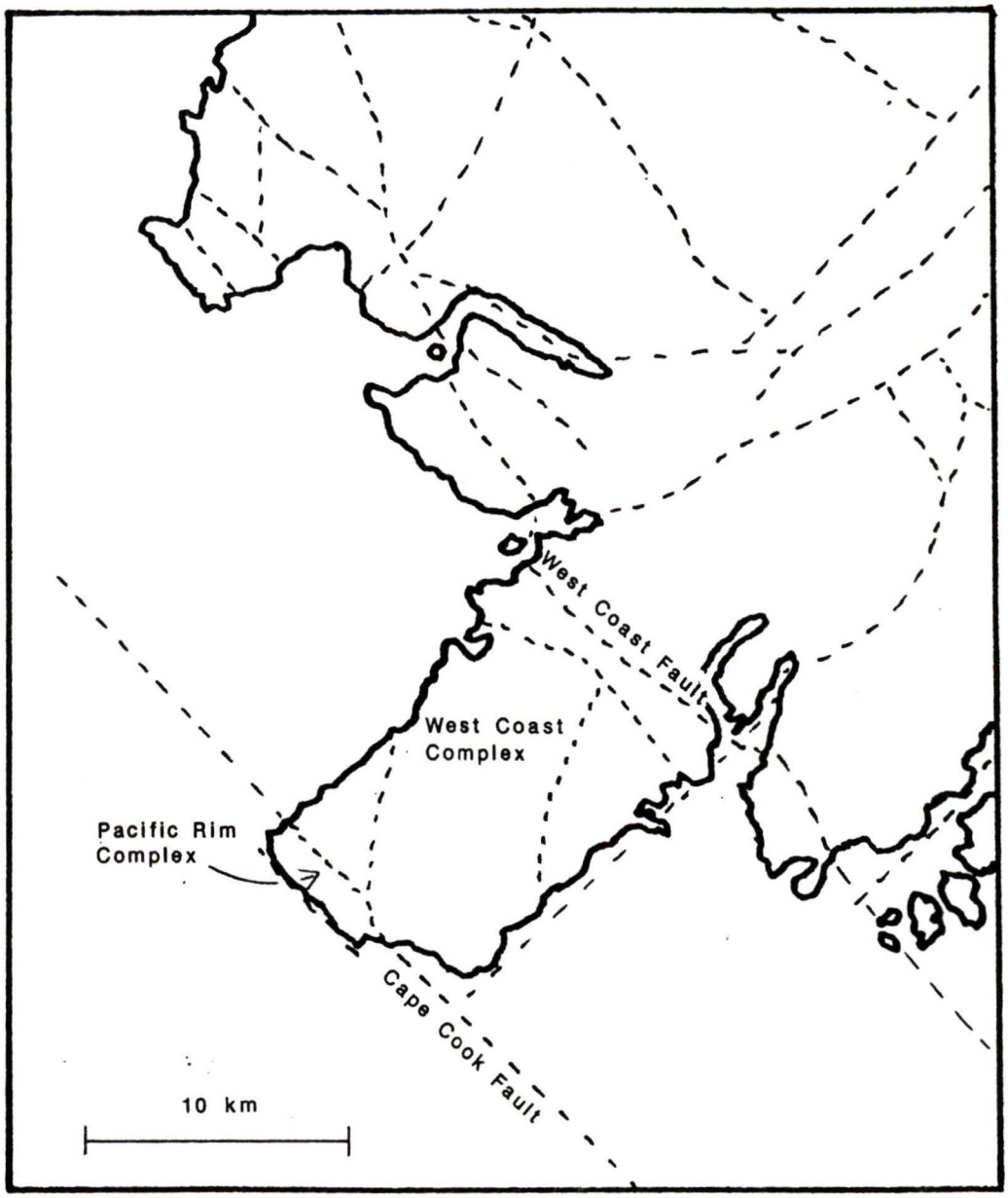

Figure 5 : Geology of the Brooks Peninsula, showing the four main geological features of the peninsula (Muller *et al.*, 1974; Smyth, 1985). Note that the West Coast Complex comprises the entire peninsula except for the Pacific Rim Complex which occupies the SW edge. Faults are shown as dashed lines.

Coast Complex and the Pacific Rim Complex.

The bulk of the peninsula is underlain by a metamorphic complex (the West Coast Complex) composed mainly of amphibolite, gneissic quartz diorite, agmatite and gabbro (Muller *et al.*, 1974). The age of the metamorphic complex has not been determined accurately but was estimated by Muller *et al.* (1974) as Jurassic or older. The Pacific Rim Complex, which occupies the southwestern edge of the peninsula, is a highly disturbed and faulted melange of exotic blocks in a matrix of black and green shale (Smyth, 1985).

The effects of the JDF-NAM-PAC triple junction occupying a stable position off the Brooks Peninsula from 10 to 4 Ma BP can be estimated from a contemporary analogue.

The Taitao Peninsula, in southern Chile, is the only known location where a mid-ocean ridge is being subducted under a continent at a triple junction (Fig. 6). The Chile Rise is being subducted at a more acute angle to the margin than the Explorer Ridge. This has resulted in the rapid northward migration of the triple point (Cande and Leslie, 1986), unlike the Brooks Peninsula. Despite the rapid motion of the triple junction, the ridge subduction greatly affected the Taitao region, forming a pull-apart basin and uplifting a block of pre-Jurassic metamorphic basement at a point near the triple junction (Forsythe and Nelson, 1985).

It follows, from the similarity of the two regimes, that the Brooks Peninsula is a fault block that has been raised by the presence of the triple junction.

1.4 Regional Seismicity

In the Brooks Peninsula region, the seismic activity is concentrated along the Nootka fault zone and the boundaries between the Explorer and Pacific plates (Fig. 7). There is very little activity along the EXP-NAM boundary north of the Nootka fault zone, except in the immediate vicinity

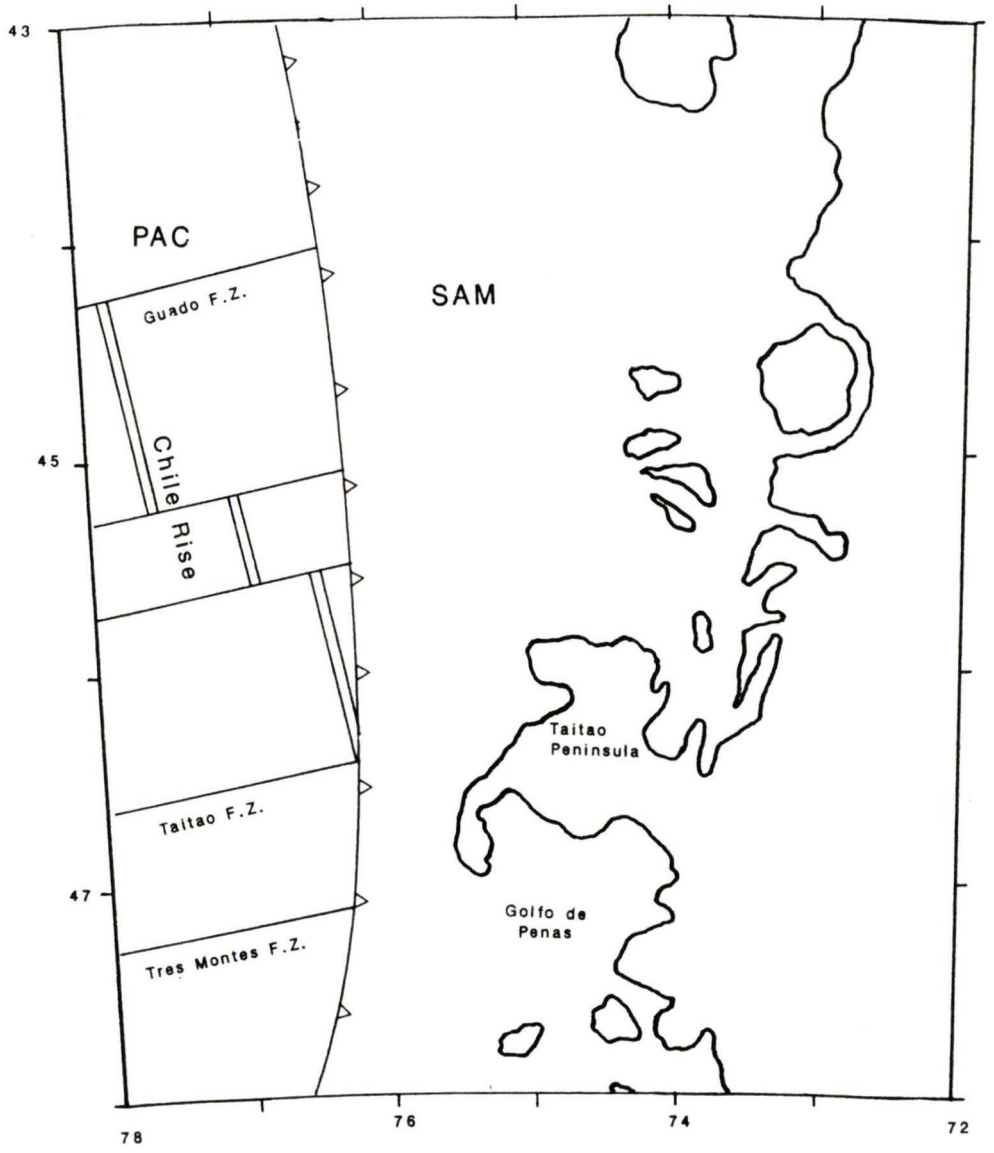

Figure 6 : Tectonic setting of the Taitao Peninsula (Cande and Leslie, 1986) in southern Chile; analogous to that of the Brooks Peninsula from 10 to 4 Ma BP. The peninsula is a fault block uplifted by the subduction of the Chile Rise. The shallow angle at which the ridge is being subducted has resulted in rapid northward migration of the triple junction.

of the Brooks Peninsula. The lack of earthquakes occurring deeper than 70 km has been ascribed to the rapid reheating of the relatively young and hot subducting slab (Riddihough and Hyndman, 1976).

The Geological Survey of Canada has located roughly 55 events in the immediate vicinity of the peninsula, between the years 1978 and 1987. The events are scattered throughout the region with no visible pattern. The two events from the summer of 1978 are the largest events to have been recorded on the peninsula itself.

Fault plane solutions for events in the Juan de Fuca plate system show either NW-SE right-lateral strike-slip or NE-SW left-lateral strike-slip motions consistent with north-south compression (Riddihough *et al.*, 1983). No events associated with underthrusting have been detected along the continental margin (Rogers, 1988), unusual for a subduction zone.

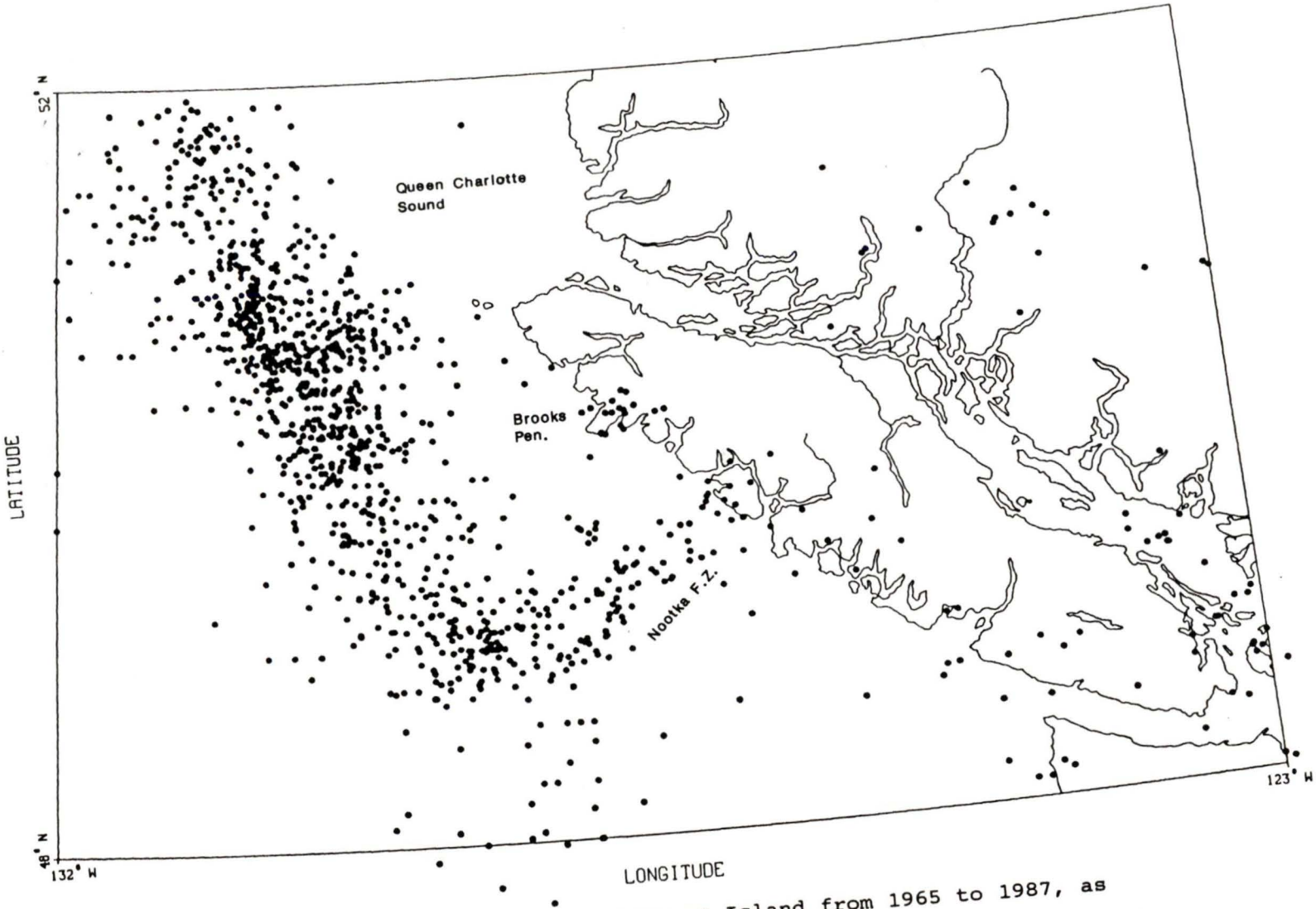

Figure 7 : Seismicity around Vancouver Island from 1965 to 1987, as determined by the G.S.C.

Chapter 2 : Aftershock Study

2.1 Introduction

Extensive aftershock sequences followed both of the Brooks Peninsula earthquakes. Events from both sequences, 15 for June and 1 for July, were located regionally using data from the G.S.C.'s permanent network. A temporary, local array was established on the peninsula by G.C. Rogers of the G.S.C. The temporary network operated from June 9th to June 12th, 1978.

The local array data were used to determine the epicentre coordinates and focal depth of the June mainshock, as well as an indication of the size of the rupture surface and the fault plane orientation. The locally detected aftershocks provided a reference position against which the regional aftershocks could be compared. Their relative locations indicated the regional location bias and provided a means of generating travel time corrections. Other earthquakes which occurred in the vicinity of the Brooks Peninsula were relocated using these corrections.

2.1.1 Chronology

The aftershock activity following each event (Fig. 8) was measured at Port Hardy (PHC), the closest permanent seismograph station at 70 km distance. The number of aftershocks, $M_L \geq 0.9$, were counted each day for 15 days after each mainshock. This minimum magnitude was chosen since it represented the smallest, clearly identifiable aftershock of the June 2nd event.

The similarity of the aftershock patterns over time is an indication of the similarity in the stress release patterns of both earthquakes. This suggests that both events may have had similar focal mechanisms and occurred on the same or adjacent faults. The lower level of activity

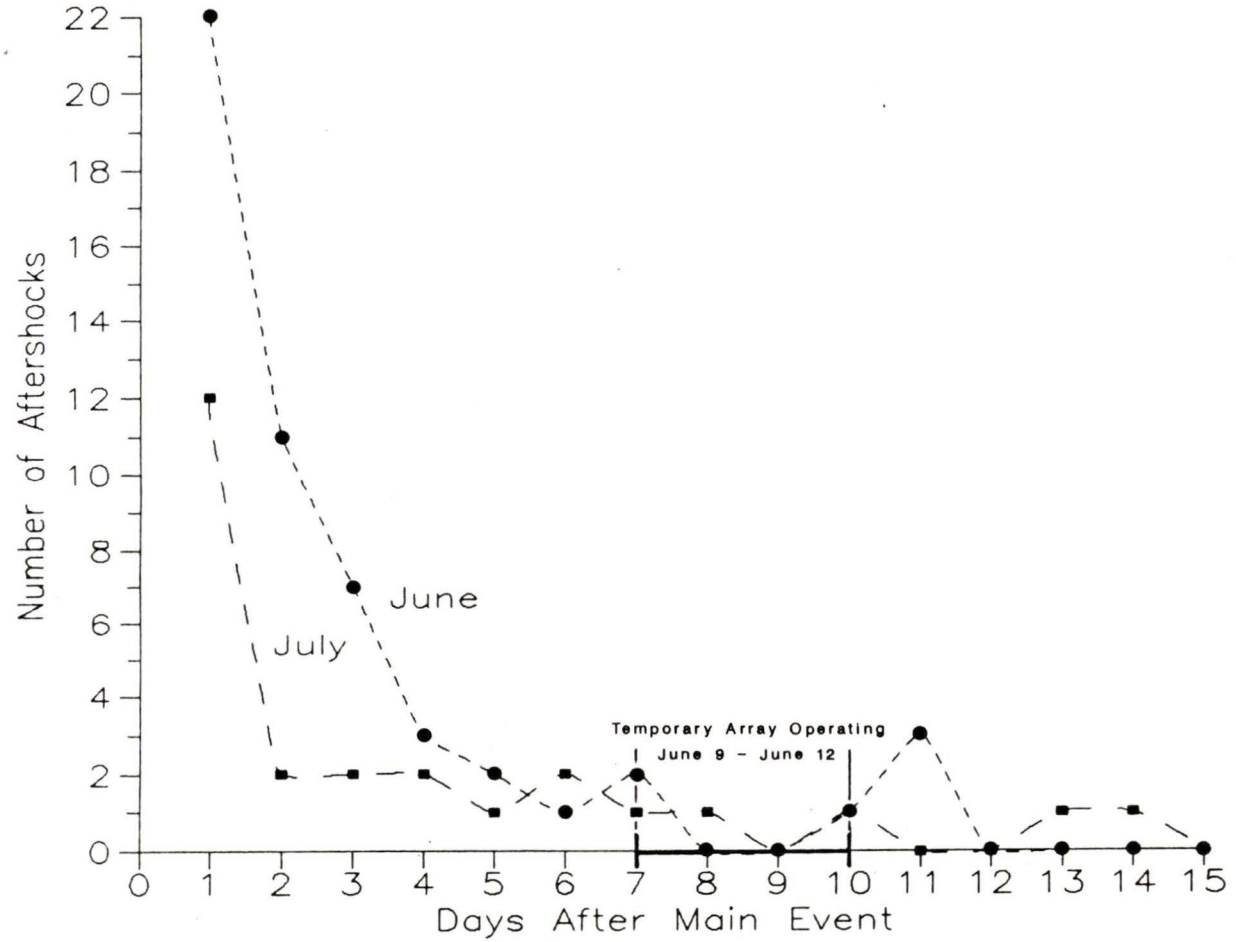

Figure 8 : Chronological distribution of aftershocks ($M_L \geq 0.9$) detected at Port Hardy for June (●) and July (■). Counts are for a 15 day period after each main shock.

following the July event is consistent with the occurrence of two earthquakes, on the same or parallel faults, where the bulk of the tectonic stress is released by the first event.

2.2 Local Study - Source Parameters

The instruments of the temporary array were deployed at Klaskino Inlet (KLA), Johnson Lagoon (JON), Cape Cook (COO) and Clerke Point (CLE), effectively surrounding the aftershock area (Fig. 9). The array functioned for only 4 days, starting a week after the main event and missing the period of the greatest activity.

While it was operating, the array detected 42 locatable events. At the same time, 4 of the locally detected events were also observed at PHC, only 1 of which was large enough (M_L 3.7) to be located using the regional data. The one common event occurred on June 12th, at 10:52 U.T. and was used as the reference event to determine travel time corrections (§ 2.3.3).

The array geometry provided good horizontal and vertical control for the local hypocentre solutions. The arrival time data were originally read by G. Rogers and reread in a few cases by the author.

2.2.1 Method

The program HYPOELLIPSE (Lahr, 1985) was used to determine the aftershock hypocentres. HYPOELLIPSE is a local hypocentre determination program which locates events by minimizing the RMS of the travel time residuals. Standard errors are computed for the geographical position, depth and origin time. The positional errors are given as vectors which are the axes of the 68% confidence error ellipsoid (Lahr, 1985). These axes describe the directions of poorest control on the solutions.

The short epicentral distances ensured that the first arrivals were all direct phases, suitable for a local hypocentre determination. The

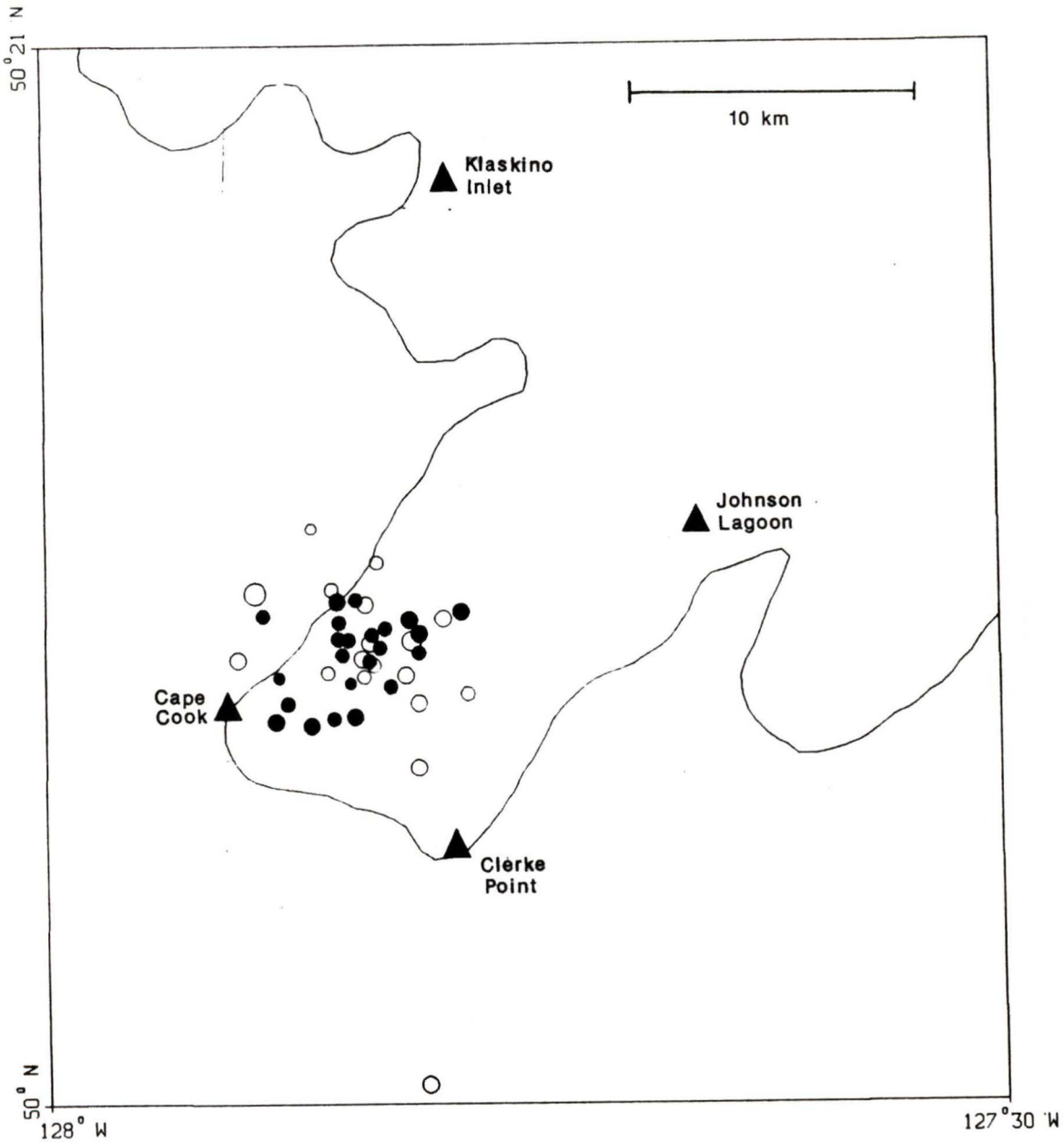

Figure 9 : Distribution of Aftershocks detected by the temporary array and placement of the instruments (▲) used in the array, June 9th to June 12th, 1978. The solid symbols indicate those events located using 2 or more *S* phases.

Layer	Velocity (km/s)	Depth (km)	Thickness (km)	V_p/V_s
1	5.50	0	1	1.73
2	6.10	1	1	1.73
3	6.40	2	2	1.73
4	6.50	4	4	1.73
5	6.60	8	4	1.73
6	6.70	12	4	1.73
7	7.00	16	4	1.73
8	7.80	20	7	1.73

Table 1 Local crustal model used for the Brooks Peninsula

earth model used to approximate the local velocity structure was a flat layered crustal model (Table 1), derived from the refraction model developed by McMechan and Spence (1983) from a transect along the length of Vancouver Island.

2.2.2 Analysis

The aftershocks were first located using all the available data. The hypocentres (Fig. 9) were scattered over a 10 km diameter area in the SW corner of the peninsula. The horizontal errors in these solutions ranged between 1 and 8 km and the errors in depth varied between 1 and 20 km. Many of the solutions had poor vertical control, having been located using only 1 or no *S* phases. Since the poor solutions generally had an error in depth of more than 5.0 km, all solutions with a vertical error of 5.0 km or more were removed. The remaining 23 aftershocks covered a 7 km diameter area with an average error in depth of 2.0 km and an average horizontal error of 1.4 km. Within the pattern, on the west side, there was a region in which no aftershocks occurred. If this void is real, then it may

represent the surface projection of the rupture surface (Mendoza and Hartzell, 1988).

The more precisely located events were used to obtain a nominal mainshock hypocentre, to estimate the area of the rupture surface and to prepare the cross-sections used to determine the fault plane orientation.

The hypocentre coordinates (Table 2) were obtained by separately averaging the latitudes and longitudes of these aftershocks. The focal depth was determined in a similar fashion, by averaging the focal depths of the same set of aftershocks. The errors were taken from the radius of the aftershock area and from the standard deviation in the aftershock depths.

Latitude	Longitude	Depth
50° 09.00′ ± 3.5 km	-127° 49.80′ ± 3.5 km	17 ± 2 km

Table 2 Nominal epicentre for the June 2nd event.

Upper and lower bounds for the estimated size of the rupture surface were obtained from the aftershock data, for the June event. The total area covered by the aftershocks (Kanamori and Anderson, 1975) gave a rupture radius 3.5 km. The void in the aftershock pattern indicated a rupture surface 1.5 km in radius.

Cross-sections were generated at azimuths perpendicular to the strikes of the nodal planes determined from the first-motion and surface wave data (Chs. 4, 5). The sections followed NW-SE or NE-SW strikes. None of these sections (Fig. 10) showed a definite alignment of hypocentres which would indicate the fault plane orientation; however, the least scatter was seen on the NW-SE section, indicating a dip to the NW.

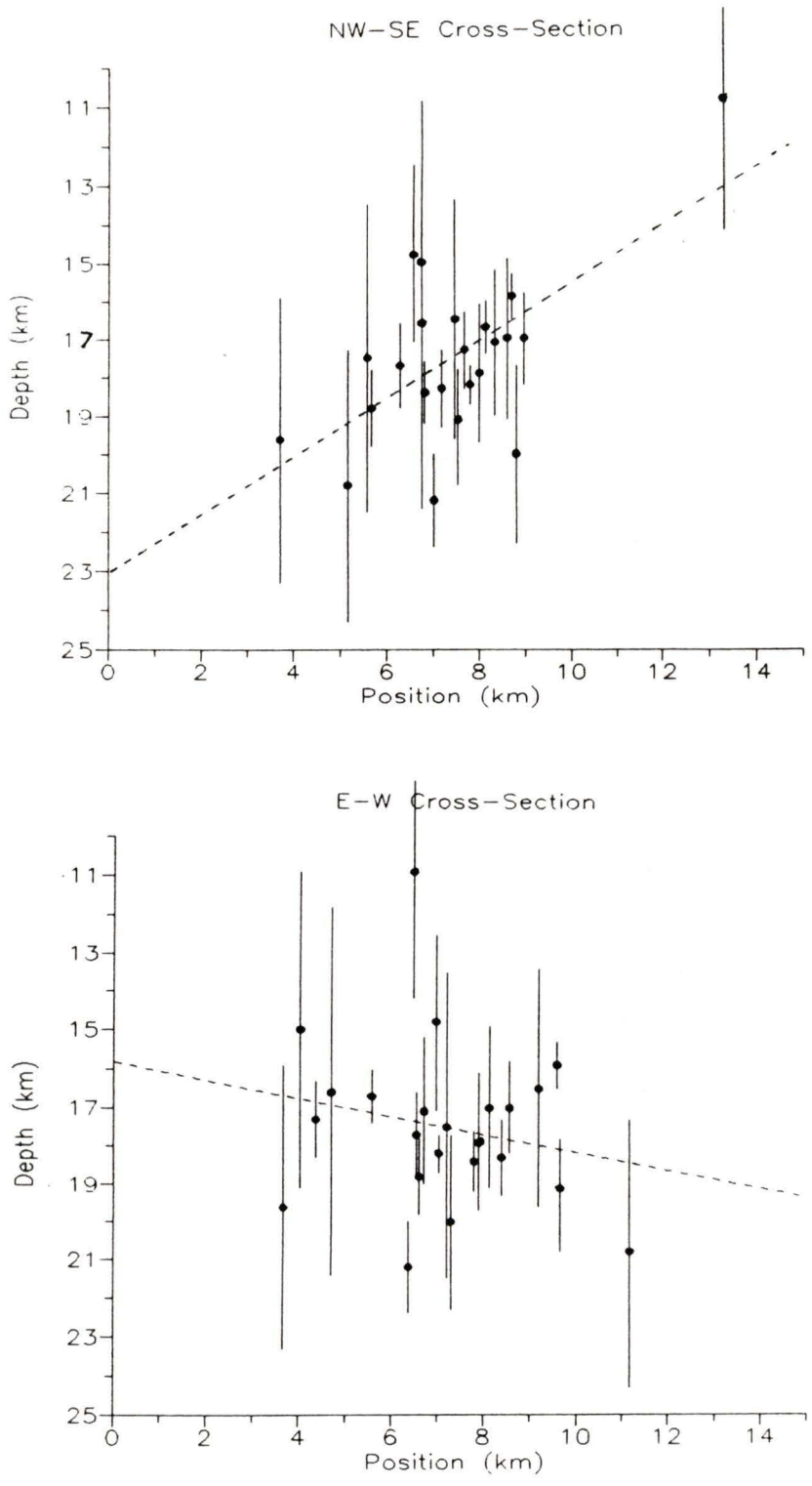

Figure 10 : Aftershock cross sections, NW-SE and E-W, employing only those solutions with an error in depth of 5 km or less. Best fit lines through the data are shown, dipping at 40° NW and 6° W.

2.3 Regional Study

The aftershocks detected by the permanent, regional stations were mislocated. This was obvious from the relative positions of the G.S.C. epicentres and the region defined by the temporary array data (Fig. 11). The subset of the data which produced the best locations, those closest to the region identified in the local study, was determined.

The regional data were extracted from the Canadian Earthquake Epicentre File (CEEF). Arrival time data and solutions were obtained for 15 aftershocks of the June earthquake and 1 aftershock of the July event (Appendix A). The G.S.C. epicentre solutions were computed using all available data, without regard for the suitability of the stations used. The locations were determined using a fixed focal depth of 18.0 km and the single-layer Canadian Shield velocity model (Table 3).

Georgia Straits Model			
Layer	Velocity (km/s)	Depth (km)	Thickness (km)
1	5.00	0	1
2	6.00	1	5
3	6.70	6	24
4	7.10	30	15
5	7.75	40	½ Space
Canadian Shield Model			
Layer	Velocity (km/s)	Depth (km)	Thickness (km)
1	6.20	0	36
2	8.20	36	½ Space

Table 3 Georgia Straits and Canadian Shield earth models

The G.S.C. solutions were widely scattered (Fig. 11), with 45 km separating the most distant epicentres. There was no chronological pattern to the distribution of events. However, each of the events had been

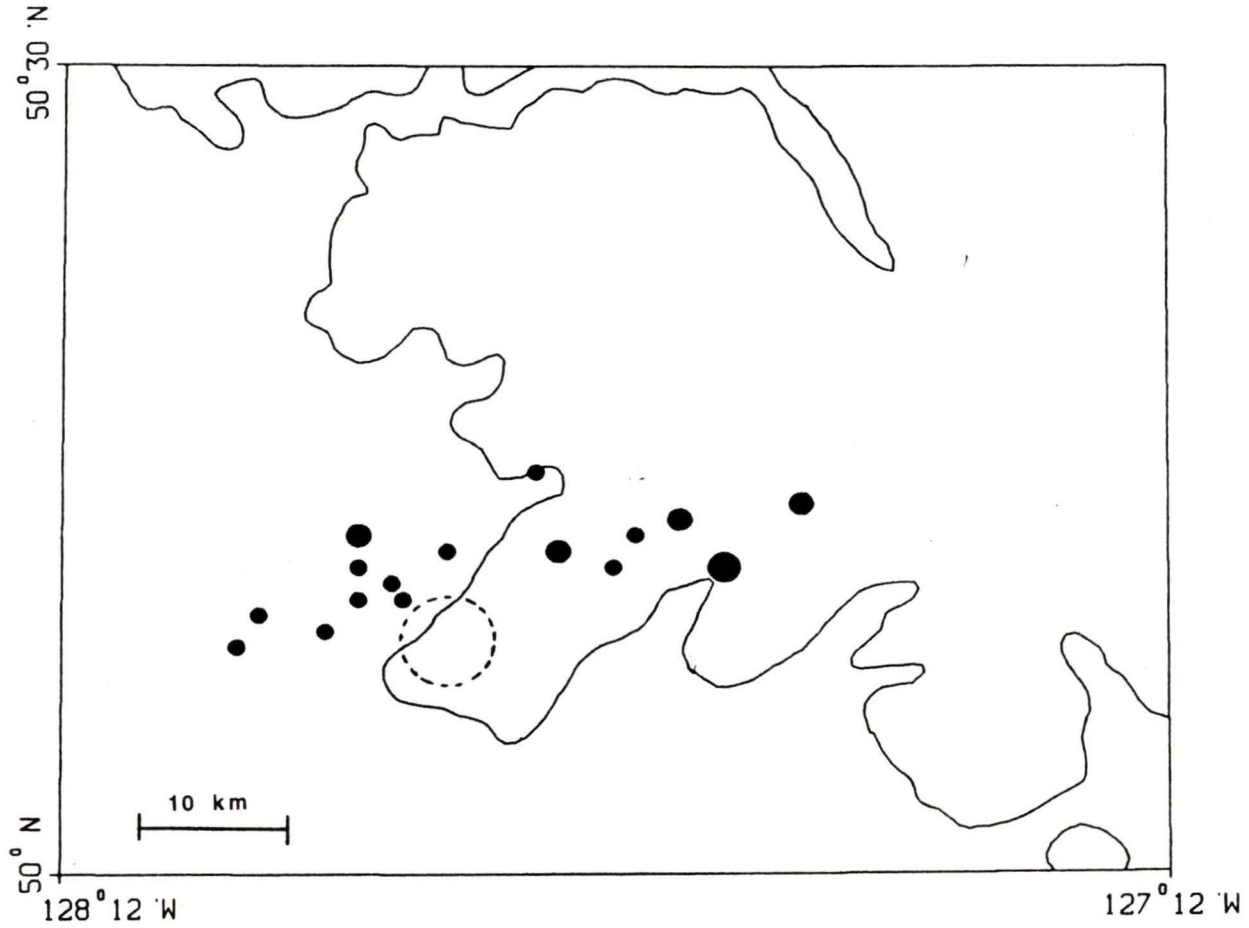

Figure 11 : Brooks Peninsula aftershocks detected by the G.S.C.'s permanent stations; original G.S.C. epicentres. The area covered by the locally detected aftershocks is delimited by a dashed circle. The two groups of epicentres are distinguished primarily by their geographical locations (§ 2.3).

located with slightly different sets of station data. The smaller events were generally located to the west of the peninsula and the larger aftershocks to the east.

2.3.1 Method

The epicentre locations were determined using the programs CANSESS (Stevens *et al.*, 1976) and HYPOELLIPSE (§ 2.2.1). The former is used by the G.S.C. for the routine location of regional events. The advantage of CANSESS was that it allowed up to four phases (*Pn*, *Pg*, *Sn* and *Sg*) at each station in the location of hypocentres, while HYPOELLIPSE allowed easier manipulation of the data and earth models. Both programs produced the same solutions using identical data sets and earth models.

The earth models used were the Canadian Shield model, which had also been used for the original solutions, and the Georgia Straits model (Table 3). With both programs, the events were located using a fixed focal depth of 18 kilometres. This value was used for the initial G.S.C. locations and was retained since it was close to the nominal focal depth obtained from the local data.

2.3.2 Relocation of Regional Aftershocks

The aftershocks were relocated using only data from stations which detected all of the events, to ensure that all of the regionally detected aftershocks were subjected to the same systematic errors. The less common stations were removed gradually in order to observe the effects of the different stations on the solutions.

The influence of stations east of B.C. and in Washington state was not examined. The Washington stations, GMW and MCW, were not included since there were data from Canadian stations at similar azimuths. Other Canadian stations, outside B.C., were excluded since they were not

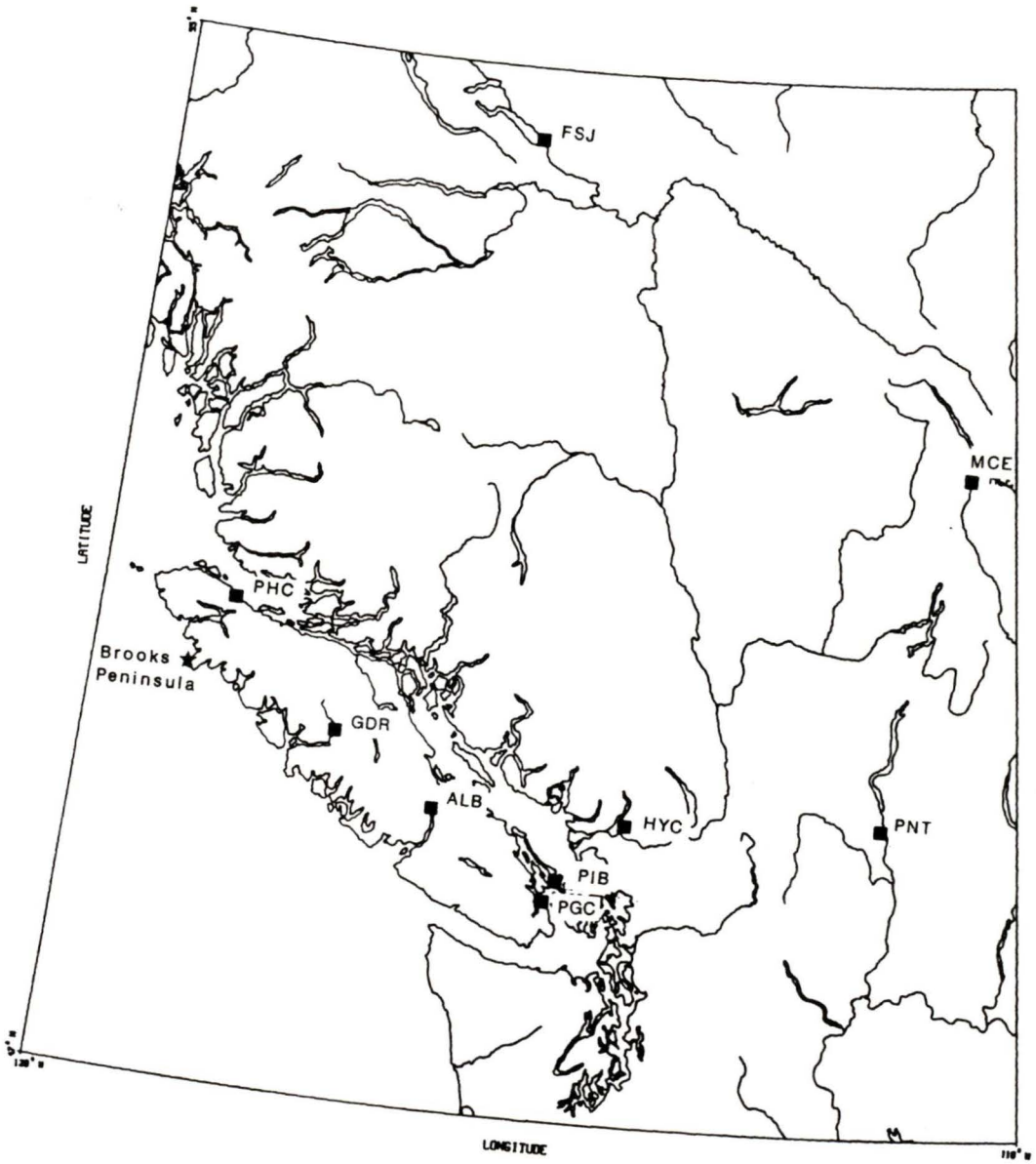

Figure 12 : Permanent seismograph stations operated by the G.S.C. in British Columbia in 1978.

appropriate for locating earthquakes on the west coast of Canada.

When the stations in the interior of B.C., FSJ, PNT and MCE, were removed, the solutions moved west by between 2 and 13 km. The elimination of HYC, PIB and PGC had a similar effect on the solutions. Thus, stations in the south and east of B.C. pull the epicentre solutions in the Brooks Peninsula to the east by 5 to 20 km.

The stations PHC, GDR and ALB were the only ones common to all events and the most common phase combinations at each station were *Pg* and *Sg*. Two aftershocks had no data from PHC, due to instrument failures, and were discarded.

The records were re-read at each of the three stations. The original picks at GDR were inconsistent, earlier arrivals had been picked for larger events and a later phase for the smaller ones. The later arrivals were not identifiable for the larger events but quite prominent in the smaller events. With the entire suite of records available, it was possible to pick the same phase on each of the GDR records. The original phase picks at PHC were consistent but had only been read to the nearest half-second. The times were re-read to the nearest tenth second. The arrivals at ALB were generally too weak to be assured of consistent phase picks, so that station was discarded. Because of this, the events were located using just PHC and GDR.

The epicentres, located using data from PHC and GDR and the Canadian Shield model, were within or up to 4 km east of the aftershock region, as defined by the local study (Fig. 13). The events were also located with the same data set and the Georgia Straits model. The epicentres (Fig. 14) retained their relative positions but were displaced 9 km west of their previous positions.

These results imply that the Canadian Shield model is a better approximation of the regional geology than the Georgia Straits model, if the solutions are judged solely on the basis of their proximity to the region defined by the locally detected aftershocks. It is possible that

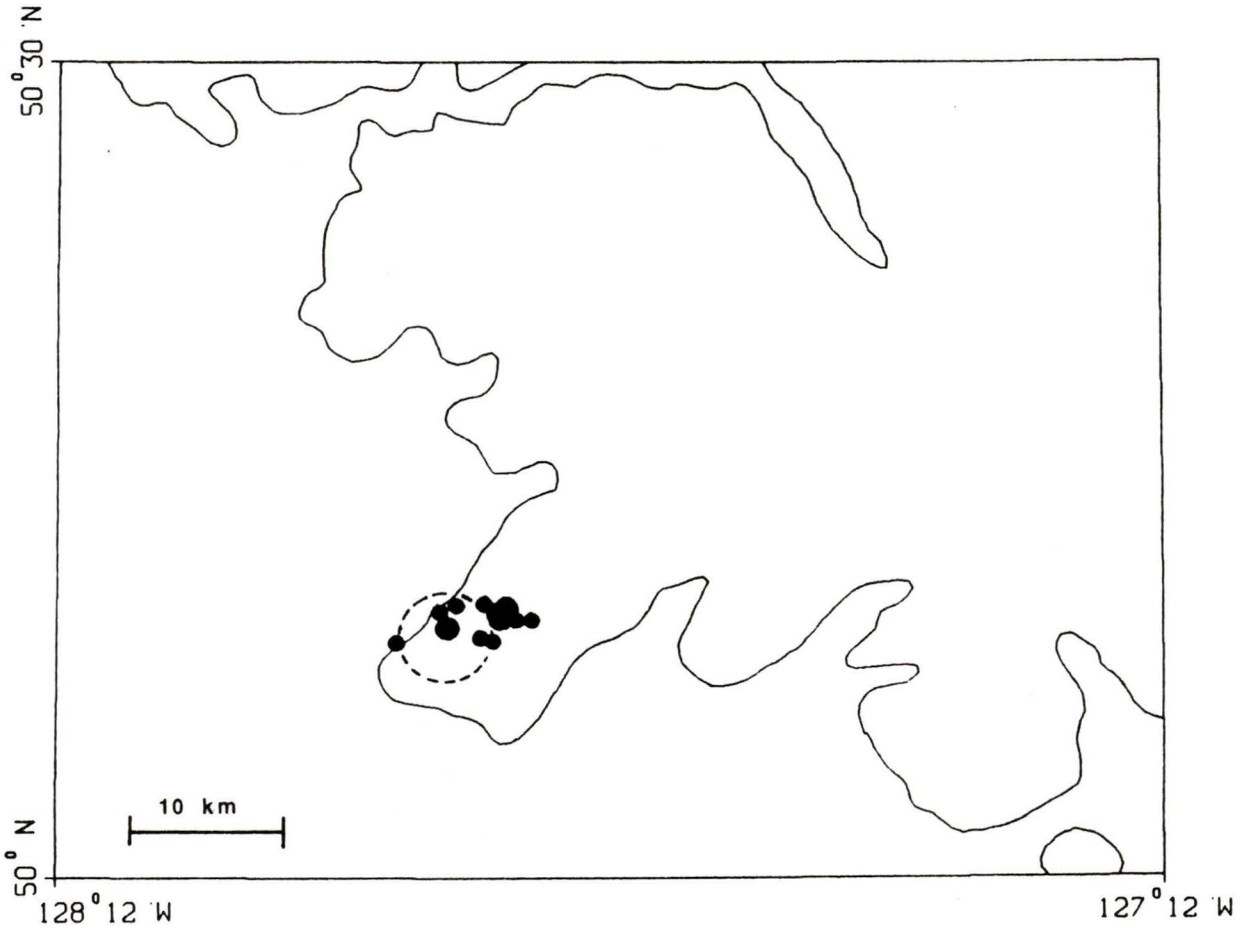

Figure 13 : Regionally detected aftershocks. Located using only re-read *Pg* and *Sg* arrivals at PHC and GDR, and the Canadian Shield model. The dashed circle denotes the aftershock area.

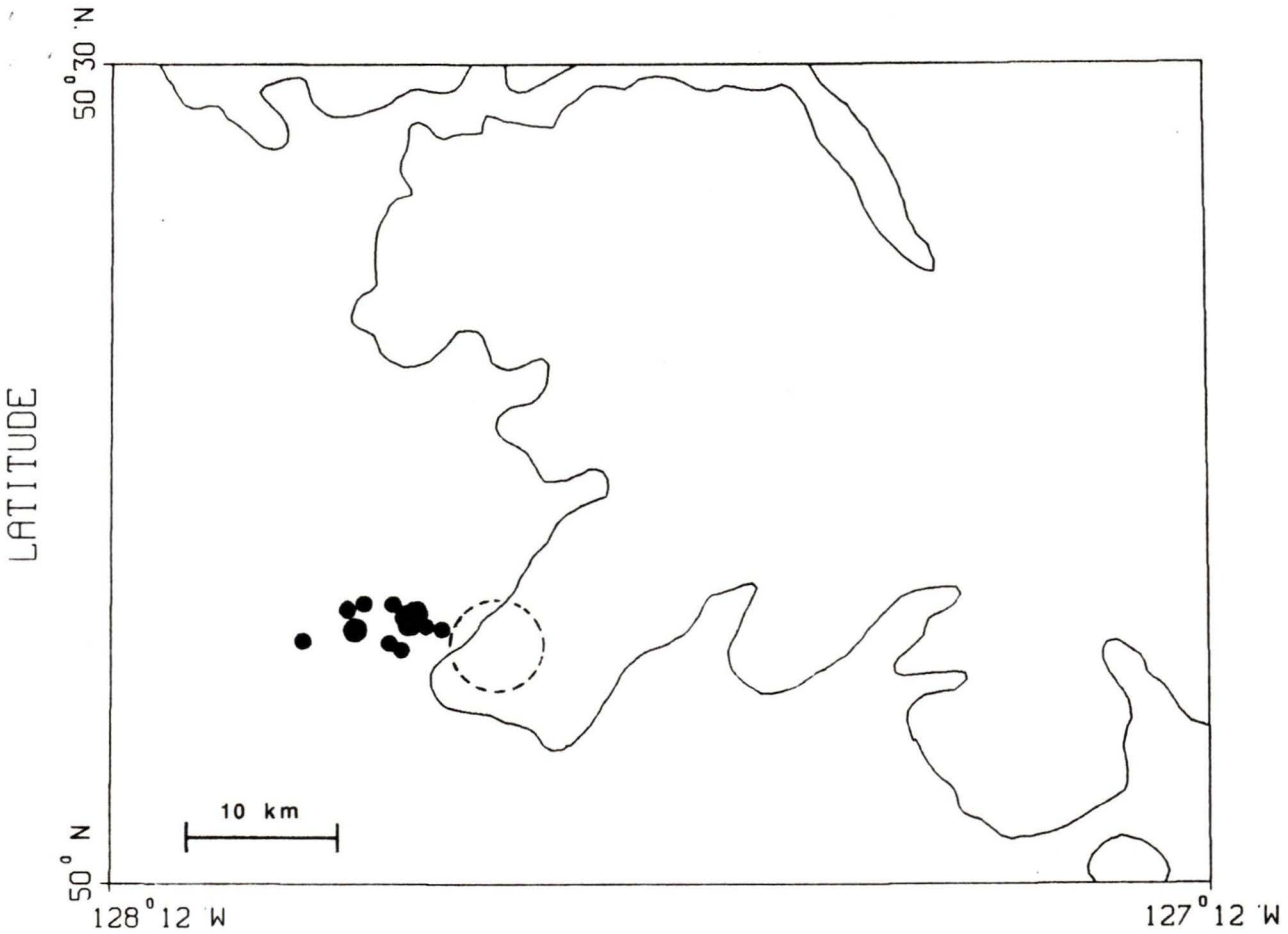

Figure 14 : Regionally detected aftershocks. Relocated with HYPOELLIPSE and the Georgia Straits model; using re-read *Pg* and *Sg* arrivals at PHC and GDR, without travel time corrections.

the regionally detected aftershocks are not coincident with the locally detected events. The Georgia Straits model was derived from refraction surveys on Vancouver Island and perpendicular to the continental margin on southern Vancouver Island (McMechan and Spence, 1983). The model was subsequently refined, using additional reflection data (Drew and Clowes, 1990), but remained similar to the original. On this basis, it is likely that the Georgia Straits model better approximates the velocity structure.

2.3.3 Determination of Corrections

In order to determine the travel time corrections, the one event detected by the regional and local networks (1978/06/12 10:52 U.T.) was used as a reference event. There were no *S* phase data for this event because of its size (M_L 3.7), which resulted in all but the first arrival being unreadable. As a result, the initial solution was poor, with horizontal and vertical errors of 8 and 20 km respectively.

Since the *S* arrivals could not be read, it was necessary to synthesize them from other events which were close to the reference event in both time and space. The nearby events were identified by re-locating all of the aftershocks using only *P* arrivals. This reduced the accuracy of the solutions but subjected all of the hypocentres to the same systematic errors. Three events occurred within both 11 km and 16 minutes of the reference event. The *S-P* intervals were obtained for each event at each station, resulting in several different combinations (Table 4).

Hypocentre solutions were computed for the reference event, using each of the dozen different combinations of *S* times. The combinations produced a closely spaced group of epicentres, spread over 10 km east-west and 2 km north-south (Fig. 15). The east-west dispersion was produced by the different *S-P* intervals at JON.

The final combination of *S-P* intervals was determined by the solution with the smallest standard deviations in the *P* and *S* residuals.

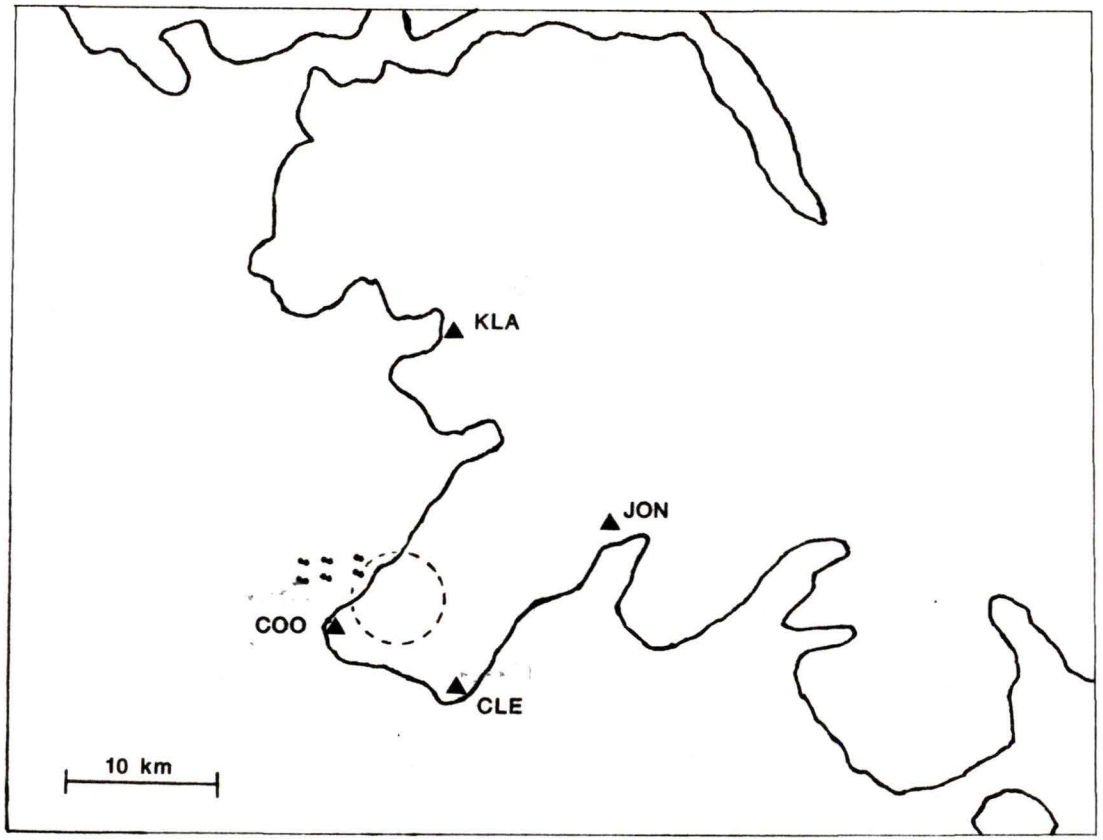

Figure 15 Various hypocentre solutions (●) for the reference event. Each location was determined using different *S-P* combinations at the temporary stations (Table 4). The dashed circle denotes the aftershock area.

Station	10:56	10:59	11:08
COO	1.5 s	1.8 s	—
CLE	—	—	1.5 s
JON	2.8 s	3.2 s	2.2 s
KLA	2.1 s	2.5 s	—

Table 4 S-P intervals at the temporary array stations. Times shown are for 3 events which occurred on 78/06/12. Final intervals for each station are underlined.

Most of the combinations would have been suitable given the close spacing of the solutions. The errors in the final solution (Table 5) were determined from the variation in the epicentre positions produced by the different *S-P* combinations.

Origin Time	Latitude	Longitude	Depth
10:52:21.9 ± 0.2 s	50° 10.18′ ± 1 km	-127° 52.72′ ± 2 km	9 ± 2 km

Table 5 Final Coordinates for the reference event.

The locally determined epicentre of the reference event was 3.5 km east of the position determined using the regional data with the Georgia Straits model (Fig. 16). The travel time corrections (Table 6) were generated by fixing the reference event at the location determined from the local array data and using the residuals at each station as the corrections. The corrections became as large as 20 s as the epicentral distance increased, an indication of the unsuitability of the more distant stations to locating events around the Brooks Peninsula.

The corrections were verified by locating the reference event using the regional data from PHC and GDR and applying the corrections. Having only 2 stations, there were two valid solutions for each event, each an equal distance to either side of the line joining the stations. A trial

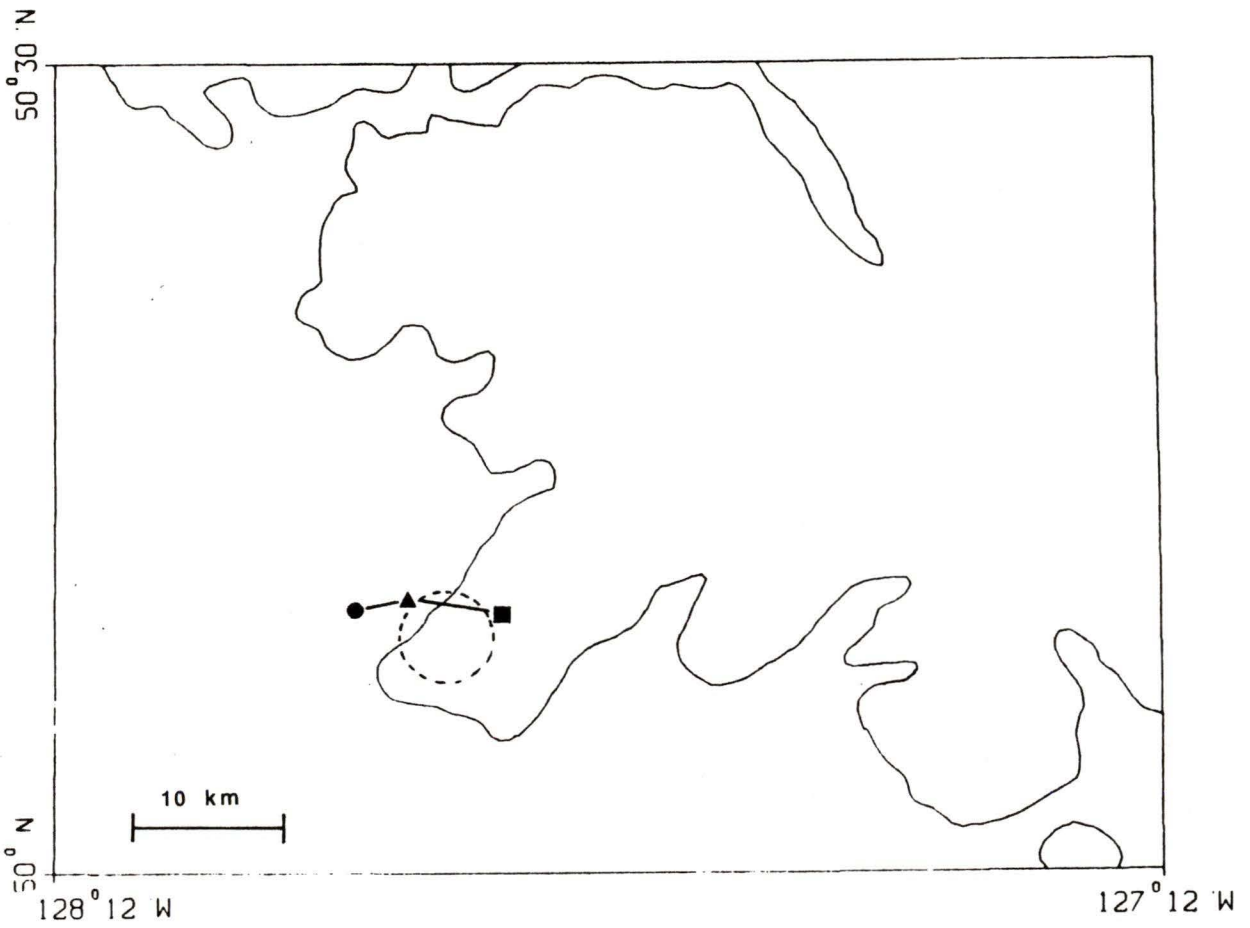

Figure 16 : Epicentre solutions for the reference event (78/06/12, 10:52) illustrating the effects of locating the events using different data sets and earth models. Solutions determined using HYPOELLIPSE with temporary array data (▲) and from regional data (●: Georgia Straits model; ■: Canadian Shield model). The dashed circle denotes the aftershock area.

Station	Georgia Straits		Canadian Shield	
	P	*S*	*P*	*S*
PHC	-0.49 s	0.28 s	-0.99 s	-1.33 s
GDR	-0.65 s	0.63 s	-1.91 s	-2.27 s
ALB	-0.12 s	3.96 s	0.12 s	5.10 s
PGC	4.70 s		6.64 s	
PIB	4.61 s		6.55 s	
HYC	-2.53 s	-2.01 s	-2.53 s	1.75 s
FSJ	-2.36 s	-16.73 s	0.82 s	-11.23 s
PNT	-2.81 s	-19.35 s	0.82 s	-13.06 s

Table 6 Travel time corrections for the regional stations. Corrections are for the Georgia Straits and Canadian Shield models for events in the Brooks Peninsula region.

location was specified on the Brooks Peninsula, forcing the solution to converge in the right area.

Relocating the regionally detected aftershocks, using the travel time corrections, pulled the epicentres 2 km east, closer to the peninsula (Fig. 17). The pattern of the aftershocks was preserved and the epicentres were spread across an area 10 km in diameter.

The process was repeated with the Canadian Shield model. The reference event was 6 km west of the position indicated by the local data (Fig. 16). The corrections were generated in the same fashion as for the Georgia Straits model. As before, the magnitude of the corrections increased with the distance of the station. The final, corrected epicentres were the same as they were for the Georgia Straits model.

The local and regional aftershock patterns were superimposed (Fig. 18); they were not coincident. The regionally detected aftershocks were located to the west of the locally detected events. It is unclear whether this offset is real or is the result of using 2 different earth models and station sets.

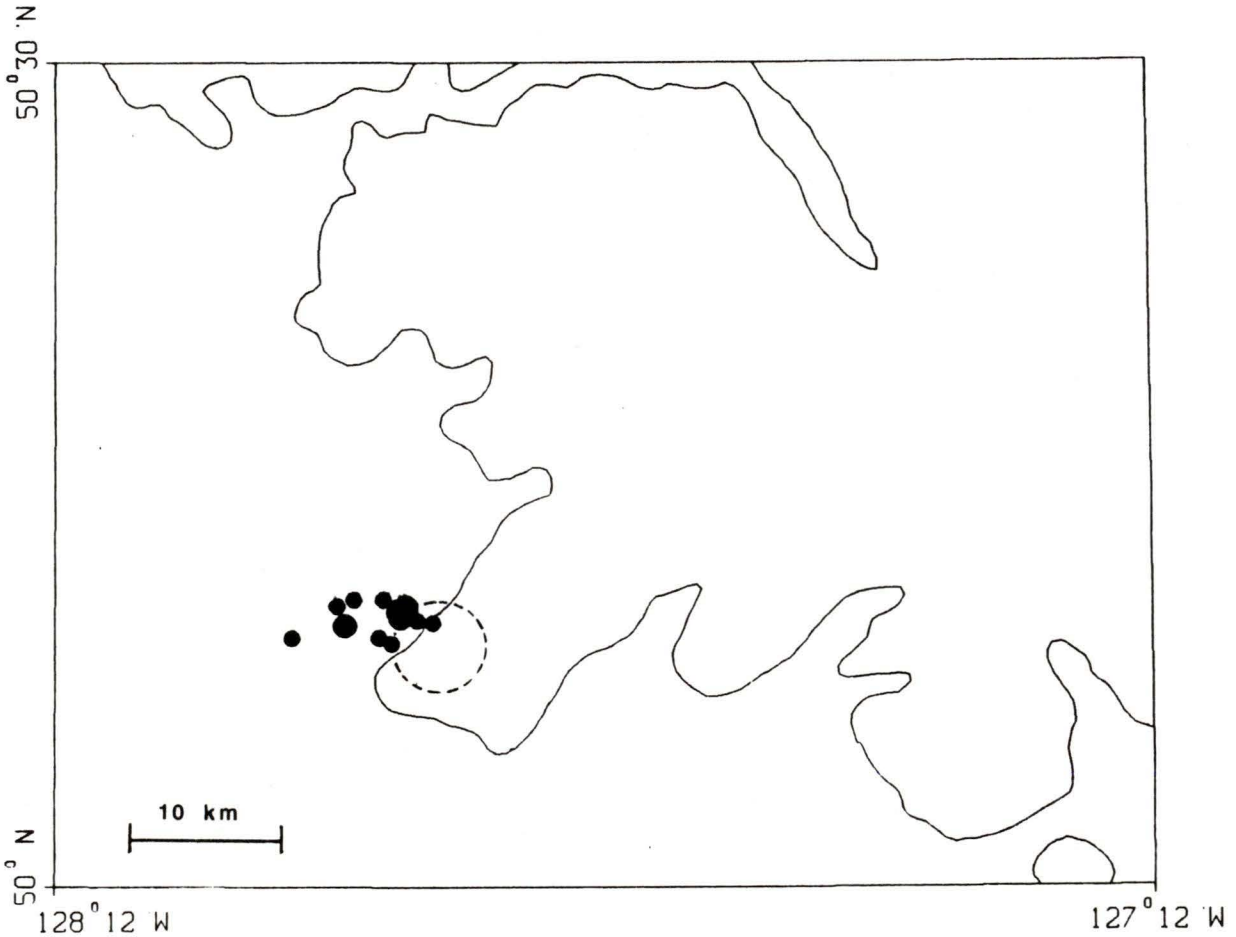

Figure 17 : Regionally detected aftershocks. Located with HYPOELLIPSE and the Georgia Straits model, using re-read *Pg* and *Sg* arrivals at PHC and GDR, with travel time corrections.

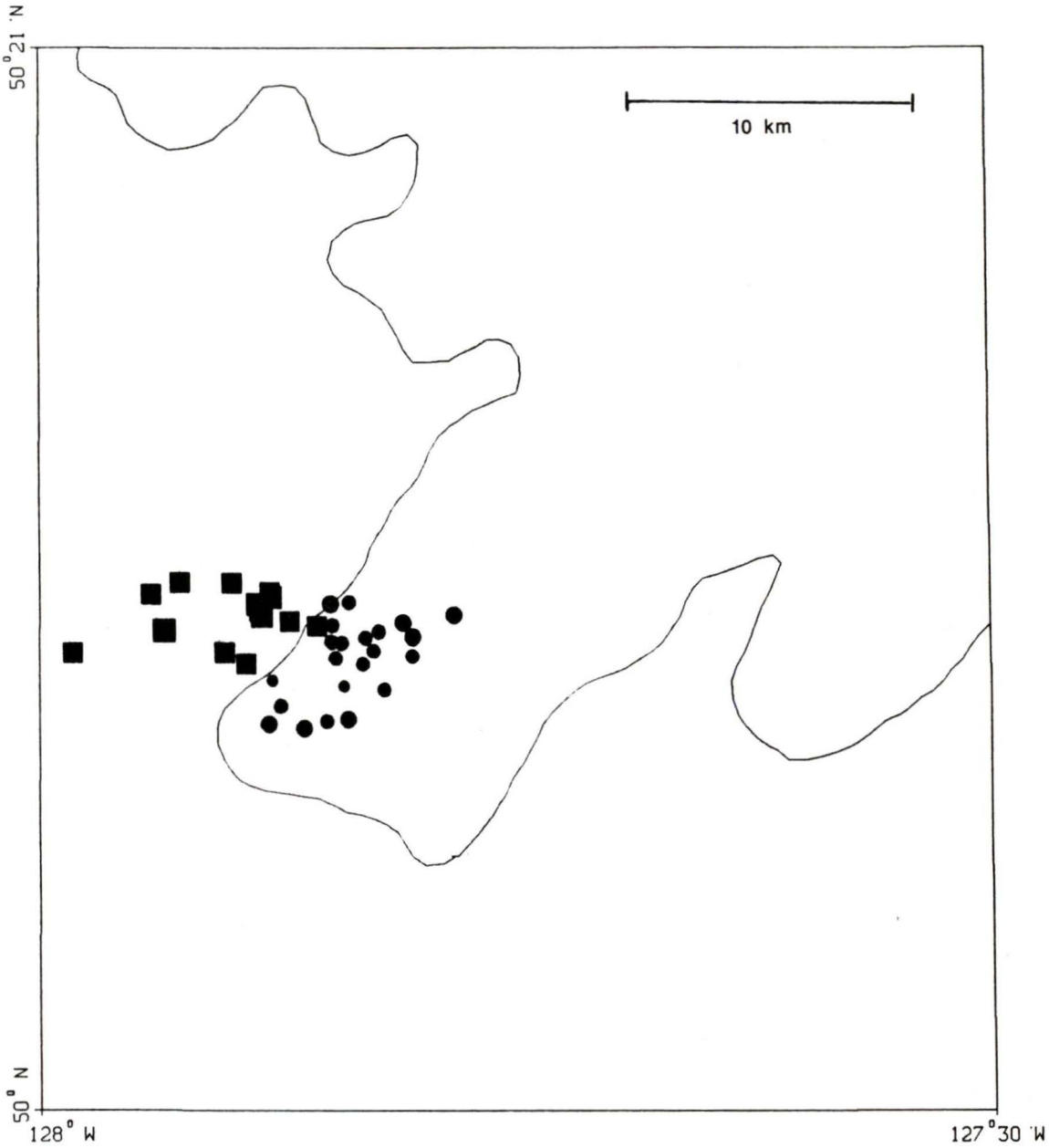

Figure 18 : Combined plot of the Brooks Peninsula aftershocks detected by the temporary (●) and regional (■) networks.

2.4 Regional Seismicity

A search of the Canadian Earthquake Epicentre File (CEEF) indicated that 61 earthquakes had occurred in the Brooks Peninsula region since the turn of the century. By excluding all but those events for which there were *P* and *S* data at PHC and GDR, the number of events was reduced to 31 (Appendix A), ranging in size from M_L 1.3 to M_L 3.3 (Fig. 19). The station ALB was rejected as a substitute for GDR since the aftershock study had shown that reliable picks could not be made at that station for events of this size.

2.4.1 Relocations

The events were located using only PHC and GDR, the Georgia Straits model and the associated travel time corrections. Most of the events moved to a 20 km diameter area west of the peninsula. However, one third of the events were dispersed over a wide area, well away from the peninsula.

The regional aftershock study showed that as the events decreased in size, it became more difficult to read the records at GDR. None of the aftershocks were smaller than M_L 2.0 and it was difficult to pick the *S* phase of the smallest of those. On this basis, events of $M_L < 2.0$ were eliminated, reducing the number of events to 17 and leaving only 5 outlying epicentres (Fig. 20).

Without examining the records, there was no way to determine whether the placement of the outlying events was real or the result of a reading error. The westerly scatter in the grouped solutions could also be the result of reading errors, which is likely since the westernmost events are also some of the smallest.

These results indicate that most of the seismic activity in the Brooks Peninsula region, from 1978 to 1987, is concentrated off the western shore of the peninsula, in the vicinity of the epicentres of the

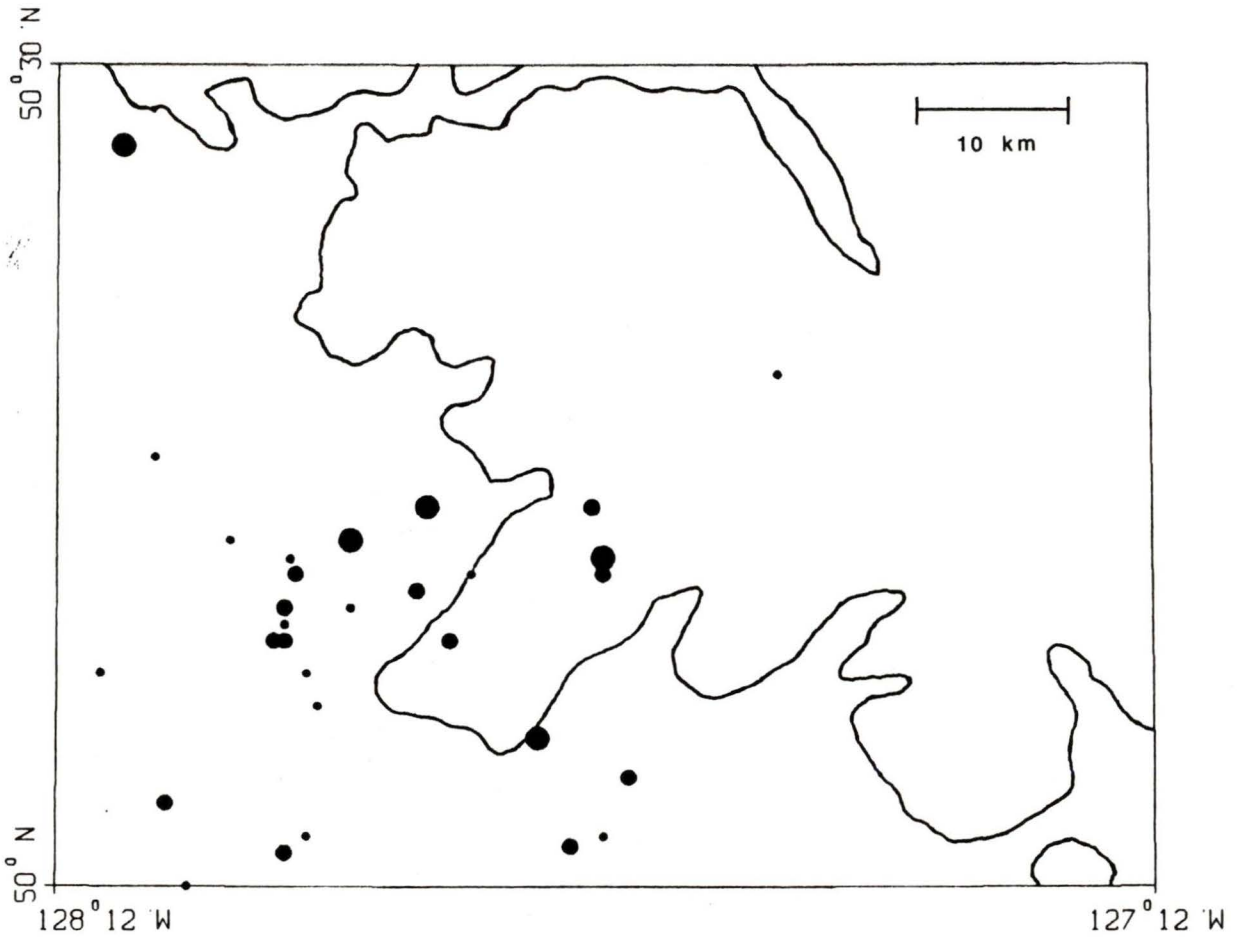

Figure 19 : Seismicity in the Brooks Peninsula region from 1978 to 1987; original G.S.C. solutions. Only those events for which *P* and *S* observations were obtained at PHC and GDR.

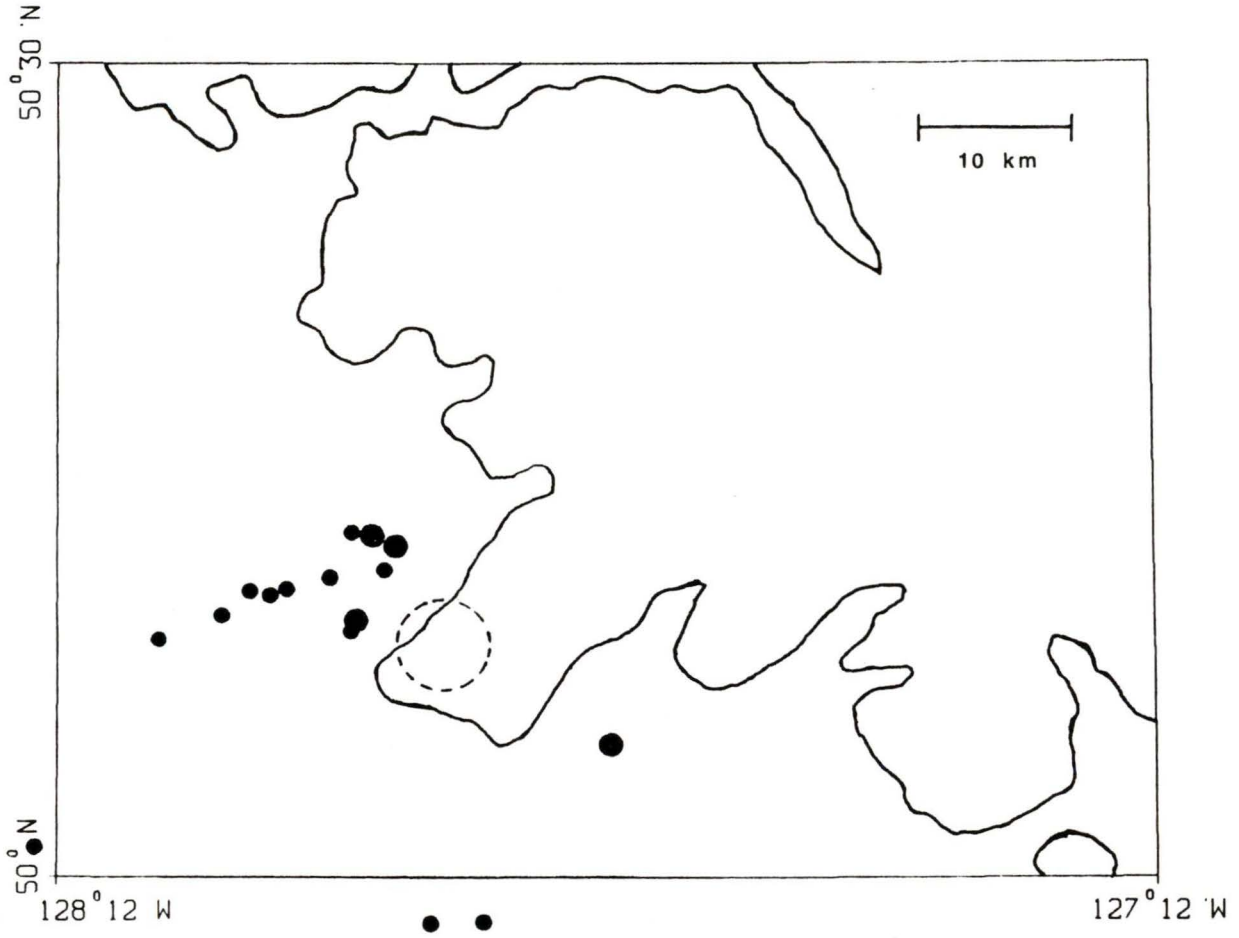

Figure 20 : Brooks Peninsula regional seismicity (1978 - 1987). Final solutions for events $M_L \geq 2.0$. The dashed circle denotes the aftershock area.

two 1978 events. The epicentres are not scattered around the region as indicated by the initial G.S.C. solutions.

2.5 Summary of Results

During the operation of the temporary seismic network on the Brooks Peninsula, from June 9th to June 12th 1978, 42 events were detected. One of these was also detected by the regional seismic stations. The hypocentres of these events were located on the NW shore of the peninsula. A nominal mainshock hypocentre was obtained by averaging the coordinates of the aftershocks located with an error in depth of less than 5.0 km. (Table 2). The rupture surface was estimated at between 11 and 66 km^2, using the same set of aftershocks. Cross-sections plotted using the same aftershock data did not suggest a fault plane orientation.

The permanent seismograph network, maintained by the G.S.C., detected 15 aftershocks for the June 2nd earthquake and 1 aftershock of the July 25th event. It was found that solutions determined using the G.S.C. stations and the Canadian Shield model were displaced east by between 5 and 25 km, depending on the station set. Using *P* and *S* arrivals at just two stations, PHC and GDR, reasonably accurate solutions were determined for the Canadian Shield and Georgia Straits earth models. Epicentres determined using the former were displaced 3-4 km to the east while the latter produced a similar displacement to the west. The mislocations were determined with respect to the position of a reference event.

Travel time corrections were determined for the Canadian Shield and Georgia Straits models from the reference event. After the application of the corrections, the regionally detected aftershocks were still located to the west of the locally detected events.

The travel time corrections were also applied to 17 other earthquakes which occurred in the region between 1978 and 1987. The events were relocated using only PHC and GDR. It was found that the seismicity in

the Brooks Peninsula region was concentrated off the NW shore of the peninsula, in the vicinity of the aftershocks.

Chapter 3 : Mainshock Epicentre Locations

3.1 Introduction

The I.S.C. epicentre solutions for the two mainshocks placed the events at the base of the Brooks Peninsula. These solutions do not coincide, within location uncertainties, with the aftershock region. The aftershock study provided an alternate location for the epicentre of the June event, 17 km southwest of the I.S.C. solutions. The alternate epicentre was the arithmetic average of the best located aftershocks, as determined from the local array data.

The purposes of the teleseismic study were to determine (1) whether the two mainshock epicentres were coincident; (2) if there was a location bias introduced by the whole earth models and (3) the focal depths of the events, using the teleseismic data.

3.2 Teleseismic Study

The travel time data used for the teleseismic locations were obtained from the *Bulletin of the I.S.C.* and from the G.S.C. (Appendix A). Arrivals identified as P_n were omitted since the location program used only direct *P* arrivals. There were 219 arrival times obtained for the June 2nd earthquake. Of these, 173 were from stations at epicentral distances greater than 20°. For the July 25th event, 204 *P* arrivals were obtained, 167 of which were from stations at distances greater than 20°. There was also a subset of 119 stations which detected both events, which provided a means for comparing the epicentre solutions of each event.

3.2.1 Method

The method used to locate the epicentres was a least-squares iterative technique, implemented in the program EPDET (Weichert and Newton, 1970). Given an initial location, the program determined the epicentre by minimizing the sum of the squares of the travel time residuals. At each step, the origin time and epicentre coordinates are adjusted using a fixed depth equation of conditions (Nordquist, 1962). The iterations terminate when the change in the RMS residual is less than one one-thousandth. I added a subroutine to determine the location errors, using the matrix of the coefficients of the normal equations (Nordquist, 1962).

The nominal epicentre coordinates, determined from the aftershock study, were used as the reference position against which the teleseismic epicentre solutions were compared. The focal depth for the teleseismic locations was fixed at 17 km, the average depth of those aftershocks with an error in depth of 5.0 km or less.

Two earth models were used to locate the epicentres, the Jeffreys-Bullen (JB) model (Jeffreys and Bullen, 1940), and the more recent Dziewonski-Anderson (DA) model, which also included station corrections (Dziewonski and Anderson, 1983).

3.2.2 Analysis : Epicentre Locations

Initially, solutions were determined using all available data; i.e., 219 observations for the June event and 204 for July. The solutions obtained were close to those of the I.S.C., although not identical. The two sets of solutions were well within the location uncertainties of one another (Fig. 21). The EPDET locations were displaced 5 km WSW of those of the I.S.C. Locating the epicentres using the I.S.C. focal depths, 13 km for June and 6 km for July, did not make any noticeable difference in the

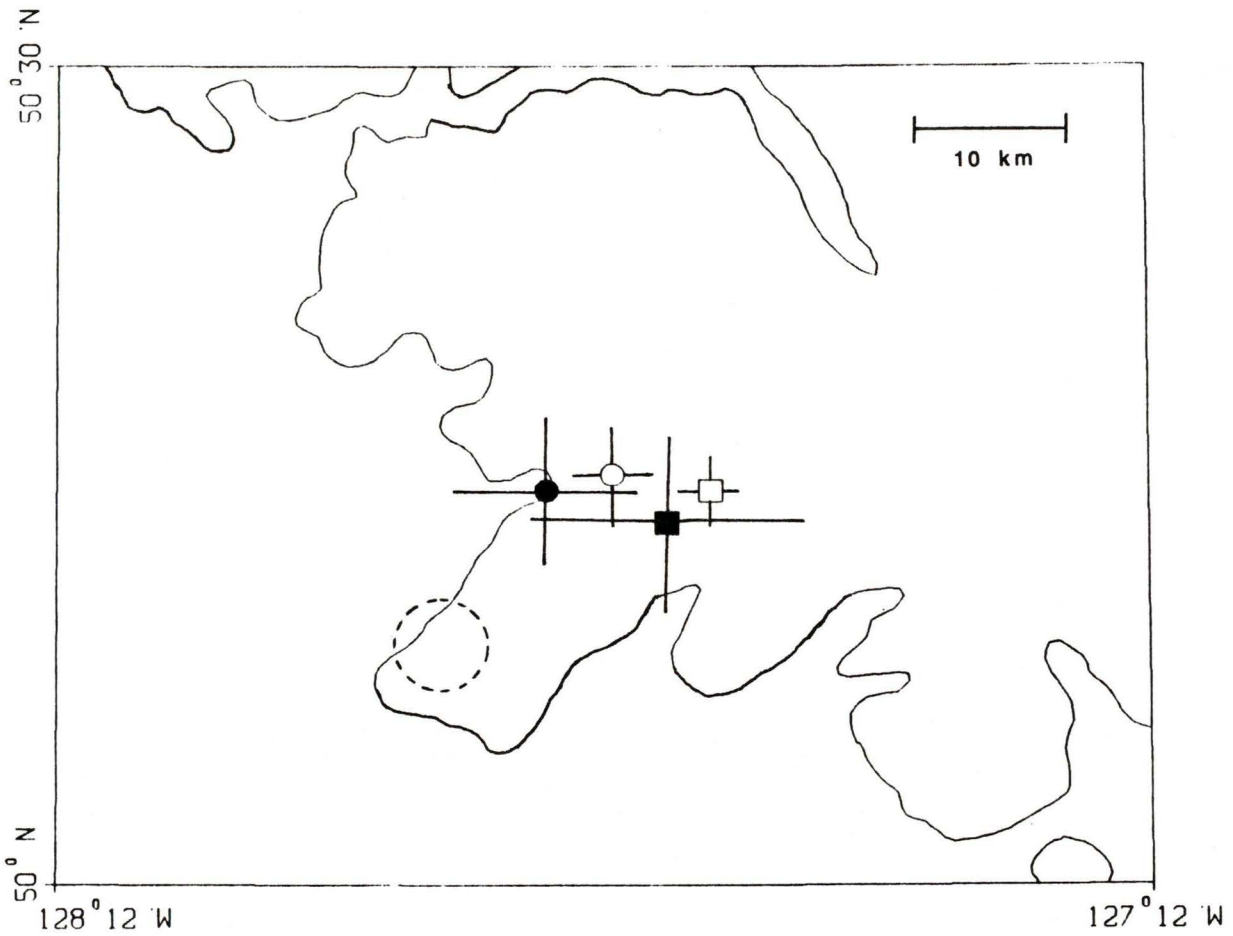

Figure 21 : Brooks Peninsula earthquakes; epicentres determined using all available data with the JB earth model (Table 7). The I.S.C. solutions (open symbols) are provided for comparison. Circles represent the June solutions and squares the July solutions.

positions. It was not possible to duplicate the I.S.C. technique exactly, since they employed additional phases (26 for June and 32 for July) and an unspecified refinement scheme (*Bulletin of the I.S.C.*, 1979). The similarity of the I.S.C. and EPDET solutions indicates that any location bias was not an artifact of the location technique.

June 2nd, 1978 20:41				
Data Set	All Data	$\Delta \geq 20°$	5 s Res.	4 s Res.
Latitude	50.24° ± 5 km	50.06° ± 9 km	50.10° ± 7 km	50.11° ± 5 km
Longitude	-127.75° ± 6 km	-127.92° ± 9 km	-127.89° ± 7 km	-127.88° ± 5 km
Origin Time (s)	43.2 ± 0.3	42.3 ± 0.5	42.4 ± 0.4	42.2 ± 0.3
RMS (s)	1.8	1.7	1.5	1.3
Number of Stations	219	173	169	165
July 25th, 1978 23:30				
Data Set	All Data	$\Delta \geq 20°$	5 s Res.	4 s Res.
Latitude	50.22° ± 6 km	50.04° ± 13 km	50.08° ± 11 km	50.12° ± 8 km
Longitude	-127.64° ± 9 km	-127.78° ± 12 km	-127.77° ± 10 km	-127.70° ± 8 km
Origin Time (s)	52.1 ± 0.4	51.2 ± 0.7	51.3 ± 0.6	51.5 ± 0.5
RMS (s)	2.0	2.0	1.9	1.6
Number of Stations	204	167	163	155

Table 7 Epicentre solutions determined using the Jeffreys-Bullen earth model. Showing the solutions obtained with each successive data set. (Figs. 21, 22).

To eliminate the effects of inhomogeneities in the crust and upper mantle, stations at epicentral distances (Δ) of less than 20° were removed. This reduced the June data set from 219 to 173 observations and the July data set from 204 to 167.

Using the JB model, both events were located with the reduced data sets and an iterative process was used to refine the solutions. Stations were gradually eliminated on the basis of the travel time residuals (Table 7), further reducing the June and July data sets by 8 and 12 observations, respectively. In the first pass, stations with residuals greater than 5.0 seconds were removed, and in the next pass stations with residuals greater than 4.0 seconds were eliminated. The final solutions (Fig. 22) were located near the aftershock area and were coincident within the location uncertainties.

Model	Jeffreys-Bullen		Dziewonski-Anderson	
Event	78/06/02	78/07/25	78/06/02	78/07/25
Latitude	50.06° ± 9 km	50.04° ± 13 km	50.07° ± 9 km	50.04° ± 13 km
Longitude	-127.92° ± 9 km	-127.78° ± 12 km	-127.93° ± 9 km	-127.80° ± 12 km
Origin Time	20:41:42.3 ± 0.5 s	23:30:51.2 ± 0.7 s	20:41:44.8 ± 0.5 s	23:30:53.6 ± 0.8 s
RMS (s)	1.7	2.0	1.6	2.1
Number of Stations	173	167	173	167

Table 8 Epicentre solutions determined using stations at $\Delta \geq 20°$, with the JB and DA models (without corrections). (Fig. 23).

The DA model's effect on the solutions, without station corrections, was examined. Locations were determined for both earthquakes using all stations at $\Delta \geq 20°$ (Fig. 23). The solutions (Table 8) were nearly identical to those obtained from the JB model with the same data set (Table 7). It was apparent from these results that the DA and JB models were basically identical.

Before applying the DA corrections, all stations outside the 30° to 90° distance range were removed. This restriction reduced the June and July data sets to 152 and 146 observations respectively, down 30% from their original sizes. These are the only distances for which the

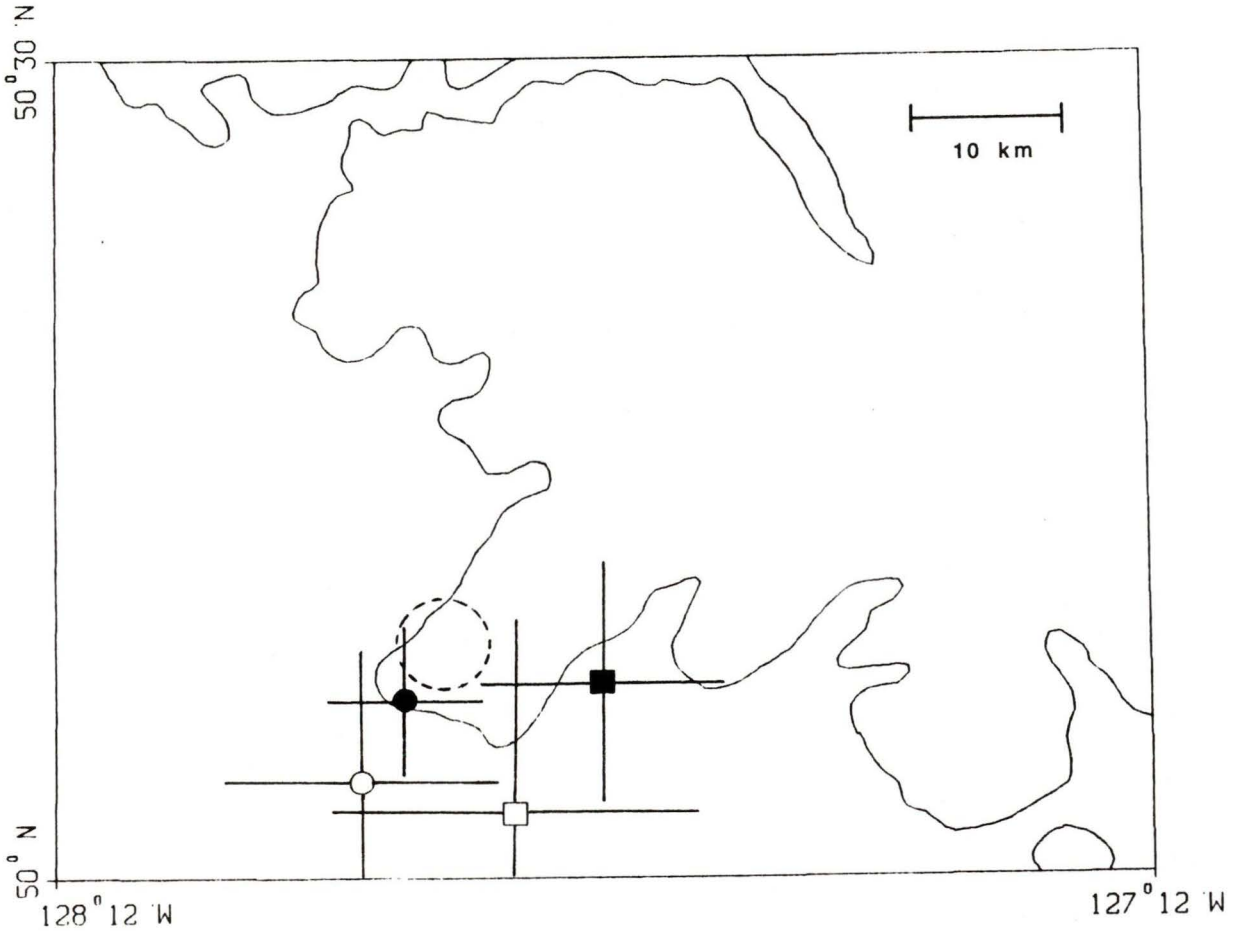

Figure 22 : Main shock epicentres determined with the JB earth model and data from ≥ 20° (Table 7). Initial (open symbols) and final solutions with large residuals removed (solid symbols). Circles represent the June solutions and squares the July solutions.

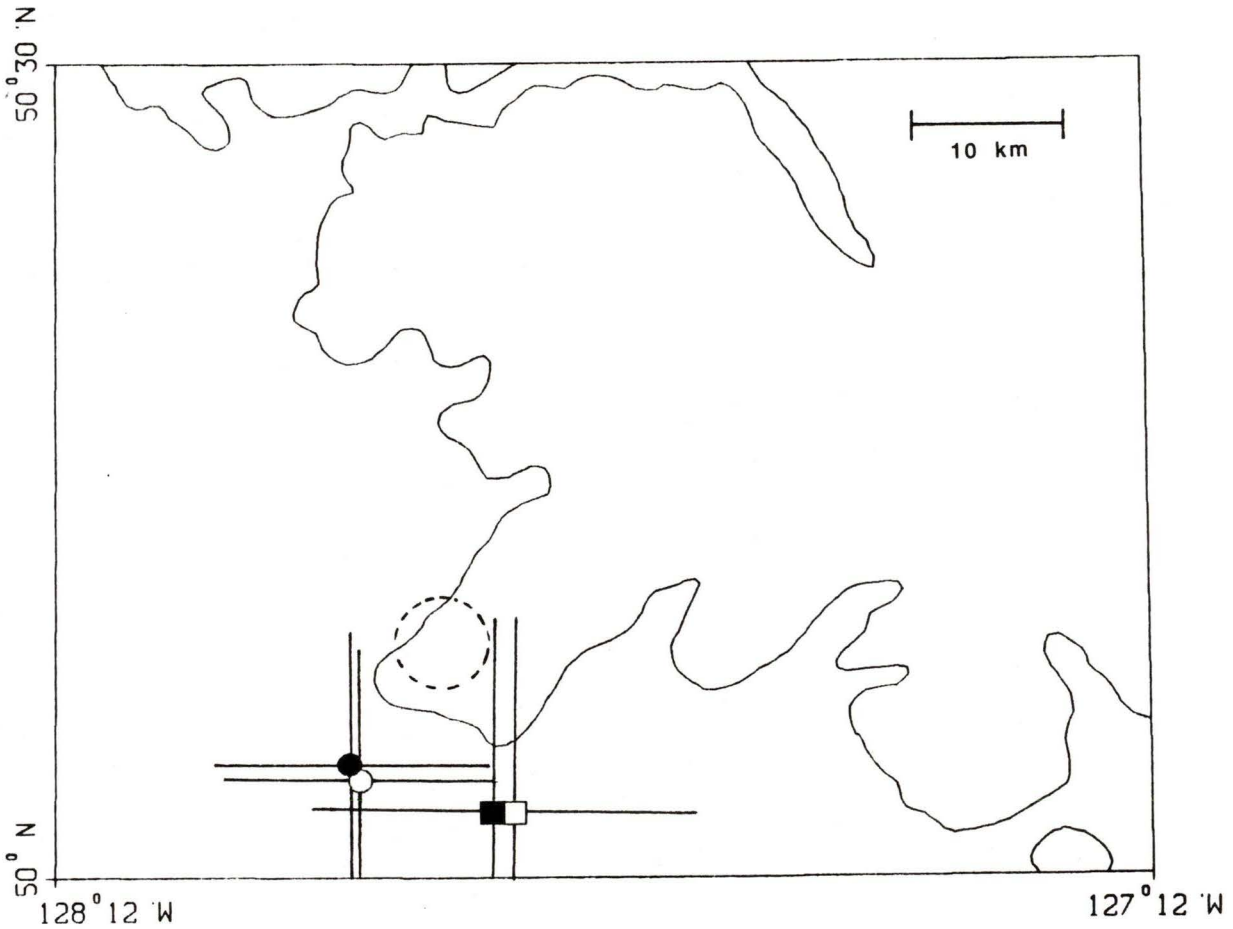

Figure 23 : Main shock epicentres determined with the DA earth model, without corrections, using data from ≥ 20° (Table 8). The solutions determined with the same data set and the JB model are provided for comparison (solid symbols). Circles represent the June solutions and squares the July solutions.

corrections are valid (Dziewonski and Anderson, 1983). Solutions were produced using the reduced, uncorrected data set in order to distinguish the effects of the smaller data set from those of the corrections.

June 2nd, 1978 20:41				
Data Set	Uncorrected	Corrected	5 s Res.	4 s Res.
Latitude	49.93° ± 12 km	49.96° ± 12 km	49.99° ± 9 km	50.00° ± 9 km
Longitude	-128.01° ± 9 km	-127.96° ± 9 km	-127.94° ± 7 km	-127.94° ± 7 km
Origin Time (s)	44.1 ± 0.6	44.1 ± 0.6	44.1 ± 0.5	44.1 ± 0.5
RMS (s)	1.6	1.6	1.4	1.4
Number of Stations	152	152	149	148
July 25th, 1978 23:30				
Data Set	Uncorrected	Corrected	5 s Res.	4 s Res.
Latitude	49.91° ± 19 km	49.90° ± 18 km	49.93° ± 16 km	49.95° ± 13 km
Longitude	-127.88° ± 15 km	-127.80° ± 14 km	-127.79° ± 12 km	-127.77° ± 10 km
Origin Time (s)	53.0 ± 1.0	52.8 ± 1.0	52.8 ± 0.9	52.9 ± 0.7
RMS (s)	2.1	2.1	1.9	1.7
Number of Stations	146	146	143	136

Table 9 Epicentre solutions determined using the Dziewonski-Anderson earth model using data in the 30° to 90° distance range. Solutions are for uncorrected and corrected data. (Fig. 24).

The uncorrected data produced epicentres located southwest of the peninsula and of the previous solutions. Since the JB and DA data sets are essentially identical, the shift of the epicentres was primarily the result of changes in the data set. The corrections shifted the epicentres slightly NNE, but otherwise had little effect on the locations. The corrected data were refined in the same way as in the earlier JB trials, pushing the solutions further to the NE. The refined solutions (Table 9)

were identical to those of the unrefined data set, within the location uncertainties, and were outside the aftershock region (Fig. 24). The corrections had less impact than the configuration of the data set.

The relative positions of the epicentres were determined by locating the events using the set of common stations, ensuring that both solutions were subjected to the same systematic errors. There was one data set for the JB model, with 119 stations ($\Delta \geq 20°$), and one for the DA model with station corrections, with 104 stations ($\Delta \in [30°, 90°]$).

Both sets of solutions (Table 10) indicated that the epicentres were coincident within the location uncertainties, and the July epicentre was consistently placed to the east of the June epicentre (Fig. 25).

Model	Jeffreys-Bullen		Dziewonski-Anderson	
Event	78/06/02	78/07/25	78/06/02	78/07/25
Latitude	50.03° ± 8 km	50.07° ± 14 km	50.00° ± 10 km	49.96° ± 18 km
Longitude	-127.95° ± 7 km	-127.78° ± 13 km	-127.92° ± 8 km	-127.79° ± 14 km
Origin Time	20:41:42.0 ± 0.4 s	23:30:51.1 ± 0.8 s	20:41:44.2 ± 0.6 s	23:30:52.9 ± 1.0 s
RMS (s)	1.4	1.9	1.4	1.8
Number of Stations	119	119	104	104

Table 10 Epicentre solutions determined using only the common stations for the JB and DA model, the latter with corrections. (Fig. 25).

3.3 Focal Depth Determination

The JB model was used with the set of common stations ($\Delta \geq 20°$) to determine the focal depths of the earthquakes. The common data set provided a basis for comparing the June and July results. The epicentre was fixed at the nominal location determined from the aftershock study and

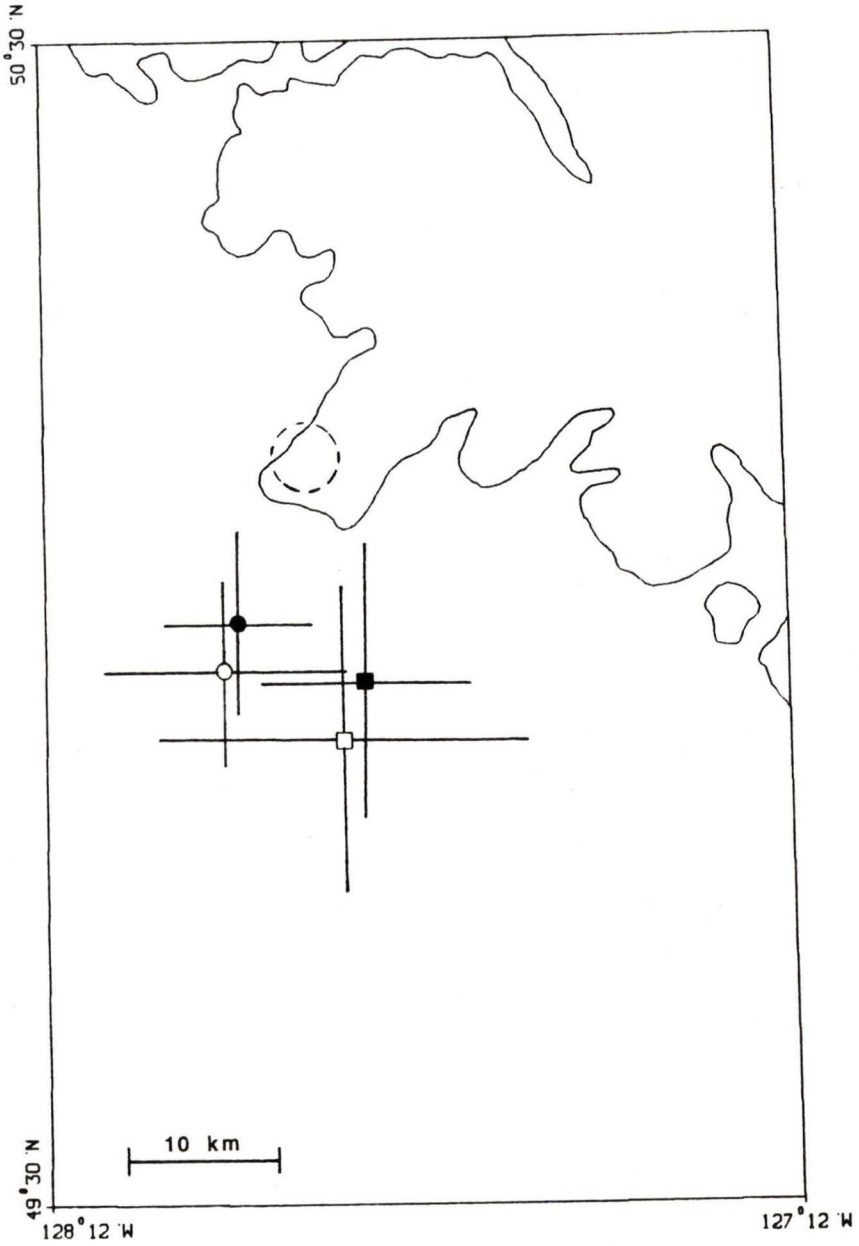

Figure 24 : Main shock epicentres determined with the DA earth model, using corrections (Table 9). Initial (open) and final (solid) solutions with large residuals removed. Circles represent the June solutions and squares the July solutions.

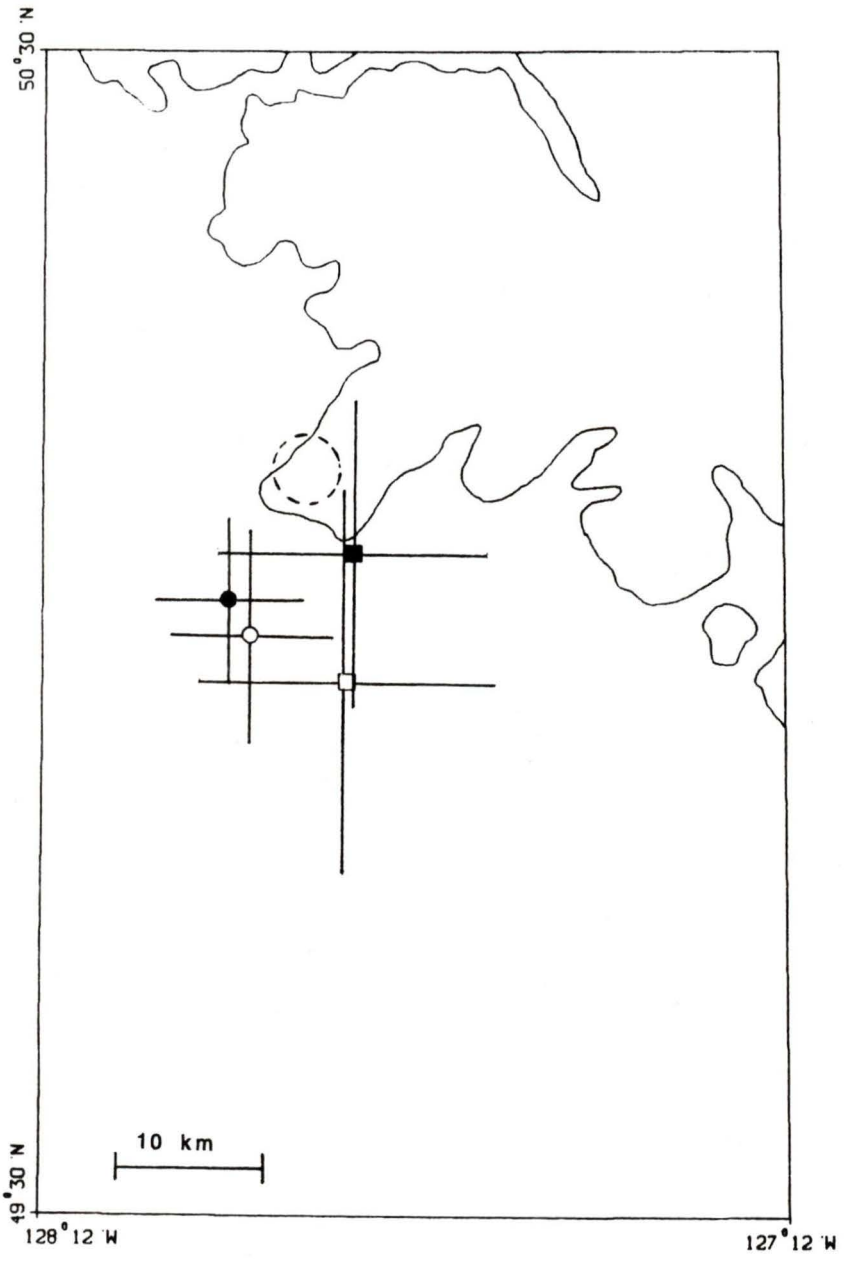

Figure 25 : Main shock epicentres determined using only the stations which detected both events (Table 10); JB model (open symbols) and DA model with station corrections (solid symbols). Circles represent the June solutions and squares the July solutions.

the depths were varied between 0 and 30 km, at 2 km intervals.

The RMS residuals associated with each solution (Fig. 26) indicated that the focal depth of the June event was 16 km and that of the July event was 11 km. Although the minima of the curves were fairly broad, the July focus was definitely shallower than the June focus. The depth for June is consistent with the aftershock results and the relative focal depths are consistent with the I.S.C. solutions.

3.4 Summary of Results

The location trials conducted using the JB and DA earth models indicated that the two mainshock epicentres were coincident within the location uncertainties. The July epicentre was consistently placed to the east of the June solution.

The relative epicentre locations could not be verified using other data sets. The regional data set, comprised of stations at $\Delta < 20°$, contained no common subset which included *S* wave arrivals, making it impossible to locate the epicentres precisely enough to determine their relative positions. It was not possible to use the *S-P* intervals at the closest stations to determine the relative placement of the epicentres, since there were no legible *S* arrivals at those stations.

It was also apparent that the local crustal and upper mantle structure distorted the epicentre locations for the JB model. With the stations at $\Delta < 20°$ removed, the epicentre solutions moved SW, towards the aftershock region. It was apparent that while the I.S.C. solutions were precise, they were not accurate if the nearby stations were included. The NE bias caused by the upper mantle structure was also observed by Wahlström and Rogers (1990).

The application of the Dziewonski and Anderson station corrections had less effect on the data than the size of the data sets. The station corrections only moved the epicentre solutions by 8 km, compared to the

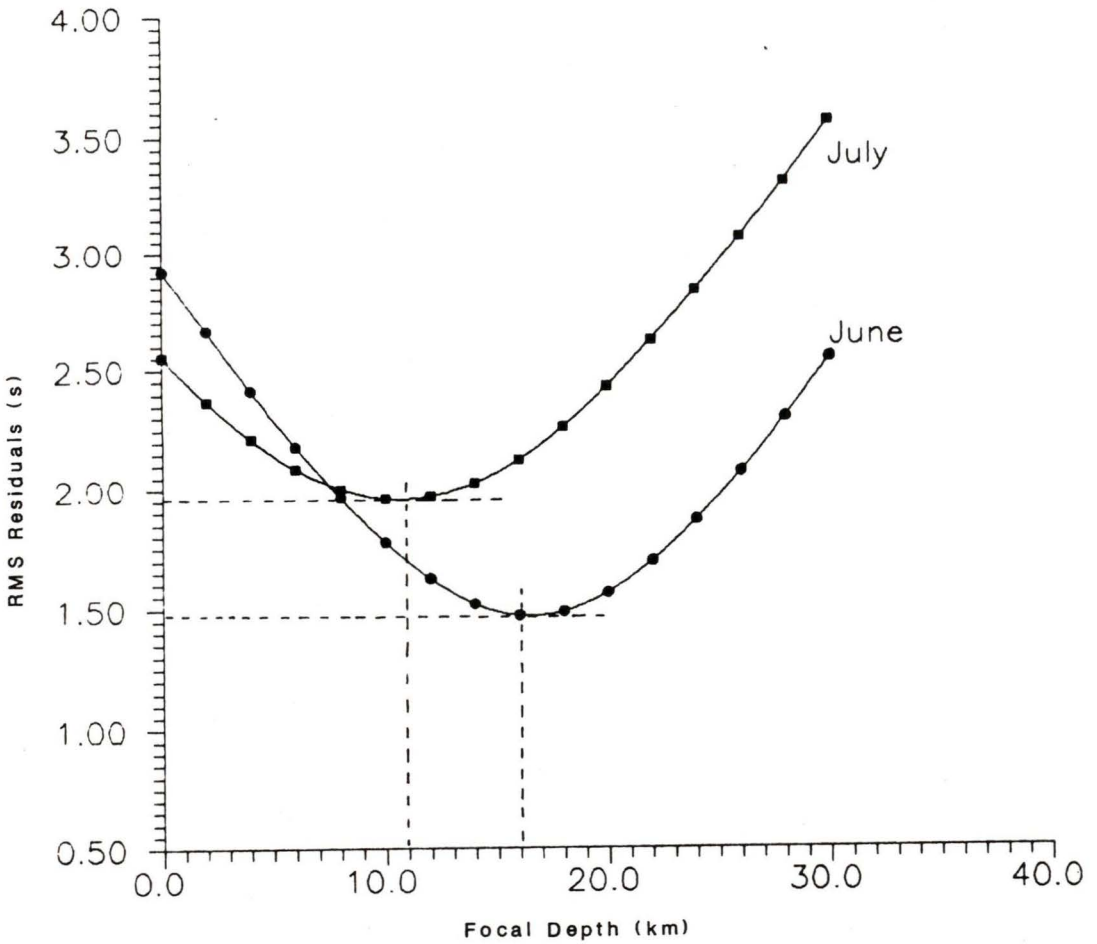

Figure 26 : Variation of the RMS residuals with depth. Epicentre solutions were determined using a fixed epicentre and the JB earth model. A cubic spline has been fitted to the data. Dashed lines indicate the minima and associated focal depths.

18 km resulting from the reduction of the data set.

Using fixed epicentres, the RMS residuals of the epicentre solutions indicated the focal depths of the events to be 16 km and 11 km for June and July respectively. These results were consistent with the aftershock study and I.S.C. solutions.

The epicentre solutions closest to the aftershock area were produced using the JB model with data at distances greater than 20°. There was no advantage to using the DA model either with or without corrections.

Chapter 4: First-Motion Analysis

4.1 Introduction

The first-motion data were used to determine the focal mechanisms of the earthquakes and to compare the first-motion waveforms at common stations. The focal mechanism work was divided into four parts, covering 1) the June mainshock, 2) the June aftershocks, 3) the combined June mainshock and aftershock data and 4) the July earthquake. The first-motion waveform analysis was conducted to determine whether the similarity of waveforms indicated the same pattern of motion on the fault for the two events.

4.2 Focal Mechanism Determination

The data used to determine the first-motion focal mechanisms were obtained from several sources. Seismograms were obtained from the CSSN and from the B.C. Hydro stations at the Mica reservoir. Records for U.S. stations and others around the world were obtained on microfiche from the U.S.G.S. Polarities were also taken from the *Bulletin of the I.S.C.* (1979). From all sources, there were 115 observations for the June event and 78 for July.

The first-motion data were divided into categories on the basis of instrument type, station location and source agency. The classifications, in order from most reliable to least were: long period, short period, I.S.C. data and readings from within the P_n refraction range.

The long period (LP) observations were taken to be the most reliable since they gave the best point source approximation. These records were the clearest, with the least chance of error in determining the first-motion polarity. There were 27 LP observations for the June event and 30

for July. The dilatations and compressions were well separated and adjacent stations did not show opposite polarities.

The short period (SP) observations were less reliable than the LP data because of the poorer point-source approximation. Short period instruments do not detect the average fault motion and may detect path effects, possibly showing first motions which do not represent the average fault motion. There were 39 SP observations for June, but only 4 were obtained for the July event since records were not requested from the University of Washington or the B.C. Hydro stations at Mica Creek. No attempt was made to obtain the U.W. records since they were of dubious value (§ 4.2.2). The records from the B.C. Hydro stations, for the July event, were not useful since they showed emergent rather than impulsive arrivals.

There were 49 first-motion polarities obtained from the I.S.C. for the June event and 44 for the July earthquake. Because these data were second-hand and could not be checked, they were considered less reliable than the LP or SP data.

Observations in the P_n refraction range, $1° \leq \Delta \leq 10°$, were also treated as the least reliable. The emergent angles of these rays are dependant on the earth model (Sutton and Berg, 1958) and may vary by as much as 30°. This implies that the positions of the observations on the focal mechanism plot may be incorrect, biasing the solutions. P_n formed part of the data obtained from SP records and from the I.S.C. for the June event and from LP instruments for the July event.

A weighting scheme was determined empirically from the analysis of the June event. The aim of the weighting scheme was to keep the mechanisms consistent with the most reliable (i.e., LP) data as each successive set was added.

Part of the June aftershock sequence was recorded by the temporary seismic network on the Brooks Peninsula. First-motion data were available for 23 of the 42 aftershocks detected by the temporary array, for a total

125 observations. These data were in the upper half of the focal sphere and had to be corrected, by reversing the station azimuths, in order to be compatible with the mainshock data. For most of these events, all four stations produced first-motion polarities. However, 10 of these events were detected at only three stations and 6 others were detected at only two stations. These data were used to construct composite focal mechanisms.

4.2.1 Method

The method used to determine the focal mechanisms was originated by Byerly (1950). The method uses the distribution of first-motions polarities to identify the nodal planes of the mechanism. Regions of compression and dilatation are defined on the focal sphere by plotting the observations by azimuth and emergent angle. The regions are separated by nodal planes, which are the fault and auxiliary planes of the mechanism. It is not possible to determine which of the nodal planes is the fault plane without introducing information from other sources.

This technique depends on the assumption that the earthquake focus can be treated as a point source. Although the focus is not truly a point source, it can be treated as such using long period data. Long period instruments give a better approximation of the average fault motion than do short period instruments and are preferred.

The focal mechanisms were determined using the program PNODAL (Wickens and Hodgson, 1967), a computer implementation of Knopoff's (1960) statistical method of focal mechanism determination. Using this method, a trial solution is assigned a score based on how well the observations fit that solution. The PNODAL program tests the data with over 4000 trial solutions in a brute force approach. An initial coarse 'grid' of trial mechanisms is generated and each solution assigned a score. A finer 'grid' is then tested in the vicinity of the best scoring mechanism.

The solutions are plotted on a Wulff equal area stereonet which represents the lower half of the focal sphere. The final solution is rotated about the null axis and the normals to the nodal planes until two additional observations are rendered incorrect, providing rough error estimates for the mechanism solutions.

The Jeffreys-Bullen earth model was the basis of the phase data table used, by PNODAL, to determine the take-off angle of each ray. The model was augmented by the extended *PKP* and *PcP* travel time tables produced by Hodgson and Allen (1954). Stations at distances less than 20° were assumed to have received P_n arrivals. After Sutton and Berg (1958), all such stations were assigned an epicentral distance corresponding to a emergent angle of 42°. The effects of a dipping Moho were not considered because of the shallow (~ 8°) dip angle (Dehler, 1991). Stations thus corrected appeared on the mechanism plot as a circle.

For stations at $\Delta < 1°$ in the JB model, rays exited from the upper half of the focal sphere. Uncorrected, these data appear in the wrong quadrant. The symmetry of the focal mechanism allows this to be corrected by changing the azimuths of these stations by 180°.

The hypocentre coordinates used for this study were determined from the aftershock data (Table 5). The same epicentre was used for both events and for the aftershocks.

4.2.2 Analysis of June Mainshock

The LP records were all re-read and assigned full weight. The SP data were then added at 10% weight with no corrections for the effects of P_n refraction. Short period readings, with polarities opposite to those of their immediate neighbours or adjacent LP stations, were re-read. Records with ambiguous first-motions were removed from the data set.

Six stations in Washington state showed dilatations while compressions were read at the adjacent long period stations. These

stations were all SP instruments in the P_n refraction range and since the reversal of so many instruments would be noticed, it is possible that the odd polarities were the result of the geology surrounding the subducting Juan de Fuca plate. Stations on or near a nodal plane often receive low amplitude first-motions which can be misread. The polarities at the nearby LP stations were not ambiguous, making it unlikely that the Washington stations are indicating the presence of a nodal plane.

Once all of the records had been re-read, several solutions were generated using various different weights for the short period data. The SP data were finally assigned a weight of 50%, the maximum weight which produced a mechanism consistent with the LP data. The SP P_n refraction data were left at 10% weight to minimize the effects of the unreliable data without discarding potentially correct readings.

The I.S.C. readings were added at 1% weight to test the fit of these data to the solution. The data did not contradict the existing solution, except where they were not self consistent. The weights of the I.S.C. data were varied between 15% and 40% with little effect on the solutions. The I.S.C. data were not given more than 40% weight since they were less

Long Period	Short Period	I.S.C.	P_n LP	P_n SP	Aftershocks
100%	50%	30%	20%	10%	10%

Table 11 First-motion weighting scheme. Used in determining the focal mechanisms of both main shocks.

reliable than the first-hand short period readings. The final weight of the I.S.C. data was 30% and that of the P_n refraction data was 10%.

The final mechanism solution for June (Fig. 27) was obtained using the final weights (Table 11) and corrections for Moho refraction. Only 10 of the 108 stations used were not consistent with the solution, 4 SP and 6 I.S.C. observations and all of which were P_n refractions.

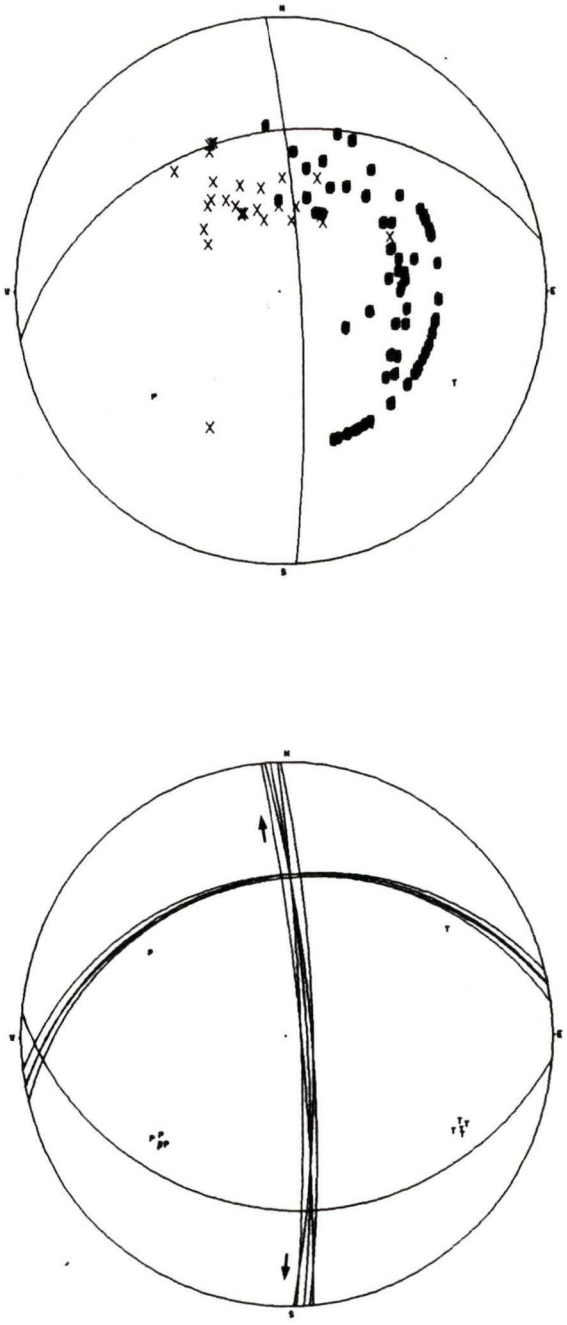

Figure 27 : Focal mechanism solution for the June mainshock, showing the data distribution and the results of rotation about the null axis and normals to the planes. Compressions (●), dilatations (×), pressure axis (P), tension axis (T) are indicated and arrows show the direction of rotation on the NE striking plane. (Table 12).

Nodal Planes	Plane A	Plane C
Strike	260°	357°
Dip	North, 41°	East, 84°
Strike Component	0.99	0.65
Dip Component	0.16	0.76
Motion Sense	Sinistral, Normal	Dextral, Normal
Horizontal Motion	073°	004°
Axes	Pressure Axis	Tension Axis
Strike	232°	118°
Plunge	38°	27°

Table 12 Focal Mechanism of the June 2nd event. (Fig. 27).

The NE striking plane was poorly constrained by the data. The dip could be varied from 40° NW to 36° SSW without rendering more than two additional stations incorrect. The north striking plane was better constrained, with less than 6° of rotation possible.

4.2.3 Analysis of Aftershock Data

The aftershock data were not used to produce focal mechanism solutions for each aftershock but instead the data were used to produce a composite focal mechanism. The azimuths and distances of each station from each aftershock were calculated independently, preserving the relative station locations for each event.

A common hypocentre was used with all of the aftershock data to compute the composite mechanism. This approach made the set of constant station positions and varying hypocentres appear as a large number of stations in close proximity, surrounding a single epicentre. This increased the apparent coverage of the focal sphere. The hypocentre coordinates were the same as those used with the June event.

Assuming that the aftershocks reflect the location and fault motions of the mainshock, the composite mechanism will, in turn, reflect the mainshock mechanism. Similarly, each station should record the same motion polarity throughout the aftershock sequence if the events are part of the same pattern of stress release.

The composite aftershock mechanism (Fig. 28) was similar to that determined for the mainshock. The NE striking plane was again poorly

Nodal Planes	Plane A	Plane C
Strike	253°	351°
Dip	North, 34°	East, 85°
Strike Component	0.99	0.56
Dip Component	0.17	0.83
Motion Sense	Sinistral, Normal	Dextral, Normal
Horizontal Motion	066°	359°
Axes	Pressure Axis	Tension Axis
Strike	230°	109°
Plunge	41°	31°

Table 13 Composite focal mechanism of the June aftershocks. (Fig. 28).

constrained, varying from a dip of 45° NW to 25° SSW, while the N striking plane was well constrained. Of the 125 observations, 10 were inconsistent with the solution. The first-motions were mostly consistent at each station; COO showed compressions for each event while the remaining three all showed dilatations. In 9 instances, 7 at COO and 2 at CLE, the polarities differed from the norm. The events which produced the anomalous readings were not unusual in any sense; however, the suspect polarities appeared near the N striking nodal plane.

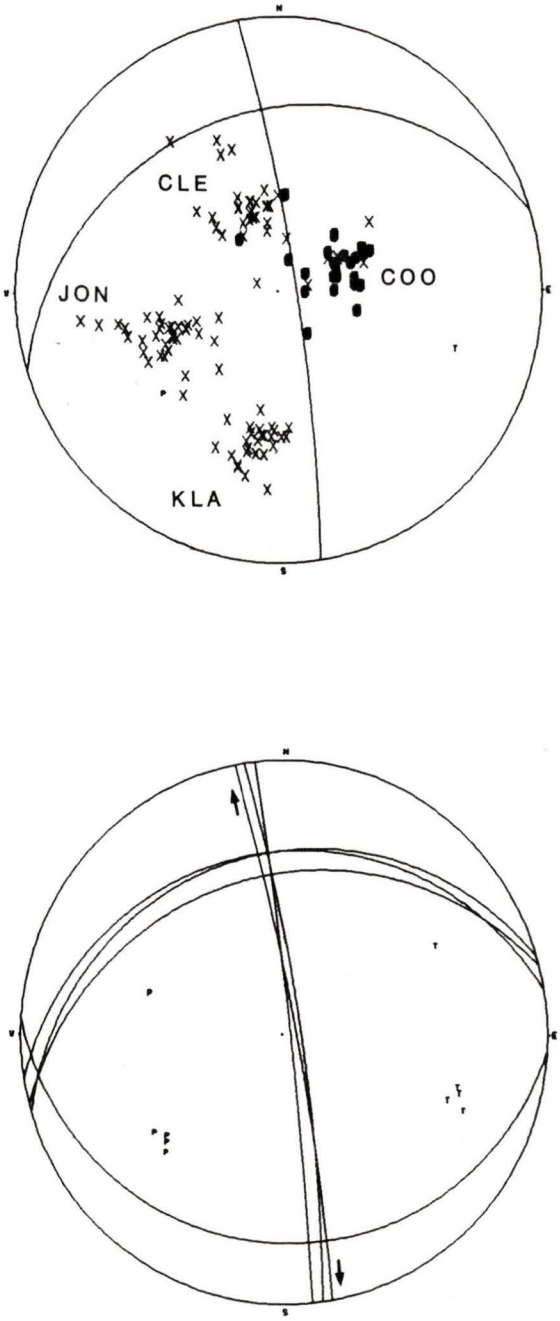

Figure 28 : Composite focal mechanism (Table 13) of the June aftershock data, showing the data distribution and the results of rotation about the null axis and normals to the planes. Compressions (●), dilatations (×), pressure axis (P), tension axis (T) are indicated. Arrows show the direction of rotation on the NE striking plane. The stations associated with each group of data are also indicated. Note that the azimuths of the stations have been reversed to account for the upper hemisphere data.

4.2.4 Composite of June Mainshock and Aftershock Data

Since the mainshock and composite aftershock mechanisms were so similar, the data sets were combined. The aftershocks provided data for the western half of focal sphere, improving the constraints on the solutions.

The mechanism (Fig. 29) was determined using the aftershock data at 10% weight. The solution was essentially identical to that determined for the June mainshock. The aftershock data served to reinforce that solution and improve the constraints on it. The N striking plane was well constrained, with only 3° of rotation possible, but the NE striking plane still varied from a dip of 41° NW to one of 25° SSW. Of the 201 observations, only 20 did not fit the solution.

Nodal Planes	Plane A	Plane C
Strike	259°	356°
Dip	North, 41°	East, 83°
Strike Component	0.98	0.65
Dip Component	0.18	0.76
Motion Sense	Sinistral, Normal	Dextral, Normal
Horizontal Motion	071°	004°
Axes	Pressure Axis	Tension Axis
Strike	230°	117°
Plunge	38°	27°

Table 14 Composite focal mechanism, June main shock and aftershock data. (Fig. 29).

4.2.5 Analysis of July Mainshock

The analysis of the data from the July earthquake was more straightforward than for the previous event. There were no aftershock data

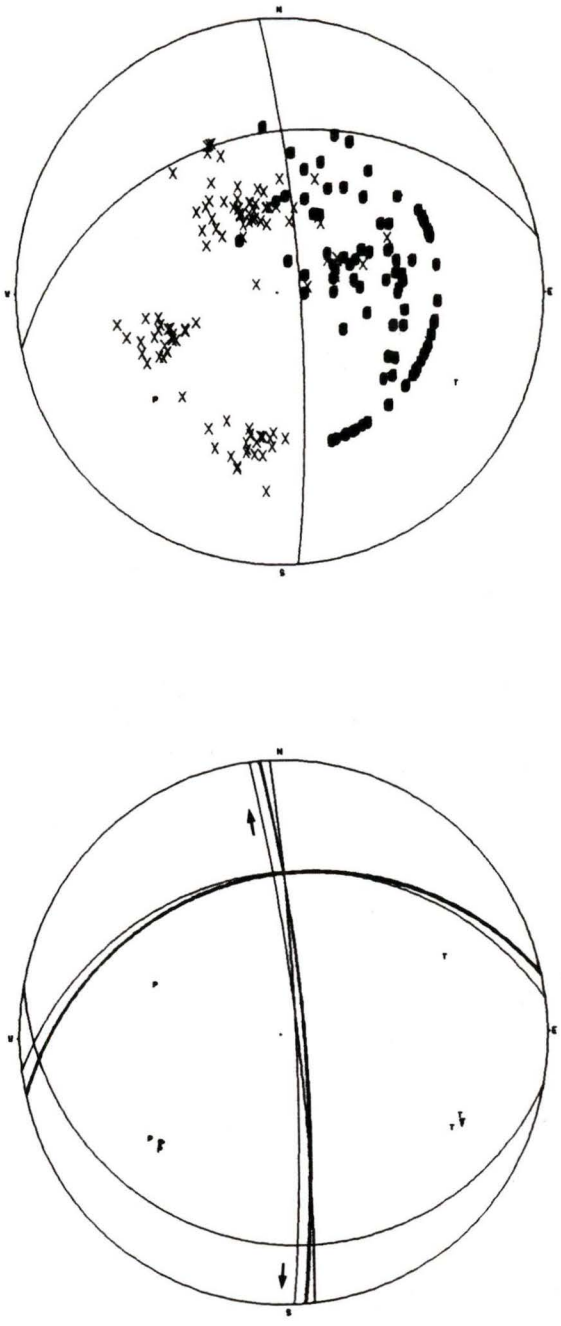

Figure 29 : Composite mechanism using June mainshock and aftershock data (Table 14), showing the data distribution and the results of rotation about the null axis and normals to the planes. Compressions (●), dilatations (×), pressure axis (P), tension axis (T) are indicated. Arrows show the direction of rotation on the NE striking plane.

to consider and the weights for the various data types had already been determined.

The development of the solution proceeded as it did in the case of the June mainshock. The data sets were added gradually and the resulting solutions compared against the LP data. The only new data were LP P_n refractions, which were assigned a weight of 20%.

The final mechanism solution for the July earthquake was similar to that obtained for the June event (Fig. 30). The steeply dipping N-S plane and the poorly constrained NE-SW striking plane were both present. In this case, 20% of the observations did not fit the mechanism, compared to only 10% for the June event.

Nodal Planes	Plane A	Plane C
Strike	246°	352°
Dip	North, 41°	East, 76°
Strike Component	0.93	0.63
Dip Component	0.36	0.78
Motion Sense	Sinistral, Normal	Dextral, Normal
Horizontal Motion	049°	008°
Axes	Pressure Axis	Tension Axis
Strike	223°	110°
Plunge	45°	22°

Table 15 Focal mechanism of the July 25th event. (Fig. 30).

The aftershock data were superimposed on the July solution to examine the fit of these data to that mechanism. The fit was poorer than it was for the June mechanism (Fig. 31). The aftershock data were not used to re-compute a mechanism solution since the aftershocks were not directly related to the July event and might have incorrectly biased the results.

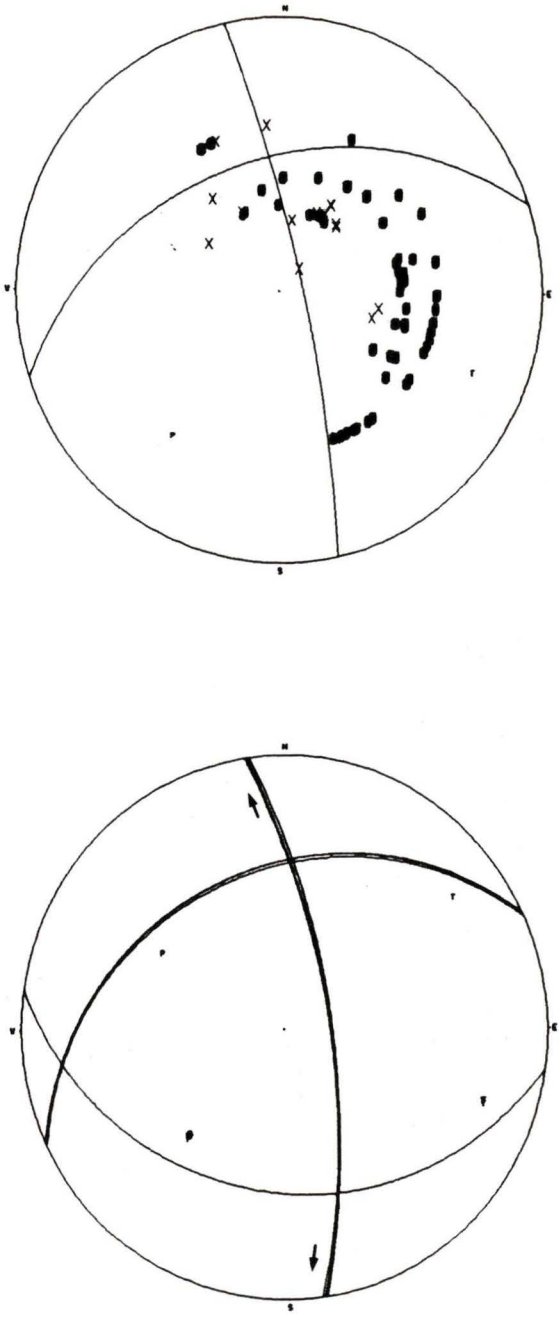

Figure 30 : Focal mechanism solution for the July mainshock (Table 15), showing the data distribution and the results of rotation about the null axis and normals to the planes. Compressions (●), dilatations (×), pressure axis (P), tension axis (T) are indicated Arrows show the direction of rotation on the NE striking plane.

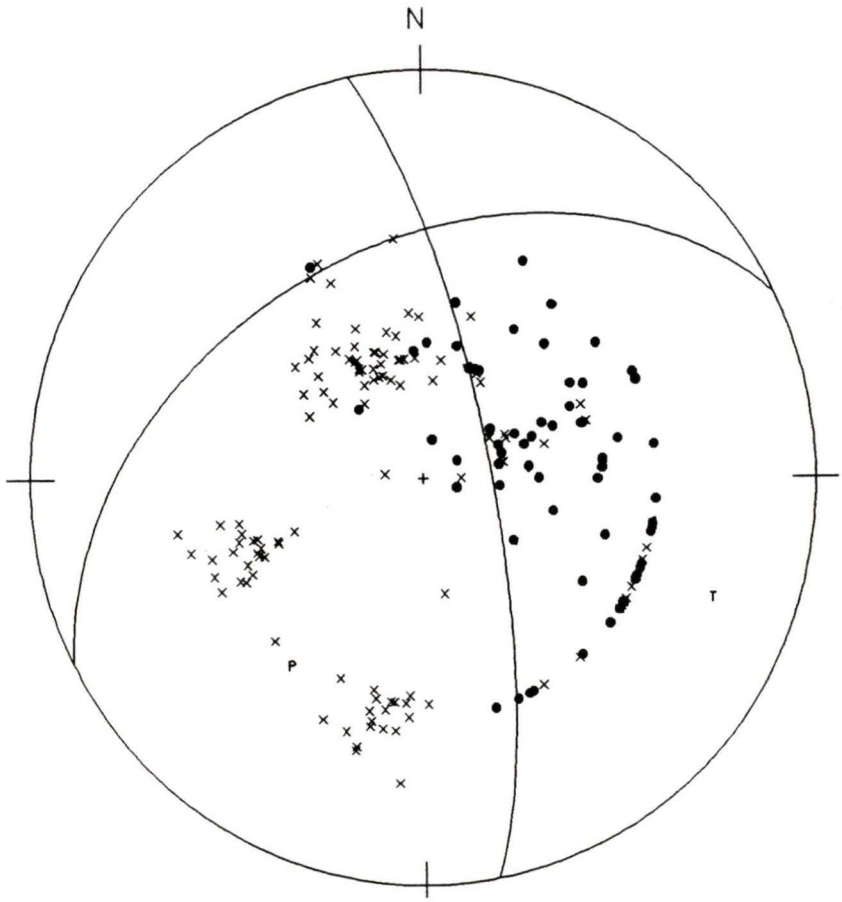

Figure 31 : Combination of July main shock and June aftershock data superimposed on the July mechanism solution. A slightly poorer fit than for June mainshock. Compressions are shown as ●, dilatations as ×, pressure axis as P, tension axis as T.

4.3 First-Motion Comparisons

The *P* waveform data for both mainshocks were obtained from the CSSN, WCTN and the USGS. Paper records were obtained from the first two, while the latter provided records on microfiche. There were 54 stations (Appendix A) which were common to both data sets and seismic records were available for 22 of those (Appendix B). The segments of interest on each record were the first 2 minutes of the recorded event.

4.3.1 Analysis

If the Brooks Peninsula events had the same focal mechanisms, the first-motions would be the same at stations which detected both events, and the waveforms would be identical. The coincidence of identical motion polarities was examined and, where the records were available, the first-motion waveforms for each event were compared.

Of the 54 stations which detected both earthquakes, only 9 recorded a different polarity for each event. In these instances the data were obtained from the I.S.C. for one or both of the events, and so involved observations which could not be checked. There were no LP data which differed.

The 22 stations for which seismograms were available all displayed the same first-motion polarity for both events. Only two of the stations, PGC and PIB, used short period instruments and one station (FFC) required the comparison of the horizontal components. All of the other stations had LP vertical records available.

The records were nearly identical for at least the first two minutes of the trace. Some differences were seen in the high frequency features and the amplitudes. The June records showed higher amplitudes, which was unexpected since the I.S.C. assigned the July event a larger magnitude (m_b

5.2) than the June event (m_b 5.0). However, this is consistent with sizes of the events as indicated by the number of aftershocks.

The records of the two earthquakes showed the same first-motions and waveforms. These data imply that the two events underwent the same pattern of faulting.

4.4 Summary of Results

The focal mechanisms were found to be very similar for both events. Each showed a well constrained N striking plane, dipping at between 75° and 85° to the east. The other plane was striking NE but was poorly constrained, the dip varying between 40° NW and 40° SSW. The faulting was normal and the motion was sinistral on the NE striking plane and dextral on the other. The horizontal motion vectors were directed more or less NE on the former and N on the latter. The P and T axes were oriented SW and ESE respectively, plunging at between 30° and 40°. The azimuth of P axis corresponds reasonably well with the convergence direction of the Explorer and North American plates.

The aftershock data produced a composite mechanism resembling that of the June mainshock. The combination of the mainshock and aftershock data improved the constraints on the mainshock slightly, the dip of the NE striking plane varied between 40° NW and 25° SSW.

The aftershock data were not combined with the July data set but the first-motion waveforms indicate that the two events were enough alike that the same restrictions should apply to both events.

The first-motion waveforms indicated that the two events had an identical pattern of faulting and that the June event was slightly larger than its successor. This makes it likely that the two events had the same focal mechanisms and further, that they are adjacent events on a common fault.

Chapter 5: Surface Wave Analysis

5.1 Introduction

The surface wave magnitudes of the events were redetermined, using the available I.S.C. and CSSN data. Digitized long period surface wave data were used to determine the focal mechanisms of the events and to constrain the first-motion mechanisms. This was accomplished using a combination of forward and inverse modelling. A Love-Rayleigh amplitude ratio (L/R) technique was employed to determine the focal depth of the June earthquake and as an alternate method of constraining the first-motion solutions.

5.2 M_s Determination

The I.S.C. assigned a surface wave magnitude of 5.2 to the June event and a magnitude of 5.1 to the July event. The I.S.C. used data from an unrestricted period range (Table 16), inappropriate for the Prague formula which was used to compute the magnitudes (*Bulletin of the I.S.C.*, 1979). In light of this and the availability of additional CSSN data, the surface wave magnitudes were redetermined.

The Prague formula (Eqn. 1) relates surface wave magnitudes (M_s) to ground motion amplitude (A), period (T) and angular distance (Δ):

$$M_s = \log_{10}(\frac{A}{T}) + 1.66\log_{10}(\Delta) + 3.3 \qquad \textbf{(1)}$$

It is only valid for periods of between 18 and 22 seconds in the distance range 25° to 130° (Duda and Nuttli, 1974). Of the 22 June magnitudes and 21 July magnitudes obtained from the I.S.C., only 11 of each were obtained for the appropriate periods.

Marshall and Basham (1972) developed a set of path and period dependent magnitude corrections for North America and Eurasia. These

Station	Azimuth	2 June 1978			25 July 1978		
		T	Comp.	M_s	T	Comp.	M_s
ANR	345°	19 s	Z	5.3	15 s	H	(5.4)
APA	008°	15 s	Z	(5.0)			
ARU	356°	20 s	Z	4.9	19 s	Z	5.1
BKS	161°				20 s	Z	4.1
CAR	106°				20 s	Z	5.3
DBN	029°	18 s	Z	5.6	20 s	Z	5.5
FRU	344°	20 s	Z	5.2			
FUR	027°	17 s	Z	(5.1)	18 s	Z	5.2
GRF	026°	20 s	Z	5.2			
HFS	020°	20 s	Z	5.0	20 s	Z	5.0
ILT	324°	13 s	Z	(5.2)	12 s	Z	(5.2)
IRK	329°	17 s	Z	(5.3)			
KHE	359°	16 s	Z	(5.1)	16 s	Z	5.1
KTG	026°	18 s	Z	5.4	19 s	Z	5.3
MAT	298°				20 s	Z	4.6
MGD	315°	16 s	Z	(5.0)	20 s	Z	4.9
MOX	026°	16 s	Z	(5.1)	17 s	Z	(4.9)
NRI	346°	16 s	Z	(5.2)	17 s	Z	(5.2)
NVS	342°	18 s	Z	5.5			
OBN	009°	20 s	Z	4.8	16 s	Z	(4.9)
PET	303°	18 s	Z	5.2	20 s	Z	4.9
SEY	318°	16 s	Z	(5.2)	16 s	H	(5.1)
TIK	335°	18 s	Z	5.3	18 s	H	5.1
TLG	342°				16 s	Z	(4.6)
YSS	304°	16 s	Z	(5.0)	16 s	Z	(4.9)
ZAK	328°	16 s	Z	(5.3)	17 s	Z	(5.3)

Table 16 M_s values obtained from the I.S.C. Values obtained at improper periods are in brackets.

corrections allow the use of data from $\Delta < 25°$ and from periods outside

the 18-22 second range. The M-B formula (Eqn. 2) includes terms dependent on amplitude (A), distance (Δ), period (T) and depth (h).

$$M_s = \log_{10}(A) + B'(\Delta) + P(T) + 0.008h \qquad (2)$$

5.2.1 Method

Eight seismograms were obtained from the CSSN for the June event and 7 for the July event. The amplitudes and periods of the largest excursions were read from the records. The ground motion amplitudes were determined from the instrument calibration curves (Shannon *et al.*, 1979). The amplitudes were obtained at periods between 12 and 17 seconds in the distance range from 18° to 47°. The M_s values were determined from the CSSN records using the method of Marshall and Basham (1972).

5.2.2 Analysis

As determined from the CSSN records, the average M_s values were 5.12 and 5.17 for June and July respectively. Using the I.S.C. data at the proper periods, the average magnitudes were found to be 5.22 and 5.00 for June and July respectively. The I.S.C. data indicate that the June event is larger than the July event, contradicting the CSSN data. However, the data sets contained different groups of stations at varying azimuths, making it difficult to compare the magnitude of one event with the other. Combining the CSSN and I.S.C. data and using only common stations, the following magnitudes were determined: M_s 5.21 for June and M_s 5.16 for July. These values are consistent with the relative sizes of the events as indicated by the levels of aftershock activity and the *P* wave amplitudes.

Plotting the distribution of magnitudes by azimuth (Fig. 32) produced a pattern of nodes and lobes. The magnitudes used were those determined from the I.S.C. data, at 18 to 22 s period and the CSSN data.

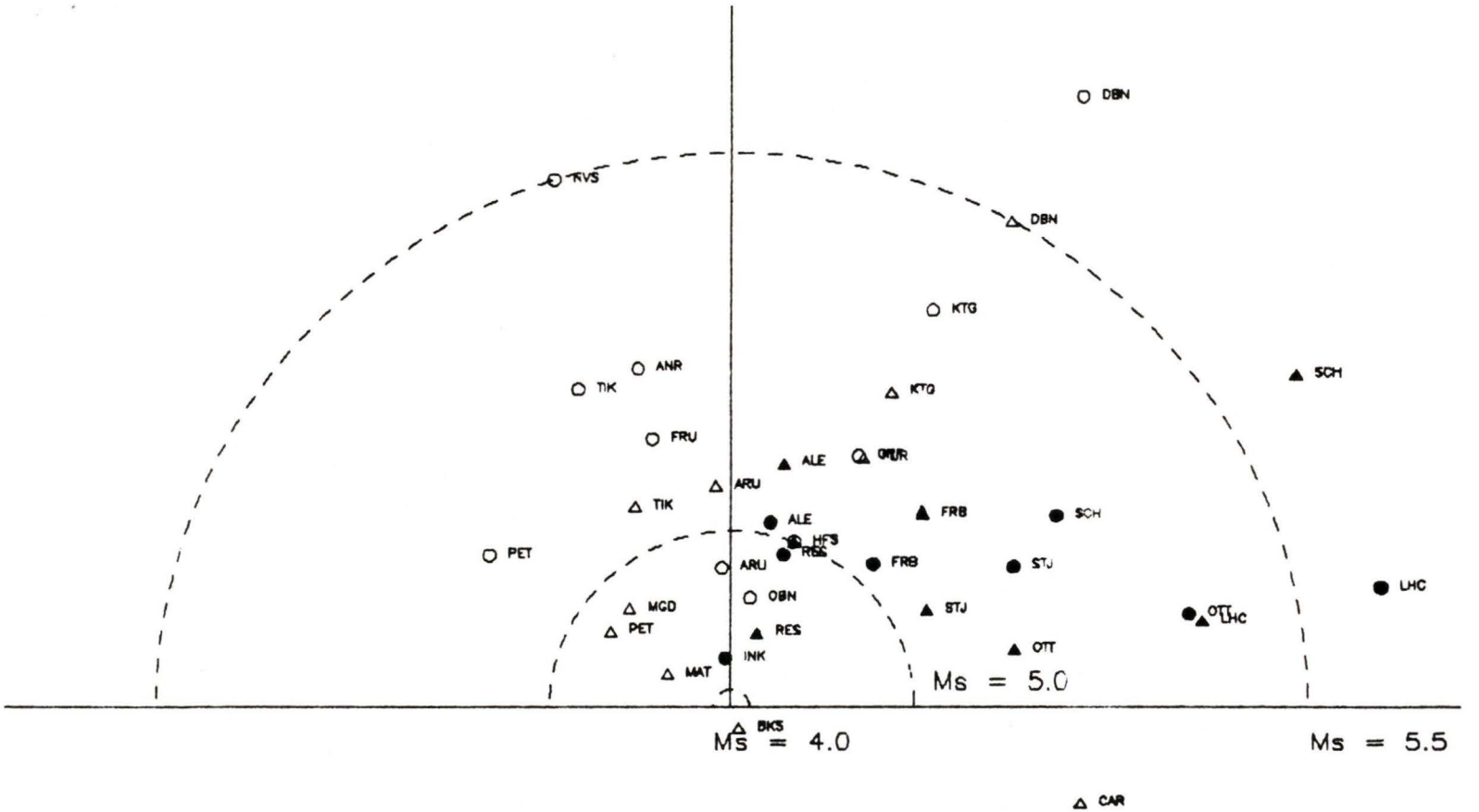

Figure 32 : Azimuthal distribution of M_s values for June (△) and July (○). Data shown are I.S.C. values, 18 s ≤ T ≤ 22 s (open symbols), and CSSN data (solid symbols) determined with the formula of Marshall and Basham (1975). Curves of constant M_s are for reference.

Station	Azimuth	2nd June 1978			25th July 1978		
		T	M_s (P)	M_s (M-B)	T	M_s (P)	M_s (M-B)
ALE	011°	15	5.56	5.03	17	5.39	5.15
FRB	044°	14	5.72	5.05	16	5.54	5.18
INK	353°	12	5.27	4.45			
LHC	079°	16	5.84	5.56	16	5.68	5.42
OTT	078°	17	5.66	5.41	16	5.56	5.20
RES	018°	14	5.59	4.96	12	5.58	4.65
SCH	059°	17	5.57	5.32	16	5.92	5.56
STJ	063°	12	6.04	5.24	12	5.87	5.08

Table 17 M_s values determined from the CSSN stations. The Prague formula values (P) have been provided for comparison with the M-B values.

To emphasize the differences between the M_s values, the data were plotted as a function of M_s: $f(M_s) = 10^{(Ms-5)}$.

The June data show a minimum at a 015° azimuth, with maxima to either side. The distribution of maxima and minima reflect the nodes and lobes in the surface wave radiation pattern for the Rayleigh vertical component (§ 5.3.2). There is also a NE linear trend of unusually high magnitudes. These anomalous magnitudes are consistent with the relatively low attenuation values observed in the Canadian Arctic (Mitchell, 1975) and probably are not a facet of the earthquake mechanisms.

The magnitudes at common stations are usually greater for the June event than for July, except in the NE quadrant where some of the CSSN stations give larger M_s values for the July event.

5.3 Surface Wave Analysis

The surface wave analysis required digital, long period, three component data. Seismograms were obtained from the CSSN and the USGS and hand digitized using a HI-PAD digitizing tablet. The actual seismograms

were available from the CSSN, while the other records were obtained from the NEIS on microfiche. The earthquakes were small enough that instruments in North America remained on scale but there were no data available from Eurasian stations. Useful data were obtained from 12 stations for the June event and 14 stations for July (Fig. 33). The June data were restricted to the NE quadrant while the July data set included 3 U.S. stations, expanding the azimuth range slightly. With restricted azimuths, a diagnostic feature like a node in the radiation pattern may not be observed, making it difficult to determine the mechanism.

Seismograms were digitized if the trace remained on scale in the digitization window and if the trace was dark enough to be followed by eye. Stations with less than three usable components were included if the vertical or both horizontal records could be digitized.

Love and Rayleigh wave attenuation coefficients ($\eta(\omega)$) for used in the inversion, forward modelling and L/R methods were derived (Eqn. 3) from Tsai and Aki's (1969) Q values for continental paths.

$$\eta(\omega) = \frac{\pi \cdot \nu}{Q \cdot U(\nu)} \qquad (3)$$

In equation 3, ν is the frequency and $U(\nu)$ is the frequency dependent group velocity (Mitchell, 1975).

The earth model (Table 18) was Ben-Menahem and Singh's (1981) continental crust model. The eigenfunctions required to compute the theoretical amplitude spectra were generated from the theoretical dispersion curves (Fig. 34) developed from the model. The programs SURAFCE, LEIGEN and REIGEN were used to accomplish this (Herrmann, 1978).

5.3.1 Method

The digitization window for each station was determined by the interval between the arrivals of the 2.5 km/s and 5.0 km/s surface waves. These velocities were chosen since the group velocities of Love and

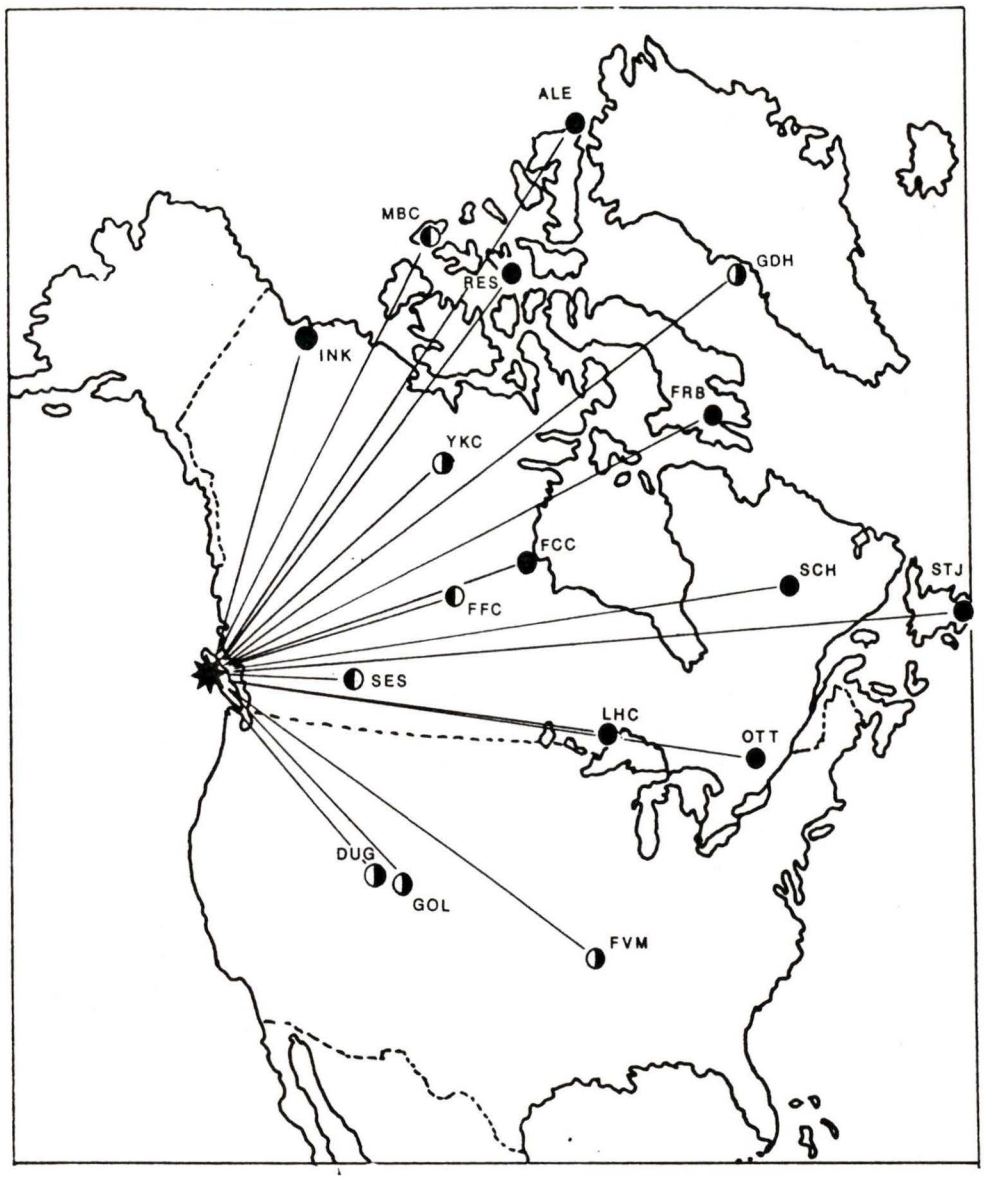

Figure 33 : North American seismograph stations from which useful surface wave data were obtained.

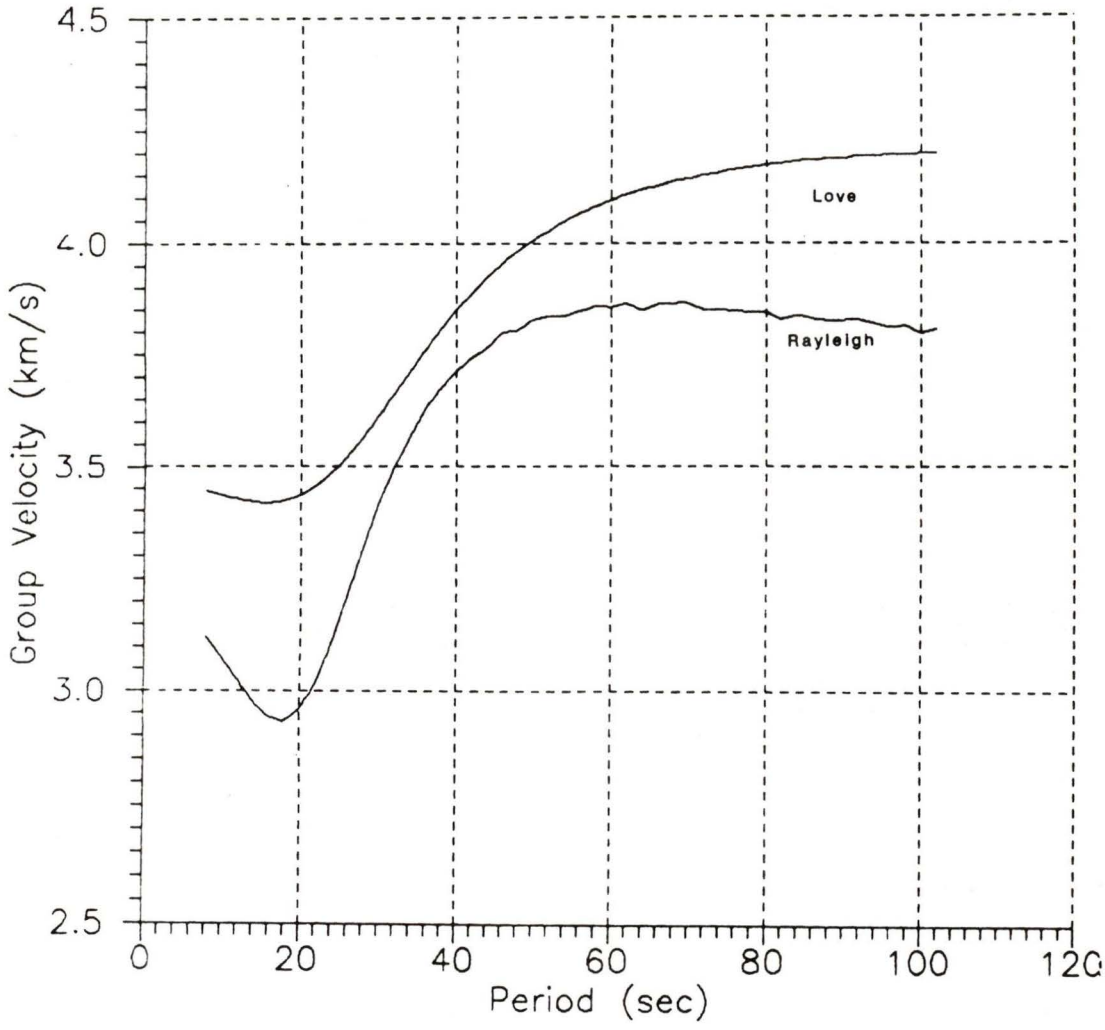

Figure 34 : Theoretical dispersion curves for Love and Rayleigh waves, determined from the Ben-Menahem and Singh earth model (1981).

Depth (km)	Thickness (km)	V_p (km/s)	V_s (km/s)	Density (g/cc)
0	1	5.00	2.93	2.20
1	21	6.03	3.53	2.78
22	15	6.70	3.80	3.00
37	13	7.96	4.60	3.37
50	25	7.85	4.50	3.39
75	50	7.85	4.41	3.42
125	75	8.00	4.41	3.45
200	50	8.20	4.50	3.47
250	100	8.40	4.60	3.50
350	100	9.00	4.95	3.63
450	100	9.63	5.31	3.89
550	100	10.17	5.63	4.13
650	100	10.59	5.92	4.33
750	100	10.96	6.14	4.49
850	100	11.28	6.29	4.60
950	150	11.46	6.38	4.69
1100	200	11.76	6.50	4.80
1300	200	12.02	6.61	4.91
1500	200	12.28	6.74	5.03
1700	200	12.54	6.85	5.13
1900	200	12.80	6.96	5.24
2100	200	13.02	7.00	5.34
2300	200	13.24	7.10	5.44
½ Space		13.48	7.20	5.54

Table 18 Continental Crust earth model (Ben-Menahem and Singh, 1981).

Rayleigh waves generally lie between 2.8 km/s and 4.6 km/s, for periods between 10 and 100 seconds, (Herrmann, 1973). Plots of the digital data were overlain on the original seismograms to ensure the accuracy of the digitization.

The data were then rotated and filtered using the program EXSPEC (Herrmann, 1978), which resolved the N-S and E-W seismograms into radial and transverse components and removed any DC offsets and linear trends. The data were also corrected for the instrument response using the station calibration curves (Shannon *et al.*, 1979). The time series data were transformed to the frequency domain and the amplitude spectra corrected for geometrical spreading, to a reference distance of 1000 kilometres.

Using the program FILTER (Herrmann, 1978), the amplitude spectra were narrow band-pass filtered to determine the spectral amplitudes of the fundamental mode. The fundamental modes were used since they were most readily identified on the dispersion curves. A Gaussian filter was used in the 20 to 50 s period range, at 2 second intervals, to minimize the effects of aliasing (Herrmann, 1973). The filter interval was chosen to provide reasonable coverage of the data interval and to keep subsequent processing time within reasonable limits. The filtering was performed in the 20-50 second range because surface waves from shallow earthquakes are most clearly recorded in the 10-50 s interval and the finiteness of the source has little effect on the data for $T > 20$ s (Tsai and Aki, 1970). Also, crustal thickness and upper mantle structure are minor factors affecting the amplitude spectra for $T > 15$ s and the attenuation coefficients, for $15 \leq T \leq 50$ s, change less rapidly than at other periods (Tsai and Aki, 1970).

The filtering produced dispersion curves with several group velocities and spectral amplitudes for each period. The group velocity-amplitude-period plots were contoured by amplitude (Appendix B). The spectral amplitudes used in the forward and inverse modelling were selected on the basis of the fit of the associated group velocities to the theoretical values (Fig. 34). The definition of the dispersion curve was also considered; poorly defined or discontinuous curves indicated mixed Love and Rayleigh energies or other contamination. Generally, the Love wave dispersion curves were better defined than either Rayleigh component.

This phenomenon has also been observed for other earthquakes in B.C. (Rogers *et al.*, 1990; Cassidy *et al.*, 1986).

The focal mechanisms were determined through an iterative process combining inverse and forward modelling. The data were inverted using a variant of Herrmann's inversion program, QUESTION (Herrmann, 1978), which employed simulated annealing (Press *et al.*, 1988).The annealing program, QUESTA, proceeded by comparing the observed data with theoretical amplitudes determined for a randomly selected, trial focal mechanism. The fit of the data to the mechanism was described by a score which was the product of the Love and Rayleigh correlation coefficients, the spectral amplitude residuals and the ratio of the seismic moments determined separately from Love and Rayleigh data (Herrmann, 1973). The fit of the focal depth was indicated by the ratio of the Love and Rayleigh seismic moments and the fit of the strike was indicated by the Love wave correlation coefficient (Herrmann, 1973).

The forward modelling was carried out using the program RADPAT (Herrmann, 1978), which computed the theoretical surface wave radiation patterns and superimposed the observed data.

5.3.2 Analysis

The initial inversions were performed using all of the available data. The solutions for each event provided approximate values for the seismic moments and crude focal mechanisms. The theoretical spectra for these mechanisms were plotted, using RADPAT, and the anomalous observations removed.

On the first pass, only those amplitudes which were more than twice as large as others at similar azimuths were eliminated. The different attenuation characteristics of the non-continental paths produced large residuals. The few stations without exclusively continental travel paths were removed. This was to prevent the different attenuation regimes from

biasing the solutions. Spectral amplitudes which showed a significant departure from the theoretical dispersion curves were also eliminated. At some stations, the horizontal components displayed a mixture of Love and Rayleigh energy on the radial and transverse components. The dispersion curves for these stations showed the energy from the two phases merging. In these cases, the dominant phase was identified and the other one removed.

The refined data sets were inverted and refined a second time. Data were removed only when one amplitude clearly differed from two or more others at the same azimuth. The data were inverted one more time to produce the final surface wave focal mechanisms.

	2 June 1978		25 July 1978	
Strike	250°	0°	259°	0°
Dip	33°	78°	45°	76°
Motion	Sinistral Normal	Dextral Normal	Sinistral Normal	Dextral Normal
Horz. Motion	270°	19°	267°	17°
P Axis Strike/Plunge	237° / 48°		229° / 47°	
T Axis Strike/Plunge	113° / 26°		120° / 24°	
Moment	1.60×10^{24} dyne·cm		1.19×10^{24} dyne·cm	
Score	0.75		0.52	

Table 19 Focal mechanisms for the Brooks Peninsula earthquakes, determined from the inversion of surface wave data. (June: Fig. 35; July: Fig. 36).

Initially there were 275 Rayleigh and 181 Love amplitudes in the June data set. After refinement, there were 167 Rayleigh and 154 Love amplitudes. The full July data set contained 335 Rayleigh observations and 216 Love amplitudes; after refinement there were 143 and 114 observations respectively. The refinement process improved the mechanism scores for both events. The June score started at 0.66 and went to 0.75, while the

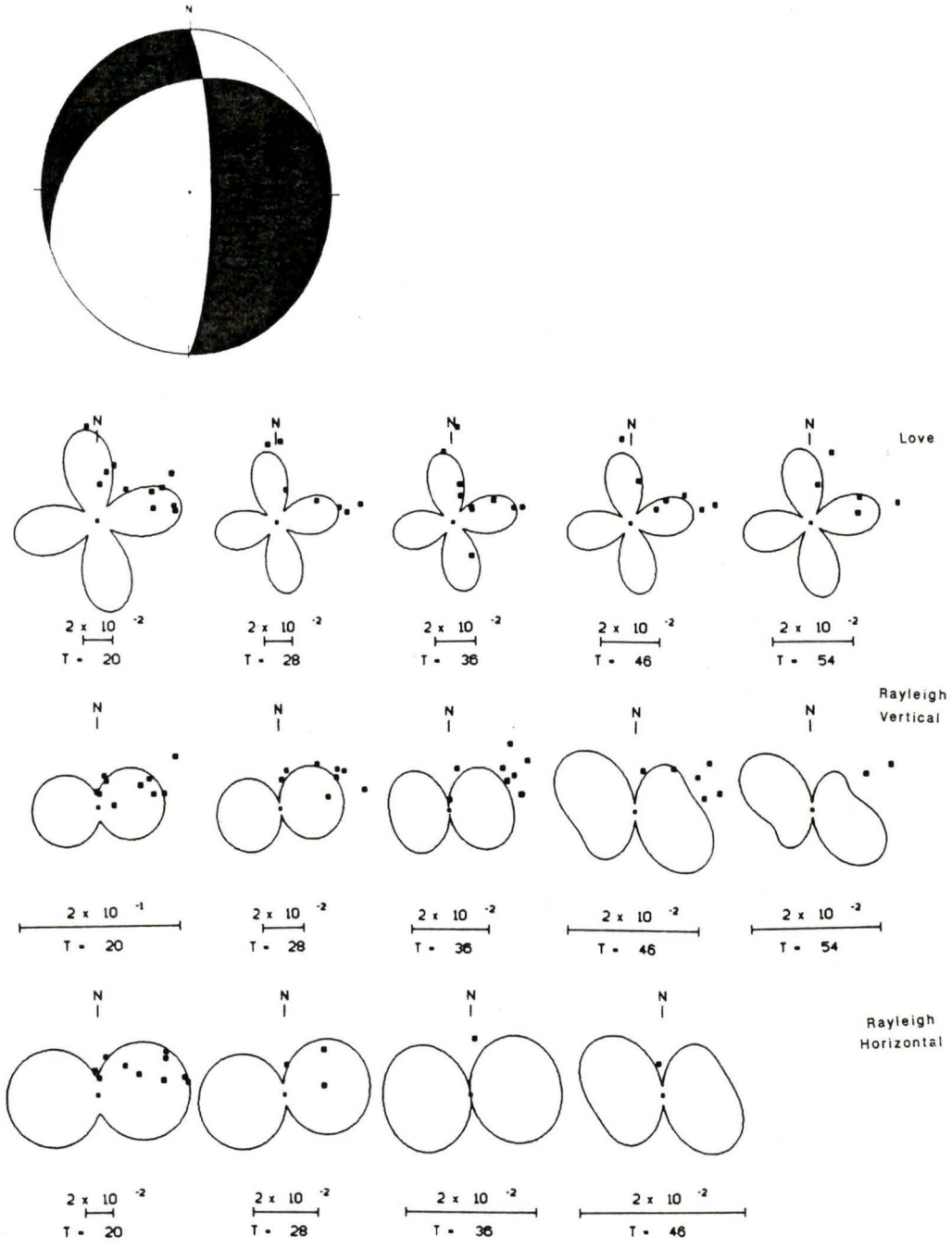

Figure 35 : Focal mechanism solution for the June 2nd earthquake, obtained from surface wave inversion (Table 19). Theoretical Love and Rayleigh surface wave radiation patterns are also shown for the inversion mechanism. The observed spectral amplitudes (■) are shown at several periods, for each component, for comparison to the theoretical curves.

change in the July score was more dramatic, increasing from 0.16 to 0.52 with refinement.

Since simulated annealing produces a "near optimum" solution, the inversions were run several times, on each data set, to test the stability of the solutions and to determine possible variations. The stability tests produced mechanisms whose parameters varied from those of the final solutions by 10° at most. Inversions were also run using several trial depths to obtain a focal depth estimate. The trial depths were varied from 0 to 20 km, at 5 km intervals. The mechanism orientations did not change significantly with depth, only the solution scores varied. The best score was obtained for a focal depth of 10 km and that depth was used throughout the remainder of the surface wave analysis.

The same surface wave radiation patterns can be generated by several equivalent focal mechanisms in which the fault slips are reversed or the planes are dipping in the opposite directions (Herrmann, 1978). Using the first-motion data, it was possible to eliminate most of these variations. The final focal mechanism solutions (Table 19) were similar to one another and to the primary P-nodal solutions. Both mechanisms showed normal faulting on a steep (75°-85°), east dipping N-S plane and a moderate (35°-45°), northwest dipping NE-SW plane. Because of the poor first-motion constraints, the latter could also be dipping to the southeast. The seismic moments were found to be 1.60×10^{24} dyne·cm for June and 1.19×10^{24} dyne·cm for July. The scatter in the July data that was observed in the dispersion curves was also seen in the surface wave radiation patterns (Fig. 36).

5.4 Constraining the P-nodal Solutions

The dips of the NE striking plane in the P-nodal solutions for each earthquake were poorly constrained. The possible variations were restricted by forward modelling with the surface wave data. The program

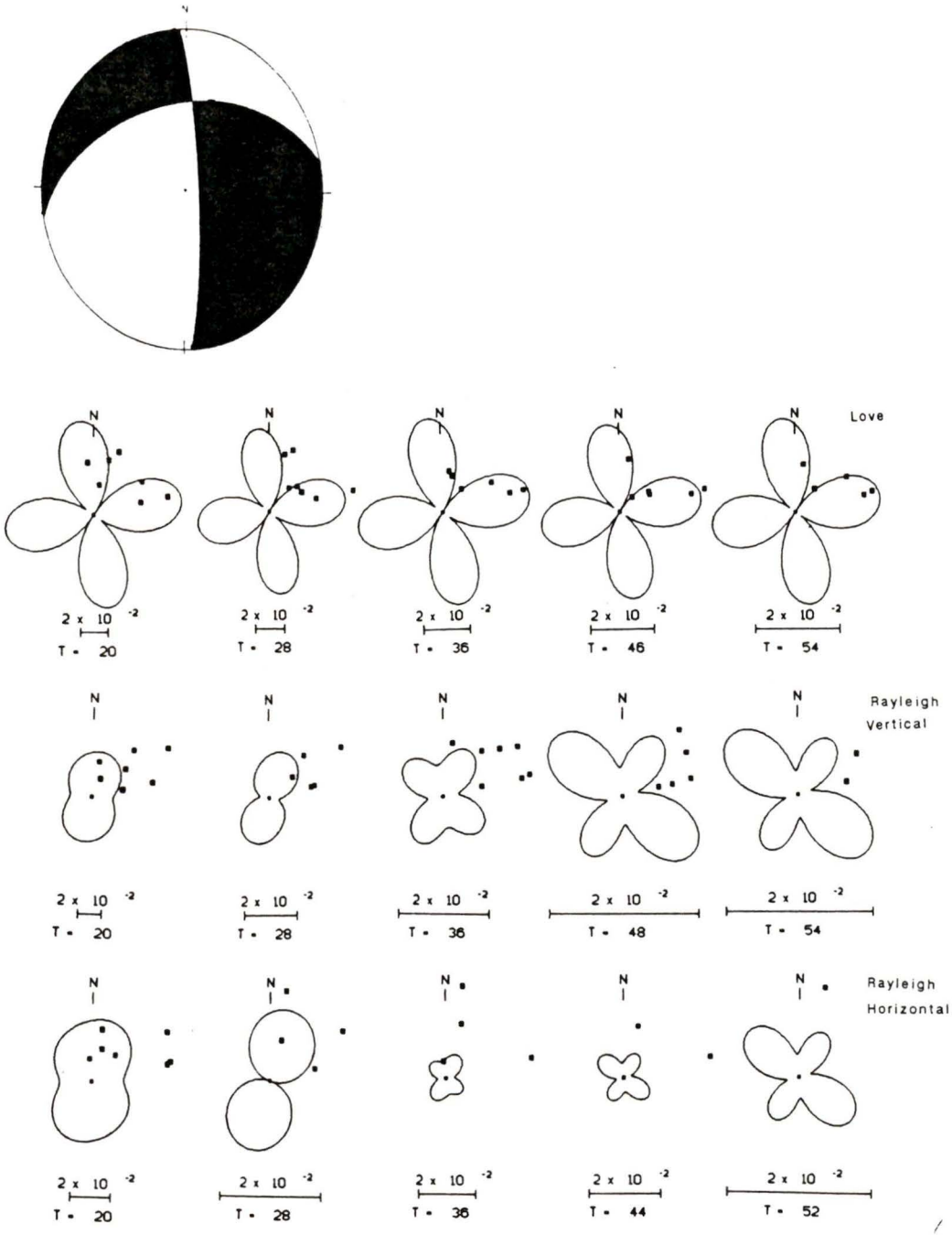

Figure 36 : Focal mechanism solution for the July 25th earthquake, obtained from surface wave inversion (Table 19). Love and Rayleigh wave radiation patterns are also shown for the inversion mechanism. Observed data are also shown (■).

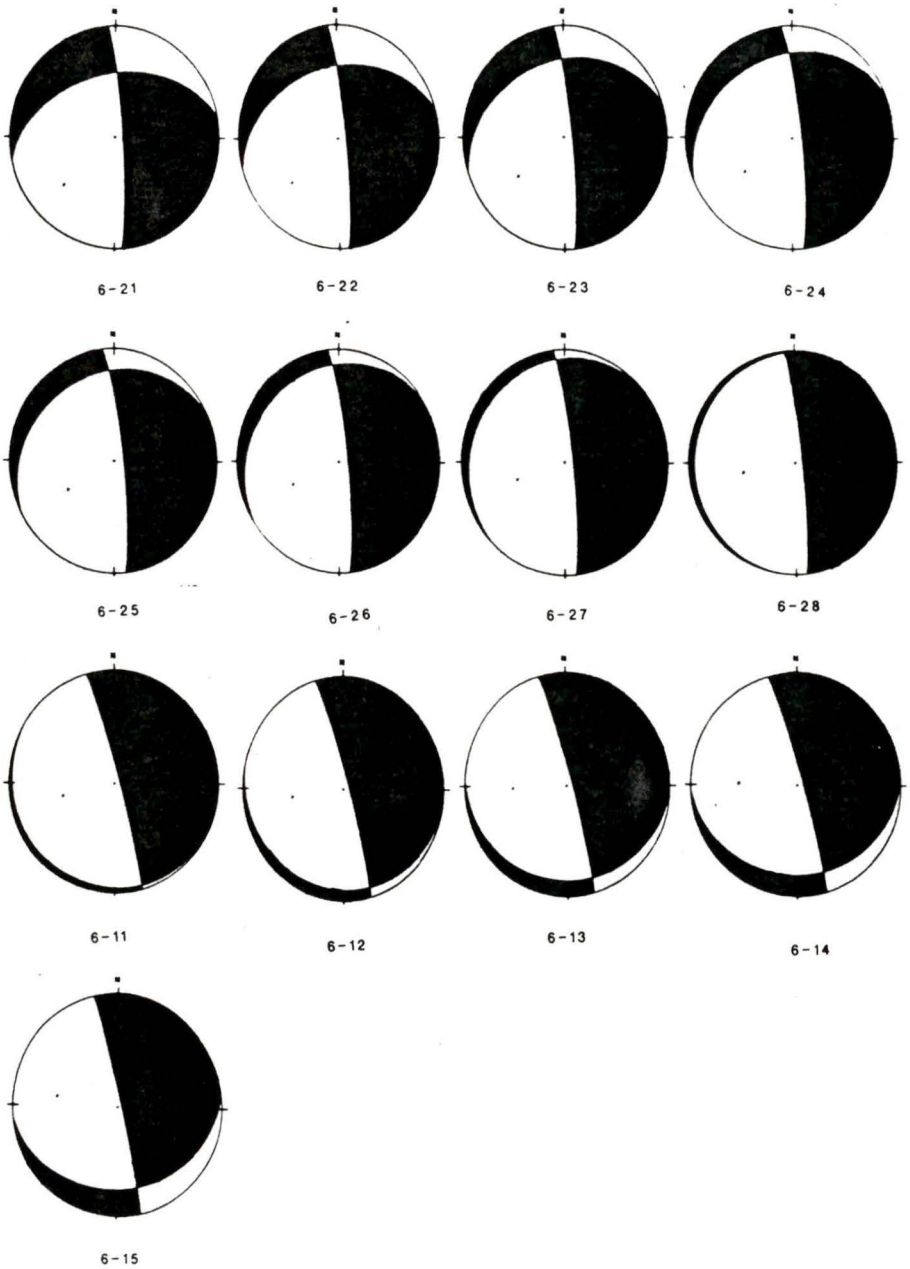

Figure 37 : Possible variations of the P-nodal solution for the June 2nd earthquake (Table 20). The mechanism numbers referred to in the text are printed below each plot. Mechanisms 6-22 through 6-25 best fit the surface wave data.

RADPAT was used along with the final, refined data sets (§ 5.3.2). Herrmann's original inversion program, QUESTION, was also used to evaluate the variations, since it computed mechanism scores for each supplied mechanism.

Mechanism	Dip	Slip	Strike	Score	L/R Residual
6-21	42°	-10°	-102°	0.56	0.808
6-22	36°	-12°	-105°	0.65	0.452
6-23	31°	-14°	-108°	0.64	0.153
6-24	27°	-18°	-113°	0.55	0.110
6-25	22°	-22°	-117°	0.45	0.343
6-26	17°	-28°	-123°	0.29	0.463
6-27	12°	-38°	-134°	0.21	0.712
6-28	6°	-72°	-168°	0.20	0.954
6-11	6°	-134°	120°	0.08	1.156
6-12	11°	-152°	101°	0.19	0.968
6-13	16°	-161°	93°	0.28	0.742
6-14	20°	-166°	87°	0.41	0.532
6-15	26°	-172°	83°	0.50	0.163

Table 20 Variation of the first-motion focal mechanism for the June event (Fig. 37). The fit of the observations is indicated by the score (see text). Slip is the motion of the hanging wall with respect to the footwall (Aki and Richards, 1980).

Thirteen different focal mechanisms, 6-21 through 6-28 and 6-11 through 6-15, were tested for the June event (Fig. 37). The Love wave data proved to be more diagnostic than the Rayleigh wave data. The former were better defined and particularly sensitive to the rotations of the NE striking plane. On the basis of the Love wave data, the solutions with planes dipping at less than 26° were eliminated. The Rayleigh wave data were relatively insensitive to the different mechanisms. The remaining mechanisms, 6-21 through 6-24 and 6-15, allowed for a plane dipping between 27° and 42° to the NW or a plane dipping at 26° to the SW. The

mechanism scores provided by QUESTION (Table 20) indicated that mechanism 6-22 best fit the data.

Mechanism	Dip	Slip	Strike	Score	L/R Residual
7-11	41°	-158°	99°	0.33	1.760
7-12	34°	-154°	102°	0.44	1.264
7-13	22°	-139°	118°	0.15	0.805
7-14	15°	-94°	164°	0.04	0.572
7-15	21°	-45°	-143°	0.15	1.037
7-16	32°	-28°	-125°	0.01	1.640
7-17	42°	-21°	-117°	0.01	2.243

Table 21 Variations of the first-motion focal mechanism for the July event (Fig. 38). The fit of the observations to the mechanisms is indicated by the score (see text).

Seven focal mechanisms, 7-11 through 7-17, were examined for the July event. Using Love wave data, solutions with planes dipping at less than 22° were eliminated. The longer period vertical component data, 30 s ≤ T ≤ 50 s, made it possible to discard the southward dipping east-west planes, 7-11 through 7-15. The two remaining solutions constrain the east-west plane to a dip of between 41° and 34°. The QUESTION scores (Table 21) showed that mechanism 7-16 best fit the data.

Because of the similarity of the two earthquakes, eliminating the southward dipping, NE striking plane from the July mechanism implies that the same can be done for the June event. This considerably improves the constraints on both solutions.

5.5 Love-Rayleigh Amplitude Ratios

The surface wave spectral amplitudes at a distant station are functions of the source mechanism, the station's position relative to the hypocentre and propagation effects (Yan and Alexander, 1990). By using a

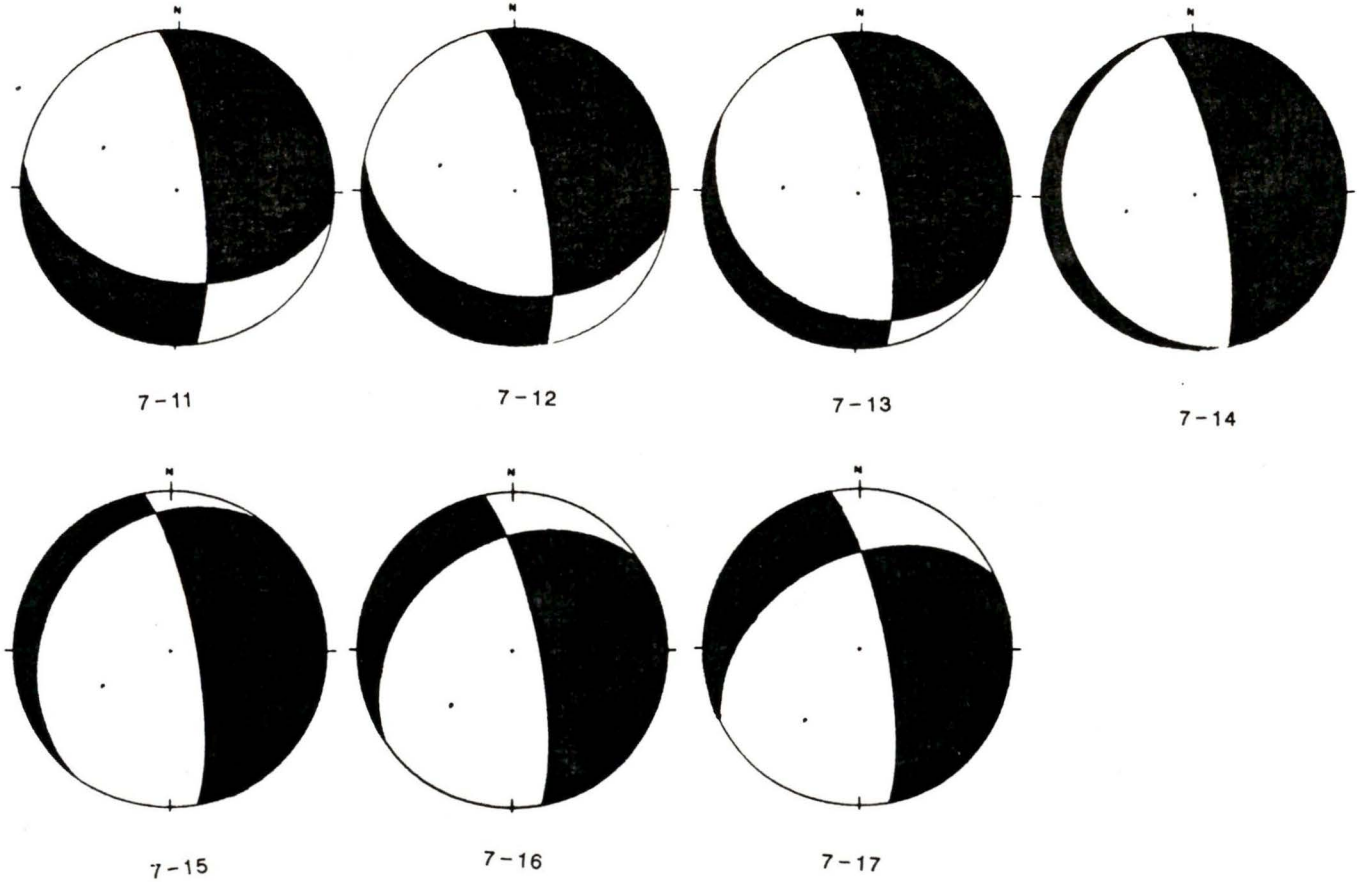

Figure 38 : Possible variations of the P-nodal solution for the July 25th earthquake (Table 21). The mechanism numbers referred to in the text are printed below each plot. Mechanisms 7-16 and 7-17 best fit the surface wave data.

L/R technique, some of these effects can be removed from consideration when comparing observed and theoretical data. The remaining factors depend only on the earth model, the mechanism orientation and focal depth. It is not necessary to know the seismic moment or to compensate for propagation effects.

An unsophisticated L/R technique was used to determine the focal depths and to constrain the P-nodal mechanism variations. The data for this study were a subset of the final set of spectral amplitudes used in the preceding sections. The L/R data sets were smaller than the originals since each Love observation required a corresponding Rayleigh amplitude at the same period.

5.5.1 Method

The program, LRR, was another adaptation of QUESTION (Herrmann, 1978). The data were corrected for attenuation and Love-Rayleigh amplitude ratios were calculated for each station and period. Theoretical spectral amplitudes were obtained for each supplied trial mechanism and the residuals at each station computed. The amplitude ratio residuals were averaged for each period and for each mechanism.

Yan and Alexander (1990) did not correct the observed data for attenuation. They maintained that the attenuation coefficients for Love and Rayleigh waves were approximately equal and could be discarded. However, using the observed data, a 20% difference was found between the corrected and uncorrected amplitude ratios.

5.5.2 Analysis

In constraining the P-nodal solutions for the June earthquake, the results were similar to those obtained from the forward modelling. Mechanism 6-24, one which fit the observed data reasonably well, had the

smallest average residual. Two other mechanisms, 6-15 and 6-23, had residuals which were only slightly greater than that of mechanism 6-24 (Table 20). Mechanism 6-15 was discarded since the forward modelling had eliminated all southward dipping planes.

The depth trials were conducted using the inversion mechanism, which had a L/R residual of 0.165, since it had the best overall fit to the observed data. Initially, depths were tested between 0 km and 30 km, at 5 km intervals; the smallest residuals were found for a focal depth of 10 kilometres. The process was repeated for the depth interval between 5 and 15 km, using a 1 km spacing. The smallest residual was again found at a focal depth of 10 km (Fig. 39).

When the July P-nodal variations were run through LRR, the smallest residuals were produced by mechanism 7-14, which is significantly different from those produced by the inversion and forward modelling. The first-motion data indicated that the June and July events had very similar focal mechanisms. The L/R results were the only ones to contradict this so the data were re-examined. From the surface wave radiation patterns for the P-nodal variations, it was apparent that the Rayleigh vertical data fit the theoretical curves poorly. The Love wave data fits to the theoretical curves for mechanism 7-14 were the poorest of all. These observations, coupled with the scatter in the July data indicate that these data were not suited to the L/R method.

5.6 Summary of Results

The surface wave magnitudes of the events (June: 5.21 and July: 5.16) were redetermined using common stations and individual M_s values computed from appropriate periods. The individual magnitudes, when plotted by azimuth, reflected the surface wave radiation pattern for the Rayleigh vertical component. This provided a crude indication of the locations of the nodes and lobes in the radiation pattern.

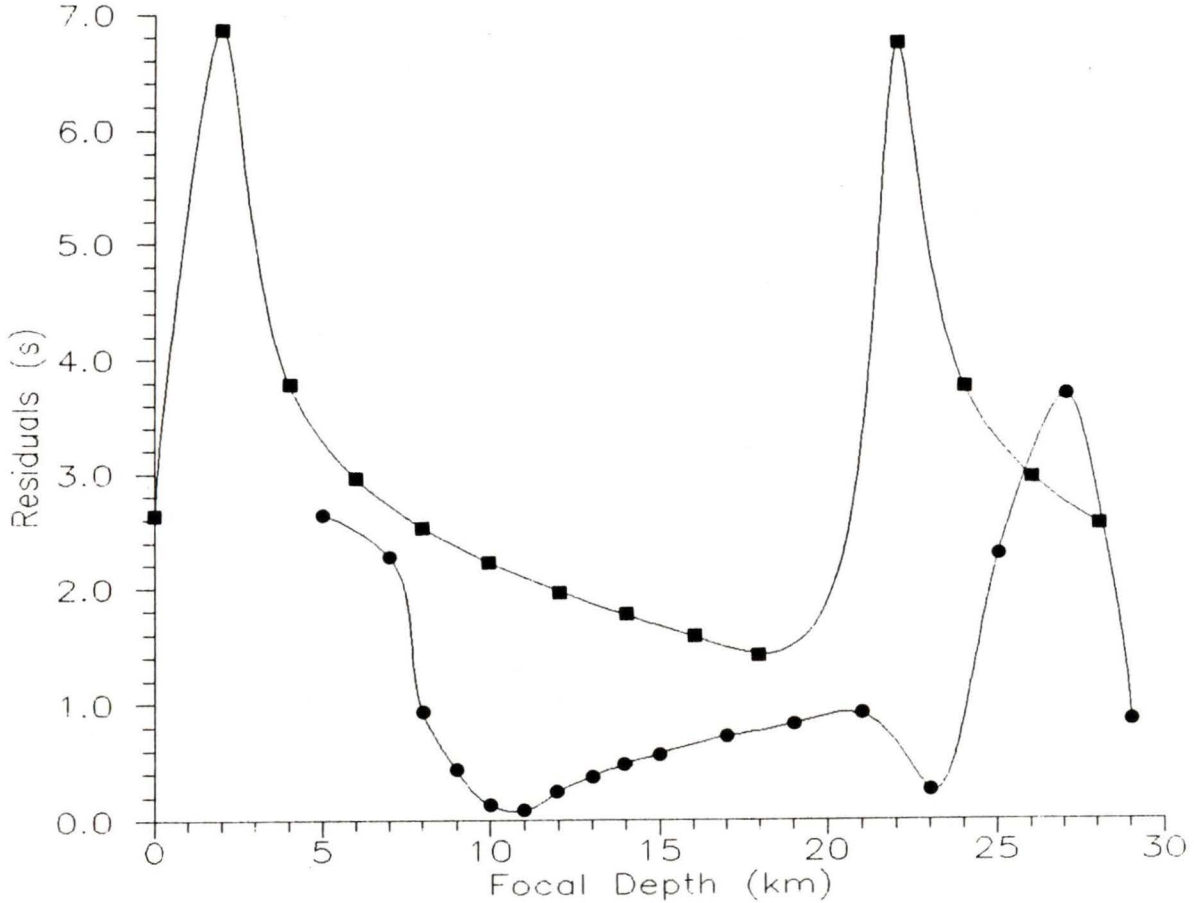

Figure 39 : Variation of the Love/Rayleigh amplitude ratio residuals by depth, for the June (●) and July (■) events.

The focal mechanisms determined from the inversion of surface wave data were similar to one another and to the principal P-nodal solutions. The July data were generally more scattered than the June data, which was reflected in the scores of the inversion solutions.

The first-motion mechanisms for both earthquakes were constrained using forward modelling and Love-Rayleigh amplitude ratios. Planes dipping south and at less than 26° were eliminated for both events. The June mechanism had a plane striking NE, dipping NW at 26°-36° and one striking N, dipping E at 75°-85°. The July mechanism was similar, with the NE striking plane dipping NW at 32°-45° and the N striking plane dipping E at 75°-85°.

The Love-Rayleigh amplitude ratio method could only be used for the June earthquake. The method was applied to the July data but the results were discarded because of inconsistencies in the data. The focal depth of the June event was found to be 10 kilometres with this method.

Chapter 6: Stress Drop Determination

6.1 Introduction

The stress drops of the events were determined from the far field displacement spectra. The stress drop data were used to estimate the size of the rupture surface.

The dynamic stress drop of an earthquake ($\Delta\sigma$) is the difference between the initial stress across the fault and the level of kinetic friction on the fault (Snoke, 1987). The dynamic stress drop provides an estimate of the static stress drop; i.e., the average difference between the initial and final stress across the fault plane. The seismic efficiency (ϵ) is the ratio of the dynamic stress drop to the static stress drop. The stress drop is complete when $\epsilon = 1$.

The data were obtained from the digital telemetered network in SW B.C. The four stations operating at the time were ALB, PGC, PIB and HYC; all of which are short period instruments.

6.2 Method

Usually, when stress drops are determined from the far field displacement spectra, broad band data are used. This is because both the long period characteristics and the high frequency decay of the displacement spectrum must be observed (Hanks and Thatcher, 1972). Under ideal conditions, the displacement spectra show the zero frequency amplitude (Ω_o), which remains constant up to the corner frequency (ν_c), when the amplitude begins to decay. The slope of the decaying spectrum is related to ϵ.

The difficulty posed by short period data is that it is difficult to estimate Ω_o. The instrument response falls off dramatically in the region of interest. When the instrument correction is applied, the spectra do not

reach a constant, low frequency level but increase continually as the noise is amplified.

The stress drops were calculated with Brune's (1971) relation, which requires Ω_o, ν_c, the epicentral distance in metres (R) and the density of the medium (ρ):

$$\Delta\sigma = 106\ \rho\ R\ \Omega_o\ \nu_c^3 \qquad (4)$$

Note that $\Delta\sigma$ varies as the cube of ν_c and is highly susceptible to errors in picking the corner frequency.

The relation between stress drop and the source dimension was defined by Brune (1971).

$$r^3 = \frac{7}{16}\frac{M_o}{\Delta\sigma} \qquad (5)$$

6.3 Analysis

The far field displacement spectra were corrected for instrument response and plotted (Figs. 40, 41). The zero-frequency level estimate was based on the largest amplitude at the low frequency end of the spectrum. The character of the spectra changed between 0 and 0.1 Hz, where the amplitudes began to increase without bound. The highest spectral amplitude before this point was selected as Ω_o. The choice of each Ω_o was entirely subjective, moderated only by how the spectra compared with one another.

The Ω_o estimates were verified by computing the seismic moment from Ω_o, using equation 6 (Hanks and Thatcher, 1972) and comparing the results with those obtained from the surface wave analysis. The resulting moments were all within a factor of 2 or 3 of the surface wave values. The S wave velocity (β) was obtained from the Georgia Straits model (Table 3).

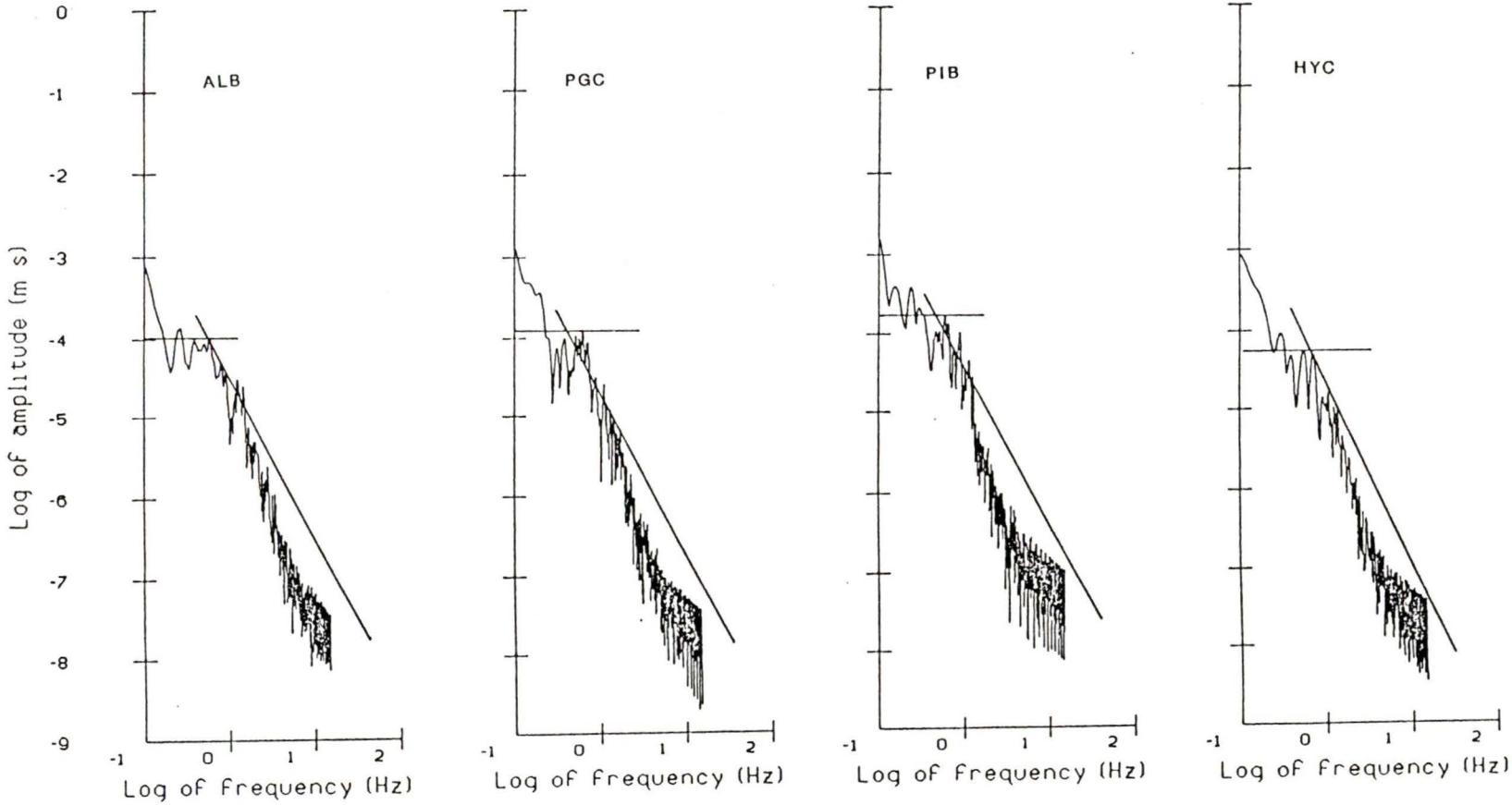

Figure 40 : Far field displacement spectra at the WCTN stations, for the June earthquake. The zero frequency levels and corner frequencies have been indicated in each case.

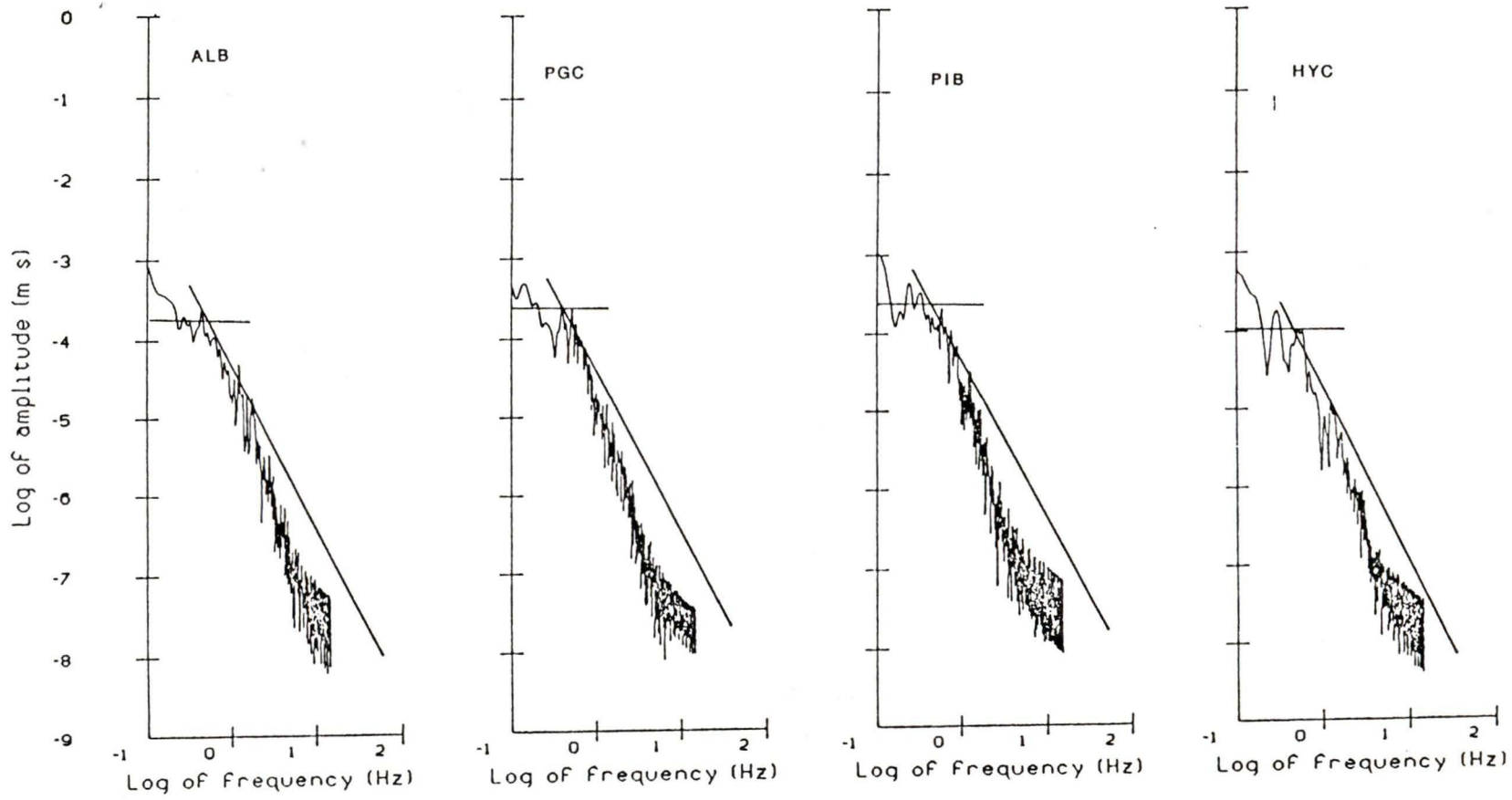

Figure 41 : Far field displacement spectra at the WCTN stations, for the July earthquake. The zero frequency levels and corner frequencies have been indicated in each case.

$$M_o = 4\pi\rho\beta^3 R\Omega_o \qquad (6)$$

The corner frequency was determined by the intersection of the zero-frequency level with the line fitted to the decaying portion of the spectrum. The latter was fitted by hand, assuming a value of 1 for ϵ.

Stations	June	July
Port Alberni	14 bars	18 bars
Haney	17 bars	11 bars
PGC	16 bars	17 bars
Pender Is.	19 bars	17 bars
Averages	16 bars	16 bars

Table 22 Stress drop estimates from the WCTN stations.

The stress drops (Table 22) were calculated using equation 4 with a density at the source of 2780 kg/m^3; from the Ben-Menahem and Singh earth model (Table 18). The average stress drop for both events was 16 bars. The individual stress drop estimates varied between 11 and 19 bars. Given the subjective nature of the corner frequency estimates, it would be reasonable to assume that the stress drops were anywhere between 10 and 20 bars.

6.4 Rupture Surface

The seismic moments used to determine the size of the rupture surface were obtained from the surface wave study. Using the average stress drops determined in § 6.3, the radii of the rupture surfaces were found to be 3.5 km for the June event and 3.2 km for July.

Estimates of the rupture surface area of the June event were also determined from the aftershock data (§ 2.2.2), using two different interpretations of the aftershock areas. The rupture surface radii were

found to be between 1.9 km and 4.6 km, after Mendoza and Hartzell (1988) and Kanamori and Anderson (1975) respectively. The rupture surface area of the June event, estimated from the stress drop, lay within these bounds.

The uncertainties involved in the stress drop estimates and aftershock locations are too great to conclude anything more than that the rupture surface area for the June event was between 11 and 66 km^2. The similarity of the Brooks Peninsula events indicates that the rupture surface of the July event was roughly the same size.

6.5 Summary of Results

The stress drops of the events were found to be between 11 and 19 bars, with an average value for each event of 16 bars. The radii of the rupture surfaces, determined from the stress drops, were found to be 3.5 km for June and 3.2 km for July, consistent with the values of 1.5 to 3.5 km determined from the aftershock data.

Chapter 7 : Discussion and Conclusion

The two earthquakes which occurred on the Brooks Peninsula in the summer of 1978, 02/06/78 and 25/07/78, are the largest events which have been recorded in the region. Both were followed by extensive aftershock sequences and a field program was mounted to monitor part of the first sequence. The data from the field program provided the means to locate the June hypocentre accurately and to determine the location bias introduced by the earth models. Teleseismic data were used to determine the relative locations of the events. The focal mechanisms of the events were determined using first-motion and surface wave data. The seismic moments and stress drops were also calculated from the surface wave data and far field displacement spectra respectively.

In this chapter, the results of each portion of the study will be summarized. A final interpretation for the earthquakes' source parameters and focal mechanisms will be given (Table 23). The discussion will focus on the implications of the results for the contemporary interactions between the Explorer and North American plates.

7.1 Summary of Results

The aftershock study indicated that the June epicentre was located on the NW shore of the peninsula (50.15°, -127.83°), with a focal depth between 10 and 20 km. The regional seismic stations detected 15 locatable aftershocks for the June event and only 1 for July. The number of aftershocks observed at PHC also indicated greater levels of activity following the earlier event. The largest June aftershock was only 0.8 magnitude units smaller than the mainshock while the only locatable July aftershock was 2.3 units smaller than the July event. The best located locally detected aftershocks indicated a rupture surface that was between 1.9 and 4.6 km in radius. Cross-sections constructed from the same data

Date	02 June 1978	25 July 1978	Comment
Origin Time	20:40:42.9 ± 0.8s	23:30:50.6 ± 0.2s	I.S.C.
Coordinates	50.15° ± 3.5 km	-127.83° ± 3.5 km	Aftershocks
Focal Depth	10-20 km		Aftershocks
M_s	5.2 ± 0.2	5.1 ± 0.2	CSSN Data and I.S.C.
Moment	1.60×10^{24} dyne·cm	1.19×10^{24} dyne·cm	Surface Wave Data
Stress Drop	16 bars	16 bars	WCTN Data
Mechanism	Normal Faulting Strike 235°-260°, Dip NW 26°-42° Sinistral, Strike-slip or Strike 350°-001°, Dip E 75°-85° Dextral, Dip-slip		First-motion and Surface wave inversion
Rupture Area	34 km^2	28 km^2	Stress Drops

Table 23 Summary of the source parameters for the Brooks Peninsula earthquakes. The source from which each was determined is also indicated.

set showed the least scatter on a NW-SE section, dipping NW.

The initial G.S.C. epicentres of the regionally detected aftershocks were scattered up to 20 km to the east of their true positions. The events were relocated using only the data from PHC and GDR. The final epicentres, after the application of travel time corrections, were 5 km west of the locally detected events. In relocating these aftershocks, it was found that the epicentres were mislocated 3-4 km to the east when the Canadian Shield model was used. A similar displacement to the west was observed with the Georgia Straits model.

The regional seismicity, from 1978 to 1987, was relocated in the same fashion as the regional aftershocks. The events were found to be concentrated off the north shore of the peninsula and not spread over the entire region, as the original G.S.C. data indicated.

The teleseismic location of the mainshock epicentres indicated that the two events were coincident within location uncertainties. The In all of the experiments, the July epicentre was always placed to the east of the June event. Epicentre solutions obtained using the Jeffreys-Bullen earth model and data from $\Delta > 20°$ were found to be the best; i.e., they were closest to the epicentre determined from the aftershocks. The location bias caused by the inclusion of the nearer stations moved the solutions roughly 12 km NE. The focal depths, determined using the teleseismic *P* wave travel time residuals at common stations, indicated that the June event was at 16 km and the July event at 11 km.

The focal mechanisms of the two earthquakes could not be uniquely determined using the first motion data. The solutions for both events were very similar but one plane was poorly constrained. The mechanisms showed normal faulting on a N striking plane, which dipped 75°-85° E, and on a poorly constrained NE striking plane. The motion on the latter was sinistral and almost entirely strike-slip while the motion was dextral and dip-slip on the former. The composite focal mechanism, constructed from the aftershock data, was almost identical to that of the June mainshock. The *P* waveforms for the two mainshocks were found to be very similar, implying that the two events occurred on the same fault plane.

Inversion of the surface wave data produced focal mechanisms for each event which were similar to one another and to the first-motion solutions. The seismic moments were found to be 1.60×10^{24} dyne·cm for June and 1.19×10^{24} dyne·cm for July. Combining the surface wave and first-motion data, it was possible to constrain the focal mechanism solutions further. Solutions with shallowly dipping or southward dipping planes were eliminated. In the final solutions, the NE striking plane was found to be dipping at between 27° and 45° (NW) and the N striking plane dipped at between 75° and 85° (E). The surface wave magnitudes were redetermined using additional data and found to be 5.2 for June and 5.1 for July, the same as the I.S.C. values. The azimuthal distribution of M_s values

reflected the surface wave radiation pattern for the vertical Rayleigh wave component. The focal depth of the June event was found to be approximately 10 km using Love/Rayleigh amplitude ratios.

Stress drops were determined from the far field displacement spectra observed at the WCTN stations. Both events showed average stress drops of 16 bars. The relatively low values indicate that the earthquakes did not occur on new or well cemented, older fractures. The rupture surfaces were found to be 3.5 km and 3.2 km in radius, for June and July respectively. The June value was consistent with the bounds established by the aftershock study.

7.2 Discussion

It is immediately apparent from these results that the Brooks Peninsula earthquakes were essentially identical. The surface wave magnitudes, seismic moments and stress drops showed both events to be of similar size. The July event was slightly smaller than its predecessor, which is reflected in the levels of aftershock activity and in the magnitudes and seismic moments.

The epicentre solutions indicated that the events were adjacent or coincident. The aftershock activity patterns, focal mechanisms and first-motion waveforms indicated that both events occurred on the same fault. Thus, it is likely that the Brooks Peninsula earthquakes were adjacent events on the same fault.

The teleseismic epicentre solutions always placed the July epicentre east of the June epicentre, independent of data set or method. There was no indication as to whether the July epicentre was located to the north or south of the June event. It was not possible to identify the *S* arrivals at nearby stations, from which the *S-P* intervals would have been diagnostic.

The focal depths of the events could not be determined precisely. However, the locally detected aftershocks indicated a focal depth of

10-20 km for the June event, as did the surface wave data. Teleseismic *P* wave data suggested a focal depth of 16 km for June and 11 km for July. These depth estimates are equal, within the 5 km uncertainties, to those of the I.S.C. (13 km for June and 6 km for July) which were determined from *pP* arrivals. The relative depths of the two events are also consistent, the I.S.C. and *P* wave data both indicate that the June event was deeper than the July event. All of the focal depth estimates place the foci in the crust, above the subducting Explorer plate (Fig. 42).

The focal mechanisms showed normal faulting on a N striking fault which dipped steeply E and on a NE striking fault which dipped moderately to the NW. The motion on the former was dextral and evenly divided between the strike and dip components. The NE striking plane showed sinistral motion which was almost entirely strike-slip. The pressure axes of the mechanisms had azimuths around 230°, with plunges of ~ 40°. The horizontal motion vectors, describing the motion of the hanging wall, were between 000° and 020° for the N striking plane and between 230° and 270° for the NE striking plane.

7.2.1 Tectonic Implications

The possibility that the Brooks Peninsula earthquakes were reflecting the subsidence of the peninsula was considered. However, using Parsons and Sclater's (1977) empirical relation for the subsidence of a mid-ocean ridge (Eqn. 7) and assuming that subsidence began at 2 Ma BP, the rate of subsidence was found to be ~ 1 mm/yr. The rate would be somewhat greater for continental crust, without sea water compensating for changes in elevation, but comparable and negligible in terms of plate motion velocities.

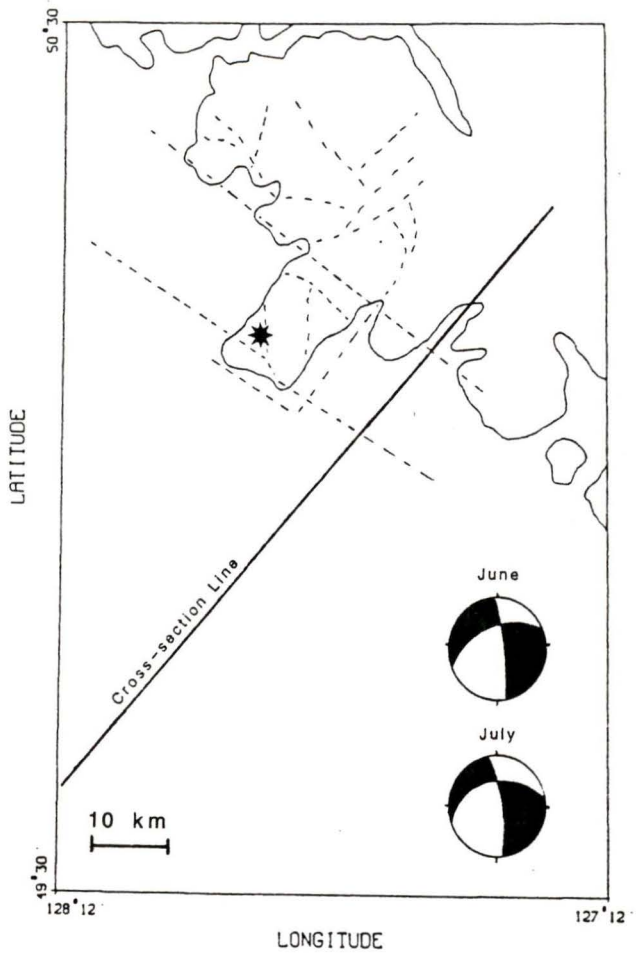

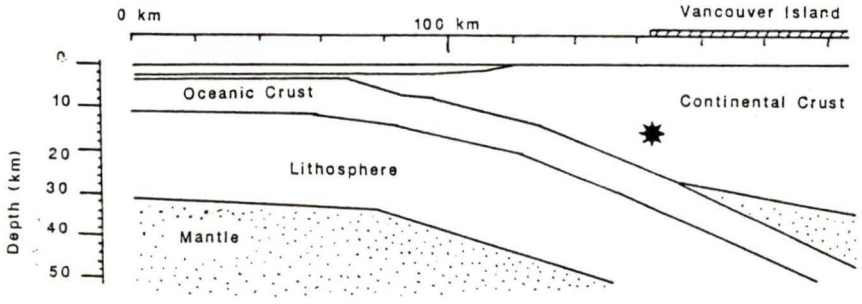

Figure 42 : Epicentres of the Brooks Peninsula earthquakes, shown in relation to geography and to the subducting plate. Also shown are the focal mechanisms. Faults are shown as dashed lines (Muller *et al.*, 1975) and only in the immediate vicinity of the peninsula. The cross section was adapted from Dehler (1991) and is based on seismic reflection and gravity models.

$$e(t) = 2500 + 350\sqrt{t} \quad (7)$$

It is more likely that the earthquakes were reflecting the relative motions of the Explorer and North American plates. As of 0.5 Ma BP they were converging in a NE direction (Riddihough, 1984). Extrapolating the present day position of the EXP/NAM rotation pole, from the positions prior to 0.5 Ma BP as determined by Riddihough (1984), placed it south of the Explorer plate (Fig. 43). Rotation about this point produces NNE convergence between the plates at the southern end of the Explorer plate. The orientation of the pressure axes of the mechanisms is consistent with NE compression. Locating the rotation pole further south would produce a more NE or ENE convergence vector. Given that the uncertainties on Riddihough's pole positions are on the order of 100 km (Riddihough, 1984), a more southern rotation pole is feasible.

In order for these earthquakes to have occurred in response to the EXP-NAM motions, there would have to be coupling between these plates along the subduction interface. The events occurred within the overlying plate and not at the interface (Fig. 42), implying that the plates are locked near that point and the stress generated by their relative motions was transmitted into the interior of the plate. However, the horizontal motion vectors may not directly reflect the relative plate motions. Shallow crustal earthquakes occur along existing faults (McKenzie, 1969), thus the horizontal motion vectors will only reflect the movements along conveniently oriented faults.

There is no conclusive evidence to indicate which is the fault plane. Both nodal planes are consistent with regional fault patterns (Muller *et al.*, 1975). The aftershock cross-sections gave no indication of the fault plane orientation. The relative mainshock epicentre locations always show the July epicentre to the east of the June event. The relative latitudes of the events are not indicated, leaving the fault strike in any direction from NE to SE, although a north-south strike was never

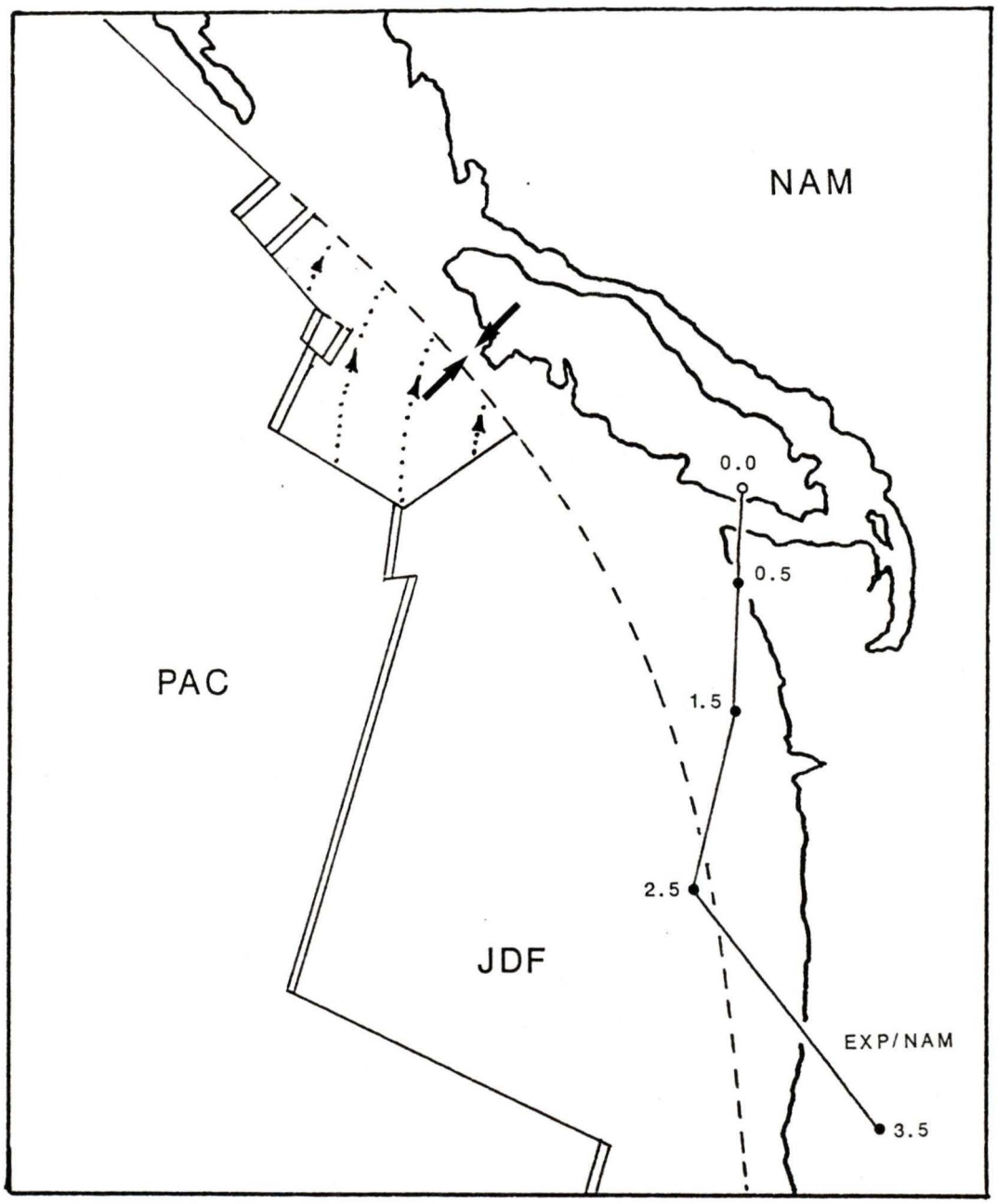

Figure 43 : Progression of the rotation pole of the Explorer with respect to the North American plate (EXP/NAM) The ages of the rotation poles (●) are given in Ma. The present position of the pole (○) has been extrapolated from the past positions. The rotation of the Explorer plate about the extrapolated pole is indicated by the dotted lines. The solid arrow indicates the P-axis strike. Transform boundaries are shown as solid lines, spreading ridges as double lines and the dashed lined is the convergent margin.

indicated. Finally, the epicentres in the regional seismicity pattern formed a NE trending line off the north shore of the peninsula, consistent with the preferred fault plane.

The regionally detected aftershocks were displaced 5 km to the west of the locally detected events. If this offset is real, then it is possible that other earthquakes in the region have also been displaced to the west. This would put the regional seismicity and the Brooks Peninsula events in the same place, off the NW coast of the peninsula.

The pattern of seismicity and the location of the Brooks Peninsula events does raise the question of why the activity is concentrated in one small area. There is obviously coupling between the North American plate and the Explorer plate but it manifests itself only in one place. A possible explanation is that the peninsula, once uplifted by the presence of the triple junction, is now subsiding with its passing. As the peninsula settles, the coupling between the plates increases, leading to a restricted region of seismicity.

7.3 Conclusion

The Brooks Peninsula earthquakes, June 2nd and July 25th 1978, occurred on the northwestern shore of the peninsula, at focal depths between 10 and 20 km. The earthquakes were found to be coincident and were indicated to be adjacent events on a common fault. Well constrained focal mechanisms were determined using first-motion and surface wave data. The mechanisms of the two events were essentially identical, also indicated by the first-motion wave forms. The preferred fault plane displayed sinistral, normal strike-slip faulting along a NE striking fault, dipping 30°-45° northwest. The alternate plane displayed dextral motion on a steeply dipping, north striking fault. There was no strong evidence to preclude the possibility of the alternate plane being the fault plane.

The aftershock sequence associated with the June event made it possible to locate the mainshock epicentres accurately. Using the aftershock data, travel time corrections were developed for events in the immediate vicinity of the peninsula.

The initial G.S.C. epicentres of regionally detected aftershocks were mislocated to the east by 20 km. This was corrected by relocating the events using only the data from the stations at Port Hardy and Gold River. The relocated solutions were slightly west of the peninsula and the travel time corrections pulled the epicentres 2-3 km east, to the NW shore of the peninsula.

Other earthquakes in the Brooks Peninsula region were relocated in the same fashion. The new epicentres indicated that the regional seismicity was confined to a small area near the NW coast of the peninsula.

When the mainshock epicentres were located using all available teleseismic data, upper mantle effects pulled the solutions 12 km to the northeast. The same effect was also noted by Wahlström and Rogers (1990) in their study of offshore events. Epicentre solutions closest to the locations determined from the aftershock study were obtained using only data from $\Delta \geq 20°$ and the Jeffreys-Bullen earth model.

Bibliography

Aki, K., and P.G. Richards, 1980, *Quantitative Seismology.*, 2 Volumes, San Francisco: W.H. Freeman and Co.

Armstrong, R.M., J.E. Muller, J.E. Hakaral, and K. Muehlenbachs, 1985, The Neogene Alert Bay Volcanic Belt of Northern Vancouver Island, Canada: Descending-Plate-Edge Volcanism in the Arc-Trench Gap, *Journal of Volcanology and Geothermal Research*, **26**, 75-97.

Båth, M.,1979, *Introduction to Seismology*. Basel: Birkhauser Verlag.

Ben-Menahem, A., and S.J. Singh, 1981, *Seismic Waves and Sources*. New York: Springer-Verlag.

Brune, J.N., 1970, Tectonic Stress and the Spectra of Seismic Shear Waves from Earthquakes. *Journal of Geophysical Research*, **75**, No. 26, 4997-5009.

Brune, J.N., 1971, Correction. *Journal of Geophysical Research*, **76**, 5002.

Bulletin of the International Seismological Centre, 1979, **15**, No. 6.

Byerly, P., 1950, Release of Energy at the Source of an Earthquake. *Publications of the Dominion Observatory*, **24**, No. 10, 303-304.

Cande, S.C., and R.B. Leslie, 1986, Late Cenozoic tectonics of the southern Chile Trench, *Journal of Geophysical Research*, **91**, 471-497.

Carbotte, S.M., J.M. Dixon, E. Farrar, E.E. Davis, and R.P. Riddihough, 1989, Geological and Geophysical Consequences of the Tuzo Wilson Seamounts: implications for plate geometry in the vicinity of the Pacific - North America - Explorer triple junction, *Canadian Journal of Earth Sciences*, **26**, 2365-2384.

Cassidy, J.F., R.M. Ellis, and G.C. Rogers, 1988, The 1918 and 1957 Vancouver Island Earthquakes. *Bulletin of the Seismological Society of America*, **78**, No. 2, 617-635.

Davis, E.E., and R.P. Riddihough, 1982, The Winona Basin: Structure and Tectonics, *Canadian Journal of Earth Sciences*, **19**, 767-788.

Dehler, S.A., 1991, Integrated geophysical modelling of the northern Cascadia subduction zone, *Ph.D. Thesis*, University of British Columbia, Vancouver, 143 pp.

Duda, S.J., and O.W. Nuttli, 1974, Earthquake Magnitude Scales, *Geophysical Surveys*, 1, 429-458.

Drew, J.J., and R.M. Clowes, 1990, A re-interpretation of the seismic structure across the active subduction zone of western Canada, *in* Studies of laterally heterogeneous structures using seismic refraction and reflection data, A.G. Green, ed., Geological Survey of Canada, Paper 89-13.

Dziewonski, A.M., and D.L. Anderson, 1983, Travel Times and Station Corrections for P Waves at Teleseismic Distances, *Journal of Geophysical Research*, **88**, No. B4, 3295-3314.

Forsythe, R., and E. Nelson, 1985, Geological manifestations of ridge collision: evidence from the Golfo de Penas-Taito Basin, southern Chile, *Tectonics*, **4**, 477-495.

Hanks, T.C., and W. Thatcher, 1972, A Graphical Representation of Seismic Source Parameters. *Journal of Geophysical Research*, **77**, No. 23, 4393-4405.

Herrmann, R.B., 1973, Some Aspects of Band-Pass Filtering of Surface Waves, *Bulletin of the Seismological Society of America*, **63**, No. 2, 663-671.

Herrmann, R.B., 1978, ed., *Computer Programs in Earthquake Seismology*, 2 Volumes, Department of Earth and Atmospheric Sciences, St. Louis University.

Hodgson, J.H., and J.F. Allen, 1965, Tables of Extended Distances for PKP and PcP, *Publications of the Dominion Observatory*, **16**, No. 10, 329-348, (Reprint).

Hyndman, R.D., C.J. Yorath, R.M. Clowes, and E.E. Davis, 1990, The Northern Cascadia Sunduction Zone at Vancouver Island: Seismic Structure and Tectonic History. *Canadian Journal of Earth Sciences*, **27**, 313-329.

Jeffreys, H., and K.E. Bullen, 1940, 1958, *Seismological Tables*. British Association for the Advancement of Science, Gray-Milne Trust.

Kanamori, H., and D.L. Anderson, 1975, Theoretical Basis of Some Empirical Relations in Seismology, *Bulletin of the Seismological Society of America*, **65**, 1073-1095.

Keen, C.E., and R.D. Hyndman, 1979, Geophysical Review of the Continental Margins of Eastern and Western Canada, *Canadian Journal of Earth Sciences*, **16**, 712-747.

Knopoff, L, 1960, Analytical Calculation of the Fault-Plane Problem. *Publications of the Dominion Observatory*, **24**, No. 10, 309-315.

Lahr, J.C., 1984, Hypoellipse/VAX : A Computer Program for Determining Local Earthquake Hypocentral Parameters, Magnitude and First Motion Pattern, *Open File Report*, U.S. Geological Survey, Menlo Park, CA., 67 pp.

Marshall, P.D., and P.W. Basham, 1972, Discriminations Between Earthquakes and Underground Explosions Employing an Improved M_s Scale, *Geophysical Journal of the Royal Astronomical Society*, **28**, 431-458.

McKenzie, D.P., 1969, The relation between fault plane solutions for earthquakes and the directions of the principal stresses, *Bulletin of the Seismological Society of America*, **59**, 591-601.

McMechan, G.A., and G.S. Spence, 1983, P-wave velocity structure of the Earth's crust beneath Vancouver Island, *Canadian Journal of Earth Sciences*, **20**, 742-752.

Menard, H.W., 1978, Fragmentation of the Farallon Plate by Pivoting Subduction, *Journal of Geology*, **86**, 99-110.

Mendoza, C., and S.H. Hartzell, 1988, Aftershock Patterns and Main Shock Faulting, *Bulletin of the Seismological Society of America*, **74**, 1438-1449.

Mitchell, B.J., 1975, Regional Rayleigh Wave Attenuation in North America, *Journal of Geophysical Research*, **80**, 4904-4916.

Muller, J.E., K.E. Northcote, and D. Carlisle, 1974, Geology and Mineral Deposits of Alert - Cape Scott Map Area, Vancouver Island, British Columbia, Canada Department of Energy, Mines and Resources, Geological Survey of Canada Paper 74-8. Ottawa.

Nordquist, J.M., 1962, A Special-Purpose Program for Earthquake Location with an Electronic Computer, *Bulletin of the Seismological Society of America*, **53**, 431-437.

Parsons, B., and J.G. Sclater, 1977, An analysis of the variation of ocean floor bathymetry and heat flow with age, *Journal of Geophysical Research*, **82**, 803-827.

Press, W.H., B.P. Flannery, S.A. Teukolsky, and W.T. Vetterling, 1988, *Numerical Recipes: The Art of Scientific Computing*, Cambridge: Cambridge University Press, 818 pp.

Riddihough, R.P., 1977, A Model for Recent Plate Interactions off Canada's West Coast, *Canadian Journal of Earth Sciences*, **14**, 384-386.

Riddihough, R.P., 1984, Recent Movements of the Juan de Fuca Plate System, *Journal of Geophysical Research*, **89**, 6980-6994.

Riddihough, R.P., R.G. Currie, and R.D. Hyndman, 1980, The Dellwood knolls and their role in triple junction tectonics off northern Vancouver Island, *Canadian Journal of Earth Sciences*, **17**, 577-593.

Riddihough, R.P., and R.D. Hyndman, 1976, Canada's Active Western Margin - the Case for Subduction, *Geoscience Canada*, **3**, 269-278.

Rogers, G.C., 1983, *Seismotectonics of British Columbia*, Ph.D. Dissertation, University of British Columbia.

Rogers, G.C., 1988, An Assessment of the Megathrust Earthquake Potential of the Cascadia Subduction Zone. *Canadian Journal of Earth Sciences*, **25**, 844-852.

Rogers, G.C., J.F. Cassidy, and R.M. Ellis, 1990, The Prince George, B.C. Earthquake of March 21, 1986. *Bulletin of the Seismological Society of America*, **80**, No. 5, 1144-1161.

Shannon, W.E., R.J. Halliday, F. Lombardo, and D.R.J. Schieman, 1979, *Canadian Seismograph Operations - 1978*, Seismological Series Number 82, Energy, Mines and Resources Canada, Ottawa.

Smyth, W.R., 1985, Geology of the Brooks Peninsula, Vancouver Island, Paper 1985-1 of the Ministry of Energy, Mines and Petroleum Resources, B.C., 161-169.

Snoke, J.A, 1987, Stable Determination of (Brune) Stress Drops. *Bulletin of the Seismological Society of America*, **77**, 530-538.

Spence, G.D., 1984, Seismc Structure Across the Active Subduction Zone of Western Canada, *Ph.D. Thesis*, University of British Columbia, Vancouver, 191 pp.

Sutton, G.H., and E. Berg, 1958, Direction of Faulting from First-Motion Studies, *Bulletin of the Seismological Society of America*, **48**, 117-128.

Stevens, A.E., W.G. Milne, R.B. Horner, R.J. Wetmiller, G. Leblanc, and G.A. McMechan, 1976, *Canadian Earthquakes - 1968*, Seismological Series Number 71, Energy, Mines and Resources Canada, Ottawa.

Tsai, Y., and K. Aki, 1969, Simultaneous Determination of the Seismic Moment and Attenuation of Seismic Waves, *Bulletin of the Seismological Society of America*, **59**, 275-287.

Tsai, Y., and K. Aki, 1970, Precise Focal Depth Determination from Amplitude Spectra of Surface Waves, *Journal of Geophysical Research*, **75**, No. 29, 5729-5743.

Wahlström, R., and G.C. Rogers, 1990, Location of Earthquakes West of Vancouver Island, British Columbia. Submitted to *Canadian Journal of Earth Sciences*.

Wahlström, R., G.C. Rogers, and R.M. Ellis, 1990, Relocations and Focal Mechanisms of Large Earthquakes West of Vancouver Island, British Columbia. Submitted to *Bulletin of the Seismological Society of America*.

Weichert, D.H., and J.C. Newton, 1970, Epicentre Determination from First Arrival Times at Canadian Stations, in *Seismological Series of the Earth Physics Branch*, No. 59, Dept. Energy, Mines and Resources, Earth Physics Branch, Ottawa, Canada.

Wickens, A.J., and J.H. Hodgson, 1965, Computer Reevaluation of Earthquake Mechanism Solutions. *Publications of the Dominion Observatory*, **16**, No. 10.

Yan, B., and S.S. Alexander, 1990, Source Mechanism Study of the 1982 New Brunswick, Canada Earthquake Sequence Using Combined Surface Wave Methods, *Bulletin of the Seismological Society of America*, **80**, No. 2, 296-312.

Appendix A : Tables

The following pages contain tables of epicentre locations for the locally and regionally detected aftershocks, a summary of the seismicity in the Brooks Peninsula region, teleseismic travel time data and the first-motion data.

Table A-1 : Hypocentres of the aftershocks detected by the temporary array established on the peninsula between June 9th and June 12th, 1978. The hypocentres were determined using HYPOELLIPSE (Lahr, 1984) and a local crustal model (Table 2.1). The horizontal errors for the hypocentre solutions varied between 1 and 10 km, except for 2 events (78/06/10 23:00, and 78/06/12 18:13), both of which were located without any *S* phases and had errors in excess of 100 km.

The revised coordiantes for the reference event (78/06/12 10:52) have also been included in brackets.

Date - Origin Time	Coordinates	Depth	M_L
78/06/09 20:44:22.73	50°07.99′ -127°52.41′	17 ± 9	0.8
78/06/09 21:03:12.39	50°09.27′ -127°50.79′	18 ± 2	0.3
78/06/10 9:31:25.51	50°09.60′ -127°50.76′	19 ± 1	0.2
78/06/10 10:06:40.06	50°08.32′ -127°49.13′	17 ± 2	0.2
78/06/10 10:15:28.61	50°09.47′ -127°49.29′	18 ± 1	0.4
78/06/10 13:54:03.34	50°08.99′ -127°48.23′	16 ± 1	0.3
78/06/10 14:54:01.94	50°08.39′ -127°50.40′	18 ± 0	-0.2
78/06/10 15:21:17.87	50°07.69′ -127°50.94′	21 ± 2	0.5
78/06/10 16:20:13.08	50°08.95′ -127°50.66′	17 ± 3	0.4
78/06/10 18:39:07.05	50°08.83′ -127°49.80′	18 ± 1	0.7
78/06/10 19:12:41.62	50°08.50′ -127°52.68′	17 ± 1	-0.2
78/06/10 21:29:24.67	50°07.63′ -127°52.79′	15 ± 9	1.4
78/06/10 22:40:28.44	50°08.86′ -127°53.99′	15 ± 11	1.2
78/06/10 23:00:17.24	49°57.23′ -128°13.65′	88 ± 99	2.1
78/06/10 23:44:23.51	50°08.55′ -127°48.64′	24 ± 13	1.6
78/06/11 2:10:33.30	50°08.52′ -127°49.97′	19 ± 11	0.9
78/06/11 2:44:47.57	50°09.19′ -127°49.78′	20 ± 16	1.0
78/06/11 2:42:12.38	50°08.75′ -127°49.64′	19 ± 11	0.7
78/06/11 6:25:56.54	50°08.00′ -127°48.24′	17 ± 11	1.3
78/06/11 6:31:30.75	50°09.96′ -127°49.92′	10 ± 11	1.1
78/06/11 7:03:01.25	50°09.23′ -127°48.45′	19 ± 11	2.2
78/06/12 10:52:21.89	50°10.19′ -127°53.43′ (50°10.18′ -127°52.72′)	9 ± 36 (9 ± 2)	3.7
78/06/12 10:56:42.34	50°08.88′ -127°50.03′	20 ± 11	1.4
78/06/12 10:59:19.77	50°06.71′ -127°48.27′	18 ± 19	1.1
78/06/12 11:08:01.36	50°10.02′ -127°50.81′	11 ± 6	1.5
78/06/12 11:13:29.12	50°09.80′ -127°46.89′	21 ± 8	1.9
78/06/12 12:10:07.43	50°09.67′ -127°47.46′	18 ± 12	1.2

Date - Origin Time	Coordinates	Depth	M_L
78/06/12 12:11:34.40	50°10.79′ -127°49.55′	19 ± 11	0.7
78/06/12 12:23:26.21	50°10.26′ -127°51.00′	9 ± 11	0.8
78/06/12 13:03:15.18	50°09.09′ -127°49.46′	17 ± 4	0.1
78/06/12 13:47:31.13	50°09.37′ -127°48.21′	19 ± 3	1.6
78/06/12 15:59:13.92	50°07.55′ -127°51.66′	17 ± 1	1.9
78/06/12 16:07:38.25	50°09.35′ -127°49.72′	18 ± 3	0.3
78/06/12 16:47:45.78	50°09.25′ -127°50.46′	15 ± 4	0.3
78/06/12 17:22:59.16	50°07.73′ -127°50.27′	18 ± 5	1.0
78/06/12 17:27:53.32	50°08.60′ -127°51.12′	17 ± 12	0.1
78/06/12 18:13:00.82	50°00.38′ -127°48.08′	62 ± 99	1.3
78/06/12 19:07:23.54	50°09.73′ -127°53.19′	20 ± 7	0.9
78/06/12 19:10:27.79	50°11.47′ -127°51.63′	12 ± 11	-0.3
78/06/12 19:24:04.38	50°09.65′ -127°48.53′	17 ± 6	1.3
78/06/12 19:29:33.75	50°08.18′ -127°46.70′	25 ± 13	0.8
78/06/12 19:30:23.61	50°10.05′ -127°50.23′	17 ± 7	0.8

Table A-2 : Regionally detected aftershocks. Original G.S.C. solutions and final epicentres (in brackets) determined using HYPOELLIPSE, the Georgia Straits model and data from only PHC and GDR. The two events without final locations were discarded because there were no data at PHC. All focal depths were fixed at 18 km.

Group I		
Date - Origin Time	Coordinates	M_L
78/06/02 20:49:05	50.19° -127.94° (50.17° -127.88°)	2.6
78/06/02 22:21:51	50.17° -127.90° (50.15° -127.98°)	2.6
78/06/03 17:04:19	50.21° -127.88° (50.15° -127.89°)	2.2
78/06/04 02:33:55	50.15° -127.97° (50.15° -127.90°)	2.5
78/06/04 03:12:23	50.16° -128.03° (50.17° -127.94°)	2.3
78/06/04 10:57:52	50.17° -127.94° (50.17° -127.88°)	2.0
78/06/04 22:47:33	50.14° -128.05° (50.17° -127.93°)	2.3
78/06/05 13:06:15	50.18° -127.91° (50.16° -127.87°)	2.1
78/07/26 06:09:39	50.21° -127.94° (50.17° -127.88°)	3.0
Group II		
Date - Origin Time	Coordinates	M_L
78/06/02 21:47:47	50.26° -127.78°	2.9
78/06/03 11:54:39	50.19° -127.61°	4.6
78/06/03 12:54:25	50.20° -127.78° (50.16° -127.93°)	3.0
78/06/05 04:13:37	50.18° -127.72° (50.16° -127.85°)	2.3
78/06/05 16:42:54	50.21° -127.70° (50.17° -127.90°)	2.2
78/06/12 10:52:23	50.23° -127.65° (50.17° -127.88°)	3.9
78/06/13 11:39:30	50.24° -127.53° (50.16° -127.88°)	3.6

Table A-3 : Hypocentre coordinates and magnitudes of the 31 earthquakes detected by the G.S.C., from 1978 to 1987, in the Brooks Peninsula region. Coordinates shown are those determined by the G.S.C. Eighteen of the events were relocated using the travel time corrections determined from the aftershock study and the stations PHC and GDR. The revised coordinates are shown in brackets.

Date - Origin Time	Coordinates	Depth	M_L
1978/05/25 21:53:44	50.20° -127.70° (50.15° -127.92°)	18	3.3
1978/07/02 12:31:49	50.03° -127.70°	18	1.8
1978/07/31 13:54:29	50.18° -127.87° (50.18° -127.90°)	18	2.1
1978/08/02 08:39:19	50.15° -127.84° (50.17° -128.02°)	18	2.1
1978/08/10 10:03:54	50.19° -127.70° (50.15° -127.93°)	18	2.8
1978/08/11 19:09:08	50.17° -127.99° (50.18° -127.94°)	18	2.2
1978/08/11 20:37:33	50.23° -127.71° (50.16° -128.04°)	18	2.5
1978/12/30 08:50:36	50.19° -127.70° (50.17° -128.00°)	18	2.4
1980/01/08 23:44:48	50.45° -128.14° (50.76° -127.52°)	18	3.0
1981/03/16 20:27:31	50.00° -128.08°	10	1.8
1981/03/17 15:07:33	50.02° -127.99° (50.01° -128.22°)	10	2.2
1981/05/22 05:18:51	50.19° -127.82°	18	1.8
1982/05/15 00:52:06	50.15° -128.00° (50.14° -128.10°)	18	2.0
1981/08/18 15:32:44	50.31° -127.54°	6	1.3
1982/06/14 18:51:01	50.21° -127.93° (50.21° -127.91°)	27 (18)	3.1
1983/05/14 09:44:10	50.23° -127.86° (50.20° -127.89°)	27 (18)	3.1
1983/10/25 00:10:33	50.19° -127.98° (50.21° -127.93°)	6 (18)	2.3
1983/11/26 13:26:35	50.05° -128.10°	5	2.0
1984/04/27 17:43:55	50.15° -127.99° (50.17° -127.98°)	1 (18)	2.6
1984/09/16 22:42:56	50.16° -127.99°	24	1.8
1984/09/22 09:14:19	50.03° -127.97°	6	1.2

Date - Origin Time	Coordinates	Depth	M_L
1985/05/15 15:09:13	50.09° -127.76° (50.08° -127.69°)	43 (18)	3.0
1985/05/24 23:10:02	50.26° -128.11°	7	1.3
1985/09/01 17:49:21	50.13° -128.16°	20	1.8
1985/09/05 13:55:59	50.13° -127.97°	20	1.5
1985/12/16 12:13:10	50.21° -128.04°	25	1.7
1985/12/17 09:22:39	50.17° -127.93°	21	1.7
1986/01/14 06:39:36	50.11° -127.96°	27	1.9
1986/05/16 05:03:03	50.02° -127.73° (49.97° -127.85°)	 (18)	2.9
1986/06/21 12:07:20	50.19° -127.98°	20	1.6
1986/06/24 00:07:05	50.06° -127.67° (49.97° -127.81°)	28 (18)	2.8

Table A-4 : Teleseismic *P* wave arrival time data used with the EPDET program (Ch. 3).

Station	2 June 1978	25 July 1978
ADK		23:37:00.0
AGM		23:38:10.0
ALE	20:48:56.0	23:38:08.5
ALI	20:54:01.0	
ALQ	20:46:35.3	23:35:44.0
ALT	20:54:39.0	23:43:47.5
AN1		23:37:15.0
AN3	20:48:07.0	
ANR	20:54:31.8	23:43:41.2
ANV		23:36:13.2
APA	20:52:07.5	
ARE		23:43:15.0
ARN	20:44:59.0	23:34:06.8
ARU	20:53:15.0	23:42:24.0
AVF	20:53:21.9	23:42:30.2
BAF	20:53:25.7	23:42:28.0
BCR	20:52:07.0	23:41:15.5
BCT	20:49:01.5	23:38:09.5
BDW	20:45:10.7	23:34:18.0
BEI	20:45:00.0	23:34:08.6
BEO		23:43:09.5
BKR	20:54:35.0	23:43:43.0
BKS	20:44:50.5	23:33:57.0
BLA	20:48:44.8	23:37:52.6
BLC	20:46:40.0	23:35:44.0
BMN	20:44:40.4	23:33:48.8
BNH	20:48:59.5	23:38:08.1
BOD	20:51:54.7	
BOG	20:52:14.0	
BRA	20:53:40.0	
BRG	20:53:22.3	23:42:28.5

Station	2 June 1978	25 July 1978
BSF	20:53:23.6	23:42:31.7
BUH	20:53:23.3	23:42:30.2
BUT		23:33:29.9
CAF	20:53:28.9	
CAR	20:52:12.0	23:41:17.0
CBM	20:49:07.1	23:38:15.2
CDF	20:53:21.6	23:42:30.1
CDR	20:53:43.9	23:42:52.2
CFR		23:43:15.0
CLE	20:48:17.6	23:37:25.0
CLL	20:53:18.0	23:42:25.0
CMP	20:54:04.0	
COL	20:45:55.0	23:35:04.0
CRO	20:47:48.6	
CRT		23:43:02.1
CSS	20:45:29.8	
CVF	20:53:53.3	23:43:01.6
CWF	20:52:40.0	23:41:54.0
DAG	20:50:04.8	23:39:16.8
DAL		23:36:48.4
DBN	20:53:04.0	
DCI	20:44:49.8	
DCN	20:52:24.6	23:41:36.8
DEV		23:43:03.0
DIX	20:53:33.0	23:42:43.0
DLA	20:48:12.2	
DMK		23:43:36.5
DOU		23:42:21.0
DSH	20:54:45.0	23:43:54.0
DUG	20:45:09.7	23:34:18.5
EAB		23:41:30.0
EAU		23:41:33.9
EBH	20:52:20.0	23:41:31.6

Station	2 June 1978	25 July 1978
EBL		23:41:35.0
EBR	20:53:47.0	23:42:54.0
ECH	20:53:23.8	
ECT		23:38:08.1
EDI		23:41:33.4
EDM	20:43:59.5	23:33:07.5
EGL		23:41:35.0
EKA	20:52:24.7	23:41:37.3
ELC	20:47:54.3	
ELF	20:48:11.1	
ELO		23:41:30.3
ELT	20:53:11.6	23:42:19.7
EMM	20:49:19.3	
EPF		23:42:42.6
EUR	20:44:57.2	23:34:06.2
FAV	20:47:33.1	23:36:42.9
FCC	20:46:28.2	23:35:36.0
FFC	20:45:28.2	23:34:35.9
FHC	20:44:06.7	23:33:15.0
FLN	20:53:03.3	23:42:12.0
FRB	20:48:24.0	23:37:31.0
FRI	20:45:12.0	23:34:17.0
FRU	20:54:19.5	23:43:27.1
FUR	20:53:33.0	23:42:40.0
FVM	20:47:44.0	
FYU	20:46:02.6	
GAR		23:43:50.9
GBV	20:48:41.3	23:37:49.3
GCA	20:45:49.9	23:34:58.2
GDH	20:49:09.2	23:38:17.7
GIL	20:45:55.4	23:35:03.5
GLA	20:46:14.0	23:35:22.0
GLD	20:46:06.7	

Station	2 June 1978	25 July 1978
GOL	20:46:05.3	23:35:13.4
GPA	20:54:31.0	
GRF	20:53:23.0	
GRR	20:53:05.4	23:42:13.8
GRS	20:54:45.0	23:43:54.0
GZR		23:43:10.0
HAD	20:54:15.0	
HAL	20:49:39.5	
HBF	20:49:07.2	
HEE	20:53:08.0	23:42:20.0
HFS	20:52:27.2	23:41:35.9
HKT	20:48:04.7	23:37:13.2
HUA		23:42:45.9
IAS		23:43:05.0
IFR	20:54:06.0	23:43:11.7
ILT	20:47:56.0	23:37:04.2
IMA	20:46:25.0	
INK	20:45:58.0	23:35:07.0
IRK	20:52:46.3	23:41:54.0
JAS	20:44:54.0	23:34:02.3
JCT	20:47:40.5	
JOS	20:53:44.0	23:42:50.0
KDC	20:45:26.0	23:34:41.5
KEV	20:51:44.0	23:40:52.0
KHC	20:53:29.0	23:42:36.6
KHE	20:50:32.6	23:39:41.8
KHO	20:54:46.0	23:43:55.0
KIR	20:51:45.0	
KJF	20:52:19.0	23:41:27.0
KON	20:52:29.0	
KPK		23:33:40.0
KRA		23:42:41.0
KRV	20:54:39.0	23:43:48.0

Station	2 June 1978	25 July 1978
KTG	20:50:32.1	23:39:40.7
LAC	20:45:54.3	23:35:02.0
LBF	20:53:22.1	23:42:30.6
LD1	20:45:12.3	
LDM	20:43:44.7	
LFF	20:53:26.2	23:42:34.5
LHC	20:47:05.3	23:36:14.4
LHS	20:48:56.2	
LMQ	20:48:53.0	
LMR	20:53:45.3	23:42:53.6
LOR	20:53:20.6	23:42:29.3
LPB	20:54:16.0	23:43:24.5
LPF	20:53:06.7	23:42:15.1
LPO		23:42:36.4
LPS	20:50:19.3	23:39:27.5
LRG	20:53:44.8	
LSF	20:53:20.6	23:42:29.3
LUB	20:47:09.0	23:36:17.0
MAG	20:49:57.0	
MAI		23:44:09.0
MAL		23:43:02.0
MAT	20:52:23.5	23:41:32.0
MBC	20:47:19.5	23:36:27.5
MEM	20:53:10.4	23:42:19.4
MFF	20:53:16.1	23:42:24.1
MGD	20:49:57.0	23:39:09.0
MHC	20:44:58.0	23:34:06.4
MHK		23:36:12.4
MIM	20:49:08.8	23:38:17.1
MIN	20:44:21.0	23:33:29.5
MLR	20:54:00.0	23:43:13.0
MNT		23:37:51.0
MNV	20:44:58.0	23:34:07.5

Station	2 June 1978	25 July 1978
MOS		23:42:27.0
MOT	20:47:20.5	23:36:29.0
MOX	20:53:19.0	23:42:25.5
MOY	20:52:57.0	23:42:06.0
MRG		23:37:43.0
MSA	20:46:24.3	23:35:31.8
MSO	20:44:03.8	
MZF	20:53:23.4	23:42:31.8
NAO		23:41:27.8
NB2	20:52:18.8	
NIE		23:42:45.0
NRI	20:51:33.4	23:40:42.0
NSC		23:38:18.2
NUR	20:52:38.0	23:41:46.0
NVS	20:53:05.0	
OAQ		23:41:36.0
OBN	20:53:21.1	23:42:29.0
OHR	20:54:17.1	
OTT		23:37:41.0
PAS	20:45:48.0	23:34:57.0
PEC	20:45:58.6	23:35:05.0
PEK	20:53:18.0	
PET	20:49:48.0	23:38:57.0
PMR	20:45:35.7	23:34:43.5
POC	20:48:54.5	
POW	20:47:49.5	
PRA	20:53:28.0	23:42:34.0
PRI	20:45:17.0	23:34:25.3
PRM	20:48:50.0	
PRU	20:53:28.0	23:42:34.5
PRZ	20:54:18.0	
PSO	20:52:24.0	23:41:31.5
PYA		23:43:31.8

Station	2 June 1978	25 July 1978
PYR	20:45:42.2	
RCC	20:50:43.0	
RES	20:47:34.0	23:36:41.0
RJF	20:53:25.5	23:42:34.0
RLO	20:47:29.3	23:36:37.7
RMP	20:54:03.0	23:43:16.0
ROB	20:53:42.0	23:42:50.0
RXF	20:43:45.4	
SAL		23:42:53.5
SAM	20:54:39.8	
SAO	20:45:07.0	23:34:13.5
SCH	20:48:46.8	23:37:55.0
SEM		23:42:42.0
SES		23:33:24.0
SEY	20:49:41.3	23:38:49.3
SGG	20:54:08.0	
SIO		23:36:32.9
SIT	20:43:41.6	23:32:49.9
SKO	20:54:15.0	
SKR		23:39:23.0
SMF	20:53:23.4	23:42:31.9
SOD	20:51:57.0	23:41:05.4
SOR	20:49:53.0	
SPC	20:53:40.0	23:42:49.0
SPF	20:53:44.7	23:42:53.0
SSC	20:53:05.6	23:42:14.0
SSF	20:53:21.0	23:42:29.4
SSR	20:54:01.0	23:43:11.0
STJ	20:50:18.0	
STR	20:53:28.0	
SVE	20:53:13.0	23:42:21.0
SVM	20:46:45.2	
SVW	20:46:05.4	

Station	2 June 1978	25 July 1978
TAS	20:54:31.5	
TCF	20:53:21.9	23:42:30.6
TIK	20:50:14.8	23:39:25.0
TIO		23:43:25.0
TLG	20:54:14.0	23:43:23.0
TNP	20:45:07.6	
TNS		23:42:27.5
TOA	20:45:26.0	23:34:34.3
TOL	20:53:40.0	23:42:47.5
TOV	20:52:04.3	23:41:14.3
TRO		23:40:44.0
TTA	20:46:15.2	
TUC	20:46:37.2	
TUL	20:47:26.7	23:36:34.6
UCT	20:49:06.5	
UME	20:52:13.1	23:41:22.0
UPP	20:52:34.1	23:41:42.5
UZH	20:53:43.0	23:42:54.0
VAN	20:54:51.0	
VAY	20:54:19.8	
VKA	20:53:39.0	23:42:46.0
VRI	20:54:01.0	23:43:10.0
WAB		23:44:04.0
WCN		23:33:50.6
WDC	20:44:14.5	23:33:22.9
WES	20:49:09.0	
WET		23:42:40.8
WHC	20:44:29.0	
WIT	20:53:02.0	23:42:12.0
WKR	20:45:21.8	23:34:30.0
WLS	20:53:23.1	
WOL	20:52:51.0	
WTS	20:53:03.0	23:42:12.0

Station	2 June 1978	25 July 1978
YAK	20:50:54.8	23:40:02.0
YKA	20:45:04.3	23:34:12.4
YKC	20:45:03.5	23:34:12.0
YSS	20:51:19.0	23:40:33.0
ZAK	20:52:58.4	23:42:07.5
ZOB	20:54:13.5	23:43:23.5
ZST	20:53:40.0	23:42:53.0
ZUL	20:53:29.5	23:42:35.0

Table A-5 : First-motion polarity data used to determine the focal mechanisms. The azimuths and distances (Δ) of each station from the epicentre are given in degrees. The polarities are indicated as compressions (C) or dilatations (D). The sources of the data are also shown; i.e., whether the data were obtained from long period (LP) or short period (SP) instruments or from the I.S.C.

Station	Azimuth	Δ°	2 June 1978		25 July 1978	
			Polarity	Source	Polarity	Source
AAM	87.3	31.1	C	LP		
ALB	106.0	2.1			C	SP
ALE	11.3	36.7	C	SP	D	LP
ALQ	127.6	22.4	C	LP		
ARU	356.2	73.7	D	ISC		
BDG	120.6	6.9	D	SP		
BEC	86.1	49.1	C	LP		
BFW	137.2	4.8	C	SP		
BKR	6.4	88.2	D	ISC	D	ISC
BKS	159.7	12.9	C	LP		
BLA	92.5	36.0	C	LP	C	ISC
BLC	37.8	21.8	C	ISC		
BLN	121.0	3.9	C	LP		
BOD	327.3	60.9	D	ISC		
BRG	24.0	74.2	C	ISC	D	ISC
BUH	28.4	74.6	D	ISC	D	ISC
CAR	106.1	63.4	C	LP		
CDR	32.4	78.2	D	ISC	C	ISC
CLE	86.9	32.5	C	ISC	C	ISC
COL	332.0	18.0	D	LP	D	SP
COR	148.5	6.3	C	LP		
CRO	84.7	31.8	C	ISC		
CRT	41.8	74.8			D	ISC
CUM	68.5	6.3	C	SP		
DAG	17.6	44.6	D	ISC	C	ISC
DAI	67.3	6.2	C	SP		
DIX	30.1	76.8			C	ISC
DLA	84.7	31.8	C	ISC	C	LP

Station	Azimuth	Δ°	2 June 1978		25 July 1978	
			Polarity	Source	Polarity	Source
DOU	29.8	72.4			D	ISC
DUG	127.2	14.5	C	ISC	C	LP
DYH	109.0	17.7	D	SP		
EAU	30.8	61.8			D	ISC
EBH	30.5	61.5			D	ISC
EDM	65.5	9.5	C	LP		
ELF	84.0	31.8	C	ISC	C	LP
ELT	339.3	73.0	D	ISC		
EPH	114.0	17.7	C	SP		
EPT	131.1	24.2	C	LP	C	SP
FAV	106.9	27.7	C	ISC	C	ISC
FCC	53.0	21.1	C	LP	C	LP
FFC	63.7	16.3	C	LP	C	LP
FHC	161.8	9.7	C	ISC	C	ISC
FPW	110.0	5.5	D	ISC		
FRB	43.4	33.2	C	LP	C	LP
FSJ	26.3	4.8	C	LP	C	LP
FUR	26.8	73.0	C	ISC	C	ISC
FVM	100.1	29.1	C	LP	C	LP
GBV	90.2	35.2	C	ISC	C	ISC
GDH	32.9	38.2	C	ISC	C	SP
GIL	332.7	17.9	D	SP		
GOL	114.8	18.9	C	LP	C	LP
GSC	147.3	16.8	C	LP	C	SP
GSM	123.2	5.0	D	SP		
HAL	71.5	41.7	C	ISC		
HYC	101.7	3.5	C	SP	C	SP
ILT	324.6	30.0	D	ISC		
IMA	329.9	20.5	D	SP		
INK	353.4	18.3	D	SP		
IRK	328.6	68.7	D	ISC	D	ISC
JAS	153.3	13.2	C	ISC	C	ISC

Station	Azimuth	Δ°	2 June 1978		25 July 1978	
			Polarity	Source	Polarity	Source
JCT	122.2	28.5	C	ISC	D	SP
JCW	113.7	4.3	C	SP		
KHE	358.7	49.4	D	ISC	C	ISC
KTG	26.0	48.4	C	ISC	C	LP
LHC	78.8	24.9	C	LP	C	LP
LLB	107.0	17.7	C	SP		
LND	83.8	32.0			C	LP
LON	128.0	5.2	C	LP	C	LP
LPB	102.4	55.9			D	ISC
LPS	124.4	46.2			C	ISC
LUB	121.0	25.2	C	LP		
MAT	297.7	65.2	D	ISC	C	LP
MBC	004.0	26.3	C	SP	C	SP
MBW	107.1	4.1	C	SP		
MCW	111.4	3.6	C	SP		
MDW	119.6	6.4	D	SP		
MEM	28.8	72.2	C	ISC	C	ISC
MGD	315.2	44.6	D	ISC		
MHC	157.7	13.3			C	ISC
MIN	153.0	10.7	C	ISC	C	ISC
MNQ	65.8	36.2	D	ISC		
MNV	144.8	13.4			C	ISC
MOY	330.1	70.3	D	ISC	C	ISC
MRG	88.2	34.5			D	ISC
MSO	102.8	9.8			C	LP
NEW	100.5	7.3	C	ISC		
NRI	345.7	55.6	D	ISC	C	ISC
OBN	9.2	74.3	D	ISC	D	ISC
OGD	82.9	37.6	C	LP	D	SP
OMK	104.0	17.7	D	SP		
OTT	77.3	34.7	C	LP	C	LP
PAS	152.0	17.4	C	ISC	C	ISC

Station	Azimuth	Δ°	2 June 1978		25 July 1978	
			Polarity	Source	Polarity	Source
PBQ	60.5	29.9	C	ISC		
PGC	114.9	3.2	C	SP	C	SP
PHC	29.4	.6	D	LP		
PIB	111.6	3.2	C	SP	C	SP
PNT	95.3	5.4	C	LP	C	LP
POC	71.1	36.8	D	SP		
PRI	156.1	14.6			C	ISC
QUE	347.3	89.2			C	LP
RES	18.0	28.0	C	LP	C	LP
RLO	107.3	27.1			C	ISC
RMW	120.9	4.8	D	SP		
SCH	58.4	35.8	C	SP	C	SP
SCP	85.1	35.1			C	LP
SES	82.0	10.8	C	LP	C	LP
SEY	318.5	42.8	D	ISC	D	ISC
SHA	108.1	35.3	C	LP	C	SP
SIT	330.5	8.1	C	SP	C	ISC
SMW	103.3	3.0	C	SP		
SPR	65.0	44.8	C	SP		
SPW	122.1	4.5	D	SP		
STJ	62.2	46.3			D	SP
STW	123.4	3.4	C	SP		
SVE	355.8	68.9	C	ISC	C	ISC
SVW	355.1	47.2	D	SP		
SYR	117.3	6.4	D	SP		
TAB	71.9	6.5	C	SP		
THO	137.8	19.9	D	SP		
TIK	335.1	47.2	D	ISC		
TLG	341.7	84.3	D	ISC	D	ISC
TOA	327.4	15.7			C	ISC
TOL	40.6	72.8			D	LP
TOV	108.8	59.6			D	ISC

Station	Azimuth	Δ°	2 June 1978		25 July 1978	
			Polarity	Source	Polarity	Source
UME	15.1	63.6	C	ISC	D	LP
UNB	71.4	39.4	C	ISC		
UZH	19.6	78.5			C	ISC
VAL	36.9	62.4			C	LP
WAT	169.4	75.3	D	SP		
WBW	106.6	6.1	D	SP		
WDC	156.2	10.2	C	ISC	C	ISC
WEN	114.0	17.7	D	SP		
WES	78.6	38.3			C	LP
WET	25.3	75.7			D	ISC
WPT	106.6	17.7	D	SP		
YAK	324.4	52.4	D	ISC		
YKC	25.7	14.3	C	LP	C	LP
YSS	304.1	55.7	D	ISC		
ZAK	328.1	70.7	D	ISC	C	ISC
ZOB	123.3	78.2	C	ISC		
ZUL	28.9	75.9			C	ISC

Appendix B - Figures

This appendix contains 3 sets of figures which were too large to include in the main body of the text. The figures in B-1 are portions of the seismic records used in the *P* waveform comparisons, B-2 contains plots of the digital data used in the surface wave analysis and the final set of figures contains the dispersion curves used in the selection of the group velocity and amplitude data and in the surface wave analysis.

B-1 : The following pages contain portions of the seismic records, from 22 stations, which were used in the *P* waveform comparisons (§ 4.3). Vertical component data are shown for all stations except FFC, where the E-W component is provided since the vertical component was unusable. Record segments for each event are shown side by side for each station and the first-motions have been indicated.

When possible, the actual seismograms were directly overlain for comparison. The actual records were available for the eleven CSSN stations.

The records for 11 of the stations are at different scales because the microfilms, from which they were copied, were made at different scales.

2 June

25 July

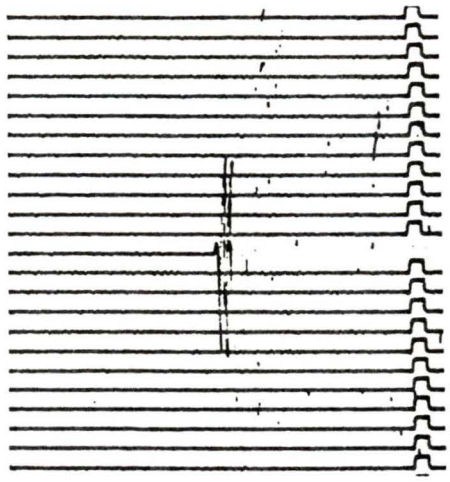

PIB

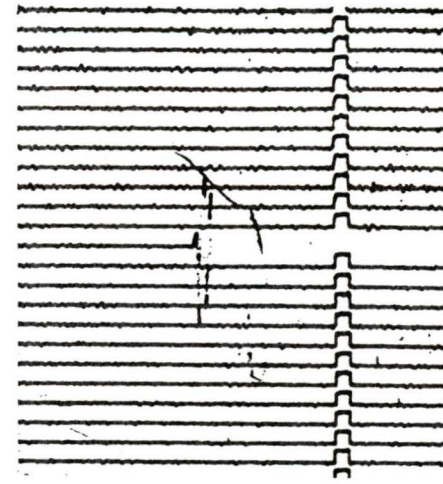

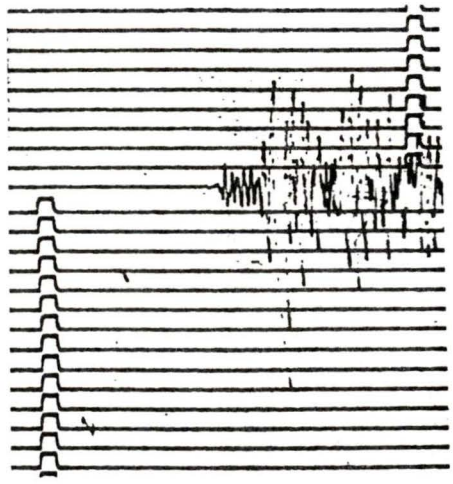

PGC

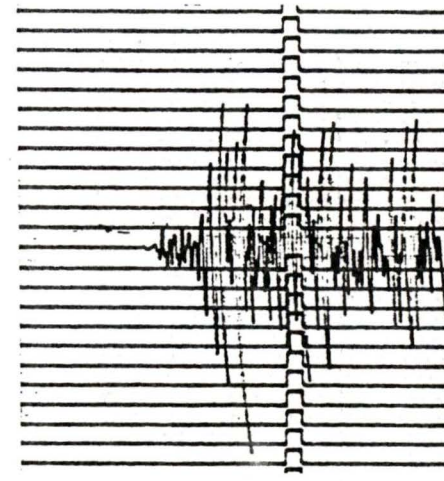

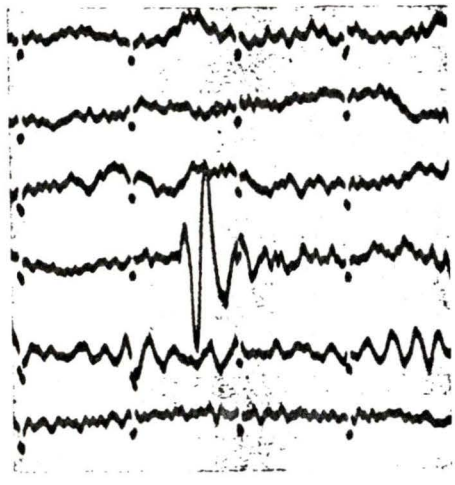

FCC

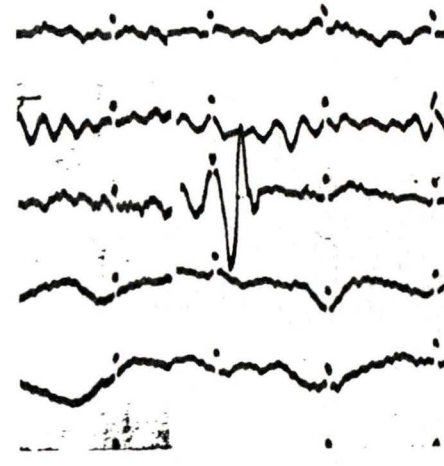

2 June

25 July

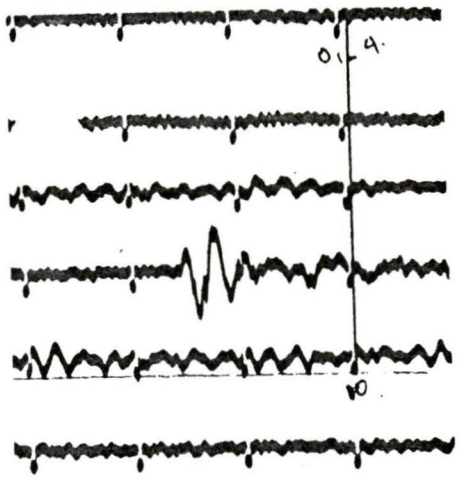

FFC

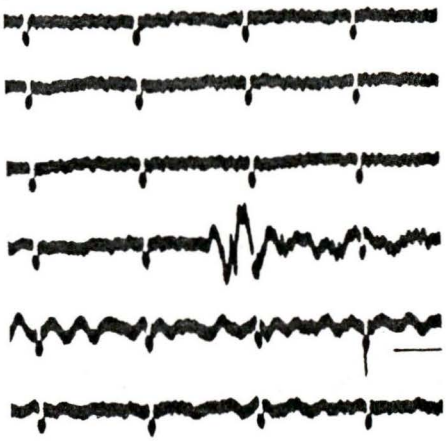

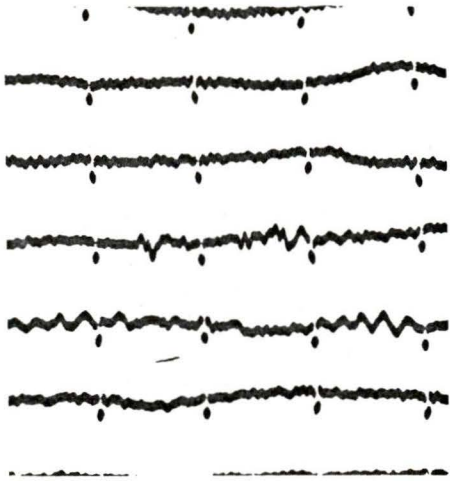

FRB

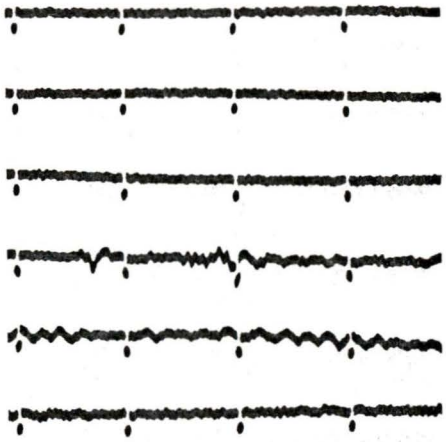

FSJ

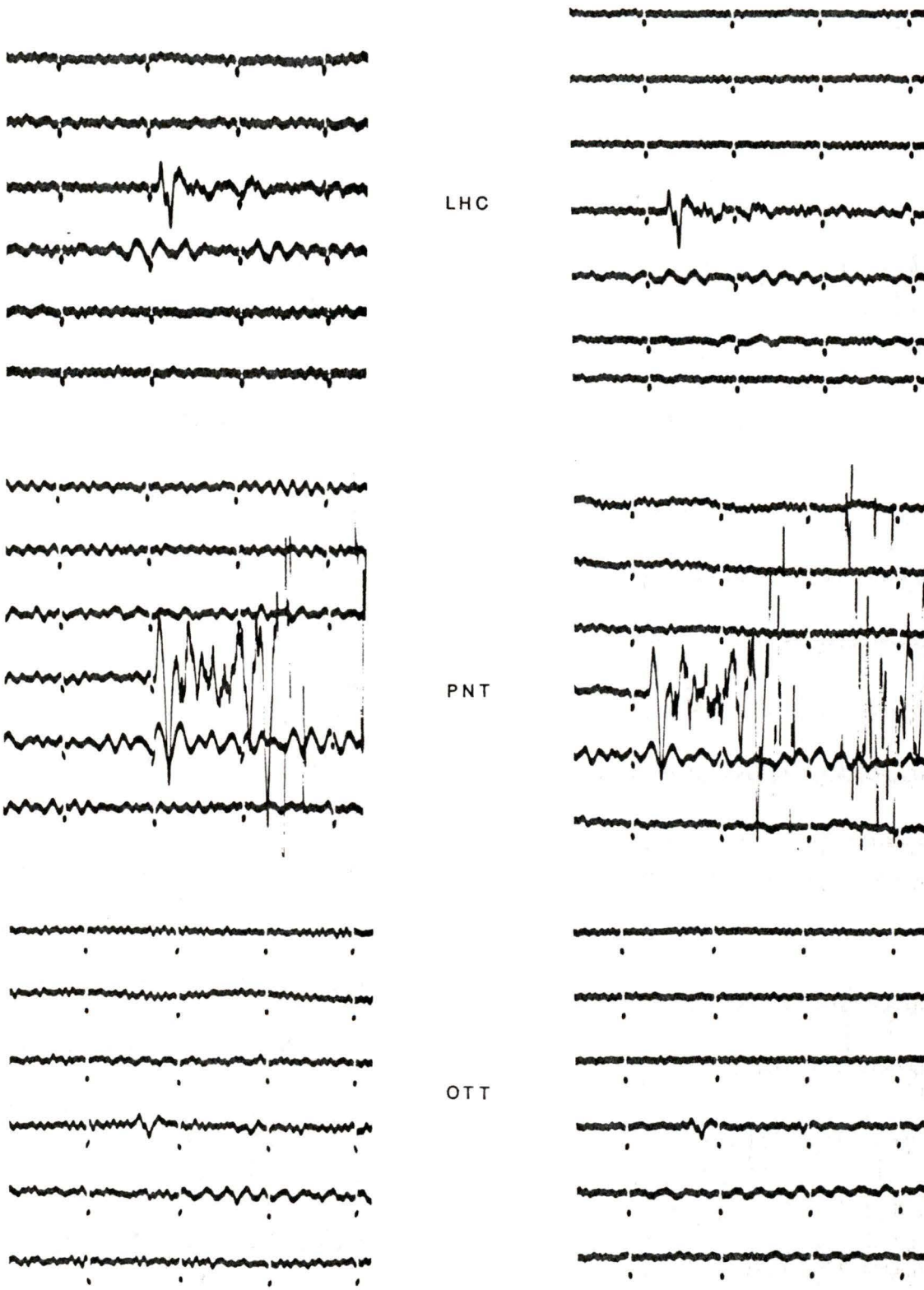
LHC
PNT
OTT

2 June

25 July

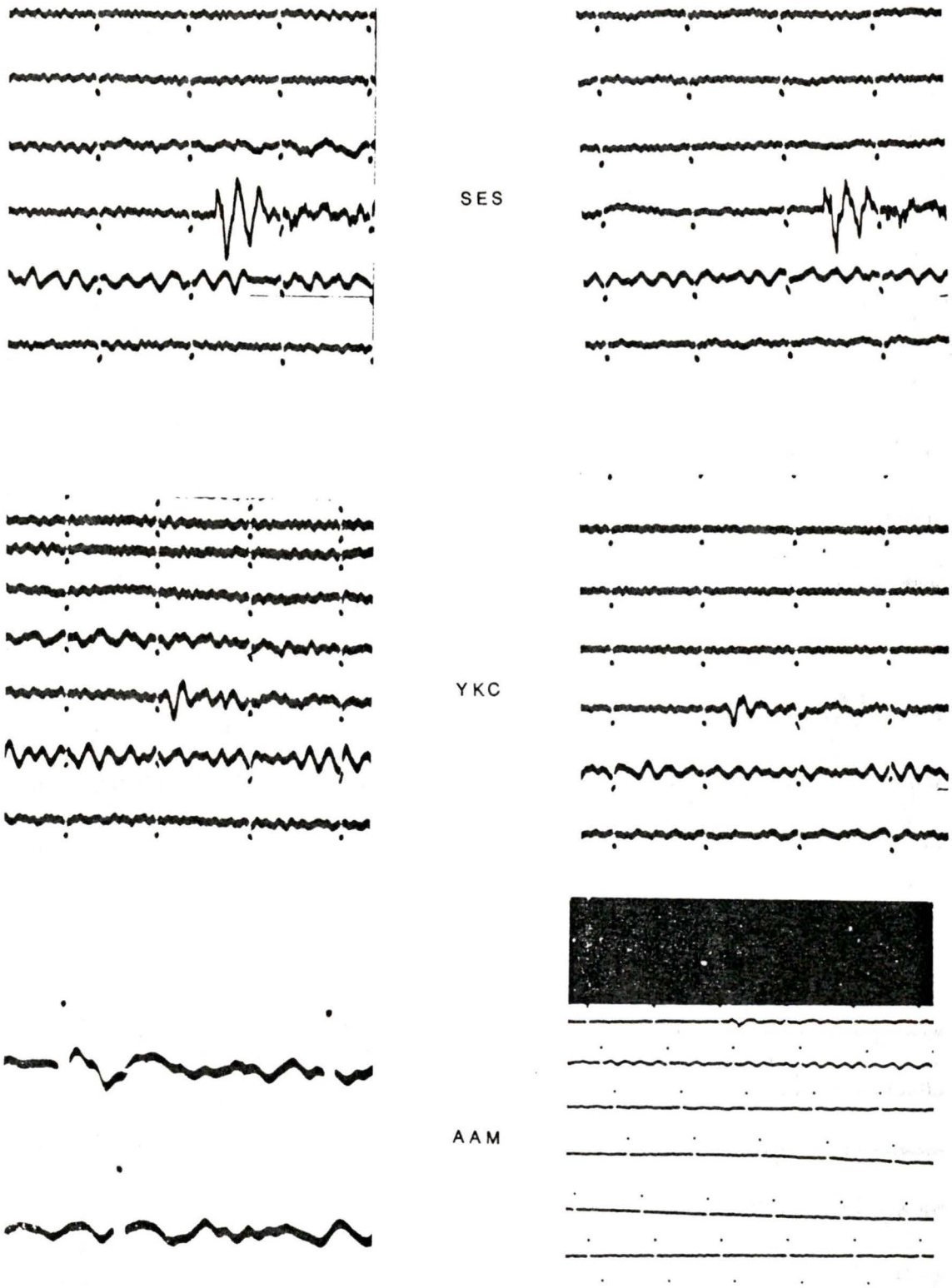

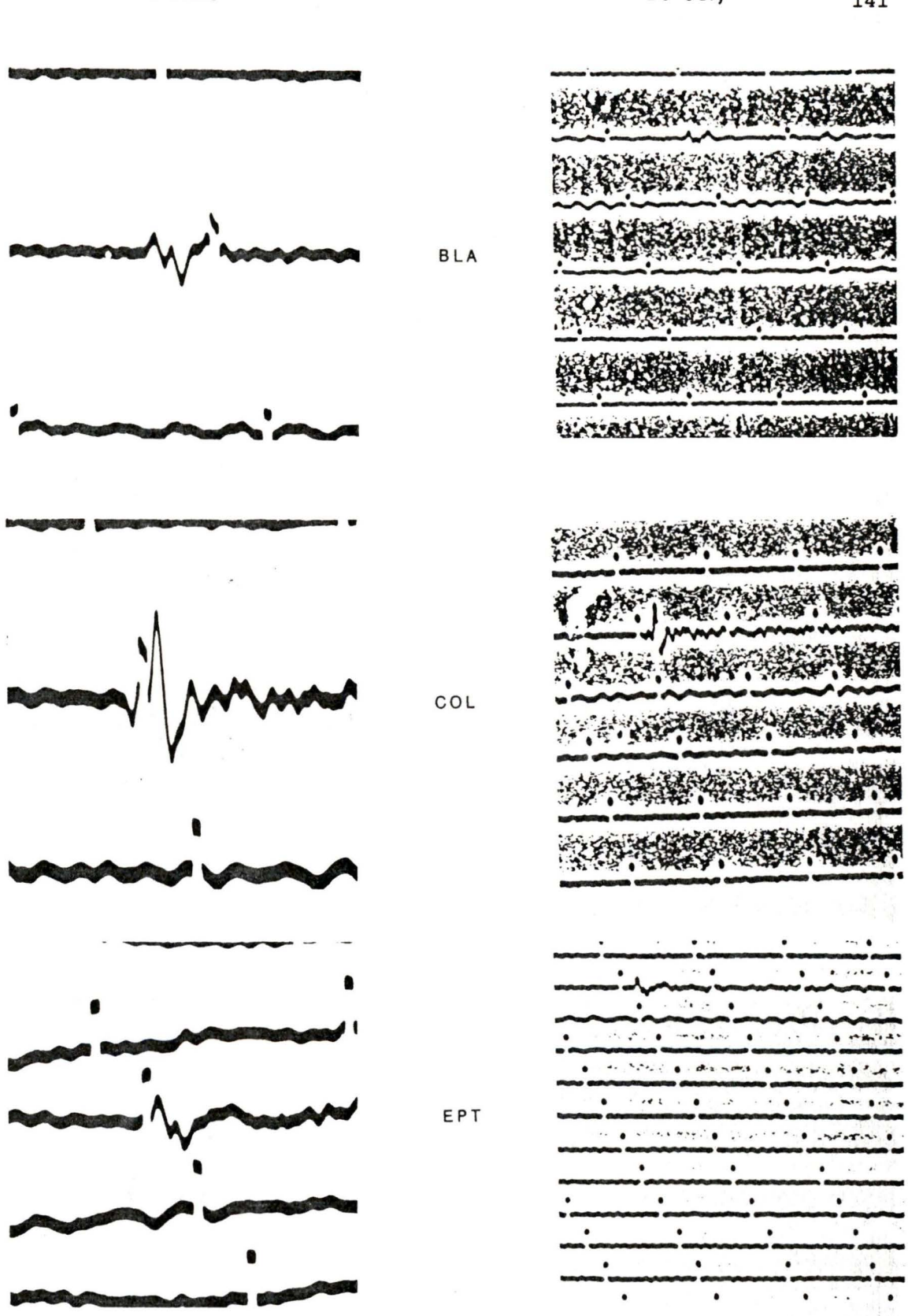
2 June
25 July
BLA
COL
EPT

2 June

25 July

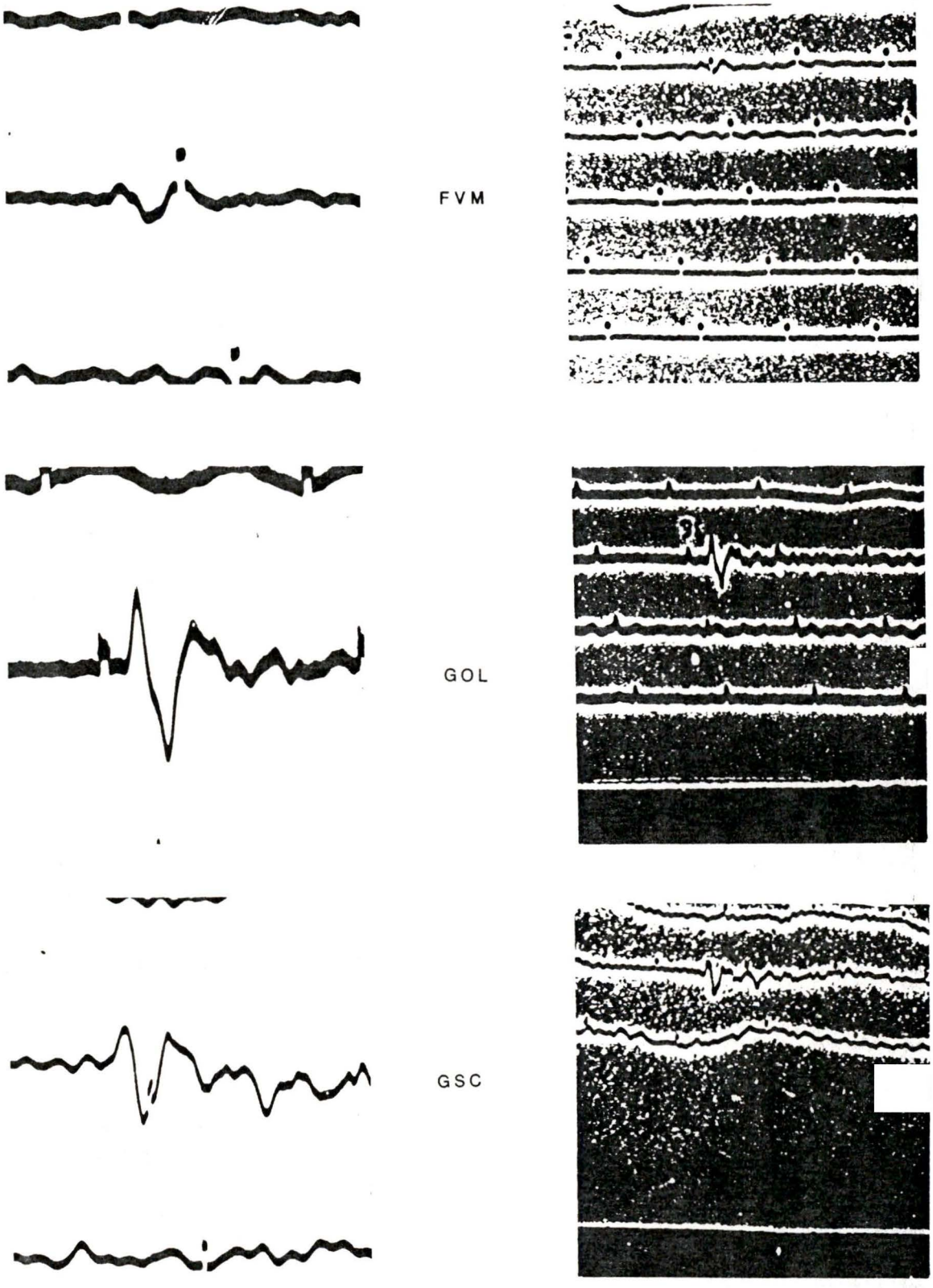

2 June

25 July

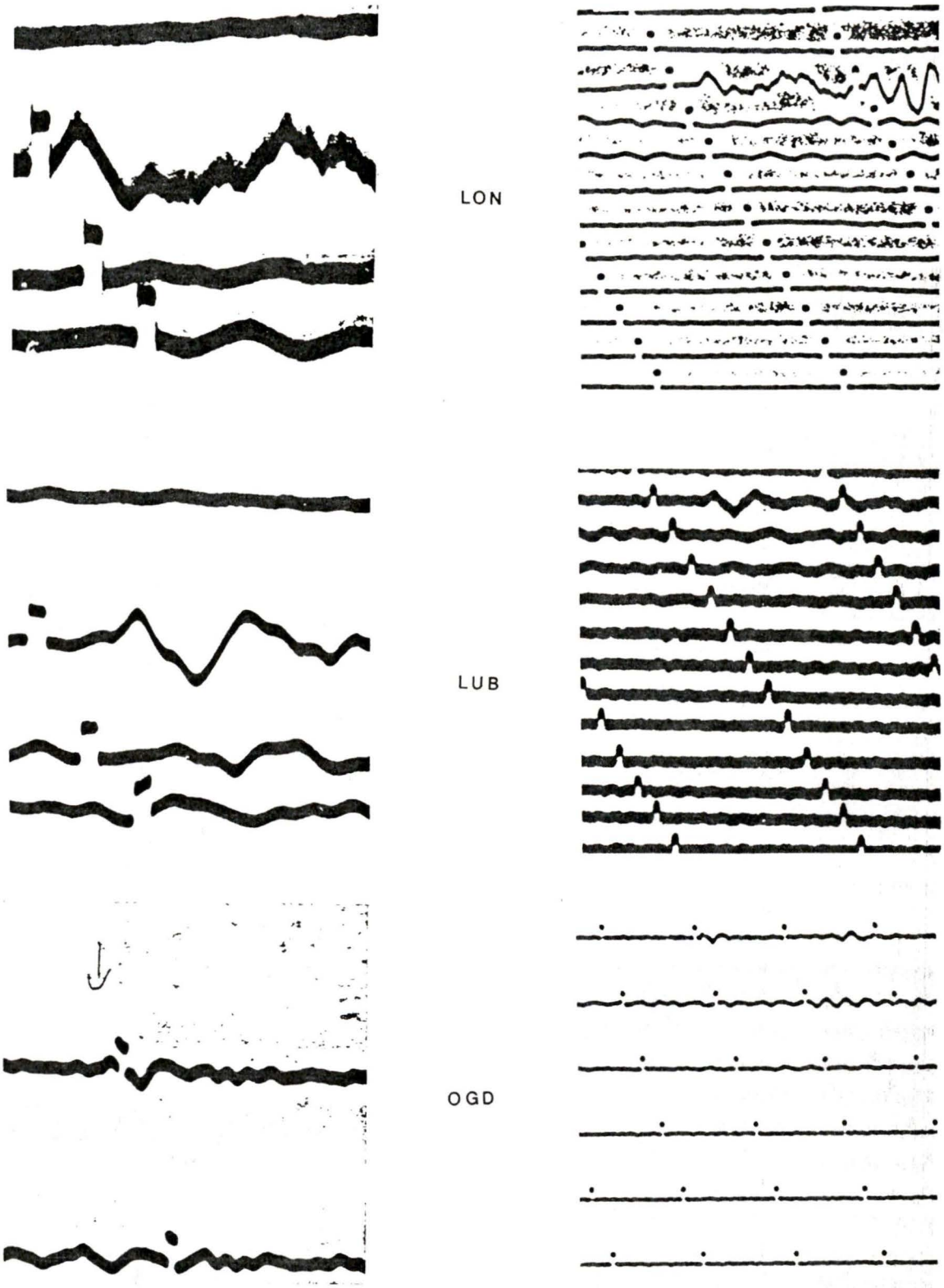

2 June

25 July

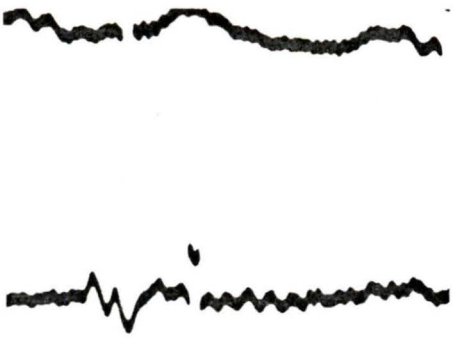

SHA

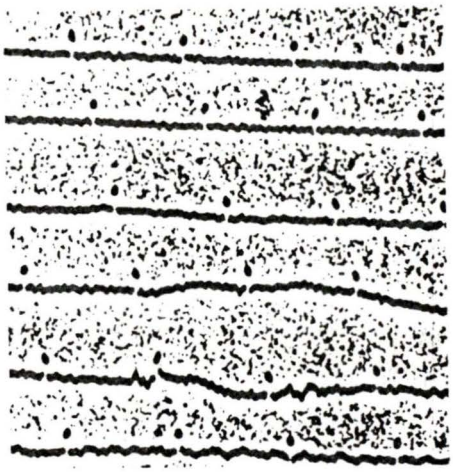

B-2 : Plots of the digital data used in the surface wave analysis (§ 5.3). Record segments are shown for each component; vertical (UZ), north-south (UN) and east-west (UE), at each station from which useful data were obtained. The stations are listed in alphabetical order for each event. The digitized data span only the interval between the arrivals of the 2.5 km/s and 5.0 km/s surface waves.

The records were digitized by hand, using a HI-PAD digitizing tablet. The accuracy of the digitization was verified by overlaying plots of the digital data on the original records.

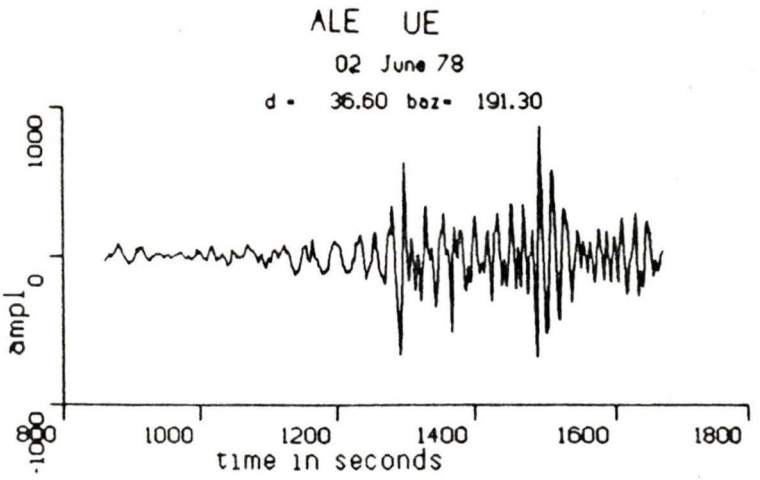
ALE UE
02 June 78
d - 36.60 baz- 191.30
ampl
1000
0
-1000
800
1000
1200
1400
1600
1800
time in seconds

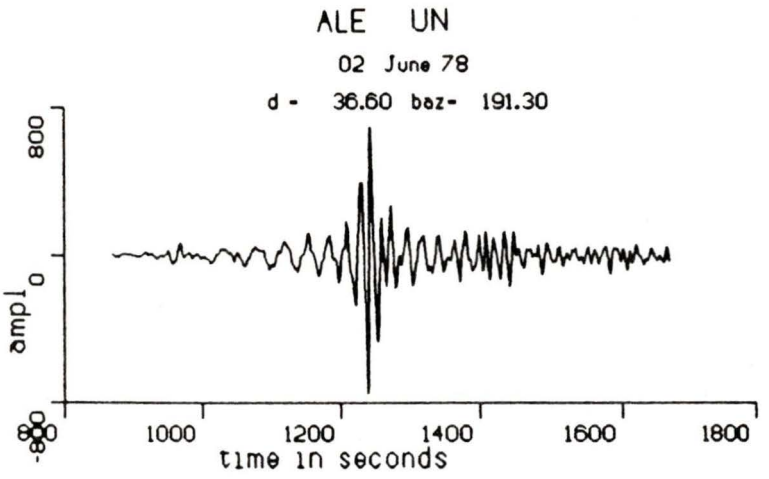
ALE UN
02 June 78
d - 36.60 baz- 191.30
ampl
800
0
-800
1000
1200
1400
1600
1800
time in seconds

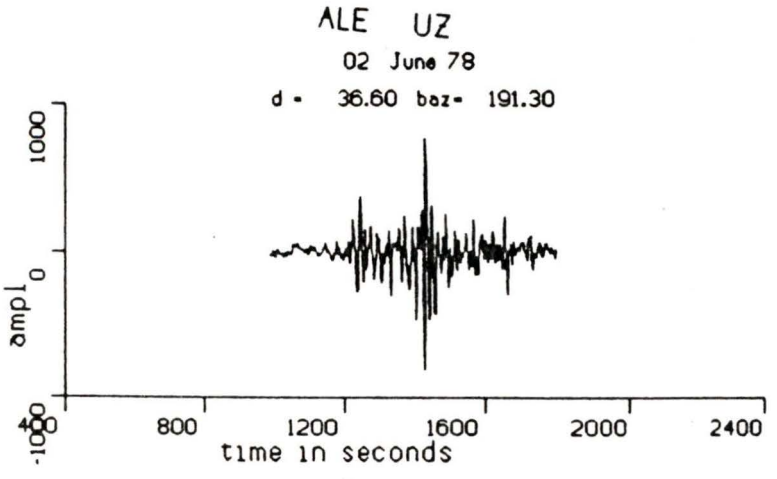
ALE UZ
02 June 78
d - 36.60 baz- 191.30
ampl
1000
0
-1000
400
800
1200
1600
2000
2400
time in seconds

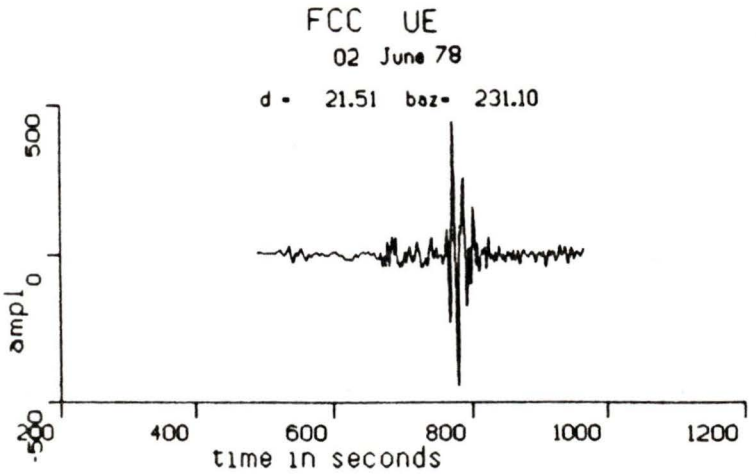
FCC UE
02 June 78
d = 21.51 baz= 231.10
500
0
-500
ampl
400
600
800
1000
1200
time in seconds

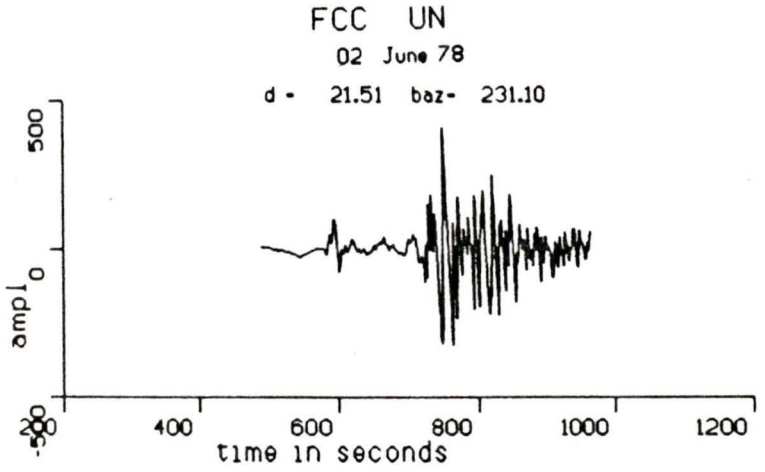
FCC UN
02 June 78
d = 21.51 baz= 231.10
500
0
-500
ampl
400
600
800
1000
1200
time in seconds

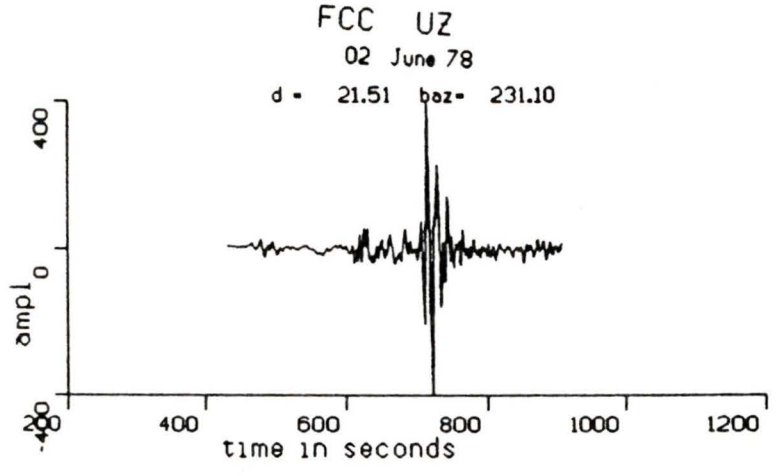
FCC UZ
02 June 78
d = 21.51 baz= 231.10
400
0
-400
ampl
400
600
800
1000
1200
time in seconds

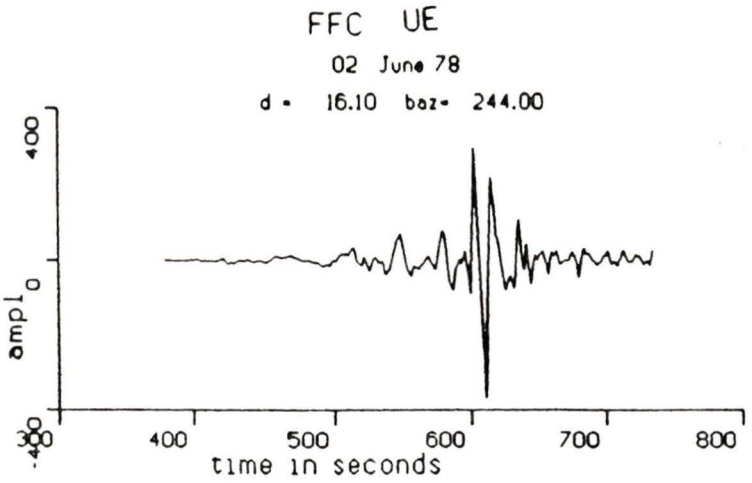
FFC UE
02 June 78
d = 16.10 baz= 244.00
ampl
400
0
-400
300
400
500
600
700
800
time in seconds

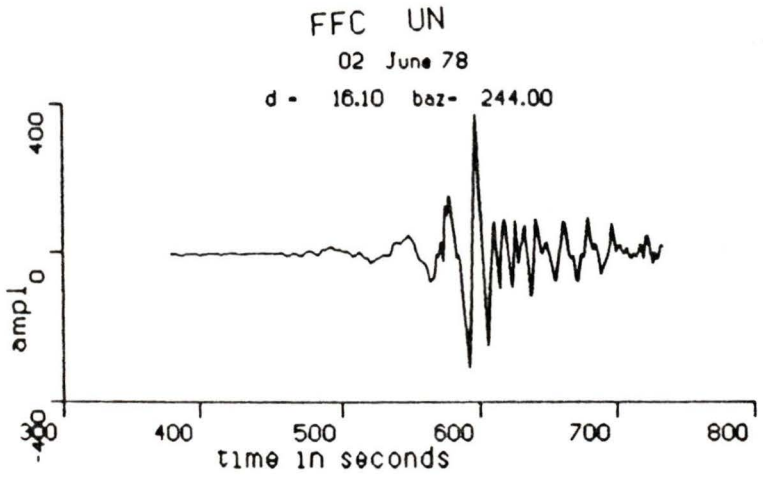
FFC UN
02 June 78
d = 16.10 baz= 244.00
ampl
400
0
-400
300
400
500
600
700
800
time in seconds

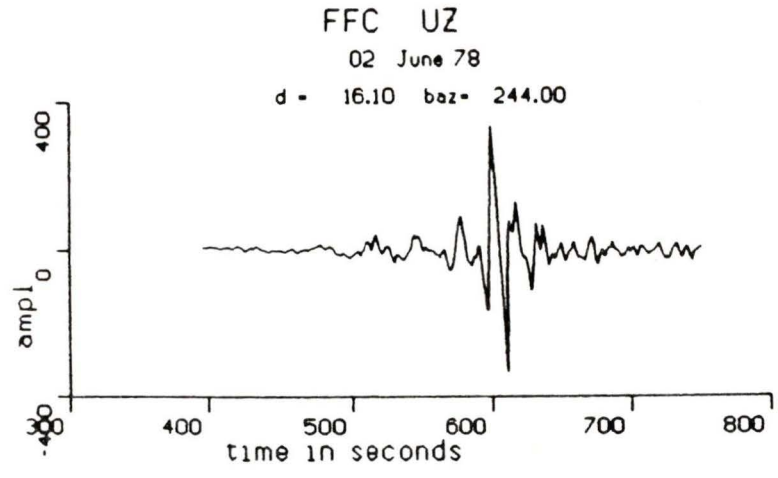
FFC UZ
02 June 78
d = 16.10 baz= 244.00
ampl
400
0
-400
300
400
500
600
700
800
time in seconds

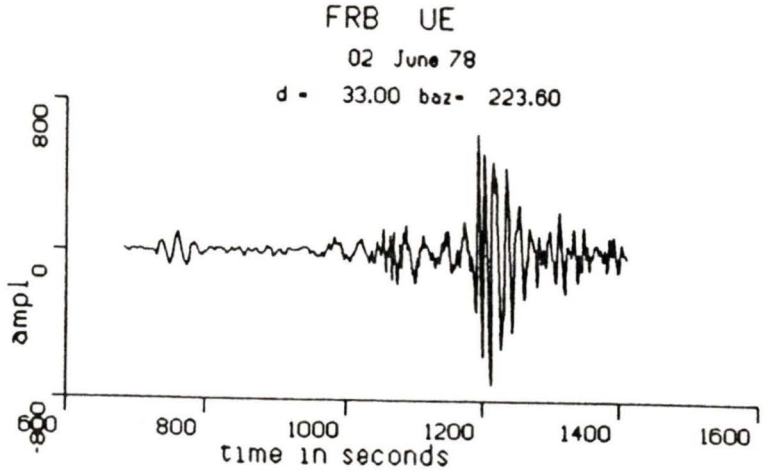
FRB UE
02 June 78
d = 33.00 baz= 223.60
800
0
-800
ampl
800
1000
1200
1400
1600
time in seconds

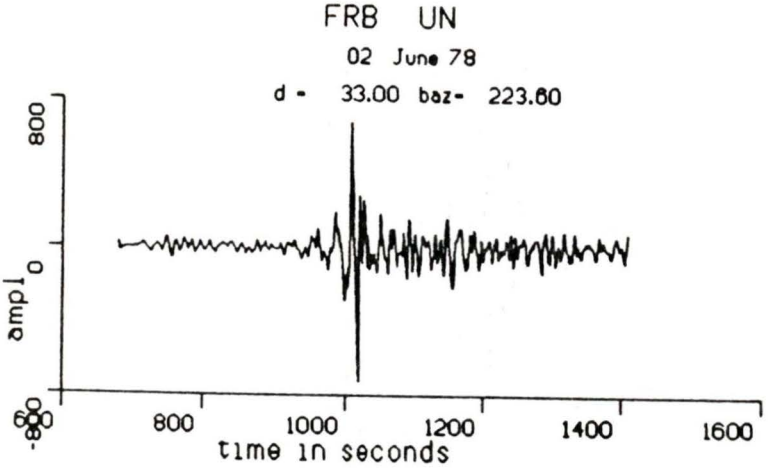
FRB UN
02 June 78
d = 33.00 baz= 223.60
800
0
-800
ampl
800
1000
1200
1400
1600
time in seconds

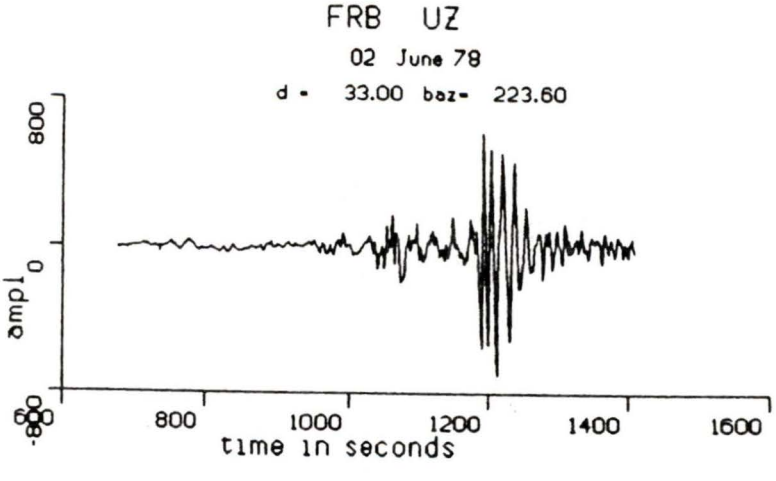
FRB UZ
02 June 78
d = 33.00 baz= 223.60
800
0
-800
ampl
800
1000
1200
1400
1600
time in seconds

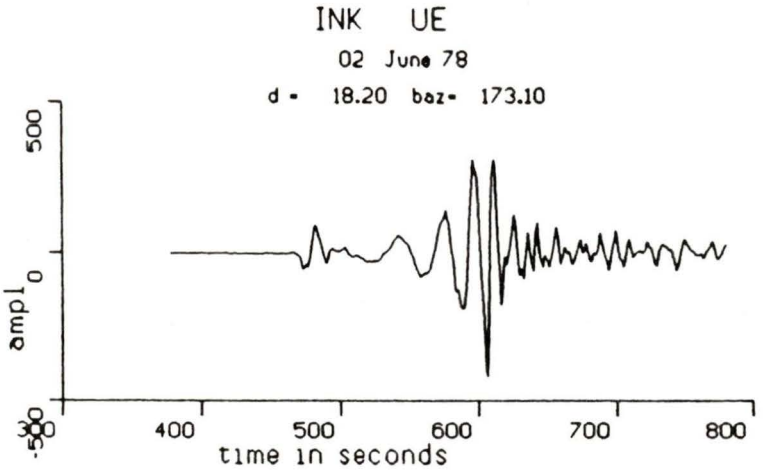
INK UE
02 June 78
d - 18.20 baz- 173.10
ampl
500
0
-500
400
500
600
700
800
time in seconds

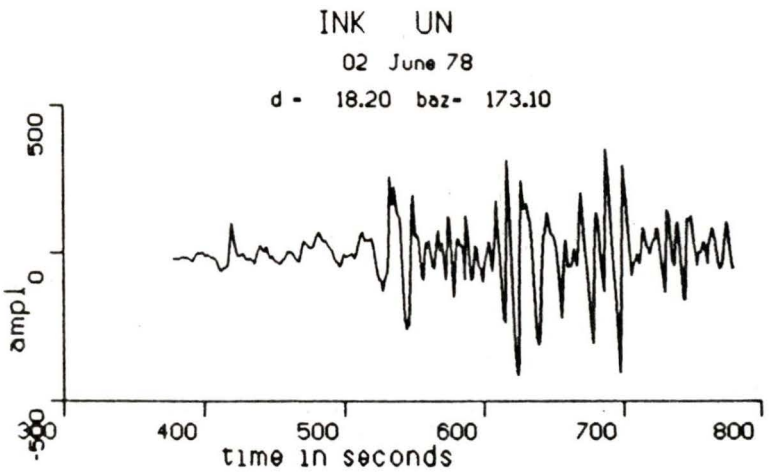
INK UN
02 June 78
d - 18.20 baz- 173.10
ampl
500
0
-500
400
500
600
700
800
time in seconds

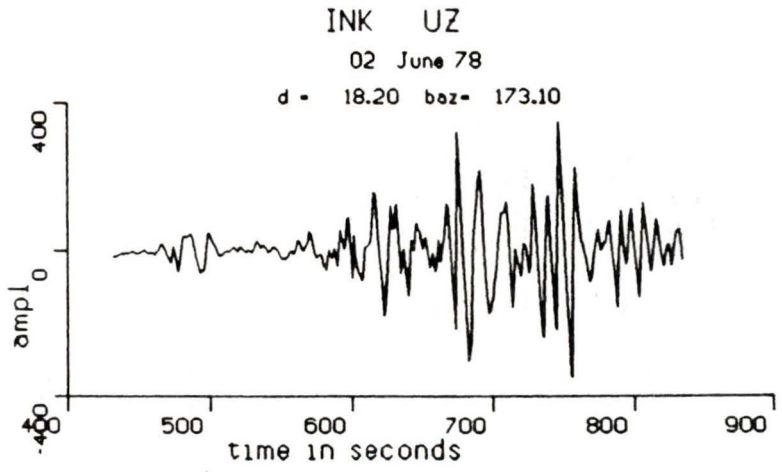
INK UZ
02 June 78
d - 18.20 baz- 173.10
ampl
400
0
-400
500
600
700
800
900
time in seconds

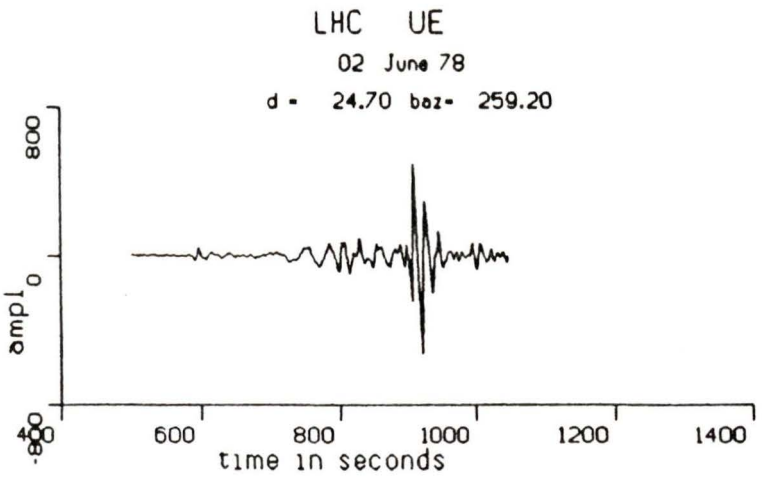
LHC UE
02 June 78
d - 24.70 baz- 259.20
800
0
-800
ampl
600
800
1000
1200
1400
time in seconds

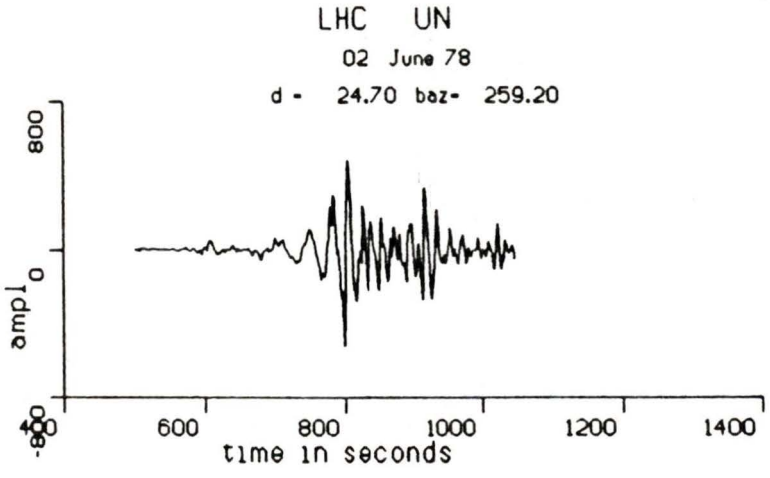
LHC UN
02 June 78
d - 24.70 baz- 259.20
800
0
-800
ampl
600
800
1000
1200
1400
time in seconds

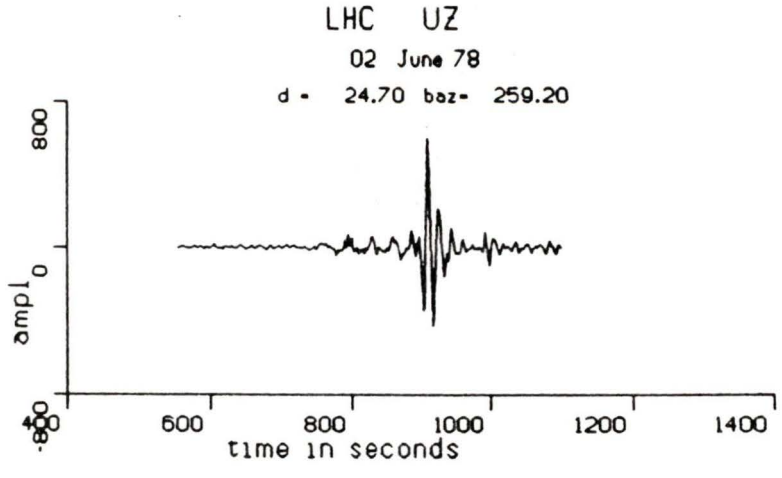
LHC UZ
02 June 78
d - 24.70 baz- 259.20
800
0
-800
ampl
600
800
1000
1200
1400
time in seconds

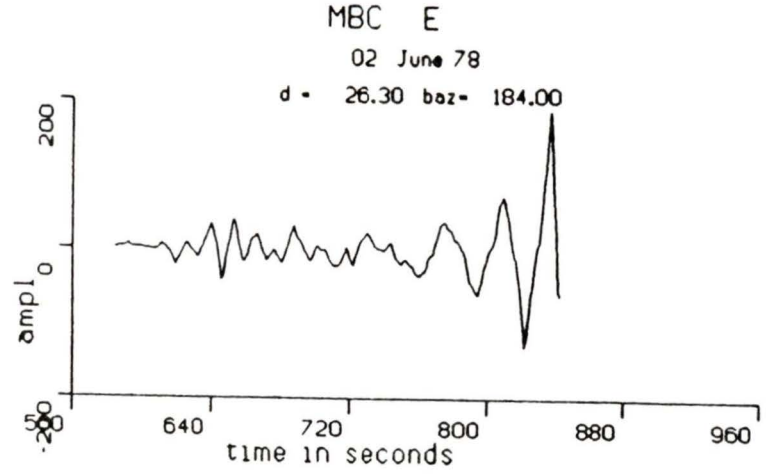
MBC E
02 June 78
d - 26.30 baz- 184.00
ampl
200
0
-200
640
720
800
880
960
time in seconds

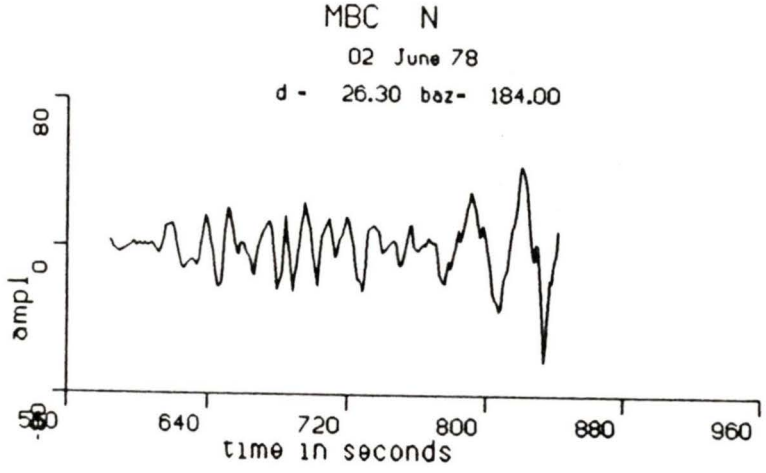
MBC N
02 June 78
d - 26.30 baz- 184.00
ampl
80
0
-80
640
720
800
880
960
time in seconds

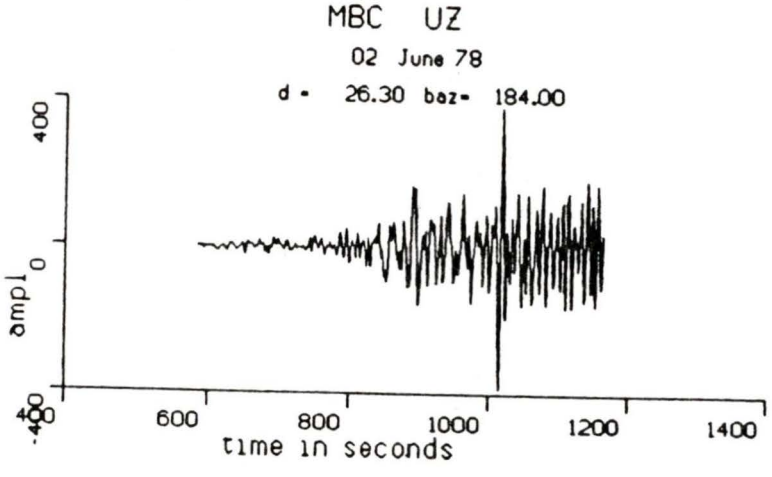
MBC UZ
02 June 78
d - 26.30 baz- 184.00
ampl
400
0
-400
600
800
1000
1200
1400
time in seconds

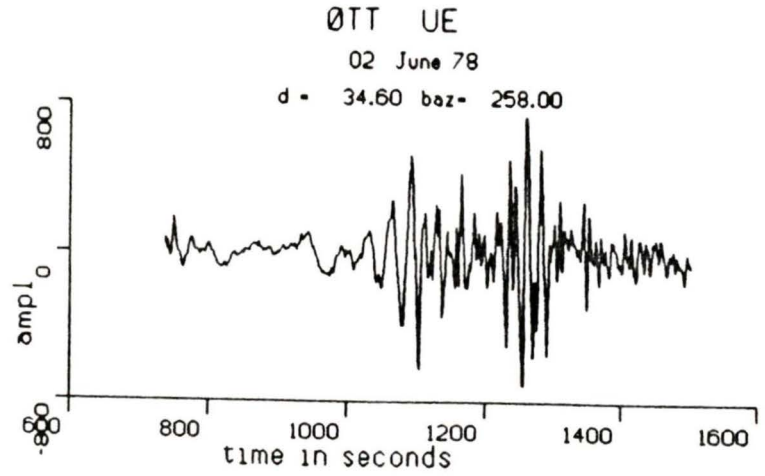
ØTT UE
02 June 78
d = 34.60 baz= 258.00
800
0
-800
ampl
800
1000
1200
1400
1600
time in seconds

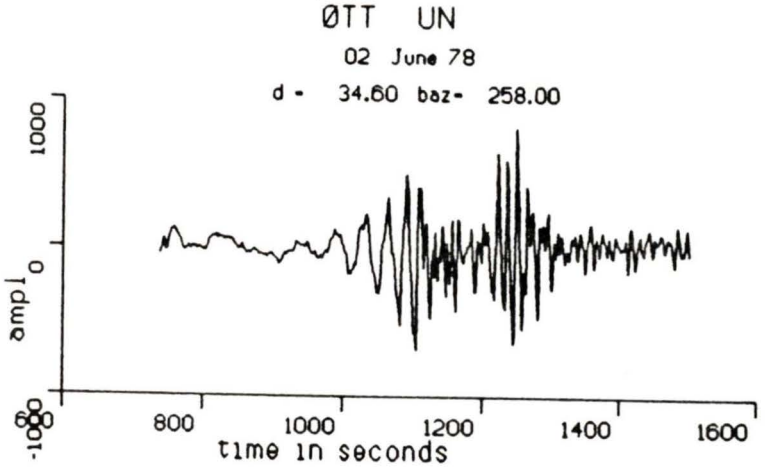
ØTT UN
02 June 78
d = 34.60 baz= 258.00
1000
0
-1000
ampl
800
1000
1200
1400
1600
time in seconds

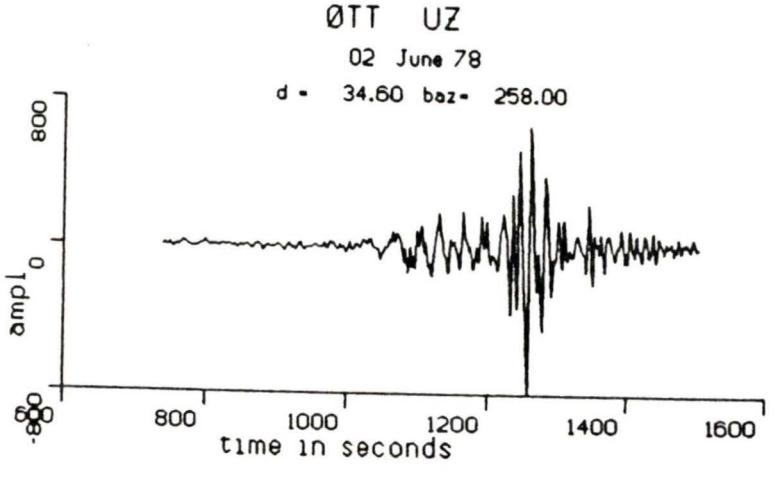
ØTT UZ
02 June 78
d = 34.60 baz= 258.00
800
0
-800
ampl
800
1000
1200
1400
1600
time in seconds

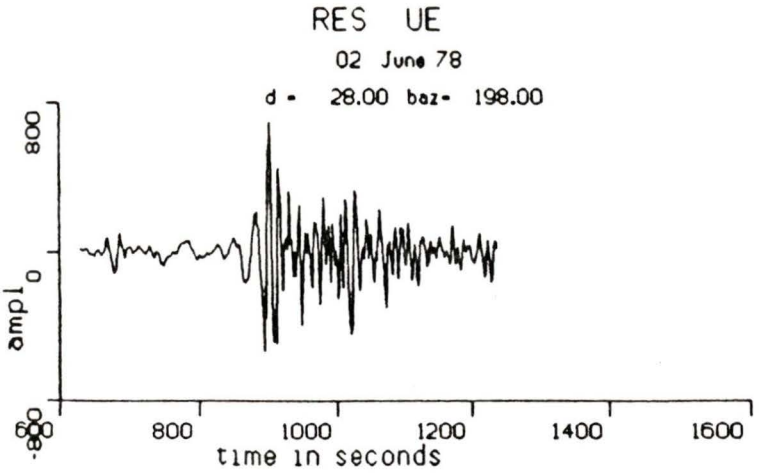
RES UE
02 June 78
d - 28.00 baz- 198.00
800
0
-800
ampl
600
800
1000
1200
1400
1600
time in seconds

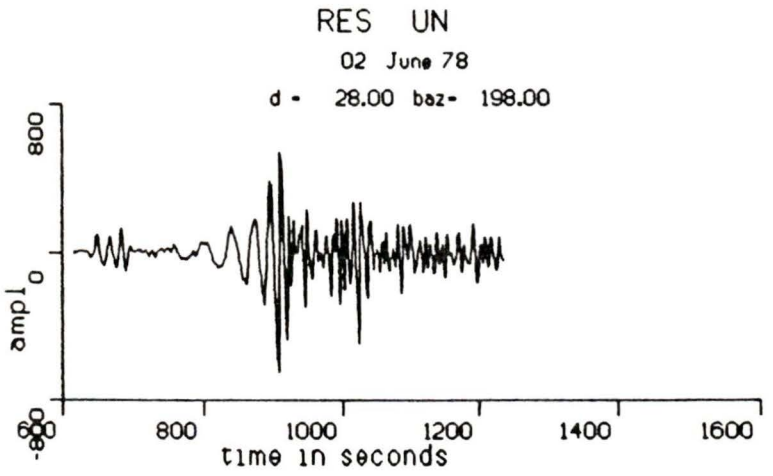
RES UN
02 June 78
d - 28.00 baz- 198.00
800
0
-800
ampl
600
800
1000
1200
1400
1600
time in seconds

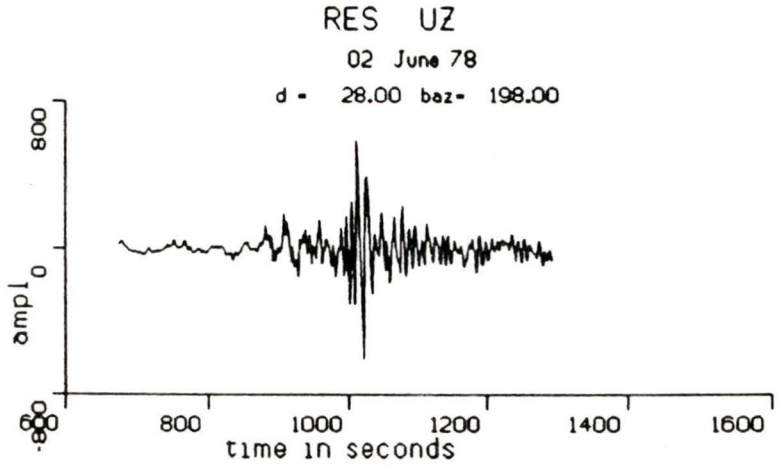
RES UZ
02 June 78
d - 28.00 baz- 198.00
800
0
-800
ampl
600
800
1000
1200
1400
1600
time in seconds

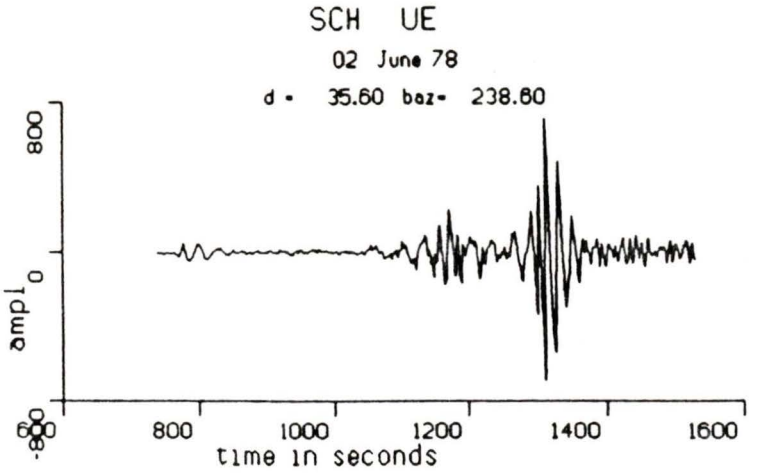
SCH UE
02 June 78
d = 35.60 baz= 238.60
800
0
-800
ampl
600
800
1000
1200
1400
1600
time in seconds

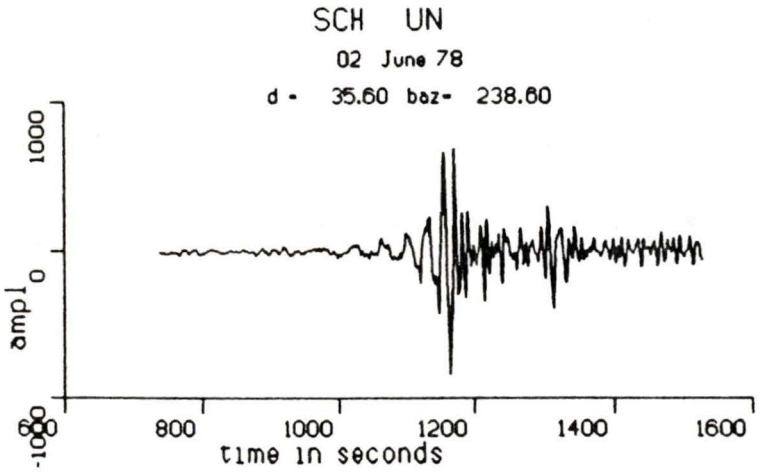
SCH UN
02 June 78
d = 35.60 baz= 238.60
1000
0
-1000
ampl
600
800
1000
1200
1400
1600
time in seconds

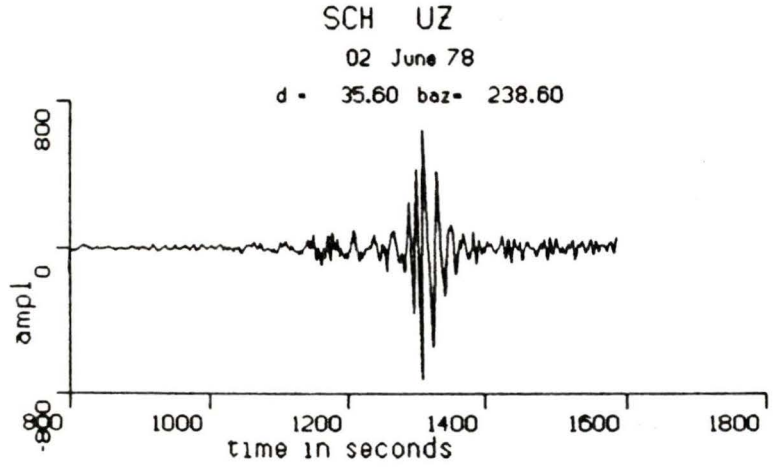
SCH UZ
02 June 78
d = 35.60 baz= 238.60
800
0
-800
ampl
800
1000
1200
1400
1600
1800
time in seconds

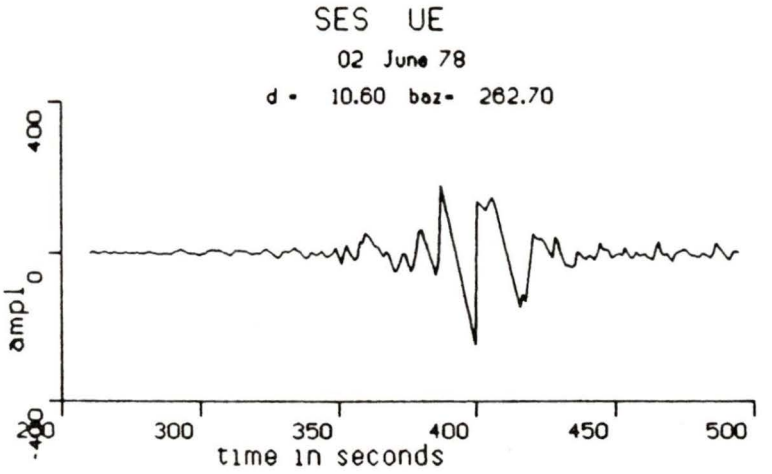
SES UE
02 June 78
d = 10.60 baz= 262.70
400
0
-400
ampl
200
300
350
400
450
500
time in seconds

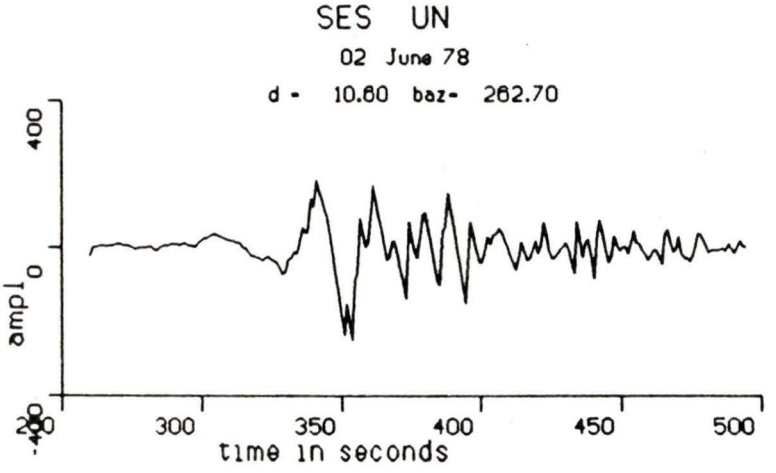
SES UN
02 June 78
d = 10.60 baz= 262.70
400
0
-400
ampl
200
300
350
400
450
500
time in seconds

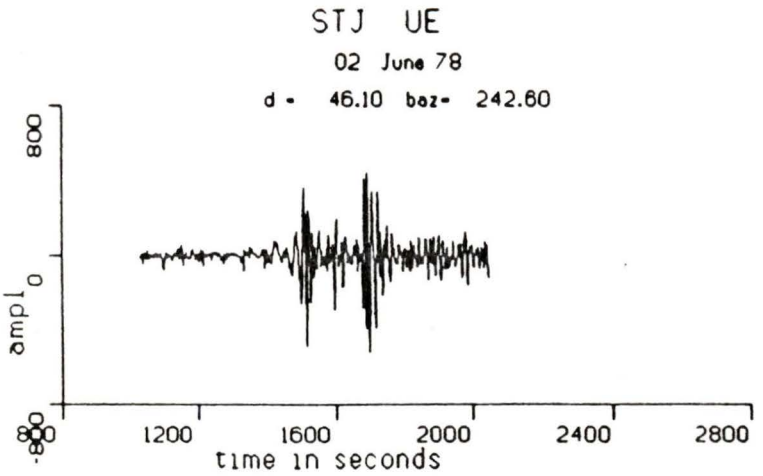
STJ UE
02 June 78
d = 46.10 baz= 242.60
800
ampl 0
-800
1200
1600
2000
2400
2800
time in seconds

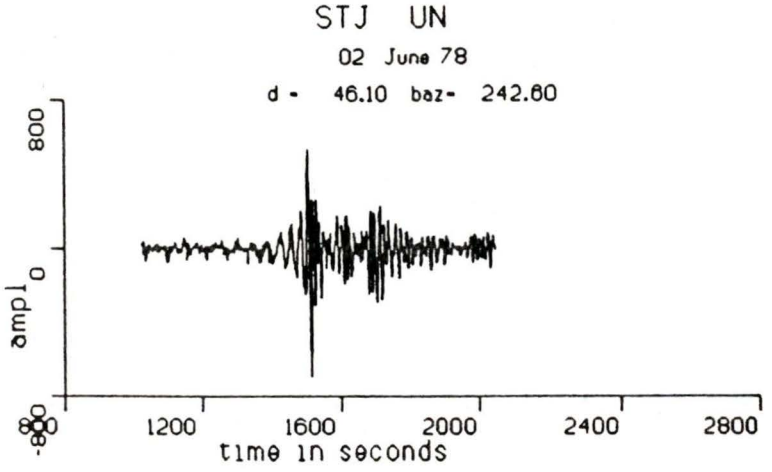
STJ UN
02 June 78
d = 46.10 baz= 242.60
800
ampl 0
-800
1200
1600
2000
2400
2800
time in seconds

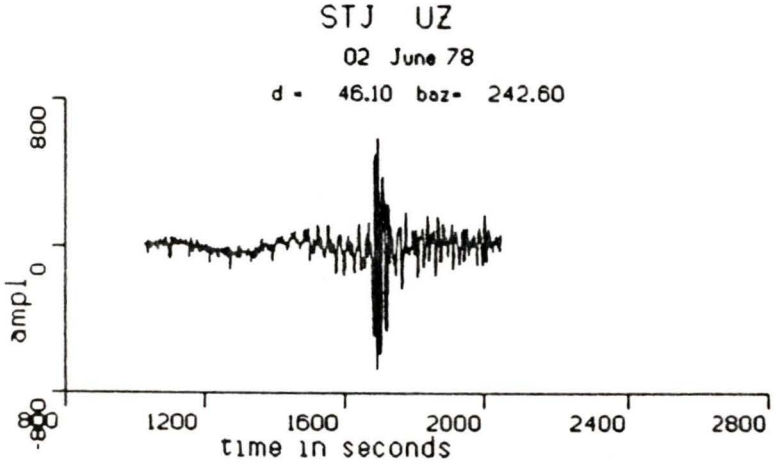
STJ UZ
02 June 78
d = 46.10 baz= 242.60
800
ampl 0
-800
1200
1600
2000
2400
2800
time in seconds

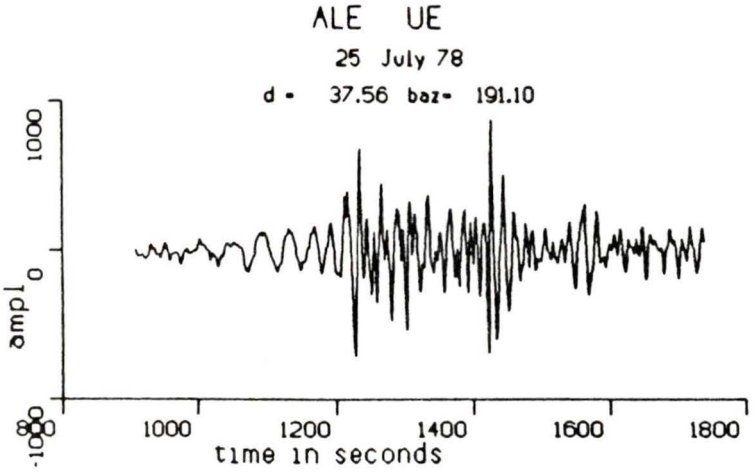
ALE UE
25 July 78
d = 37.56 baz= 191.10
ampl
1000
0
-1000
1000
1200
1400
1600
1800
time in seconds

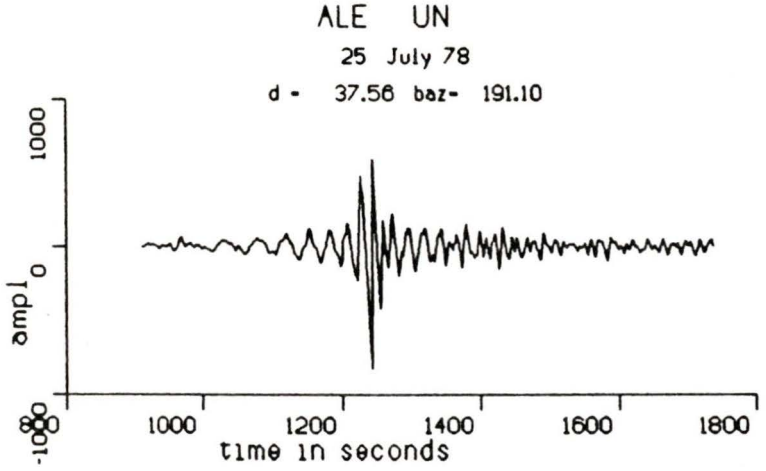
ALE UN
25 July 78
d = 37.56 baz= 191.10
ampl
1000
0
-1000
1000
1200
1400
1600
1800
time in seconds

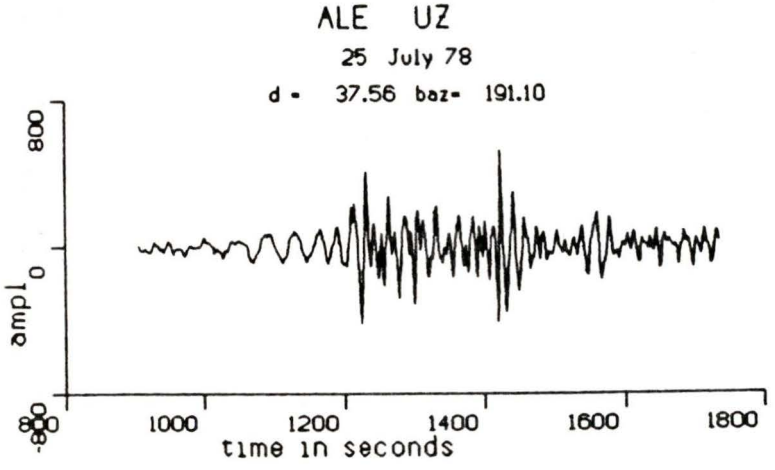
ALE UZ
25 July 78
d = 37.56 baz= 191.10
ampl
800
0
-800
1000
1200
1400
1600
1800
time in seconds

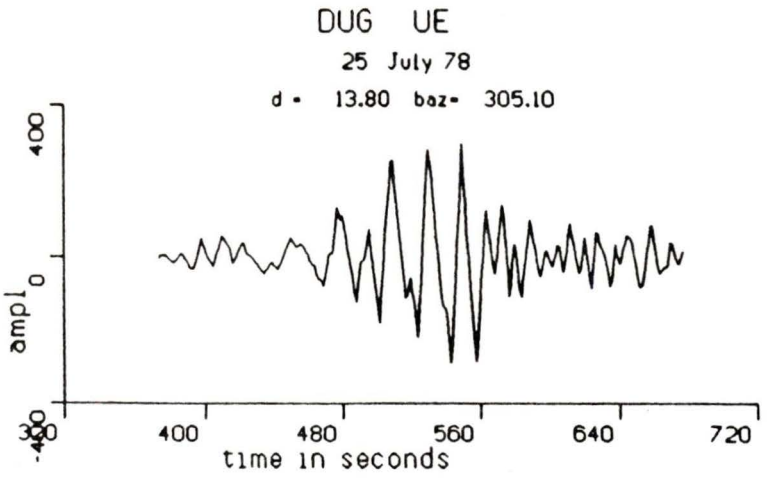
DUG UE
25 July 78
d = 13.80 baz= 305.10
400
0
-400
ampl
400
480
560
640
720
time in seconds

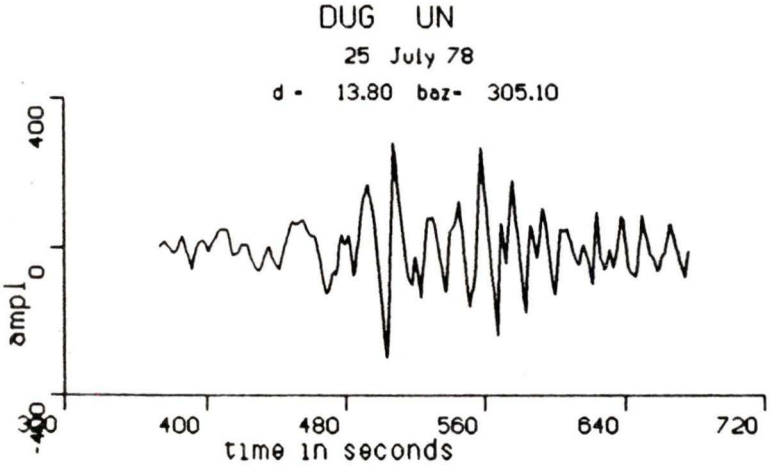
DUG UN
25 July 78
d = 13.80 baz= 305.10
400
0
-400
ampl
400
480
560
640
720
time in seconds

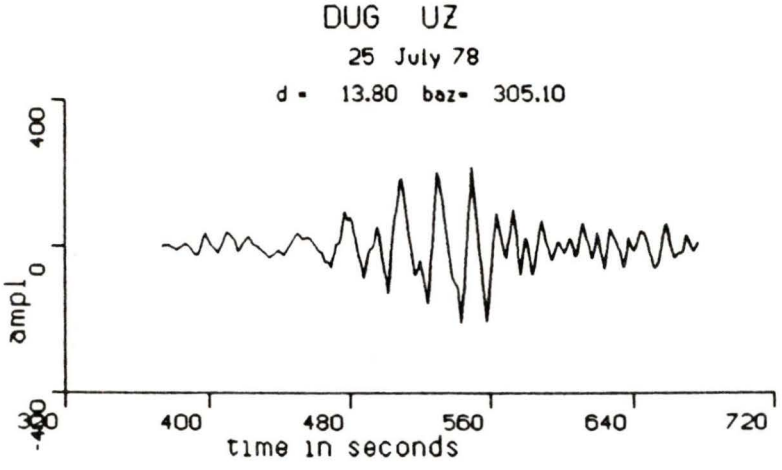
DUG UZ
25 July 78
d = 13.80 baz= 305.10
400
0
-400
ampl
400
480
560
640
720
time in seconds

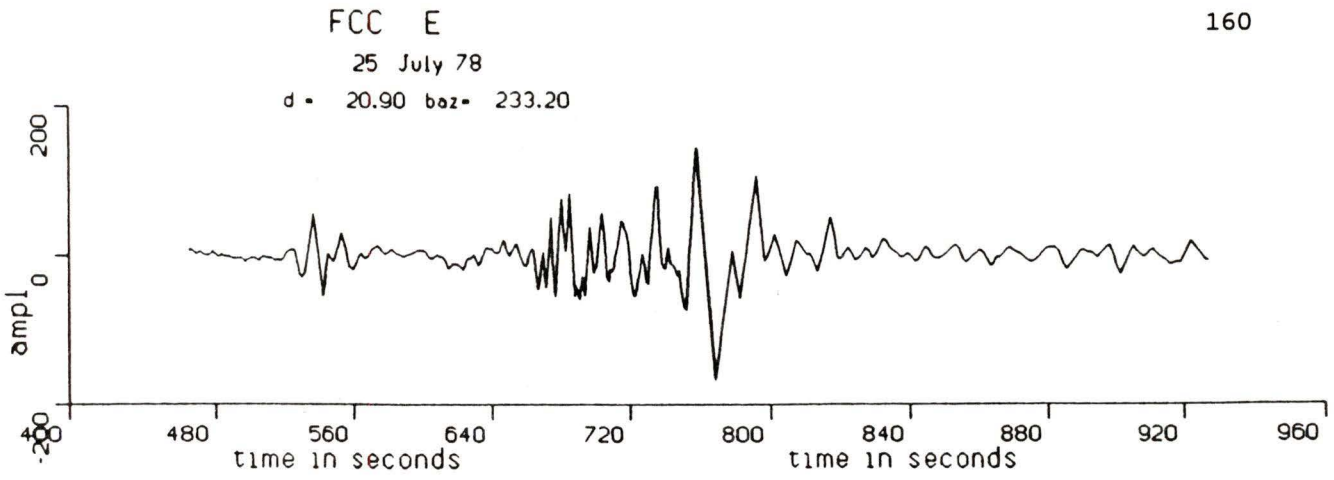
FCC E
25 July 78
d = 20.90 baz= 233.20
ampl
200
0
-200
480
560
640
720
800
840
880
920
960
time in seconds
time in seconds

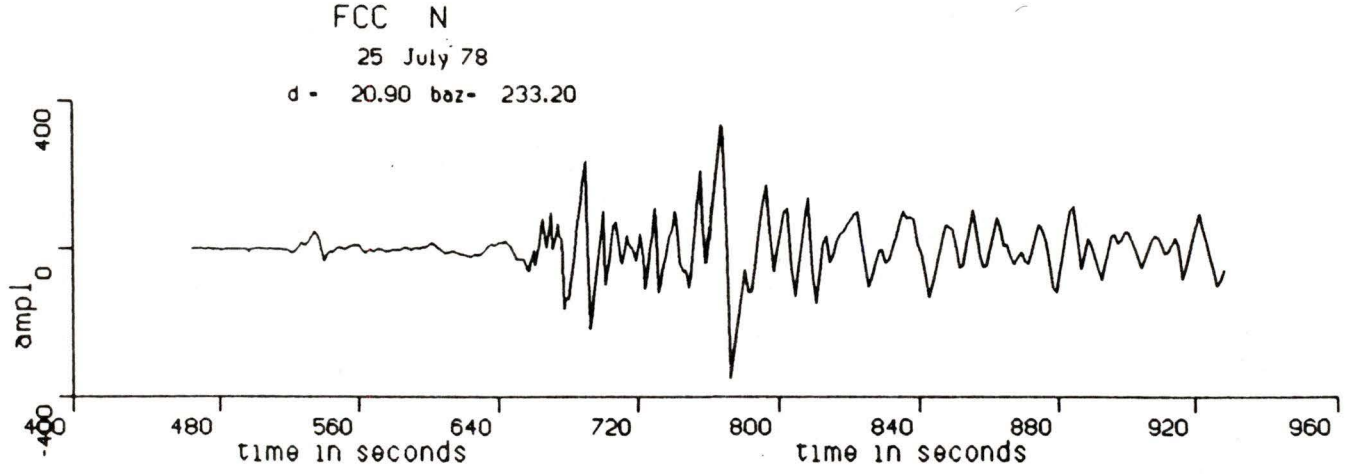
FCC N
25 July 78
d = 20.90 baz= 233.20
ampl
400
0
-400
480
560
640
720
800
840
880
920
960
time in seconds
time in seconds

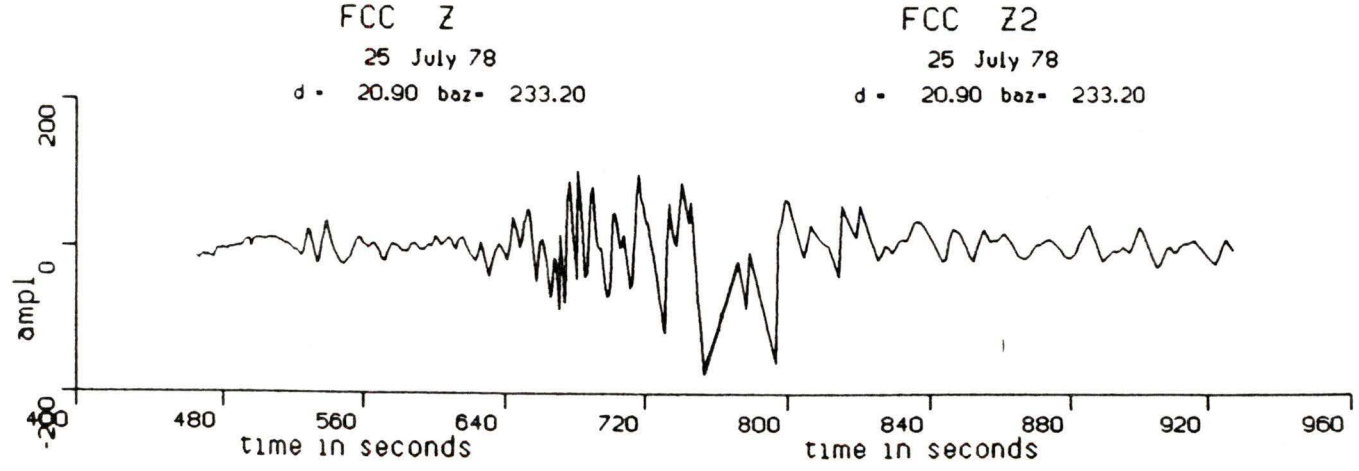
FCC Z
25 July 78
d = 20.90 baz= 233.20
FCC Z2
25 July 78
d = 20.90 baz= 233.20
ampl
200
0
-200
480
560
640
720
800
840
880
920
960
time in seconds
time in seconds

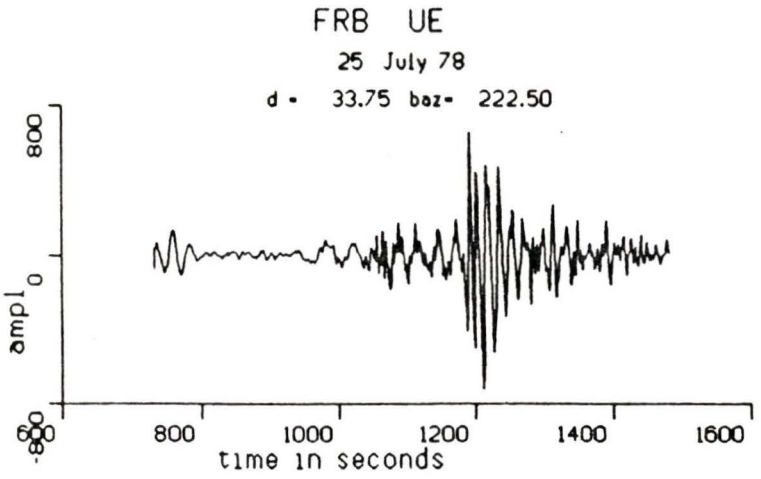
FRB UE
25 July 78
d = 33.75 baz= 222.50
800
0
-800
ampl
800
1000
1200
1400
1600
time in seconds

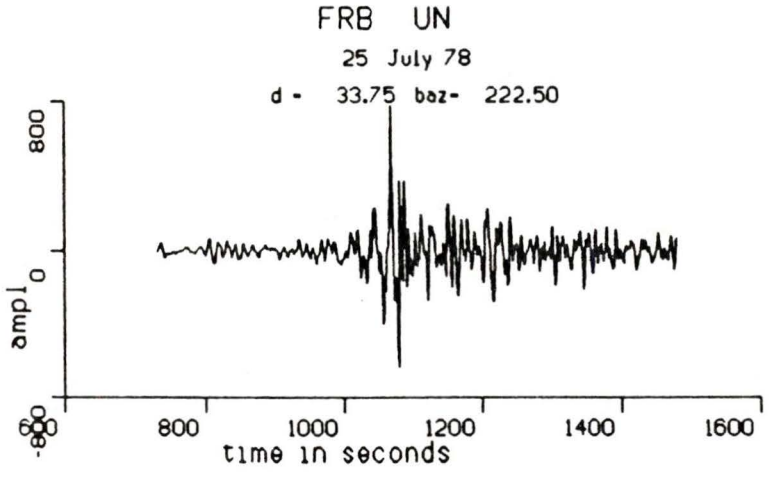
FRB UN
25 July 78
d = 33.75 baz= 222.50
800
0
-800
ampl
800
1000
1200
1400
1600
time in seconds

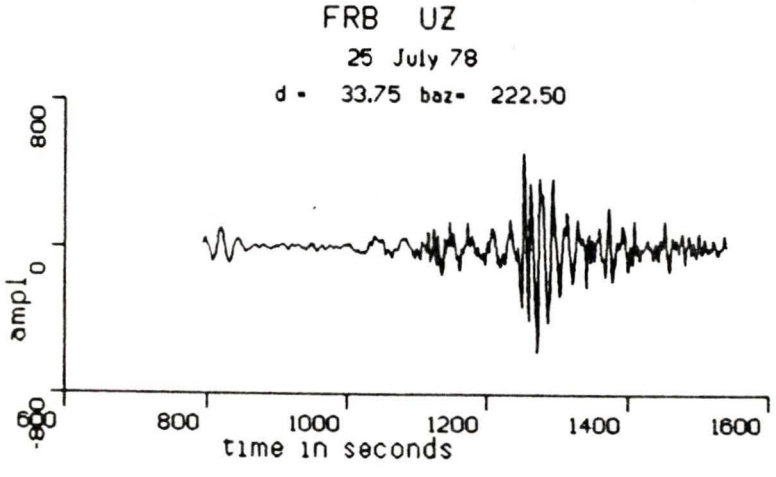
FRB UZ
25 July 78
d = 33.75 baz= 222.50
800
0
-800
ampl
800
1000
1200
1400
1600
time in seconds

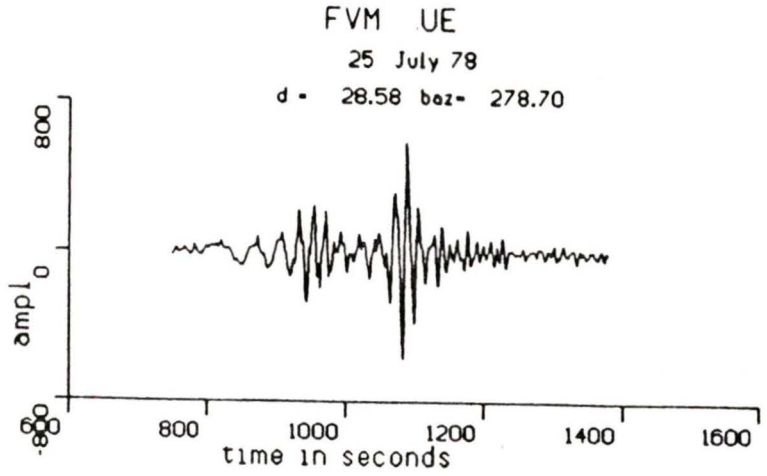
FVM UE
25 July 78
d = 28.58 baz= 278.70
800
0
-800
ampl
800
1000
1200
1400
1600
time in seconds

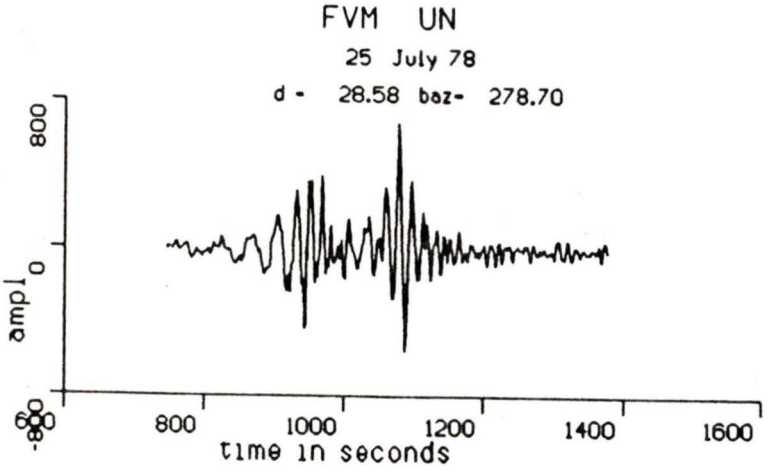
FVM UN
25 July 78
d = 28.58 baz= 278.70
800
0
-800
ampl
800
1000
1200
1400
1600
time in seconds

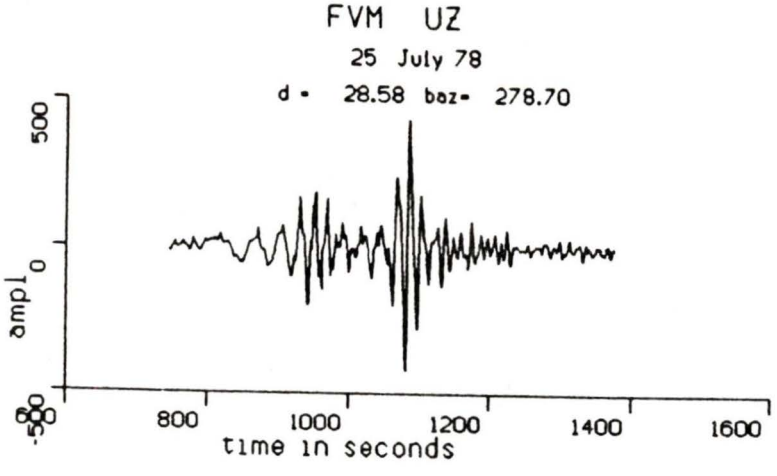
FVM UZ
25 July 78
d = 28.58 baz= 278.70
500
0
-500
ampl
800
1000
1200
1400
1600
time in seconds

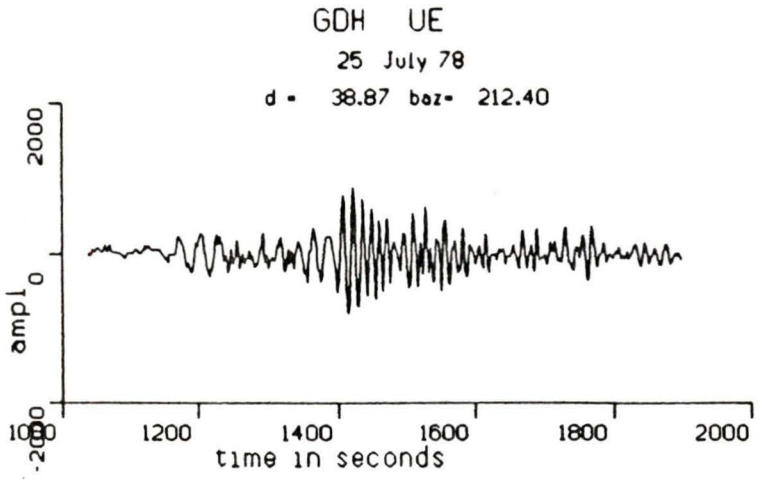
GDH UE
25 July 78
d = 38.87 baz= 212.40
2000
0
-2000
ampl
1000
1200
1400
1600
1800
2000
time in seconds

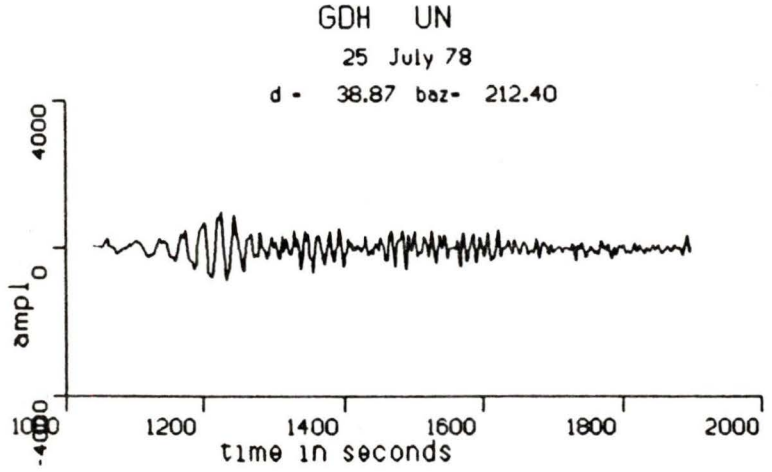
GDH UN
25 July 78
d = 38.87 baz= 212.40
4000
0
-4000
ampl
1000
1200
1400
1600
1800
2000
time in seconds

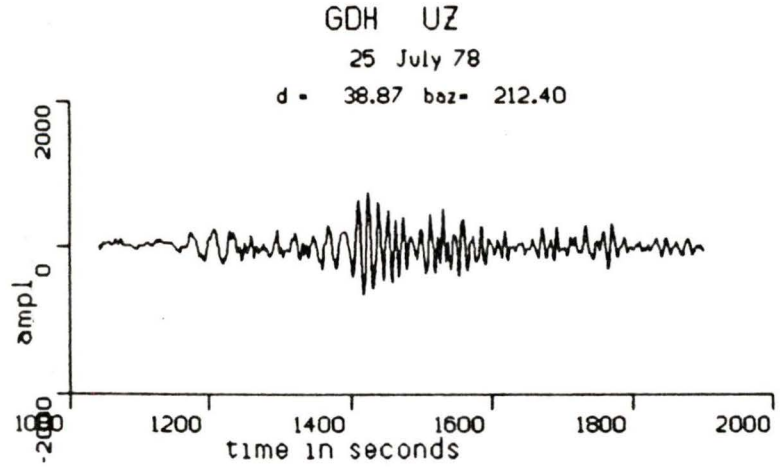
GDH UZ
25 July 78
d = 38.87 baz= 212.40
2000
0
-2000
ampl
1000
1200
1400
1600
1800
2000
time in seconds

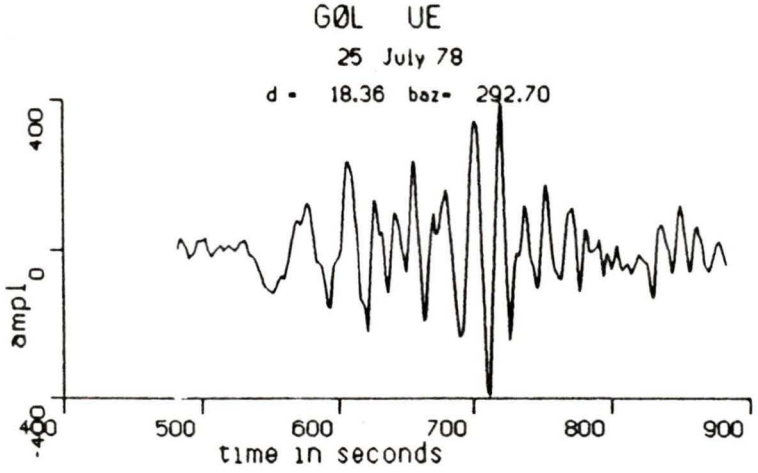
GØL UE
25 July 78
d = 18.36 baz= 292.70
ampl
400
0
-400
500
600
700
800
900
time in seconds

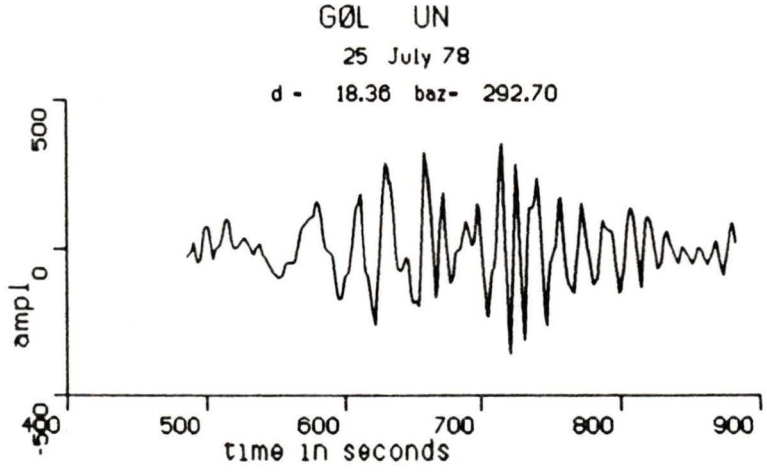
GØL UN
25 July 78
d = 18.36 baz= 292.70
ampl
500
0
-500
500
600
700
800
900
time in seconds

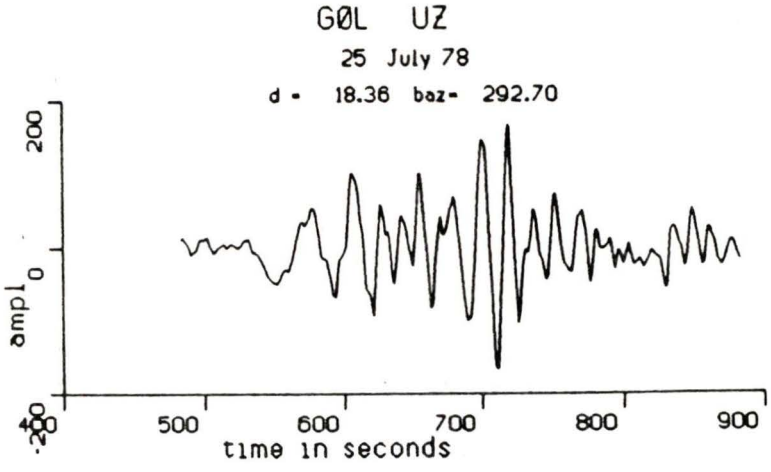
GØL UZ
25 July 78
d = 18.36 baz= 292.70
ampl
200
0
-200
500
600
700
800
900
time in seconds

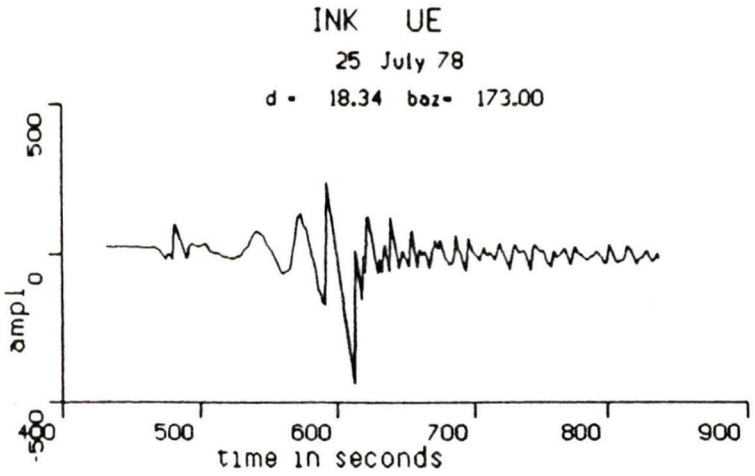
INK UE
25 July 78
d = 18.34 baz= 173.00
ampl
500
0
-500
500
600
700
800
900
time in seconds

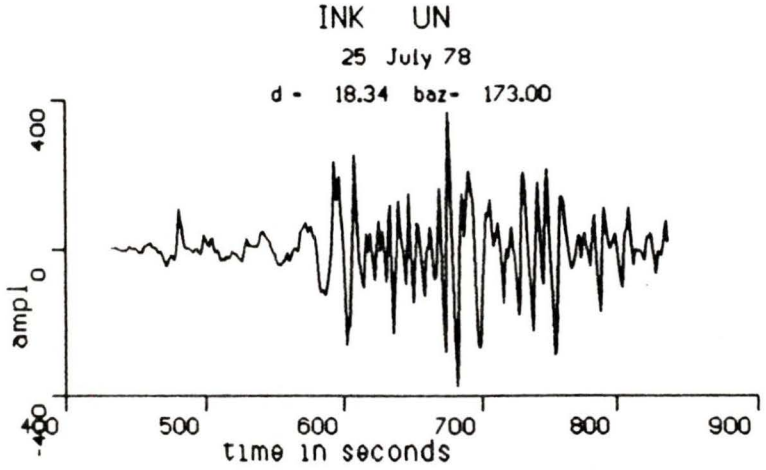
INK UN
25 July 78
d = 18.34 baz= 173.00
ampl
400
0
-400
500
600
700
800
900
time in seconds

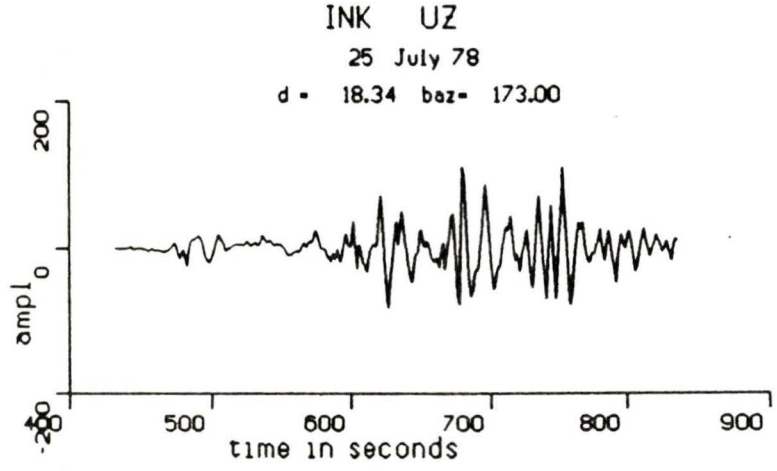
INK UZ
25 July 78
d = 18.34 baz= 173.00
ampl
200
0
-200
500
600
700
800
900
time in seconds

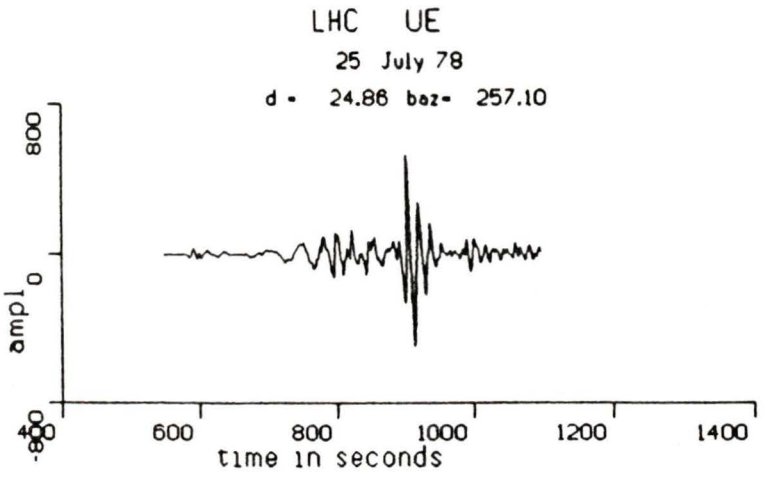
LHC UE
25 July 78
d = 24.86 baz= 257.10
800
0
-800
ampl
400
600
800
1000
1200
1400
time in seconds

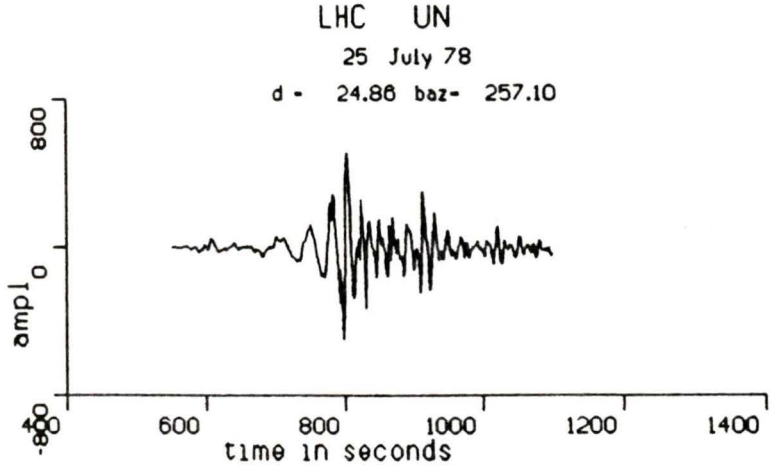
LHC UN
25 July 78
d = 24.86 baz= 257.10
800
0
-800
ampl
400
600
800
1000
1200
1400
time in seconds

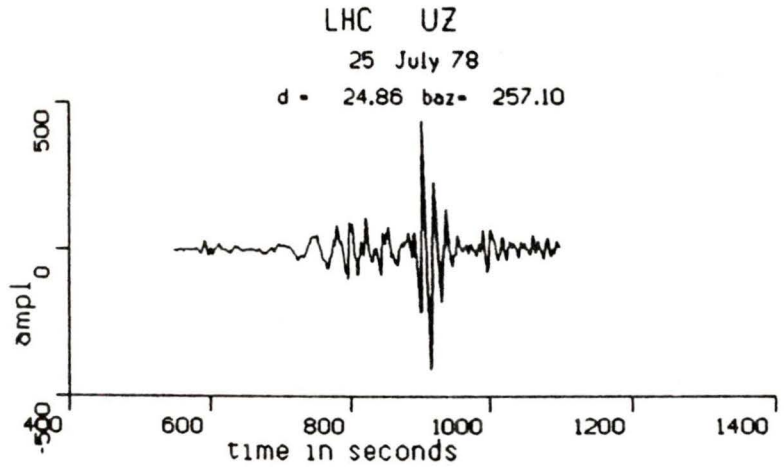
LHC UZ
25 July 78
d = 24.86 baz= 257.10
500
0
-500
ampl
400
600
800
1000
1200
1400
time in seconds

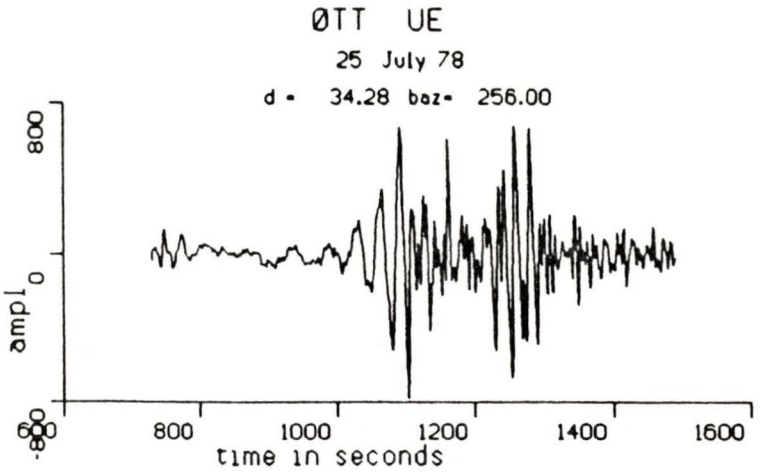
ØTT UE
25 July 78
d = 34.28 baz= 256.00
800
0
-800
ampl
800
1000
1200
1400
1600
time in seconds

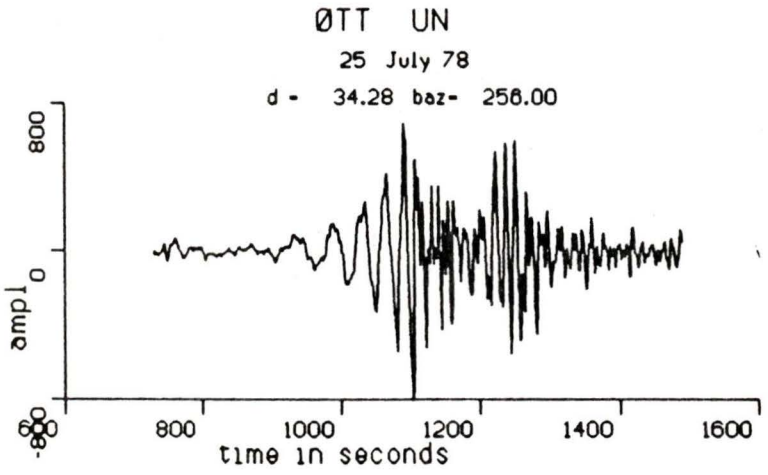
ØTT UN
25 July 78
d = 34.28 baz= 256.00
800
0
-800
ampl
800
1000
1200
1400
1600
time in seconds

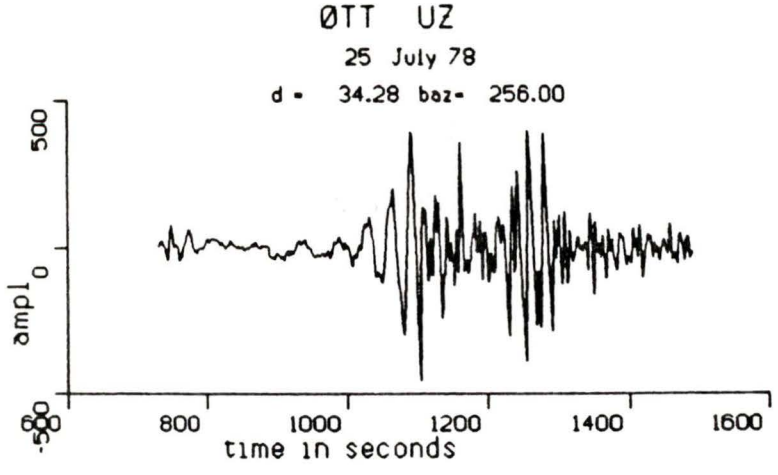
ØTT UZ
25 July 78
d = 34.28 baz= 256.00
500
0
-500
ampl
800
1000
1200
1400
1600
time in seconds

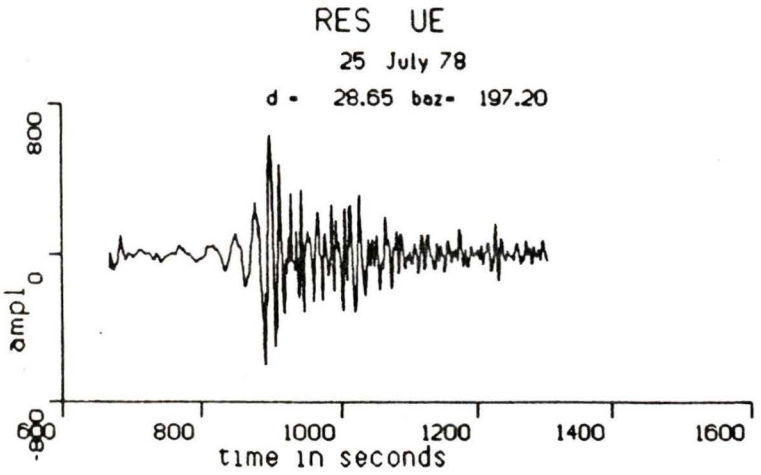
RES UE
25 July 78
d = 28.65 baz= 197.20
800
0
-800
ampl
800
1000
1200
1400
1600
time in seconds

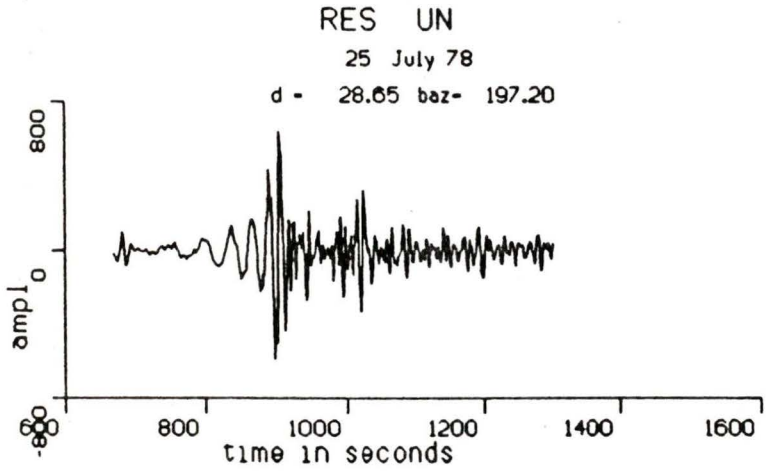
RES UN
25 July 78
d = 28.65 baz= 197.20
800
0
-800
ampl
800
1000
1200
1400
1600
time in seconds

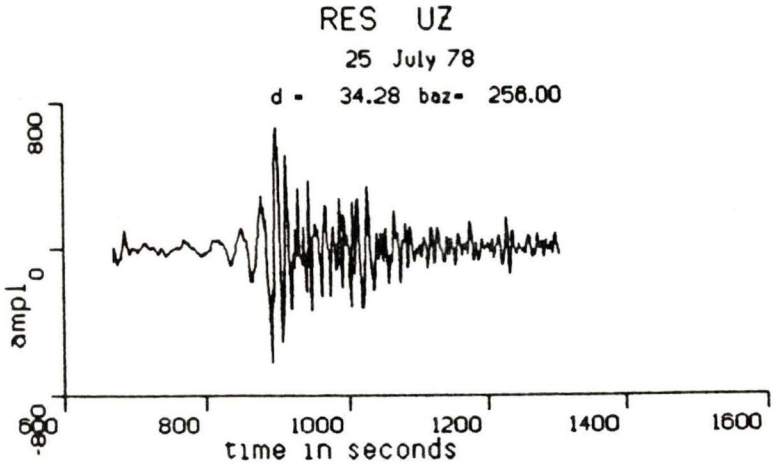
RES UZ
25 July 78
d = 34.28 baz= 256.00
800
0
-800
ampl
800
1000
1200
1400
1600
time in seconds

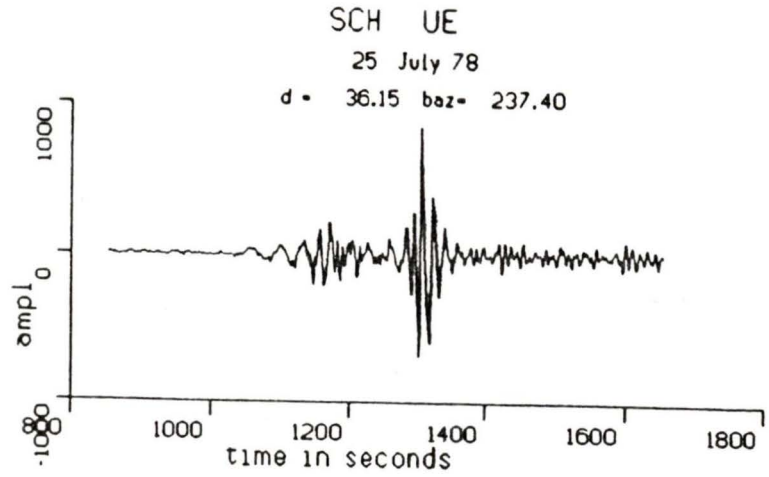
SCH UE
25 July 78
d = 36.15 baz= 237.40
1000
0
-1000
ampl
1000
1200
1400
1600
1800
time in seconds

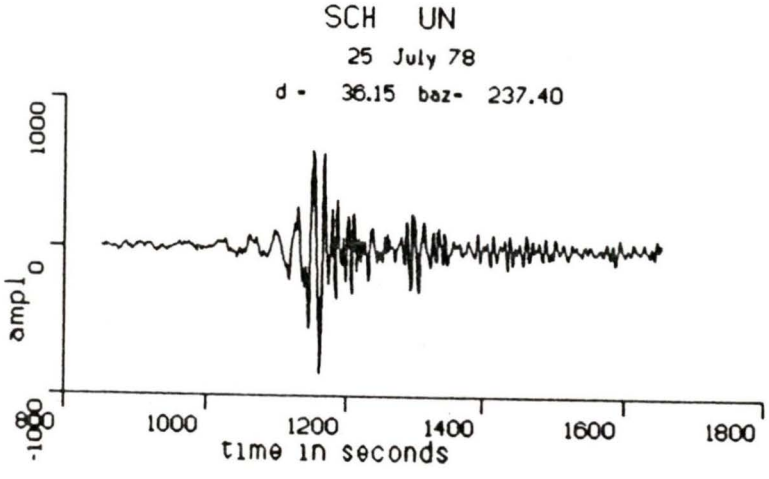
SCH UN
25 July 78
d = 36.15 baz= 237.40
1000
0
-1000
ampl
1000
1200
1400
1600
1800
time in seconds

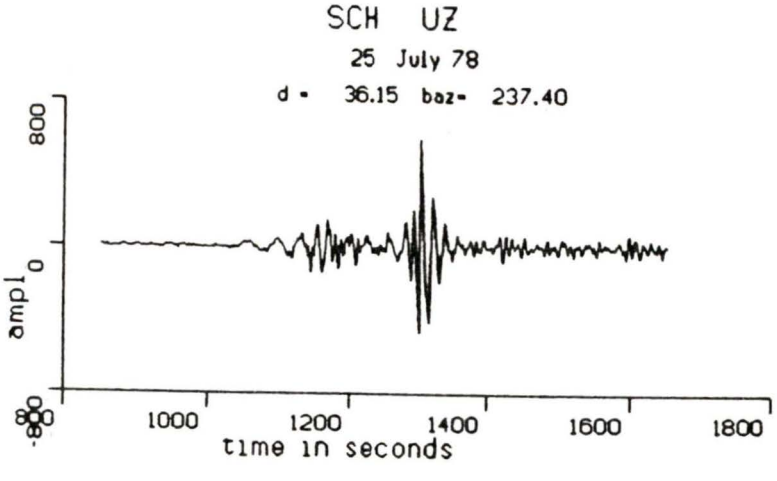
SCH UZ
25 July 78
d = 36.15 baz= 237.40
800
0
-800
ampl
1000
1200
1400
1600
1800
time in seconds

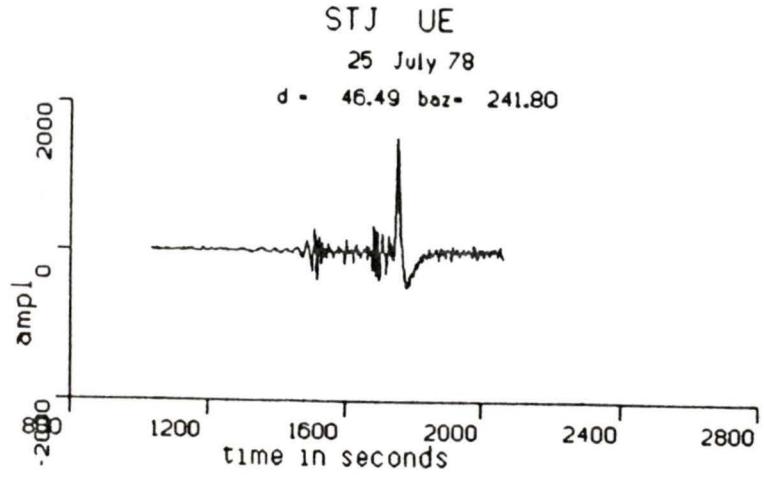
STJ UE
25 July 78
d = 46.49 baz= 241.80
2000
0
-2000
ampl
1200
1600
2000
2400
2800
time in seconds

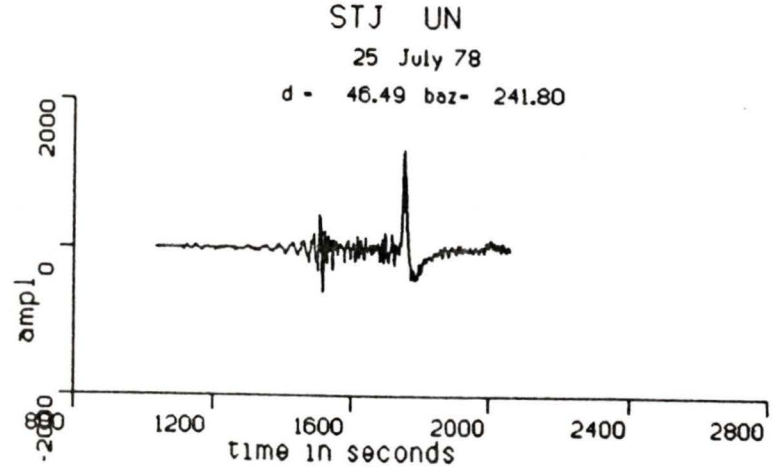
STJ UN
25 July 78
d = 46.49 baz= 241.80
2000
0
-2000
ampl
1200
1600
2000
2400
2800
time in seconds

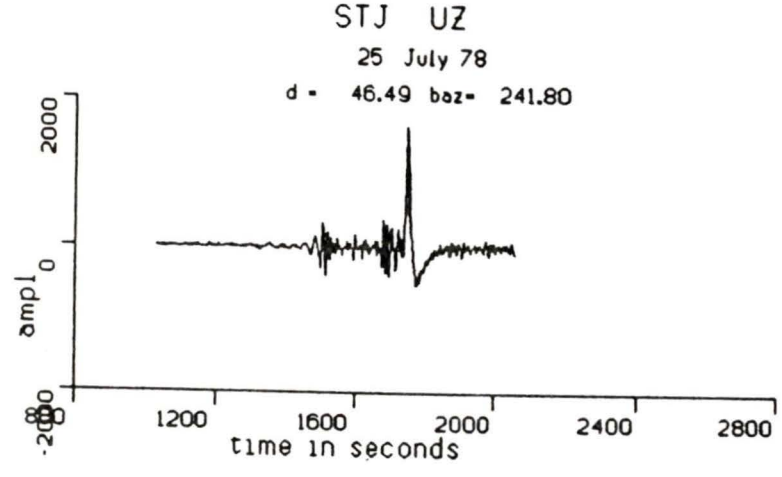
STJ UZ
25 July 78
d = 46.49 baz= 241.80
2000
0
-2000
ampl
1200
1600
2000
2400
2800
time in seconds

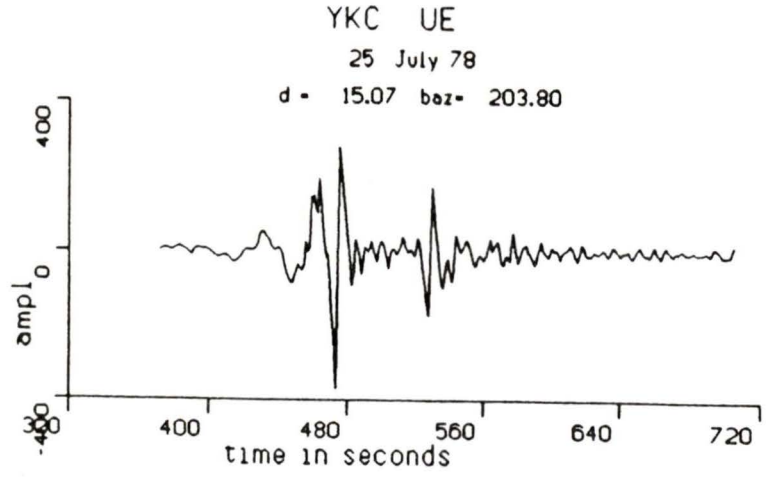
YKC UE
25 July 78
d = 15.07 baz= 203.80
400
0
-400
ampl
400
480
560
640
720
time in seconds

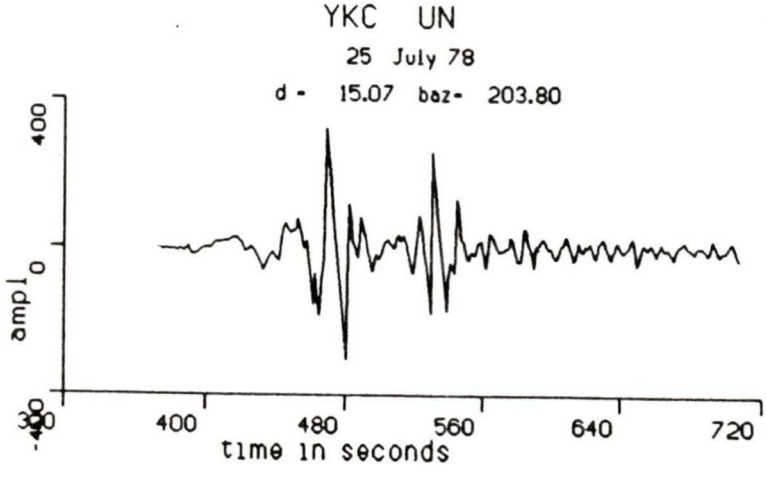
YKC UN
25 July 78
d = 15.07 baz= 203.80
400
0
-400
ampl
400
480
560
640
720
time in seconds

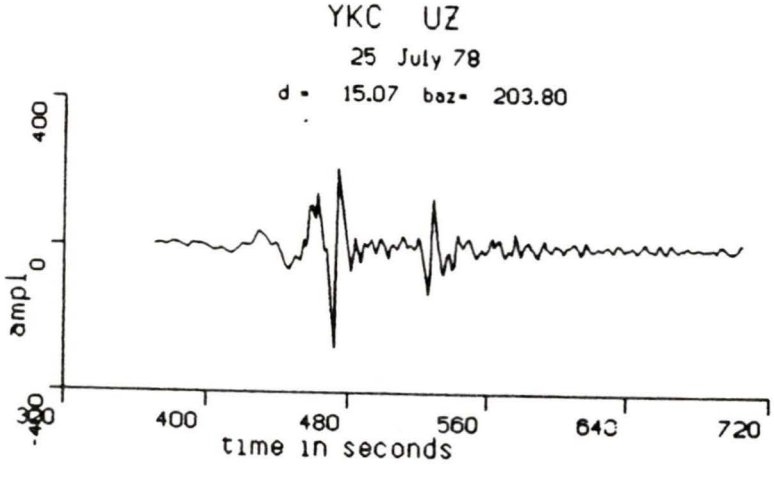
YKC UZ
25 July 78
d = 15.07 baz= 203.80
400
0
-400
ampl
400
480
560
640
720
time in seconds

B-3 : Group velocity dispersion curves for each of the stations which provided useful surface wave data. The plots were produced by the program FILTER (Herrmann, 1978) which was used to determine the spectral amplitudes through band-pass filtering (§ 5.3.1). The stations are listed in alphabetical order for each event. The curves show the distribution of spectral amplitudes for a given group velocity (vertical axis) and period (horizontal axis). The data have been contoured by spectral amplitude. Each component is represented: vertical (Rayleigh), radial (Rayleigh) and transverse (Love).

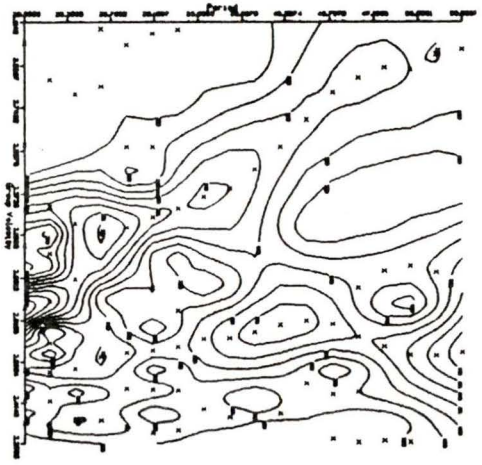

ALE

Vertical

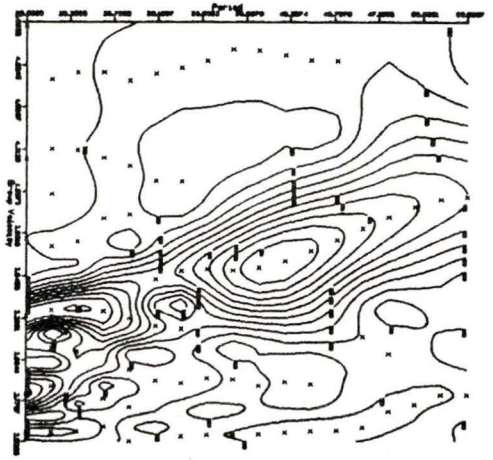

Transverse

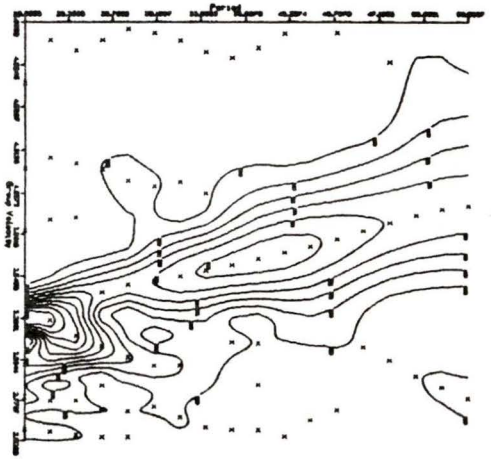

Radial

2 June

FCC

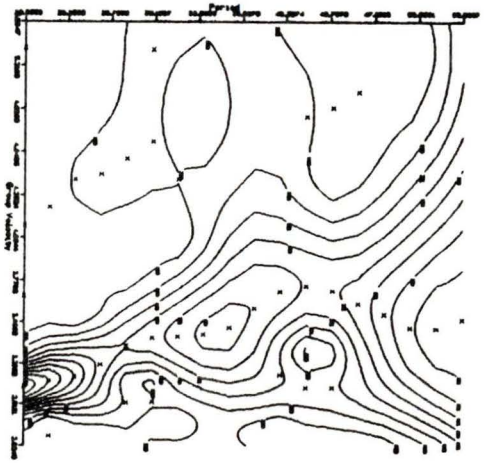

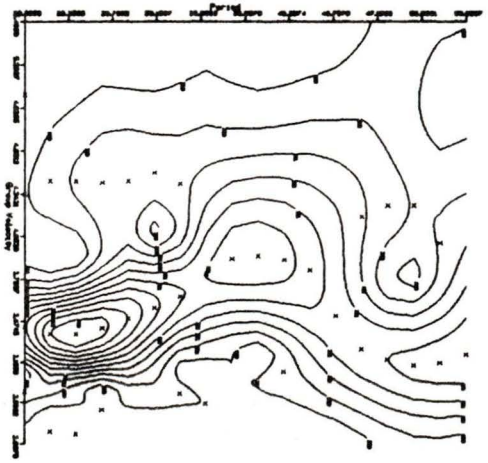

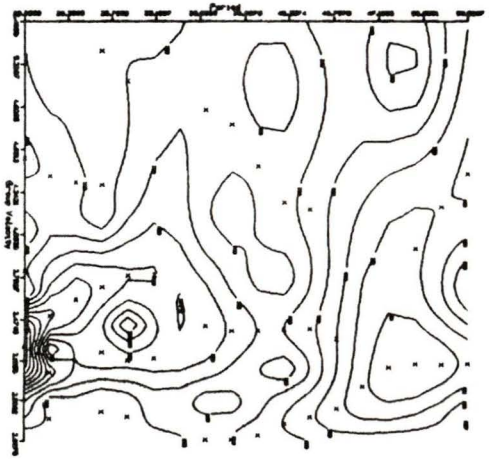

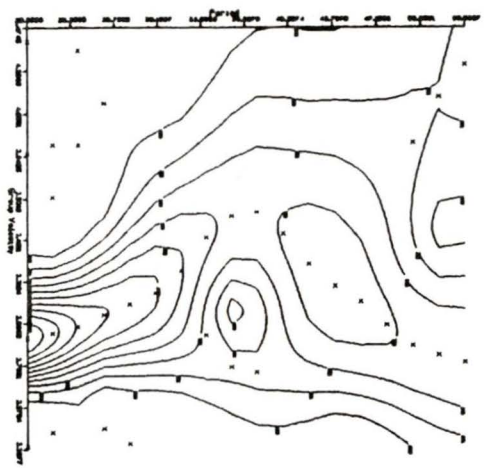

FFC

Vertical

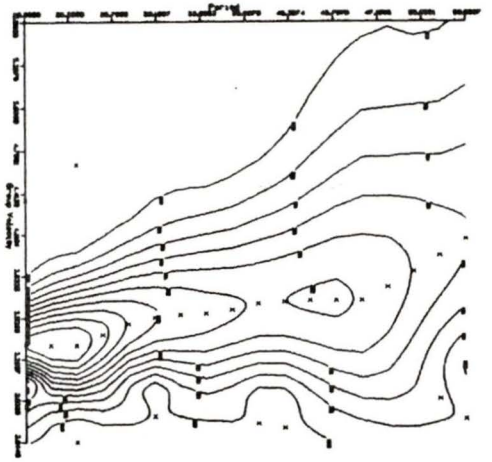

Transverse

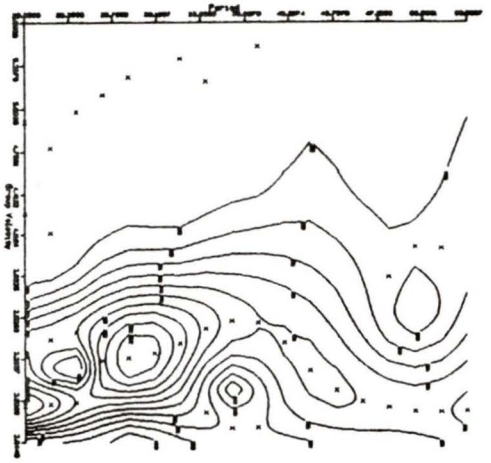

Radial

2 June

FRB

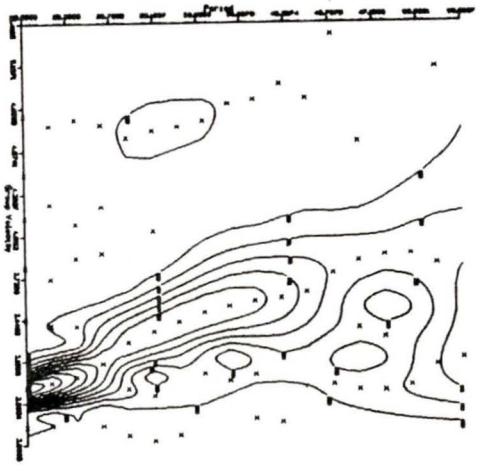

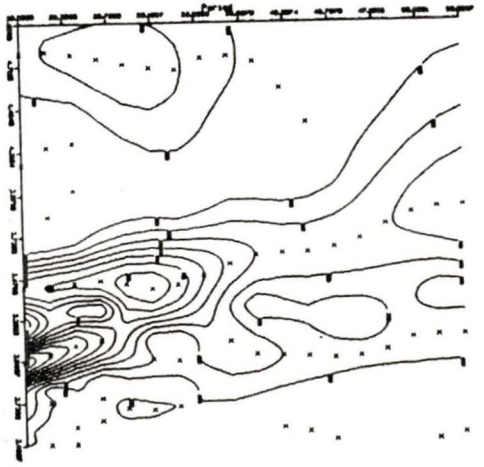

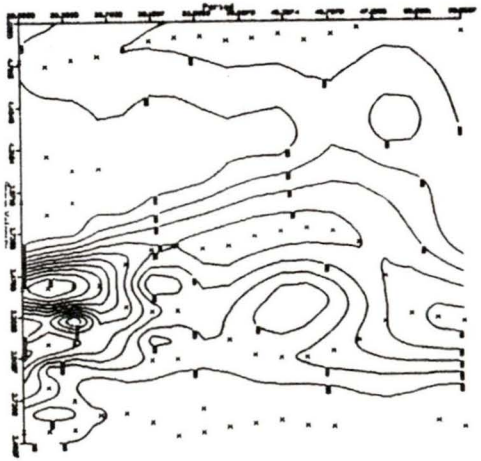

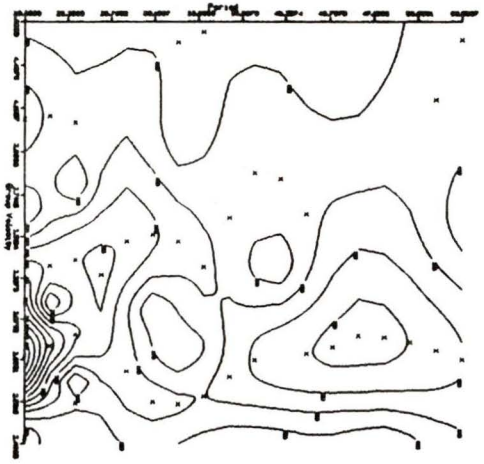

INK

Vertical

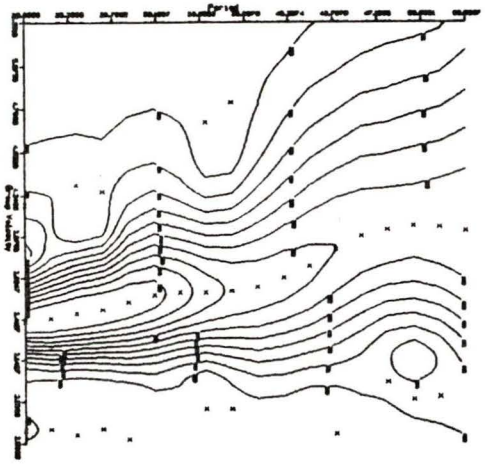

Transverse

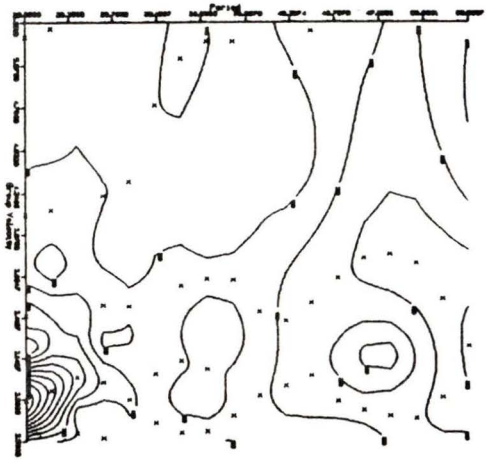

Radial

2 June

LHC

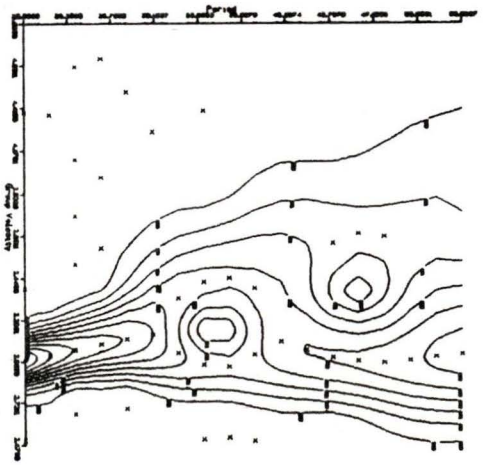

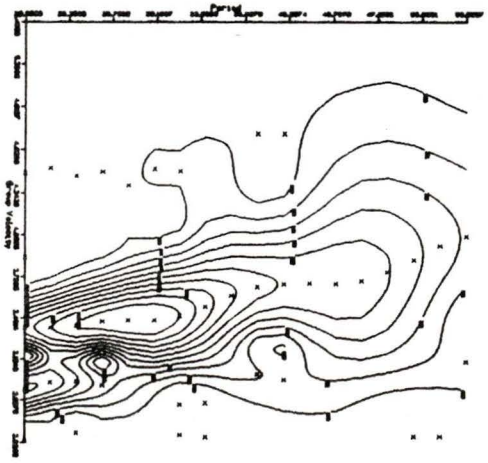

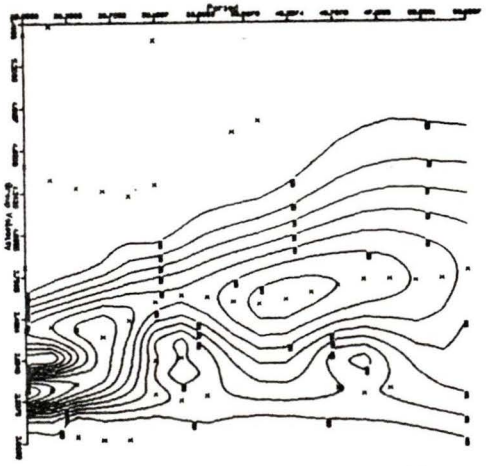

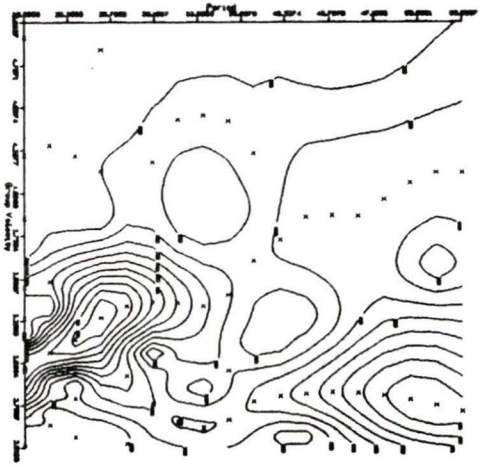

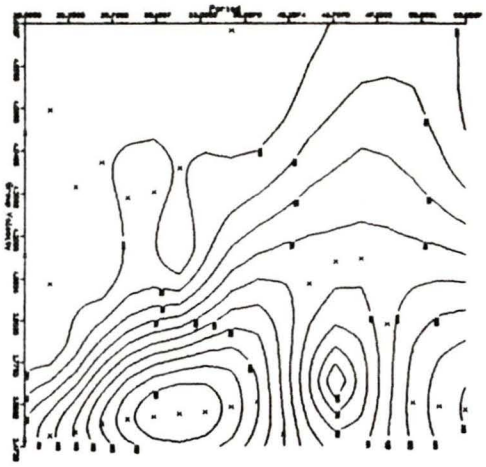

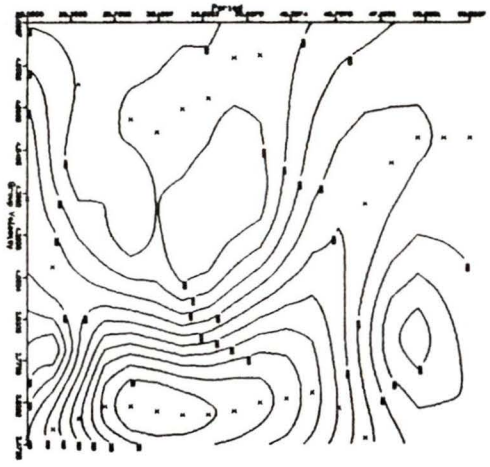

MBC

Vertical

Transverse

Radial

2 June

OTT

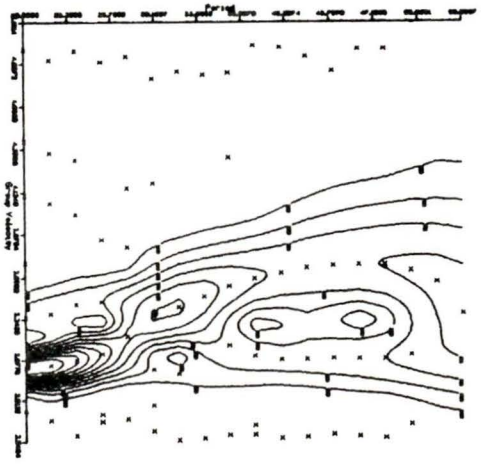

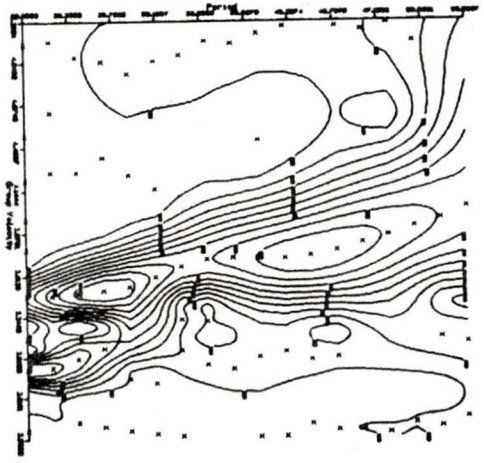

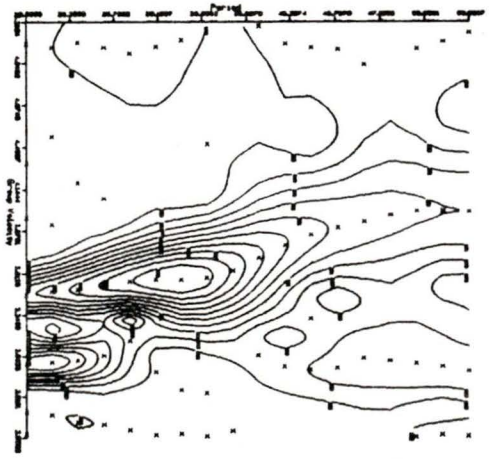

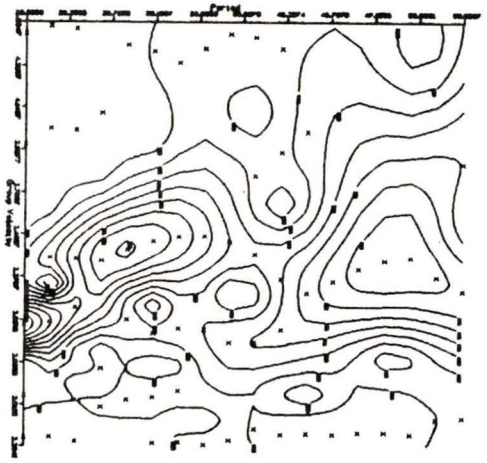

RES

Vertical

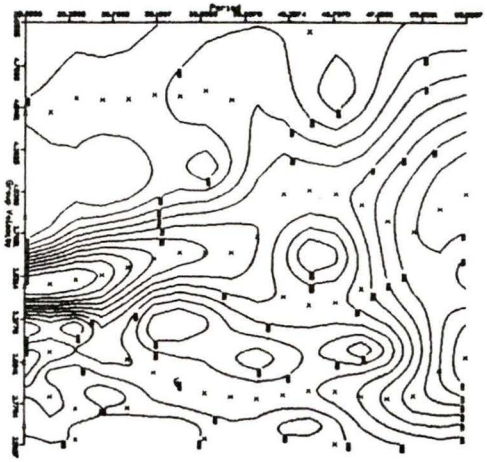

Transverse

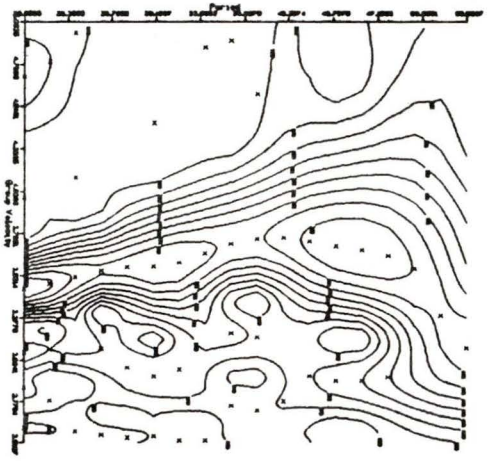

Radial 2 June

SCH

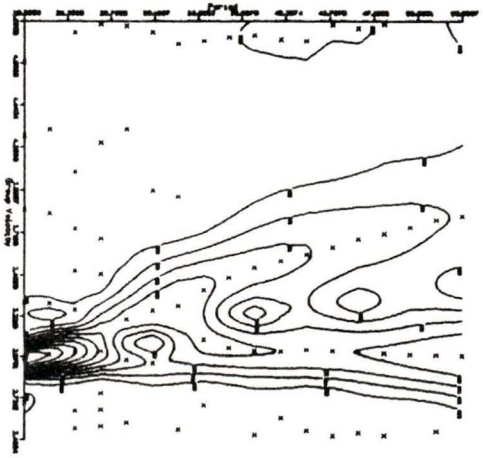

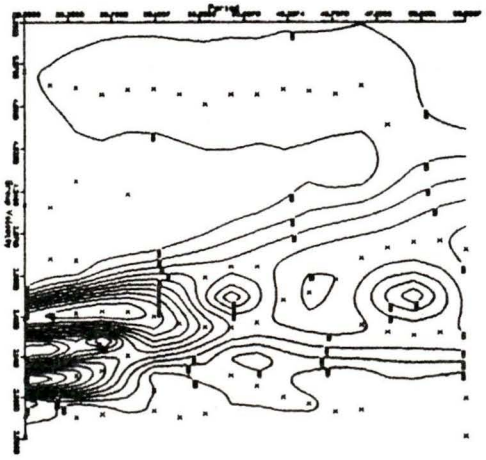

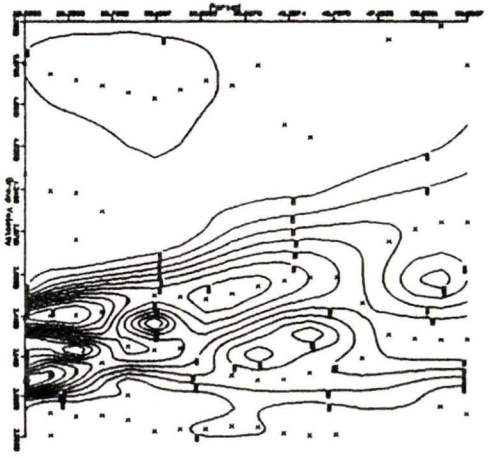

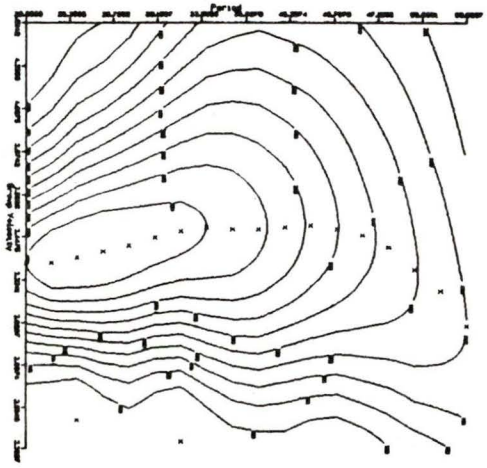

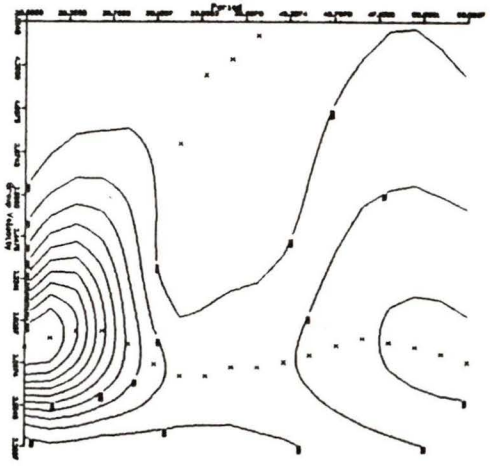

SES

Vertical

Transverse

Radial

2 June

STJ

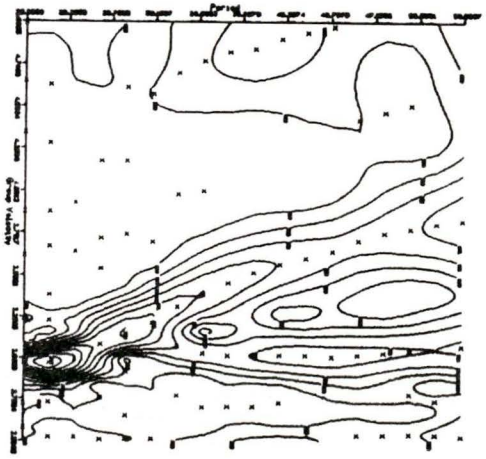

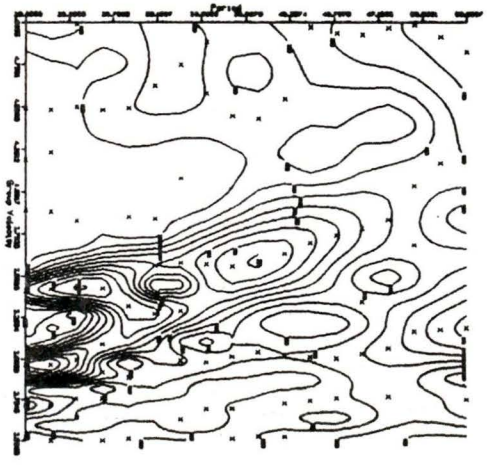

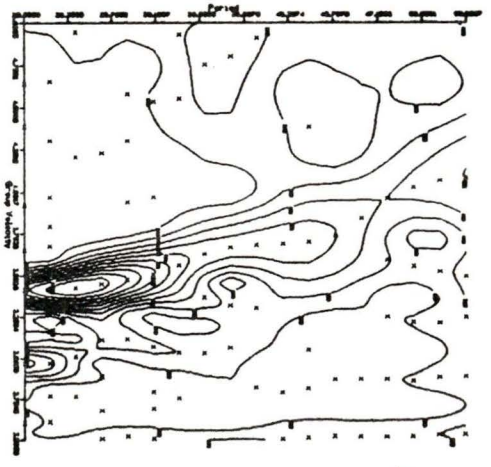

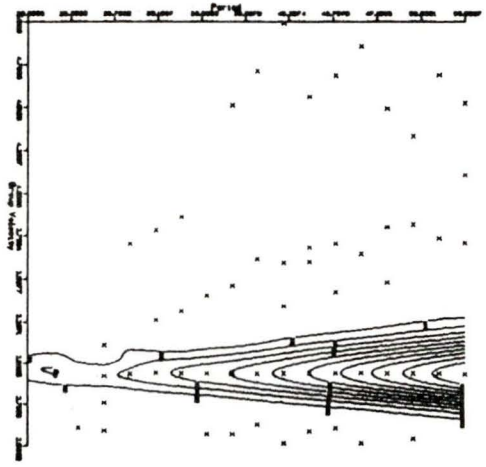

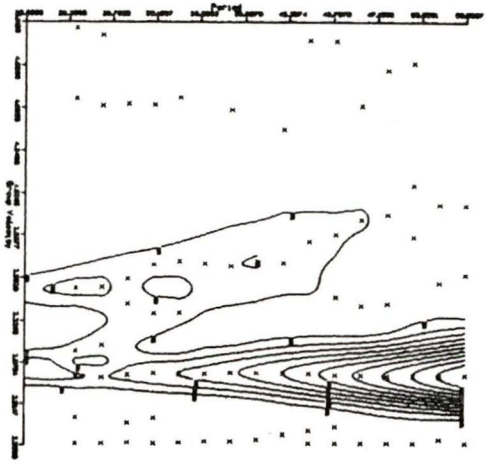

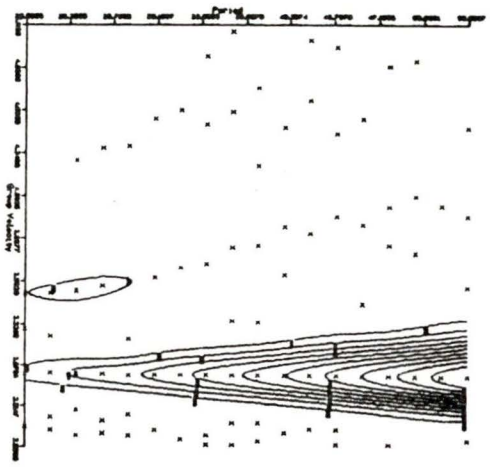

STJ

Vertical

Transverse

Radial

25 July

YKC

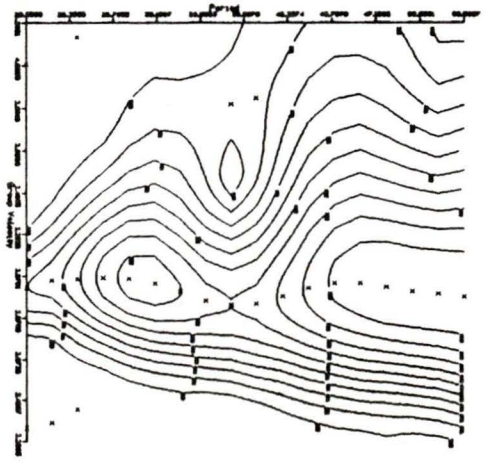

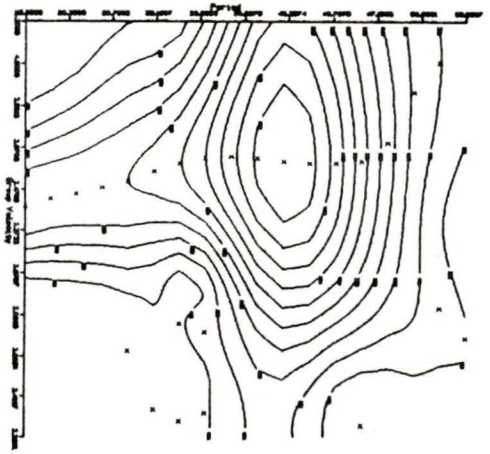

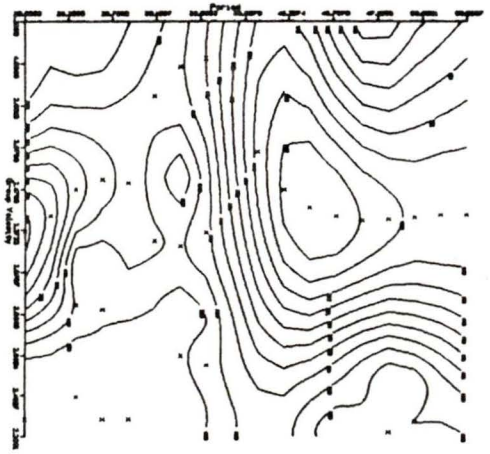

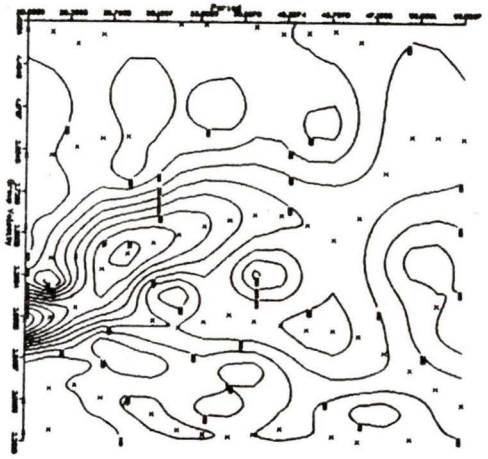

RES

Vertical

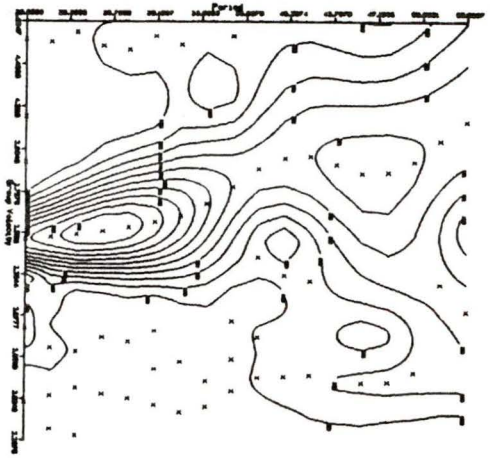

Transverse

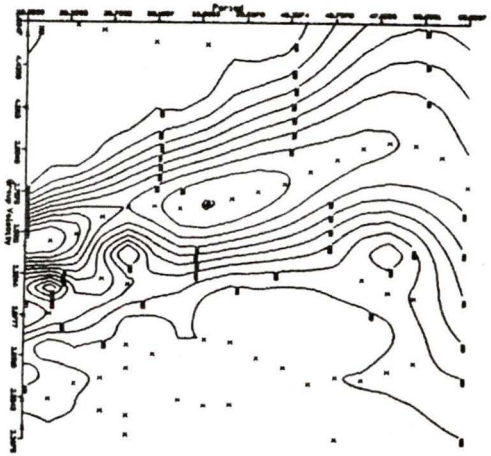

Radial 25 July

SCH

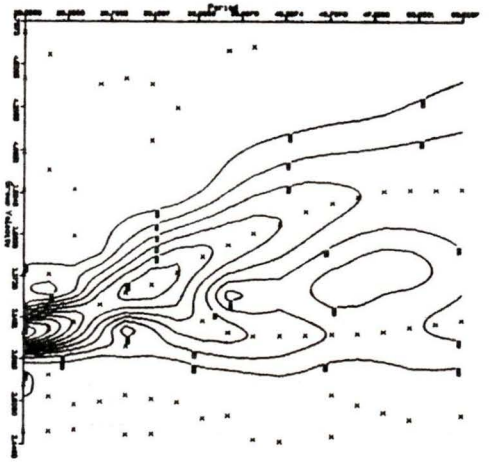

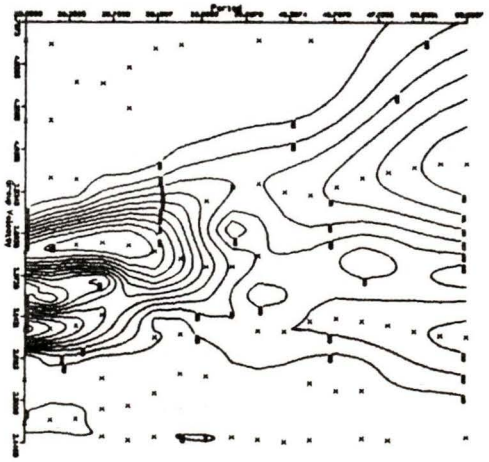

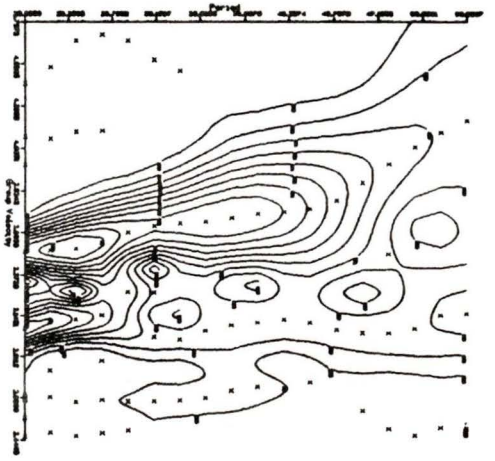

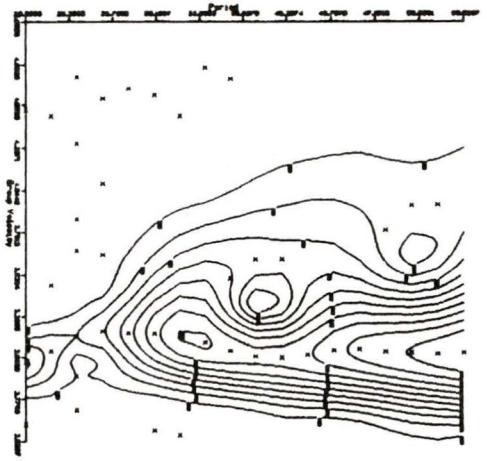

LHC

Vertical

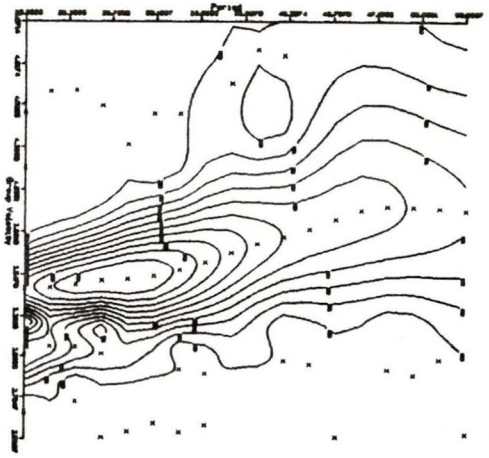

Transverse

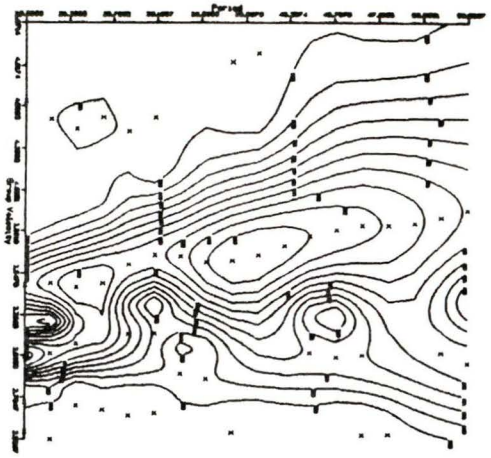

Radial

25 July

OTT

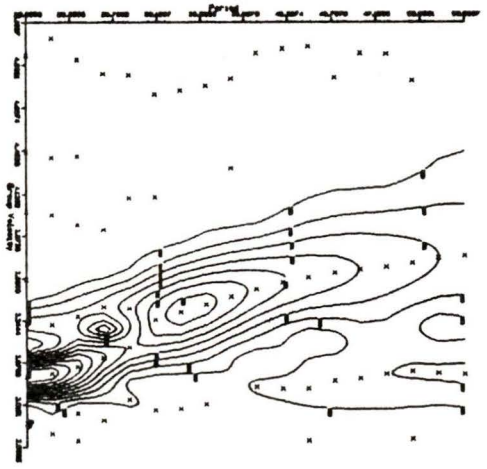

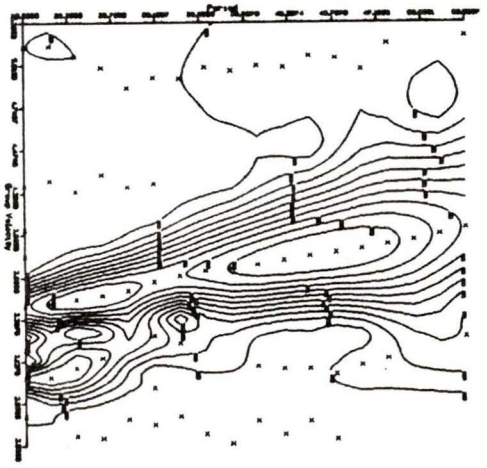

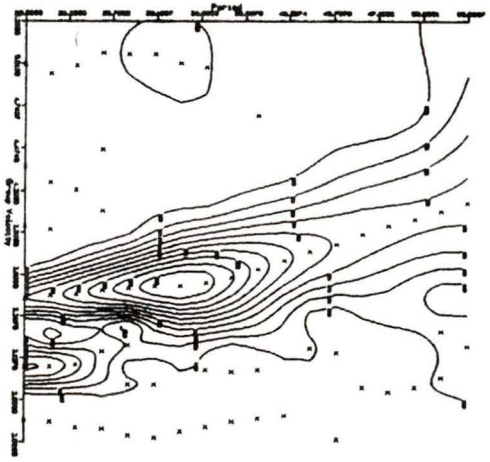

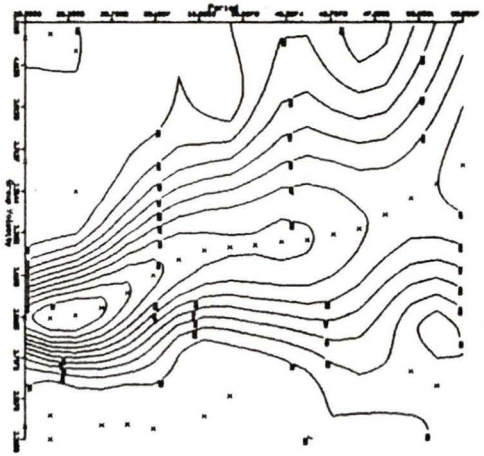

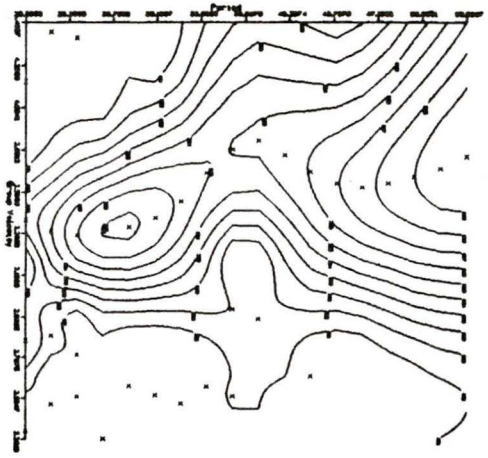

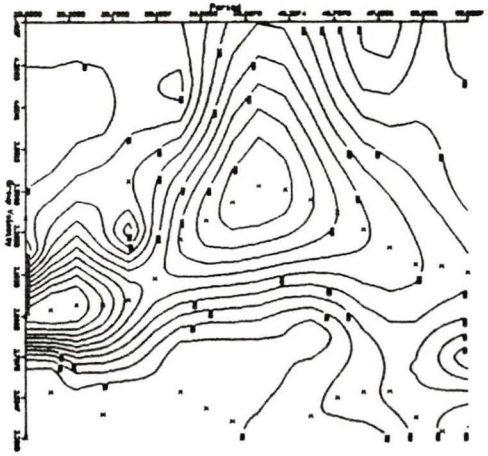

GOL

Vertical

Transverse

Radial

25 July

INK

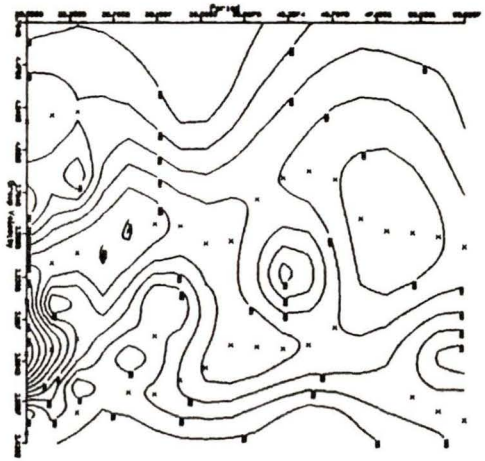

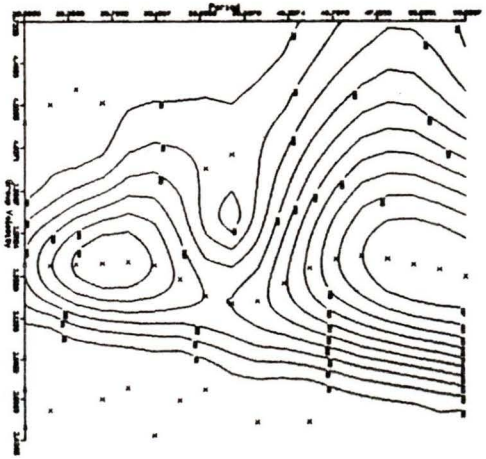

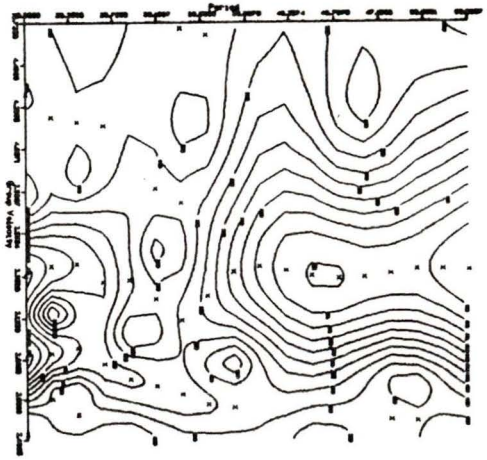

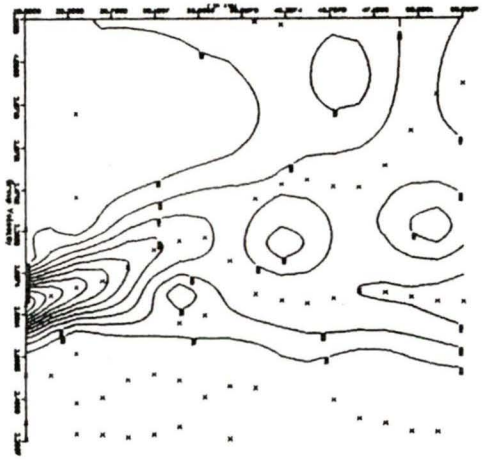

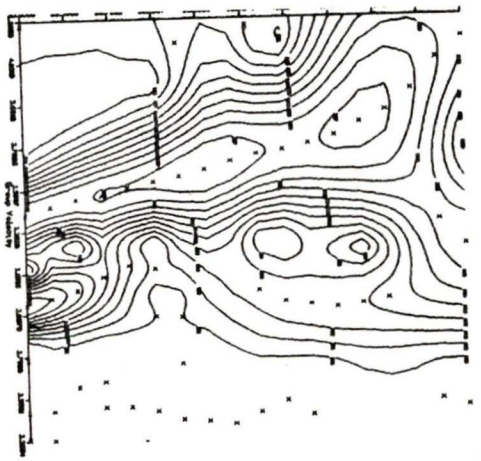

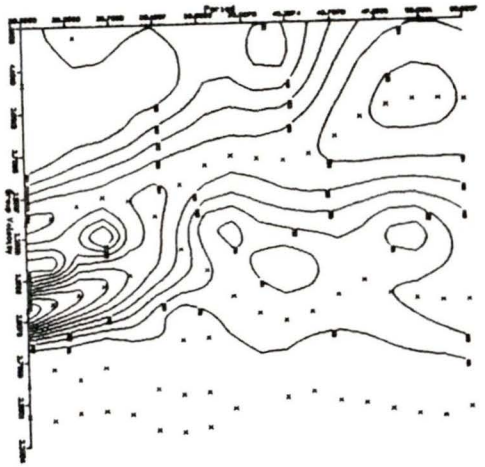

FVM Vertical

Transverse

Radial

25 July

GDH

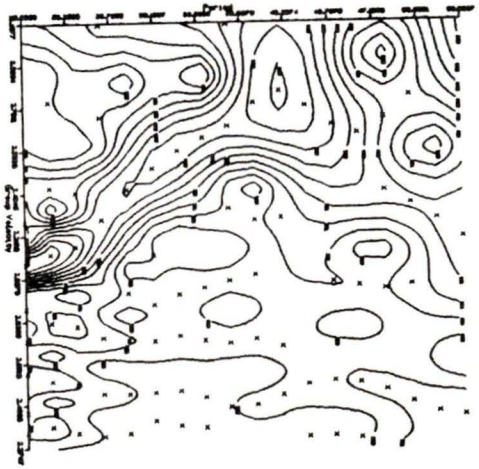

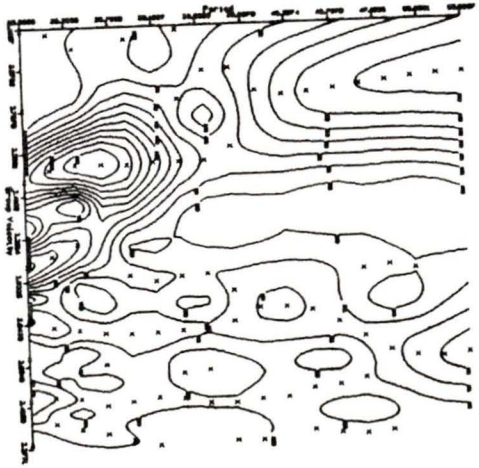

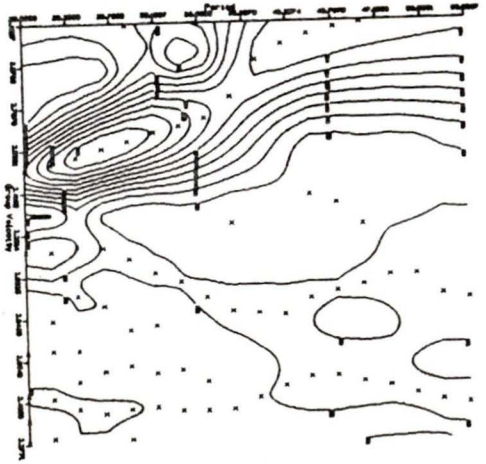

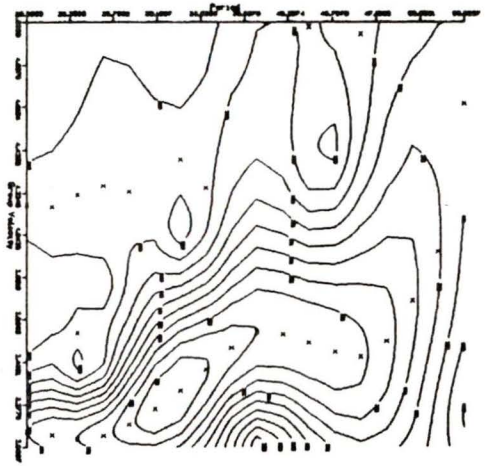

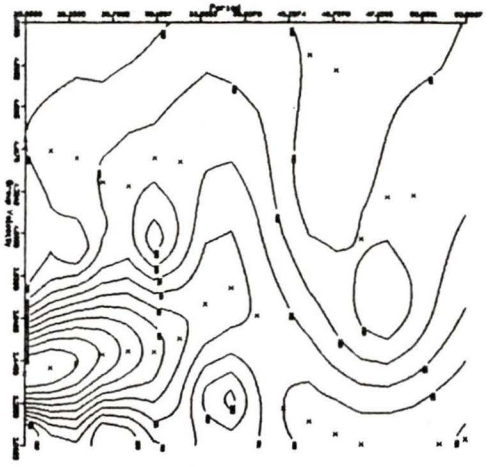

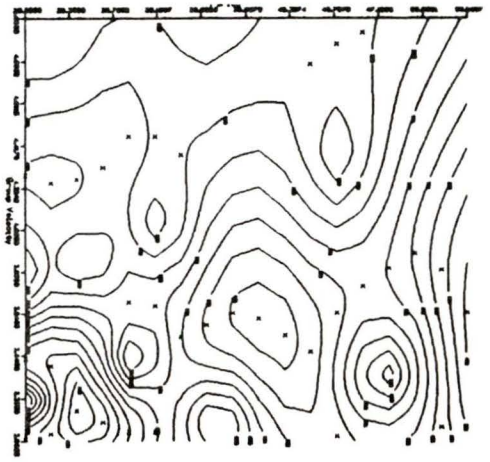

FCC Vertical

Transverse

Radial 25 July

FRB

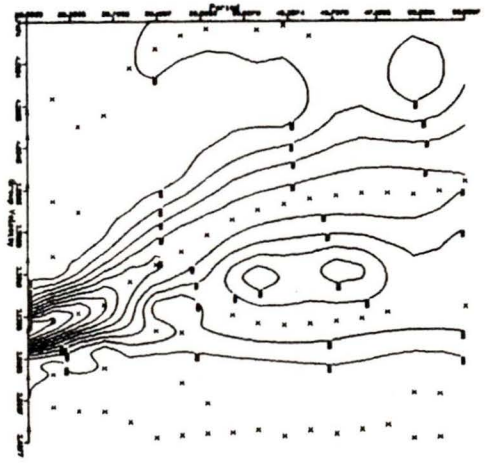

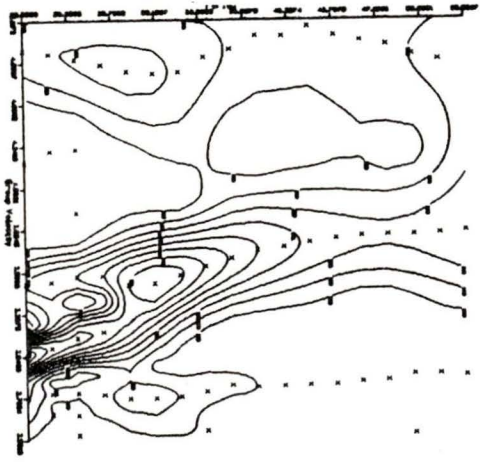

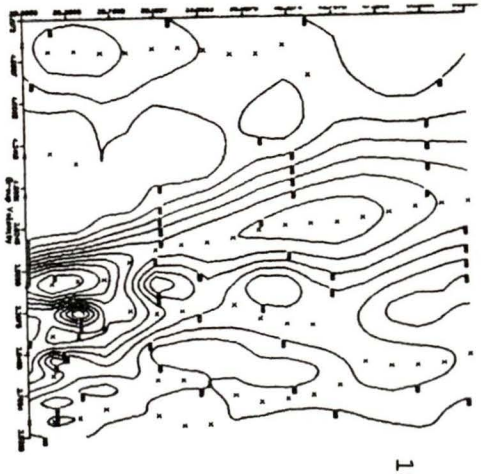

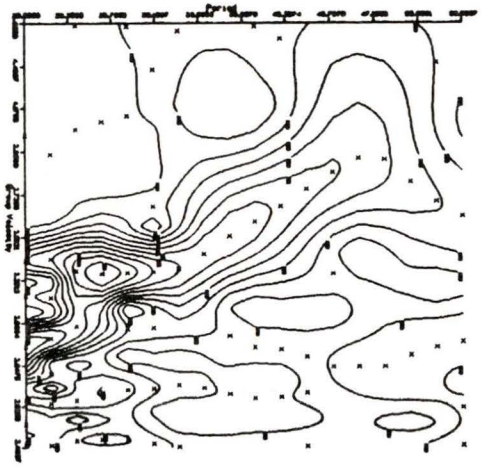

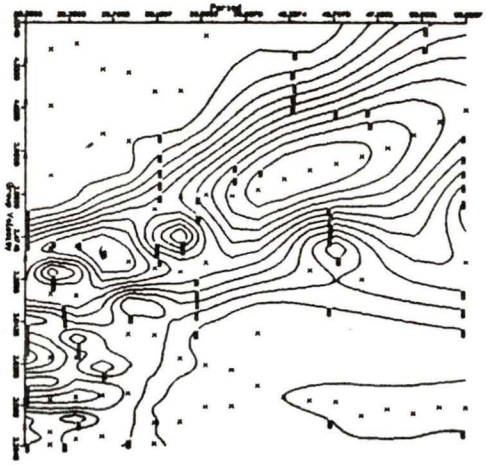

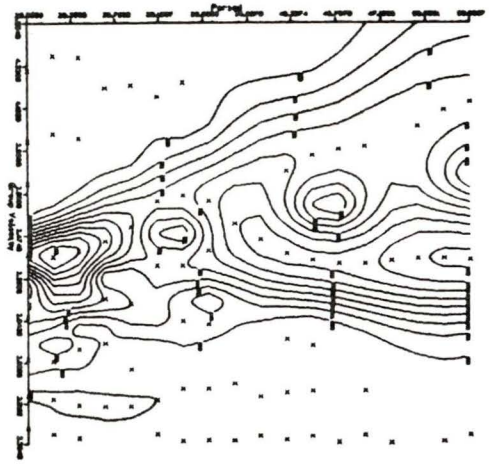

ALE

Vertical

Transverse

Radial

25 July

DUG

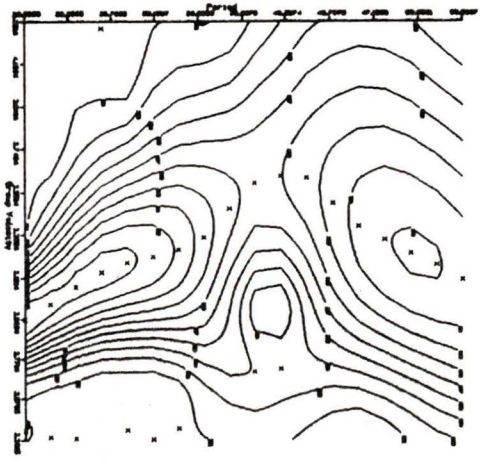

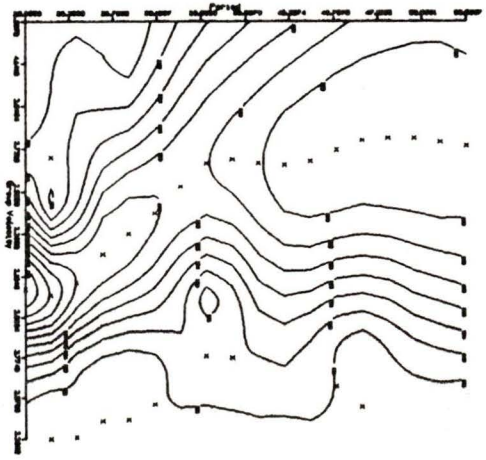

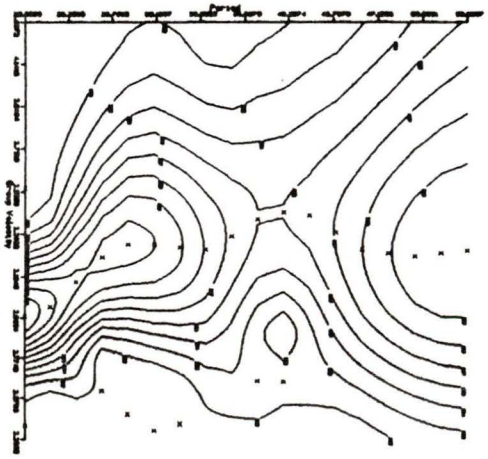

VITA

Surname: Spindler Given Names: Christopher W.L.

Place of Birth: Quebec City, Quebec Date of Birth: 3 April, 1965

Educational Institutions Attended

University of Victoria	1983 to 1988
University of Western Ontario	1988 to 1991

Degrees Awarded

Certificate of Honours Standing (Geophysics)	University of Western Ontario	1988
B.Sc.	University of Western Ontario	1987

Honours and Awards

U.W.O. Geophysics Scholarship for Excellence	1985
C.S.E.G. Scholarship	1984

Publications

Rogers, G.C., C. Spindler, and R.D. Hyndman, Seismicity along the Vancouver Island Lithoprobe Corridor. *Proceedings of the Lithoprobe Workshop*, 3-4 March, 1990, University of Calgary, pp. 166-169.

Spindler, C., and G.C. Rogers, 1989, The 1978 Brooks Peninsula, Vancouver Island Earthquakes (Abstract). *Seismological Research Letters*, **60**, p 7.

PARTIAL COPYRIGHT LICENSE

I hereby grant the right to lend my thesis to users of the University of Victoria Library, and to make single copies only for such users or in response to a request from the Library of any other university, or similar institution, on its behalf or for one of its users. I further agree that permission for extensive copying of this thesis for scholarly purposes may be granted by me or a member of the University designated by me. It is understood that copying or publication of this thesis for financial gain shall not be allowed without my written permission.

Title of Thesis: Analysis of the 1978 Brooks Peninsula, Vancouver Island, Earthquakes

Author [redacted]

Chris Spindler

25 April 1991